



THÈSE

En vue de l'obtention du

DOCTORAT DE L'UNIVERSITÉ DE TOULOUSE

Délivré par:

Université Toulouse 3 Paul Sabatier (UT3 Paul Sabatier)

Présentée et soutenue par:

Syed Asad Ali GILLANI

le jeudi 18 mai 2017

Titre:

Degradation of the residual strength of concrete: Effect of fiber-reinforcement and of rubber aggregates - Application to thin bonded cement-based overlays

École doctorale et discipline ou spécialité:

ED MEGEP: Génie Civil

Unité de recherche:

Laboratoire Matériaux et Durabilité des Constructions (LMDC) Toulouse

Directeurs de Thèse:

Pr. Anaclet TURATSINZE

Dr-HDR Ahmed TOUMI

Jury:

M. Christophe PETIT

M. Pierre ROSSI

Mme. Armelle CHABOT

M. Rashid HAMEED

M. Ahmed TOUMI

M. Anaclet TURATSINZE

Rapporteur

Rapporteur

Examinatrice

Examineur

Co-Directeur de Thèse

Directeur de Thèse

Professeur-Université de Limoges

Directeur de Recherche-IFSTTAR, Marne la Vallée

Directrice de Recherche-IFSTTAR, Bouguenais

Associate Professor-UET Lahore, Pakistan

Maître de conférences (HDR)-Université de Toulouse III

Professeur-Université de Toulouse III

DEDICATION

TO MY BELOVED PARENTS AND RESPECTABLE TEACHERS

ACKNOWLEDGEMENT

It is a great honor for me to express my heartfelt appreciation and special thanks to my respected supervisors Prof. Anaclet Turatsinze and Dr. Ahmed Toumi for sharing their firm knowledge and research experience to accomplish this research work. During all the lengthy scientific discussions, I have learnt a lot, not just about my subject but also about the attitude towards research. They have been a source of motivation for me throughout the thesis.

I am gratefully indebted to all jury members of the thesis defense committee, Prof. Christophe Petit from Université de Limoges, Dr. Pierre Rossi from IFSTTAR Marne la Vallée, Dr. Armelle Chabot from IFSTTAR Bouguenais and Dr. Rashid Hameed from University of Engineering & Technology Lahore, Pakistan for their valuable comments and suggestions on this thesis. It is an honor for me also that my thesis is reviewed by the renowned and expert researchers of this field.

I am thankful to Ex-Director of Laboratoire Matériaux et Durabilité des Constructions (LMDC) Prof. Gilles Escadeillas for providing me an opportunity to work in this prestigious laboratory equipped with latest equipments required to carry out this research work. I am also thankful to the current director of LMDC Prof. Alain Sellier who is very much helpful and co-operative.

I would like to thank all the technical staff of LMDC for their cooperation and assistance throughout my experimental work, especially, Bernard Attard, Carole Soula, Guillaume Lambaré, René Boujou, Yann Bouaskeur, Frédéric Leclerc, Sylvain Dos Santos, Alexis Bloyer. And my special thanks to laboratory secretaries Ghislaine Dupouey, Fabienne Lacoste and Fatima Assabi for the all administrative assistance.

I am thankful to University of Engineering & Technology Lahore, Pakistan for awarding me a scholarship and providing me this opportunity to study in France.

Also, special thanks to all my colleagues, Kahina Agred, Maha Al-Soudani, Mohamed Mosa, Quan Nguyen, Thomas Verdier and Wu Long Zhang for their immense support throughout my research work. My deepest appreciation goes to Dr. Rashid Hameed, not only as a research mate but also as a colleague, thanks a lot for all of the support, help and guidance. I have no words to express my gratitude to Dr. Muhammad Muneeb and Syed Shabbir Hussain Shah, they were always with my family during my absence from Pakistan.

I would like to pay special regard to my respectful parents who always supported me with love and prayers and even sacrificed, to help me reach at this point. It is all their encouragement and support, which made me able to accomplish this research work. My sincere thanks to my sister Arooj Zanjani for her love and care, you are my pride.

Above all, I am thankful to God, the most Merciful and Generous, who gave me the strength and knowledge to achieve this milestone of my life.

Syed Asad Ali GILLANI

TITLE: Degradation of the residual strength of concrete: Effect of fiber-reinforcement and of rubber aggregates - Application to thin bonded cement-based overlays

ABSTRACT

This work is devoted to the study of the debonding of thin bonded cement-based overlays from the concrete substrate under mechanical loading. As repair materials, fiber-reinforced and rubberized cement-based mortars are used. Under these conditions, assessment of durability of the repairs necessarily involves the study of the degradation of the bridging strength under fatigue loading. In this context, tensile fatigue tests controlled by crack mouth opening displacement (CMOD) are conducted on composite specimens in order to establish the degradation law of fiber-reinforced and/or rubberized mortar.

The bridging strength decreases with the number of fatigue cycles for the same maximum crack width, whatever the nature of the composite. The maximum cyclic bridging strength degradation occurs in plain mortar. The cyclic bridging strength degradation for large pre-cracked widths is limited for mortar reinforced with metallic fibers. In case of rubberized mortar, cyclic bridging strength degradation is limited at less pre-cracked width values. A combine use of rubber aggregates and fibers in mortar appeared to be a suitable solution to limit the cyclic bridging strength degradation for a wide range of pre-cracked widths. It confers to the composite an interest for durable application such as cement-based thin bonded overlays.

Taking into account the main cause of distress in thin bonded cement-based applications i.e. cracking and interface debonding, different surface preparation techniques were evaluated in this research. Among them, the sandblasting one is usually implemented in actual conditions.

In order to investigate the structural performance, composite beams consisting of a thin repair layer on top of sandblasted substrates are subjected to three point bending tests (monotonic and fatigue). For monitoring the evolution of cracking in the repair layer and of debonding at interface, digital 3D image correlation technique is used. It emerges as a conclusion that the rubber aggregates incorporation in repair material is helpful to control micro-cracking, which results in the delay of the debonding initiation. Moreover, a fiber-reinforcement of repair material is also helpful to limit the interface debonding propagation by restraining opening of the crack. So, the dual-use of rubber aggregates and fibers in the repair material of thin

bonded cement-based overlays can be a suitable solution to delay the debonding initiation and also to limit the interface debonding propagation. This shows that the synergetic effect provided by the combine use of rubber aggregates and fibers remains valid under fatigue loading also.

The used rubber aggregates are obtained by grinding end-of-life tyres. In such conditions, the approach brings an added value, the recycling of this industrial by-product being also a contribution to the maintenance of a clean environment. Incidentally, this approach also helps towards the development of a circular economy.

Key words: Repair, fiber-reinforcement, rubber aggregates, substrate surface preparation, durability, fatigue, interface debonding, digital image correlation

TITRE: Dégradation de la résistance résiduelle en traction d'un béton : Effet d'un renfort par des fibres et des granulats en caoutchouc - Application aux rechargements minces adhérents à base cimentaire.

RESUME

Ce travail est centré sur l'étude du décollement de couches minces adhérentes à base cimentaire sur un substrat en béton sous chargement mécanique. Comme matériaux de réparation, des mortiers renforcés par des fibres et/ou incorporant des granulats en caoutchouc sont utilisés. Dans ces conditions, l'étude de la durabilité des réparations implique nécessairement celle de la dégradation de la résistance sous chargement de fatigue. Dans ce contexte, des essais de fatigue par traction, contrôlés par l'ouverture de la fissure (CMOD) sont effectués sur des échantillons composites afin d'établir la loi de dégradation de la résistance du mortier renforcé par des fibres et / incorporant des granulats en caoutchouc.

Les résultats montrent que, pour une ouverture de fissure maximale donnée, la résistance résiduelle diminue avec le nombre de cycles et ce quelle que soit la nature du composite. La dégradation maximale de la résistance résiduelle se produit dans le cas du mortier non fibré. Pour des grandes ouvertures de fissure, un renfort par des fibres permet de limiter cette dégradation sous un chargement de fatigue. Dans le cas du mortier incorporant des granulats en caoutchouc, la dégradation de la résistance résiduelle est limitée pour les petites ouvertures de fissure. Une association granulats caoutchouc-renforcement par des fibres permet de limiter les dégâts sur une large étendue d'ouvertures de fissure. Cette solution confère au composite un intérêt pour une application durable dans le cas des réparations minces adhérentes à base cimentaire.

En tenant compte des principales pathologies rencontrées dans cette application tels que la fissuration de la couche de réparation suivie par le décollement de l'interface, différentes techniques de préparation de la surface du support ont été évaluées. Parmi celles-ci, un traitement de la surface par sablage, facile à mettre en œuvre dans les conditions réelles, a été utilisé.

Pour évaluer la performance structurale, des poutres composites constituées d'un rechargement mince sur des substrats dont la surface a été préalablement traitée par sablage ont été soumises à des essais de flexion trois points (monotone et fatigue). Pour le suivi de l'évolution de la fissuration dans le rechargement et du décollement à l'interface, la technique

de corrélation d'image 3D est employée. Il en résulte que l'incorporation des granulats caoutchouc dans le matériau de réparation est efficace pour contrôler la fissuration, et par conséquent pour retarder l'initiation du décollement. De plus, le renforcement du matériau de réparation par des fibres est également efficace pour limiter la propagation du décollement en contrôlant l'ouverture de la fissure. Ainsi, l'utilisation simultanée des granulats caoutchouc et des fibres dans le matériau de réparation par couches minces à base cimentaire peut être une solution appropriée pour retarder l'initiation du décollement et également pour limiter sa propagation, autrement dit pour la durabilité de l'application. Les granulats en caoutchouc utilisés étant obtenus par broyage de pneus usagés non réutilisables, cette approche apporte une valeur ajoutée en valorisant un sous produit industriel et en contribuant à la sauvegarde d'un environnement sain.

Mots clés: Réparation, renforcement de fibres, granulats de caoutchouc, préparation des surfaces du substrat, durabilité, fatigue, décollement, technique de corrélation d'images.

TABLE OF CONTENTS

GENERAL INTRODUCTION.....	1
I. LITERATURE REVIEW	11
I.1 INTRODUCTION.....	11
I.2 RELATED PAST RESEARCH WORKS	11
I.2.1 <i>Effect of incorporating rubber aggregates and fibers on shrinkage cracking of mortar</i>	12
I.2.2 <i>Mechanical behaviour of mortars incorporating rubber aggregates and steel fibers</i>	14
I.2.3 <i>Effect of using fiber-reinforced and rubberized repair mortar on the durability of thin bonded cement-based overlays.....</i>	17
I.2.4 <i>Effect of using high performance fiber-reinforced concrete on the durability of repair system.....</i>	19
I.2.5 <i>Behaviour of fiber-reinforced concrete under fatigue loading.....</i>	21
I.2.6 <i>Impact of substrate surface preparation on bond behaviour between repair and substrate.....</i>	31
I.2.7 <i>Detection and measurement of cracking by using Digital Image Correlation technique.....</i>	39
I.3 CONCLUDING REMARKS	40
II. MECHANICAL CHARACTERIZATION OF STUDIED CEMENTITIOUS COMPOSITES.....	45
II.1 INTRODUCTION.....	45
II.2 SELECTION OF MATERIALS	46
II.2.1 <i>Mortar Constituents</i>	46
II.2.2 <i>Fibers</i>	46
II.2.3 <i>Rubber Aggregates</i>	47
II.3 MORTAR MIX COMPOSITIONS.....	48
II.4 MECHANICAL CHARACTERISTICS	49
II.4.1 <i>Compressive Strength</i>	49

II.4.1.1	Testing Procedure	49
II.4.1.2	Results and Discussion	49
<i>II.4.2</i>	<i>Modulus of Elasticity in Compression</i>	50
II.4.2.1	Testing Procedure	50
II.4.2.2	Results and Discussion	52
<i>II.4.3</i>	<i>Direct Tensile Strength</i>	53
II.4.3.1	Testing Procedure	53
II.4.3.2	Results and Discussion	55
II.4.3.3	Highlights	58
<i>II.4.4</i>	<i>Mass Loss and Shrinkage</i>	59
II.4.4.1	Total Shrinkage.....	60
II.4.4.2	Autogenous Shrinkage.....	63
II.4.4.3	Drying Shrinkage.....	64
II.5	CONCLUDING REMARKS	66

III. IMPACT OF SUBSTRATE SURFACE PREPARATION ON BOND STRENGTH .

.....	71	
III.1	INTRODUCTION.....	71
III.2	SUBSTRATE SURFACE PREPARATION	72
III.2.1	<i>Cutting/Sawing Method</i>	72
III.2.2	<i>Wet Sandblasting Method</i>	72
III.3	BOND TENSILE STRENGTH.....	75
III.3.1	<i>Testing Procedure</i>	75
III.3.2	<i>Results and Discussion</i>	78
III.3.3	<i>Summary</i>	80
III.4	BOND TENSILE STRENGTH BETWEEN UNTREATED SUBSTRATES AND DIFFERENT TYPE OF REPAIR MATERIALS	80
III.4.1	<i>Results and Discussion</i>	80
III.4.2	<i>Summary</i>	82
III.5	BOND TENSILE STRENGTH BETWEEN SANBLASTED SUBSTRATES AND DIFFERENT TYPE OF REPAIR MATERIALS	83
III.5.1	<i>Results and Discussion</i>	83
III.5.2	<i>Summary</i>	86
III.6	CONCLUDING REMARKS	86

IV. FIBER REINFORCED AND RUBBERIZED MORTAR UNDER TENSILE FATIGUE LOADING	91
IV.1 INTRODUCTION.....	91
IV.2 CRACK BRIDGING DEGRADATION OF FIBER REINFORCED AND RUBBERIZED MORTAR UNDER FATIGUE TENSION	92
IV.2.1 Testing Procedure.....	94
IV.2.2 Results and discussion	98
IV.2.3 Highlights.....	104
IV.3 INTERFACIAL BOND DEGRADATION IN THIN BONDED CEMENT-BASED OVERLAYS UNDER FATIGUE TENSION	104
IV.3.1 Testing Procedure.....	104
IV.3.2 Results and discussion	106
IV.3.3 Highlights.....	113
IV.4 CONCLUDING REMARKS	113
V. STRUCTURAL BEHAVIOUR OF REPAIRED BEAMS UNDER FLEXURAL LOADING	117
V.1 INTRODUCTION.....	117
V.2 MANUFACTURING OF COMPOSITE SPECIMENS.....	118
V.3 THREE POINT BENDING TEST UNDER MONOTONIC LOADING	120
V.3.1 Mechanical behaviour of composite beams.....	122
V.3.1.1 Relationship between force and opening of notch.....	122
V.3.1.2 Relationship between force and deflection.....	125
V.4 FLEXURE TESTING ALONG WITH DIGITAL 3D IMAGE CORRELATION TECHNIQUE	128
V.4.1 Digital image correlation Technique.....	128
V.4.2 Detection of interface debonding initiation through 3D digital image correlation technique.....	130
V.5 BENDING TESTS UNDER FATIGUE LOADING.....	137
V.5.1 Experimental protocol of fatigue testing.....	137
V.5.2 Results and discussions.....	142
V.5.2.1 Evolution of notch opening with the number of cycles.....	142
V.5.2.2 Interface debonding propagation with number of cycles	146
V.6 CONCLUDING REMARKS	150

CONCLUSIONS AND PROSPECTS	155
REFERENCES.....	163
ANNEXES	175

LIST OF FIGURES

Figure I-1: Debonding induced by load and differential shrinkage (T-H. Nguyen et al., 2010)	12
Figure I-2: Shrinkage cracking pattern after 55 days (A. Turatsinze et al., 2006)	14
Figure I-3: Pseudo tensile Stress versus notch opening (A. Turatsinze et al., 2005).....	15
Figure I-4: Load vs. deflection in four-point of flexure tests, effects of rubber aggregates and fiber reinforcement incorporation (A. Turatsinze et al., 2006).....	15
Figure I-5: Tensile stress vs. displacement: Influence of rubber aggregates and fiber reinforcement (T-H. Nguyen et al., 2010)	17
Figure I-6: Cross section of specimens (M. Skazlic et al., 2008)	20
Figure I-7: Results of flexural loading test of concretes at 28 days (M. Skazlic et al., 2008).21	
Figure I-8: Simulated flexure stress versus CMOD curves for plain concrete, SSFRC and HSFRC beams under three-point bending, shown together with experimental data (J. Zhang et al., 1999)	24
Figure I-9: Relationship of maximum flexure stress with fatigue life (J. Zhang et al., 1999).25	
Figure I-10: Typical stress-crack width curve of fatigue tension test (J. Zhang et al., 2000) .26	
Figure I-11: Relationship between normalized maximum bridging strength and number of fatigue cycles (J. Zhang et al., 2000)	28
Figure I-12: Relations of normalized maximum bridging strength and maximum pre-cracked width for SSFRC, showing results after 10, 10 ² , and 10 ⁵ cycles, respectively (J. Zhang et al., 2000)	29
Figure I-13: Relations of normalized maximum bridging strength and maximum pre-cracked value of HSFRC, showing results after 10, 10 ² , and 10 ⁵ cycles, respectively (J. Zhang et al., 2000)	30
Figure I-14: Surface profile registered with mechanical profilometer (A. Garbacz et al., 2006)	31
Figure I-15: Factors affecting bond between concrete substrate and repair material (J. Silfwerbrand., 1990)	32
Figure I-16: Examples of concrete surface views after: (a) grinding; (b) sandblasting; (c) shotblasting; and (d) mechanical milling [magnification: 100×-SEM/SE] (A. Garbacz et al., 2006)	34

Figure I-17: Sand test for surface roughness evaluation (L. Courard et al., 2014).....	36
Figure I-18: Failure modes on pull-off test scheme for surface tensile strength evaluation and examples of type B1 [superficial], B2 [middle] and B3 [deep] self defined failure modes (L. Courard et al., 2014)	38
Figure I-19: Failure modes on pull-off test scheme for bond strength evaluation and examples of type A/B and B failure modes (L. Courard et al., 2014)	38
Figure II-1: Amorphous metallic fibers of 30mm length.....	46
Figure II-2: Rubber aggregates and sand	47
Figure II-3: Grading curves of sand and rubber aggregates	48
Figure II-4: Compressive strength of different mortar mixes.....	50
Figure II-5: Testing set-up for compressive modulus of elasticity	51
Figure II-6: Modulus of elasticity in compression.....	52
Figure II-7: Notched test specimen for direct tension tests (dimensions are in mm)	53
Figure II-8: Complete experimental testing set-up for tension test	54
Figure II-9: COD attached at notch (direct tension test).....	55
Figure II-10: Tensile strength of different mortar mixes	56
Figure II-11: Effect of rubber aggregates and fibers on straining capacity	56
Figure II-12: Effect of rubber aggregates and fibers on strain capacity (enlarged view)	57
Figure II-13: Material behaviour in direct tension test	57
Figure II-14: Softening behaviour of different type of mortar mixes	58
Figure II-15: Weighing balance for mass loss determination.....	60
Figure II-16: Apparatus for shrinkage measurement.....	60
Figure II-17: Evolution of total shrinkage in different mortar mixes during period of 150 days	61
Figure II-18: Evolution of mass loss in different mortar mixes during period of 150 days	62
Figure II-19: Total shrinkage vs. mass loss curves for different mortar mixes	62
Figure II-20: Evolution of autogenous shrinkage in different mortar mixes during period of 150 days	63
Figure II-21: Evolution of drying shrinkage in different mortar mixes during period of 150 days	65
Figure II-22: Drying shrinkage vs. mass loss curves for different mortar mixes	65
Figure III-1: Substrate surface prepared with sawing method.....	72
Figure III-2: Substrate surface prepared by sandblasting	73
Figure III-3: View of surfaces obtained after different preparation techniques	73

Figure III-4: Enlarged view of reference surface (RS) without any treatment	74
Figure III-5: Enlarged view of sandblasted surface (SB)	74
Figure III-6: Enlarged view of cut surface (CS)	75
Figure III-7: Notch created by adhesive tape before casting repair	76
Figure III-8: Specimen after repair casting	76
Figure III-9: Notched specimen for bond tensile strength test (dimensions are in mm)	76
Figure III-10: View of notched specimen for bond tensile tests controlled by COD	77
Figure III-11: Bond tensile strength variation with different surface preparation techniques.	78
Figure III-12: Strain capacity behavior of overlays with different substrate surface textures.	79
Figure III-13: Post Peak Bond Softening Behavior of overlay with different substrate surface textures	79
Figure III-14: Bond tensile strength variation with different repair materials.....	81
Figure III-15: Strain capacity behavior with different overlay repair materials	81
Figure III-16: View of broken sample with 30R0F repair, showing the fracture mainly occurred in the repair material	82
Figure III-17: Bond Tensile strength variation with different repair materials on sandblasted substrates.....	84
Figure III-18: Strain capacity behavior with different overlay repair materials on sandblasted substrates.....	84
Figure III-19: Strain capacity behavior with different overlay repair materials on sandblasted substrates (enlarged view).....	85
Figure III-20: View of broken sample with 30R30F repair, showing the fracture mainly occurred in the repair material	85
Figure IV-1: Notched test specimen for uniaxial tensile fatigue tests (dimensions are in mm)	92
Figure IV-2: Complete experimental testing set-up for conducting uniaxial fatigue tension test.....	93
Figure IV-3: COD attached at notch.....	93
Figure IV-4: Selection of COD_{max} for tensile fatigue loading corresponding to control mortar	94
Figure IV-5: Direct tension test upto $COD_{max} = 0.025\text{mm}$	95
Figure IV-6: Typical loading - unloading loops of crack bridging strength under cyclic loading for control mortar.....	96

Figure IV-7: Test results of maximum bridging strength vs. number of cycles for control mortar corresponding to $COD_{max} = 0.025$ mm.....	97
Figure IV-8: Test results of normalized maximum bridging strength vs. number of cycles for control mortar corresponding to $COD_{max} = 0.025$ mm	97
Figure IV-9: Relationship between normalized maximum bridging strength and number of fatigue cycles corresponding to $COD_{max} = 0.025$ mm	99
Figure IV-10: Relationship between normalized maximum bridging strength and number of fatigue cycles corresponding to $COD_{max} = 0.025$ mm on logarithmic scale.....	99
Figure IV-11: Normalized maximum bridging strength degradation values in different mortar mixes corresponding to $COD_{max} = 0.025$ mm at 10^4 cycles	100
Figure IV-12: Relationship between normalized maximum bridging strength and number of fatigue cycles corresponding to $COD_{max} = 0.010$ mm	100
Figure IV-13: Relationship between normalized maximum bridging strength and number of fatigue cycles corresponding to $COD_{max} = 0.010$ mm on logarithmic scale.....	101
Figure IV-14: Normalized maximum bridging strength degradation values in different mortar mixes corresponding to $COD_{max} = 0.010$ mm at 10^4 cycles	101
Figure IV-15: Comparison of normalized maximum bridging strength degradation values in different mortar mixes, corresponding to different pre-cracked widths (COD_{max}) at 10^4 cycles	102
Figure IV-16: Relationship between normalized maximum bridging strength and maximum crack width for different mortar mixes, showing results after 10, 10^2 , 10^3 and 10^4 cycles, respectively	103
Figure IV-17: Notched specimen for interfacial bond strength degradation (dimensions are in mm).....	105
Figure IV-18: Complete experimental testing set-up for determining interfacial bond strength degradation.....	105
Figure IV-19: Selection of COD_{max} for tensile fatigue loading corresponding to control mortar repair	106
Figure IV-20: View of broken sample with 30R0F repair after conducting bond tension test	107
Figure IV-21: Relationship between normalized maximum bond strength and number of fatigue cycles corresponding to $COD_{max} = 0.010$ mm	108
Figure IV-22: Relationship between normalized maximum bond strength and number of fatigue cycles corresponding to $COD_{max} = 0.010$ mm on logarithmic scale.....	108

Figure IV-23: Normalized maximum bond strength degradation with different repair mortar mixes corresponding to $COD_{max} = 0.010$ mm at 10^4 cycles	109
Figure IV-24: Relationship between normalized maximum bond strength and number of fatigue cycles corresponding to $COD_{max} = 0.020$ mm	109
Figure IV-25: Relationship between normalized maximum bond strength and number of fatigue cycles corresponding to $COD_{max} = 0.020$ mm on logarithmic scale.....	110
Figure IV-26: Normalized maximum bond strength degradation with different repair mortar mixes corresponding to $COD_{max} = 0.020$ mm at 10^4 cycles.....	110
Figure IV-27: Comparison of normalized maximum bond strength degradation for different repair material, corresponding to different pre-cracked widths (COD_{max}) at 10^4 cycles	111
Figure IV-28: Relationship between normalized maximum bond strength and maximum crack width with different repair mortar mixes, showing results after 10, 10^2 , 10^3 and 10^4 cycles, respectively	112
Figure V-1: Casting of repair on top of substrate	119
Figure V-2: Complete dimensions of composite specimen	119
Figure V-3: Detail of a composite specimen	120
Figure V-4: Schematic diagram of a composite specimen under three point bending test....	120
Figure V-5: Complete testing setup for three point bending test.....	121
Figure V-6: Load versus opening of notch (COD) curves for 0R0F (CC) repair	123
Figure V-7: Load versus opening of notch (COD) curves for 0R30F repair	123
Figure V-8: Load versus opening of notch (COD) curves for 30R0F repair.....	124
Figure V-9: Load versus opening of notch (COD) curves for 30R30F repair.....	124
Figure V-10: Load versus opening of notch (COD) curves for composite repaired beams with different repair mix compositions.....	125
Figure V-11: Load versus deflection curves for CC repair.....	126
Figure V-12: Load versus deflection curves for 0R30F repair	126
Figure V-13: Load versus deflection curves for 30R0F repair	127
Figure V-14: Load versus deflection curves for 30R30F repair	127
Figure V-15: Load versus deflection curves for composite repaired beams with different repair mix compositions.....	128
Figure V-16: Sample preparation for bending test along with 3D digital image correlation technique.....	129
Figure V-17: Complete experimental testing setup for three point bending test along with 3D digital image correlation technique.....	130

Figure V-18: Selected strain visualizations for crack observation and use of artificial extensometer for detecting the load at which crack reach at interface location	131
Figure V-19: Force vs. opening of artificial extensometer (D1): detection of load at which crack reach at interface location and debonding initiated.....	132
Figure V-20: Force vs. debonding length at interface for 0R0F (CC) repair	134
Figure V-21: Force vs. debonding length at interface for 0R30F repair	134
Figure V-22: Force vs. debonding length at interface for 30R0F repair	135
Figure V-23: Force vs. debonding length at interface for 30R30F repair	135
Figure V-24: Force vs. debonding length at interface for different repair layers	136
Figure V-25: Debonding length vs. opening of notch for different repair layers under monotonic loading	137
Figure V-26: Experimental protocol of cyclic loading for 30R0F repair	138
Figure V-27: Strain field color contrast showing propagation of crack from notch tip to interface location under monotonic loading for 30R0F repair.....	139
Figure V-28: Strain field color contrast showing interface debonding location and using artificial extensometer to determine the debonding length for 30R0F repair (100000 cycles)	139
Figure V-29: Seven Strain fields showing interface debonding propagation with number of cycles and using artificial extensometer to determine the debonding length for 30R0F repair	141
Figure V-30: Snapshot of MTS acquisition during fatigue test, showing opening of notch (COD) due to the application of cyclic loading between P_{max} and P_{min}	141
Figure V-31: Opening of notch at P_{max} with number of cycles for 0R0F (CC) repair.....	143
Figure V-32: Opening of notch at P_{max} with number of cycles for 0R30F repair.....	143
Figure V-33: Opening of notch at P_{max} with number of cycles for 30R0F repair.....	144
Figure V-34: Opening of notch at P_{max} with number of cycles for 30R30F repair.....	144
Figure V-35: Opening of notch at P_{max} with number of cycles for different repair mortar mixes.....	145
Figure V-36: Curve between COD and image number (recorded at every 20000 cycles), showing evolution of notch opening with number of cycles	145
Figure V-37: Propagation of debonding length at interface with number of cycles for 0R0F (CC) repair	146
Figure V-38: Propagation of debonding length at interface with number of cycles for 0R30F repair	147

Figure V-39: Propagation of debonding length at interface with number of cycles for 30R0F repair	147
Figure V-40: Propagation of debonding length at interface with number of cycles for 30R30F repair	148
Figure V-41: Propagation of debonding length at interface with number of cycles for different repair mortar mixes	148
Figure V-42: Debonding length at interface vs. opening of notch for different repair mortar mixes	149

LIST OF TABLES

Table I-1: Load (kN) necessary to initiate interface debonding: analytical results versus numerical and experimental ones (A. Toumi et al., 2013).....	19
Table I-2: Results of pull-off strength tests (A. Garbacz et al., 2006).....	35
Table I-3: Results of Surface Roughness Index (SRI), surface tensile strength and pull-off bond strength vs. surface treatment technique (L. Courard et al., 2014).....	37
Table II-1: Characteristics of amorphous metallic fibers (Fibraflex saint-gobain)	47
Table II-2: Mix design and proportioning (Values in kg/m ³)	49
Table V-1: Load at which crack reached at interface and debonding at interface started	133



GENERAL INTRODUCTION

GENERAL INTRODUCTION

Concrete has been used in the construction industry from thousands of years and with the passage of time distresses or decrement of load carrying capacity of existing structures has been observed. In the upcoming years, the challenge which civil engineers will have to face is the repair and strengthening of these existing structures. Moreover, the number of concrete structures keeps growing, and therefore need of repair or retrofiting also increases. There can be different approaches for rehabilitation of concrete. Among them, thin bonded overlay is found to be the most economical alternative (B. Bissonnette et al., 2011). This overlay repair technique is particularly suitable with the structures having large surface areas, where it can be either sprayed or poured. The application of these types of overlays is of special concern: slabs on grade (e.g. industrial floors), pavements, bridge decks, walls and tunnels.

The primary purpose of overlays is to extend the service life of the existing concrete structures, either by restoring the smooth finish surface or by improving the load carrying capacity of concrete by increasing the thickness of concrete.

Some other benefits from overlaying slabs/concrete pavements include:

- ✚ To match the level of an adjacent slab
- ✚ To remove the deteriorated concrete and placing a new layer which act as a protection to the structure (especially its reinforcement)
- ✚ To provide more durable wearing surface
- ✚ To improve the frictional characteristics of top surface for pavements or bridge decks
- ✚ To restore architectural features such as color or texture.
- ✚ To replace a corrosion damaged bridge decks or slabs with a more durable concrete

The main problem in overlay concrete is bond sustainability and durability of bonded overlay systems and is of main concern to the world. The durability of these overlays is jeopardized if cracking cuts new repair layer, because this cracking initiates the debonding mechanism (T-H. Nguyen et al., 2010). Debonding generally starts at the joints, boundaries and cracks in the overlay, and further propagated by curling effects in the debonding area. This leads to new cracks and increased debonding, which accelerate the damage process and soon leads to the need of renewed repairs. Two mechanisms or their combination are involved in debonding phenomena:

- ✚ First is due to applied loads on the overlaid structure
- ✚ Secondly, due to the differential length changes of the overlay and of substrate

According to some previous numerical studies, use of high tensile strength materials as a repair material reduces risks of cracking (Q-T. Tran et al., 2008). Moreover, by using repair material having low Young's modulus is more beneficial because it improves strain capacity, which in turn is helpful in delaying crack localization, particularly the cracks which normally developed due to restrained shrinkage as a result of differential length change between the substrate and the overlay (Q-T. Tran et al., 2008). Unfortunately, it is a bit difficult to achieve this kind of ideal matrix having characteristics of low modulus and high strength simultaneously. Several studies prove this fact that by incorporating metallic fibers in mortar, various properties improves, mainly the ductility of mortar. Previous laboratory and field studies also showed that use of metallic fibers in overlays, restrains the cracking phenomena, which in turn delays debonding initiation and propagation (A. Turatsinze et al., 2005; A. Turatsinze et al., 2006; T-H. Nguyen et al., 2010). Reinforcing steel bars or welded wire mesh can also be used to restrain the cracking, but the main problem associated with that, these can only be used in sufficient thick overlays. Another advantage of using metallic fibers instead of steel bars is that one can reduce the risk of corrosion (S-U Balouch and J-L Granju., 1999). So in the light of previous research, it can be said that cracking and debonding in overlays can be controlled by increasing the bond tensile strength at the interface and improving the repair material properties to restrain cracking.

Previous Research Works

Several studies have been devoted to this topic of cement-based repairs out of which some research works were conducted in Laboratoire Matériaux et Durabilité des Constructions (LMDC), Toulouse. Chronologically we can enumerate:

- ✚ F. Grandhaie (F. Grandhaie., 1993) studied the effectiveness of using fibers in repair material.
- ✚ J-L. Granju (J-L. Granju., 1994) study was focused on mechanism of debonding in repair system.
- ✚ H. Chausson (H. Chausson and J-L. Granju., 1996) used fibers in the repair material in order to improve its mechanical properties.
- ✚ A. Turatsinze (A. Turatsinze et al., 2003) studied the shrinkage behaviour of fiber-reinforced concrete.
- ✚ V. Sabathier (V. Sabathier., 2004) studied the mechanical aspects and modeling of the repair system.
- ✚ A. Garbacz (A. Garbacz et al., 2006) performed characterization of concrete surface roughness and determine its relation to adhesion in repair system.
- ✚ Q-T. Tran (Q-T. Tran., 2006) studied the structural behaviour of repair system and his work was mainly focused on the evolution of interface debonding under fatigue loading.
- ✚ E. Brühwiler (E. Brühwiler and E. Denarié., 2008) utilized High Performance Fiber-Reinforced Concrete (HPFRC) as repair material, for the rehabilitation of concrete structures.
- ✚ T-H. Nguyen (T-H. Nguyen., 2010) studied the mechanical properties of different repair materials and also the sustainability of cement-based repair systems.
- ✚ L. Courard (L. Courard et al., 2014) studied different properties near to the concrete substrate surface which can affect the bond strength in repair system.

- ✚ Bassam A. Tayeh (Bassam A. Tayeh et al., 2013) performed characterization of the interfacial bond between old concrete substrate and ultra high performance fiber concrete repair composite.
- ✚ A. Toumi (A. Toumi et al., 2015) carried out finite element modelling for predicting the debonding propagation of fiber-reinforced and rubberized cement-based overlays under fatigue loading.
- ✚ Zena R. Aljazeera (Zena R. Aljazeera and John J. Myers., 2016) evaluated the fatigue and flexural behaviour of reinforced-concrete beams strengthened with fiber-reinforced cementitious matrix

Problem Statement and Research Objectives

It is recognized that the incorporation of fibers and rubber aggregates in concrete can favorably modify the residual post cracking strength and its strain capacity. In this regard, a positive synergetic effect with material bridging can be expected by using them in overlays. However, in actual cases, fatigue loading is more relevant. So under these conditions, it is necessary to investigate the contribution of fiber-reinforcement and of rubber aggregates under fatigue loading and to compute material degradation in residual post-cracking resistance. In this context, this research work has the following main objectives:

- ✚ To conduct uniaxial tensile fatigue tests controlled by crack mouth opening displacement (CMOD) on mortar mixes incorporating rubber aggregates and/or metallic fibers, in order to compute the cyclic bridging degradation behaviour.
- ✚ To develop the cyclic bridging degradation law, the so-called stress-crack width relationship of fiber-reinforced and/or rubberized mortar.
- ✚ To study the impact of substrate surface preparation on bond behaviour of the repair system.
- ✚ To monitor crack propagation and interface debonding in thin bonded repaired beams by using 3D Digital Image Correlation (DIC) technique under monotonic and fatigue loading.

- ✚ To study the structural performance of thin bonded repaired beams under monotonic and fatigue loading.

Thesis Organization

This thesis comprises of total five chapters. These chapters are organized as follows:

Chapter 1:

This chapter includes a literature review and relevant work done by previous researchers on thin bonded cement-based overlays. Complete mechanisms are presented in order to understand the sustainability of repair system. The influence of mechanical loading and shrinkage on behaviour of fiber-reinforced and a rubberized mortar is presented here. The impact of using fiber-reinforced and rubberized repair mortar on the durability of thin bonded cement-based overlays is explained. Also, the cyclic crack bridging behaviour of fiber-reinforced concrete is highlighted. The effect of utilizing high performance fiber-reinforced concrete for rehabilitation of concrete structures is discussed. Further, the impact of substrate surface preparation on bond behaviour of repair system is discussed. Finally, the adequacy of using DIC technique to detect cracking in concrete and bituminous material is presented.

Chapter 2:

This chapter describes the selection of different materials used for cement-based overlays and mechanical characterization of studied mix compositions. Complete properties of materials like cement, sand, fibers, rubber aggregates, super-plasticizer, viscosity agent, etc. are presented here. For mechanical characterization of studied mix compositions, in first step the behaviour is evaluated in direct compression and direct tension. After that, modulus of elasticity in compression will be presented. In this chapter, the influence of using rubber aggregates on strain capacity, improvement in post cracking behaviour by use of metallic fibers and positive synergetic effect of combined use of rubber aggregates and fibers is also discussed. At the end, total shrinkage, autogenous shrinkage, drying shrinkage and mass loss of studied mortar mix compositions are presented with the aim of studying the effect of incorporating rubber aggregates (material with high deformation capacity) and metallic fibers on shrinkage behaviour.

Chapter 3:

This chapter reports the impact of substrate surface preparation on the bond behaviour of the repair system. Different surface preparation techniques are evaluated by conducting bond tensile tests. Bond tensile strengths along with the softening behaviour of treated and untreated substrate surfaces are explained here. The bond behaviour of treated and untreated substrate bases is also evaluated by overlaying these bases with kind of composite repairs.

Chapter 4:

In this chapter, the cyclic bridging degradation laws of fiber-reinforced and/or rubberized mortars are presented. These degradation laws are developed by subjecting studied mortar mixes under uniaxial tensile fatigue loading at different pre-cracked width values. And comparison will be made among different type of mortar mixes, which allows us to know how fiber-reinforcement and rubber aggregates incorporation in mortar is helpful to control cyclic bridging degradation. Further, the impact of pre-cracked width value on cyclic bridging degradation behaviour is also evaluated here. Finally, the cyclic interfacial bond degradation of composite specimens (repair materials on top of sandblasted substrates) is evaluated at different pre-cracked width values.

Chapter 5:

The primary objective of Chapter 5 is to study the structural performance of repaired beams under flexure loading (monotonic and fatigue). For this purpose, composite beams consisting of a thin repair layer on top of sandblasted substrates (simulating repaired structure) are tested in bending. Firstly, the behaviour of composite beams subjected to three point bending tests under monotonic loading is evaluated. From simple monotonic tests, the following parameters are determined: the relationship between the force and deflection, the relationship between force and opening of the notch, the force at which crack reaches the substrate-repair interface, the load at which debonding initiates at interface and total debonding lengths at the interface. Finally, at the end of this chapter, the behaviour of composite beams is studied under cyclic loading. Since, fatigue loading on repairs is more realistic in practical field

condition. The evolution of crack opening and debonding length with respect to the number of cycles was examined with the aim of evaluating the effectiveness of fiber-reinforced and/or rubberized repair mortar towards the durability of thin bonded cement-based overlays. In order to monitor the evolution of cracks and to measure the debonding along the interface, digital 3D image correlation technique is used.

Based on the experimental investigations, general conclusions and perspectives are discussed at the end of the thesis.



Chapter I

LITERATURE REVIEW

I. LITERATURE REVIEW

I.1 INTRODUCTION

By giving a synthesis of the research work on repairs, this chapter presents the main research results on the subject. The list of works presented does not pretend to be exhaustive, but nevertheless it covers the subject from old works to recent ones.

It is a recognized fact that early degradation of concrete strength reduces the service life of structures. In order to repair the structure, extra cost is required, which as a result increase the overhead charges of the structure. This matter yields to the development of new materials and technologies for repair of concrete structures.

There can be different approaches for rehabilitation of concrete. Among them, a common way to restore the performance of a deteriorated pavement is thin bonded cement-based overlay. Since, all over the world this technique of thin bonded cement-based overlays proves to be very effective, especially for large concrete areas (J-L. Granju., 1996; G. Chanvillard et al., 1989). But uptill now these repairs possessed some durability problems. The durability of these overlays is mainly in danger due to cracking of the repair layer, followed by interface debonding from the substrate.

I.2 RELATED PAST RESEARCH WORKS

According to some previous researches (J-L. Granju., 1996; Q-T. Tran et al., 2006; B. Bissonnette et al., 2011), the debonding between overlay and substrate is majorly caused by mechanical loading and differential shrinkage as described in Figure I-1. In both mechanisms, this lack of adherence primarily begins from edges, cracks and joints. It is a known fact that the addition of fibers in concrete improves several of its properties like cracking resistance, ductility, wear resistance etc. Recent research work (T-H. Nguyen et al., 2010; T-H. Nguyen et al., 2012; A. Toumi et al., 2013; A. Turatsinze et al., 2016) also pointed out that the use of rubber aggregates obtained from grinding of end-of-life tyres is a suitable solution to improve

the strain capacity of cement-based materials. These two properties are without any doubt essential in the durability of bonded cement-based overlays.

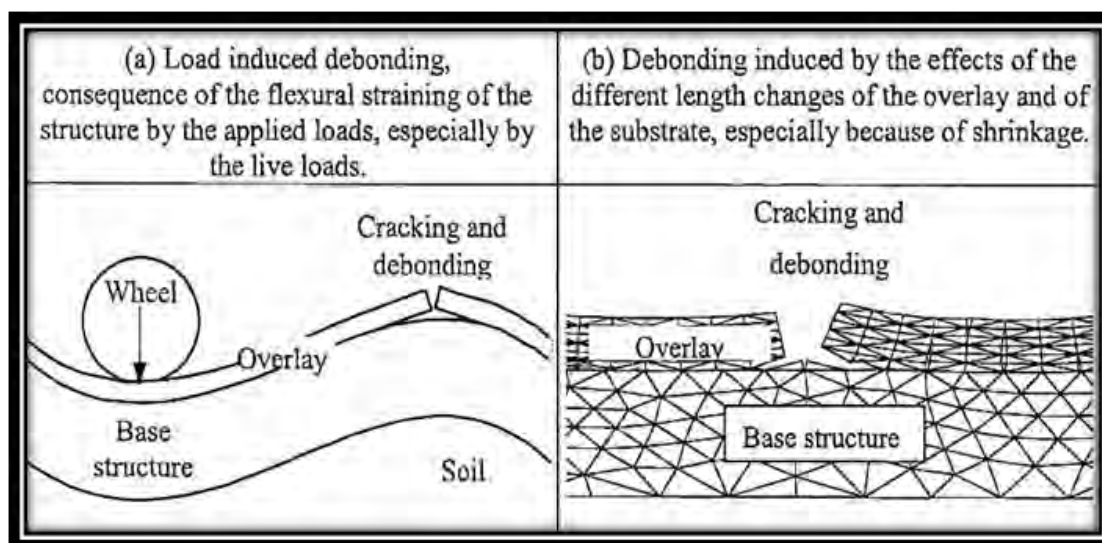


Figure I-1: Debonding induced by load and differential shrinkage (T-H. Nguyen et al., 2010)

In order to get enhance the durability of cement-based overlays, one can suggest that the use of repair material incorporating rubber aggregates and/or metallic fibers can be a promising solution. But, before using this innovative cement-based material as a repair material, it is necessary to know the mechanical behaviour of this composite. Several studies have been conducted in the past for evaluating the shrinkage behaviour and mechanical properties of cementitious composites incorporating rubber aggregates and metallic fibers. So, out of those, some works are presented below.

1.2.1 Effect of incorporating rubber aggregates and fibers on shrinkage cracking of mortar

Cement-based materials are always sensitive to cracking, especially shrinkage cracking. This cracking is more pronounced in cases where shrinkage is restrained, e.g. cement-based overlays. The cracking induced due to restrained shrinkage causes serious durability issues in thin bonded cement-based overlays (J-L. Granju., 1996; A. Turatsinze et al., 2003). A continuous effort is going on to develop such cement-based matrix which exhibits good resistance against the shrinkage cracking.

So, in this context, A. Turatsinze (A. Turatsinze et al., 2006) utilized the rubber aggregates and steel fibers in mortars and evaluated the shrinkage cracking behaviour of this unique

mortars mix. The primary objective of this research work was to design such cement composite which shows more strain capacity before the macro-cracking. In order to design such kind of matrix, aggregates possessing low modulus of elasticity like rubber aggregates were incorporated in the mortar. For this purpose, shredded non-reusable tyres were used which also helps to maintain a clean environment. These rubber aggregates were incorporated as a partial replacement of sand. Two percentage replacements were used, i.e. 20% and 30% by an equivalent volume of mineral aggregates. The particle size of used rubber aggregates is almost identical to sand particle size i.e. 4 mm. As far as the incorporation of fibers is concerned, two dosages of fibers were selected, i.e. 20 and 40 kg/m³.

The ring tests were conducted for evaluating the propensity for shrinkage cracking. Results demonstrated that by rubber aggregates substitution in mortar, on one hand shrinkage cracking is delayed and on the other hand multiple cracking with thinner crack opening was observed in rubberized mortars (30R0F) as shown in Figure I-2. It was also observed that for controlling shrinkage cracks, the mix substituted with 30% of rubber aggregates (30R0F) found to be more efficient than the mix reinforced with 40 kg/m³ of fibers (0R40F). In the case of fiber-reinforced mortar (0R40F), the cracks crossed the whole height of the specimen as evident from Figure I-2.

However, in case of specimens incorporating both rubber aggregates and metallic fibers (30R40F), multiple cracking with reduced crack length was observed. The opening of the crack is also limited in this type of mortar mix. So, this indicates the positive synergetic effect of the combine use of rubber aggregates and fibers.

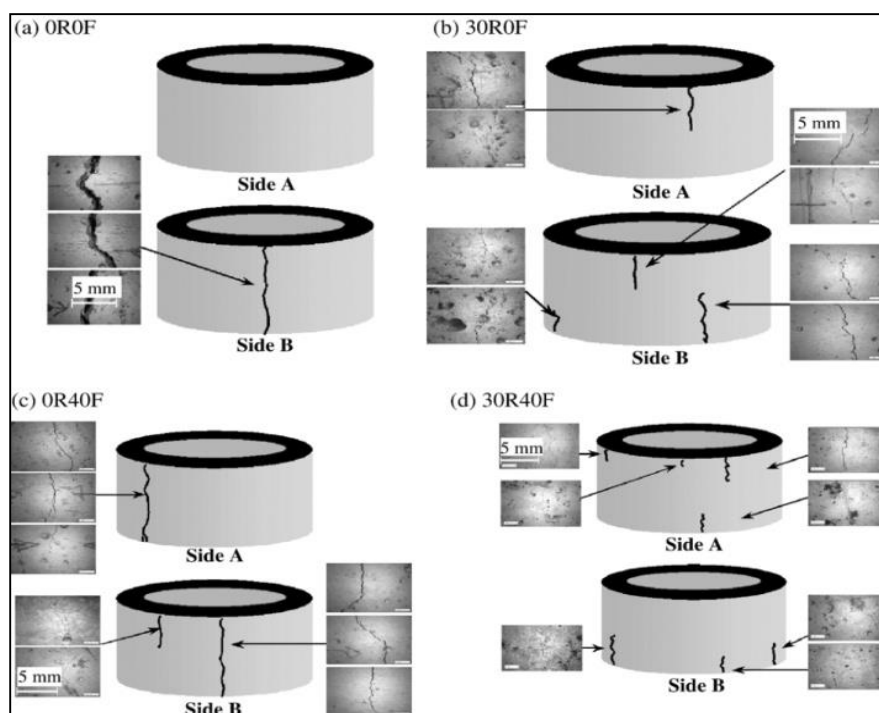


Figure I-2: Shrinkage cracking pattern after 55 days (A. Turatsinze et al., 2006)

I.2.2 Mechanical behaviour of mortars incorporating rubber aggregates and steel fibers

A. Turatsinze (A. Turatsinze et al., 2005) studied different mechanical properties of mortar incorporating rubber aggregates and compared the behavior of rubberized mortar with the conventional plain mortar and mortar reinforced with metallic fibers. Rubber aggregates were incorporated in mortar as a partial replacement of sand by an equivalent volume. Two percentage replacements of sand were used, i.e. 20% and 30%. The maximum particle size of rubber aggregates used is almost identical to sand particle size i.e. 4mm. For fiber-reinforced mortar, straight steel wire fibers of 13mm in length and 0.2mm in diameter were incorporated at two dosage rates, i.e. 20 kg/m³ and 40 kg/m³.

A significant reduction in compressive strength, tensile strengths and in modulus of elasticity was observed by the incorporation of rubber aggregates in mortar as compared to reference control mortar. For determining tensile strength, direct tension tests on the notched specimens were conducted. The curves presented in Figure I-3 show that the pseudo-strain corresponding to the peak load is significantly increased in rubberized mortar (30R0F). Also, the combine use of rubber aggregates and of fibers shows the positive synergetic effect by

enhancing the strain capacity along with the post cracking residual strength. So, this proves that the benefits of rubber aggregates and fiber-reinforcement can be drawn simultaneously.

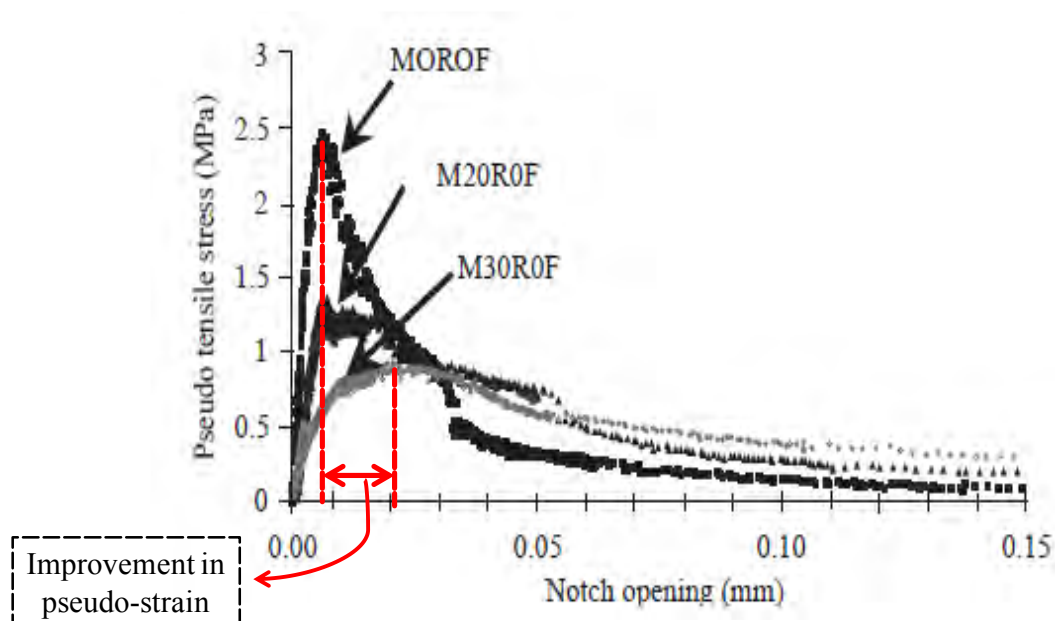


Figure I-3: Pseudo tensile Stress versus notch opening (A. Turatsinze et al., 2005)

A. Turatsinze (A. Turatsinze et al., 2006) investigated the strain capacity of fiber-reinforced and/or rubberized mortars by conducting four point bending test on prismatic specimens (85×50×420 mm). The behaviour of different mortar mixes under flexural loading is presented in Figure I-4.

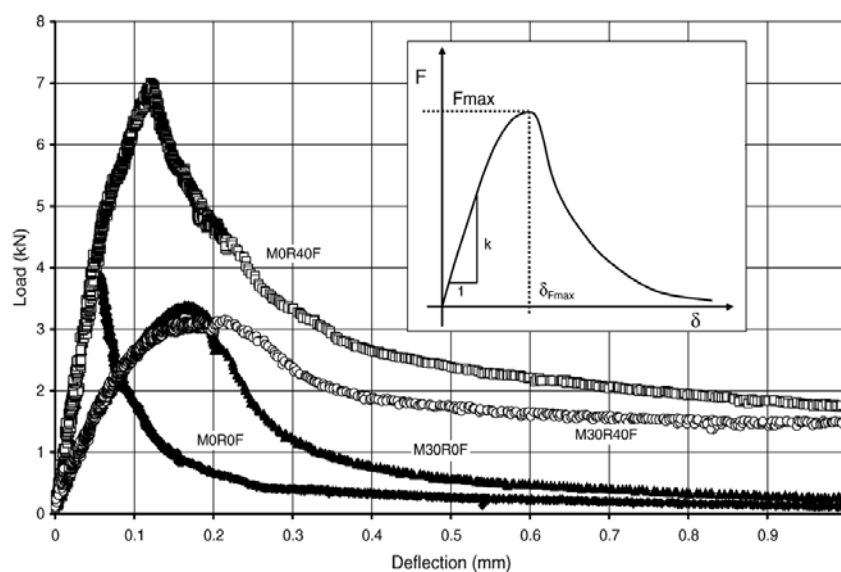


Figure I-4: Load vs. deflection in four-point of flexure tests, effects of rubber aggregates and fiber reinforcement incorporation (A. Turatsinze et al., 2006)

The bending tests show that the flexural load bearing capacity is significantly reduced in mortars incorporating rubber aggregates, even if it is reinforced with fibers. The positive effect obtained by the addition of rubber aggregates is the improvement in strain capacity, here defined as deflection corresponding to peak load which is also evident from Figure I-4. The results also demonstrate that the presence of rubber aggregates along with the fibers in mortar didn't change the role of fiber reinforcement.

T-H. Nguyen (T-H. Nguyen et al., 2010) studied the different mechanical properties of steel fiber reinforced and rubberized mortars. Amorphous metallic fibers (24 μm thick, 1.0 mm wide and 15 mm long) were used in cement-based mortar with a content of 20, 30 and 40 kg/m³. Along with the fibers, two percentages of rubber aggregates were used, i.e. 20% and 30% by volume as a partial replacement of mineral aggregates. Since, rubber aggregates have lower density (1.2) as compared to sand (2.7), so these rubber aggregates are highly sensitive to segregation. In order to improve segregation resistance, viscosity agent (Sika 300) was used. Along with the viscosity agent, super plasticizer was also used for ensuring the workability.

In accordance with the previous research (A. Turatsinze et al., 2005), significant reduction in compressive strength, tensile strength and modulus of elasticity was observed by incorporating rubber aggregates in mortar. Although, rubber aggregates incorporation in mortar reduces tensile strength, but fiber-reinforcement partly tends to counterbalance this negative effect. Also, the strain capacity before macro-crack localization is increased with the incorporation of rubber aggregates and this phenomena is further emphasized with the fiber-reinforcement.

Further, it can be concluded that the presence of rubber aggregates along with the fibers didn't change the traditional ability of metallic fibers to provide a residual post cracking strength as depicted from Figure I-5. Additionally, the use of rubber aggregates obtained by grinding of these shredded non-reusable tyres in cement-based material can be considered as a solution to maintain a clean environment by limiting the landfill for residual waste.

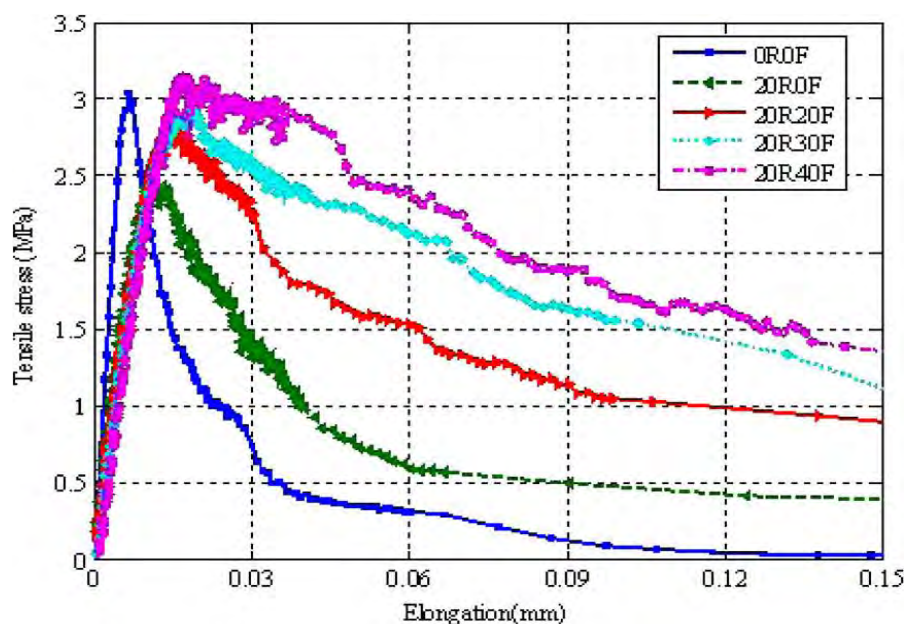


Figure I-5: Tensile stress vs. displacement: Influence of rubber aggregates and fiber reinforcement (T-H. Nguyen et al., 2010)

The above studies show the different benefits which one can attain by incorporating rubber aggregates and metallic fibers in a mortar. In the past, some studies have been conducted in order to evaluate the structural behaviour of overlays repaired with fiber-reinforced and rubberized material. So, out of those, some works related to the performance of thin bonded cement-based overlays incorporating rubber aggregates and steel fibers is presented below.

1.2.3 Effect of using fiber-reinforced and rubberized repair mortar on the durability of thin bonded cement-based overlays

A. Toumi (A. Toumi et al., 2013) carried out a study on debonding of thin rubberized and fiber-reinforced cement-based repairs under monotonic bending load. In this research, a simple analytical approach was used to predict the debonding initiation between substrate and overlay and comparison was made with the experimental and numerical model results. This study also illustrates, different benefits obtained by incorporating material with high straining capacity before cracking localization (thanks to rubber aggregates) and high post cracking residual strength (thanks to fiber-reinforcement) in thin bonded cement-based overlays.

For analytical modeling, they used conventional composite beam model firstly proposed by Suo and Hutchinson (Z. Suo and JW. Hutchinson., 1990) and then developed by Li and Thouless (S. Li et al., 2004). As reported in previous research (J-L. Granju., 2001), debonding

in thin bonded cement-based overlays is always initiated by tensile forces perpendicular to interface. Therefore, in this model they considered normal tensile stress only near to debonding tip.

For numerical modeling, special attention was paid on durability of composite structure (overlay and substrate). Normally, when load applied on this composite structure, crack initiates from the tension face of overlay and propagate towards the substrate. When this crack reached at interface two possibilities may occur:

- ✚ If interface bond strength between overlay and repair material is strong enough then crack will propagate towards substrate which depicts the monolithic behavior.
- ✚ In second possibility, if the interface bond strength is not so strong then it initiates debonding between repair material and substrate.

First situation depicts that bond between substrate and overlay is strong enough and provides sufficient resistance against debonding which was not targeted in this investigation. Their work was emphasized on a second scenario in which interface debonding occurs.

For experimental investigation, they conduct three point bending test on composite specimens. A composite specimen (overlay on top of the substrate) simulates that structure is repaired. In overlay material, metallic fibers along with the rubber aggregates were incorporated. Commercially available amorphous metallic fibers with a content of 40kg/m^3 were used along with the two percentage replacement of rubber aggregates i.e. 20% and 30% by volume of mineral aggregates. Plain cement mortar was used for casting of substrate. Before casting repair, these substrate bases were cured at 20°C and at RH of 100% for a period of 6 months. In order to monitor crack propagation and detecting interface debonding, video micro-scope with magnification 175x was used.

The load corresponding to debonding initiation, computed by using an analytical approach for different types of specimens was reported in Table I-1. Experimental results along with the numerical results obtained by using finite element modeling were also presented in the same table. In all cases, test results proved that fiber-reinforcement of repairs confer a post cracking residual strength which is a solution to delay the repair debonding.

Table I-1: Load (kN) necessary to initiate interface debonding: analytical results versus numerical and experimental ones (A. Toumi et al., 2013)

Specimen	Experimental results	Numerical results	Analytical results
OROF	4.53	4.90	4.58
OR40F	7.40	6.85	7.16
2OR40F	7.30	6.54	7.14
3OR40F	8.53	7.56	8.36

A. Toumi (A. Toumi et al., 2013) also concluded that the fiber-reinforcement of repair material appeared as a suitable solution for improving the durability of thin bonded cement-based overlays. These fibers restrain the growth of crack opening and delay the interface debonding. Further, the combine use of rubber aggregates and fibers in thin bonded overlays exhibits a positive synergetic effect by limiting the interface debonding propagation.

In the light of above results, it can be concluded that the use of fiber-reinforced and rubberized repair material is helpful to enhance the durability of thin bonded cement-based overlays. In the past, some researchers also tried to improve the durability of the repair system by utilizing high performance fiber-reinforced cementitious repair material. Some studies are presented below in which high performance fiber reinforced concrete was used as a repair material for rehabilitation purpose.

1.2.4 Effect of using high performance fiber-reinforced concrete on the durability of repair system

The early degradation of concrete does not only reduce the service life of the structure, but also increase the overhead maintenance charges. Due to this fact, a continuous effort is doing to develop new materials and technologies for repairing the damaged concrete structures. (E. Brühwiler and E. Denarié., 2008) utilized High Performance Fiber-Reinforced Concrete (HPFRC) as repair material for rehabilitation of concrete structures. They concluded that the rehabilitated structure shows significantly improved stability, serviceability and durability properties.

M. Skazlic (M. Skazlic et al., 2008) also studied the effect of utilizing high performance fiber-reinforced micro-concrete (HPFRMC) as a repair material on concrete beam. The performance of concrete beams repaired with HPFRMC was evaluated by conducting flexural

tests. The gross dimensions of the beam used were $150 \times 150 \times 600$ mm. Three different types of beams were cast having same gross dimensions, but different thickness of repair material as shown in Figure I-6 and comparison was made with the beams without any repair (R).

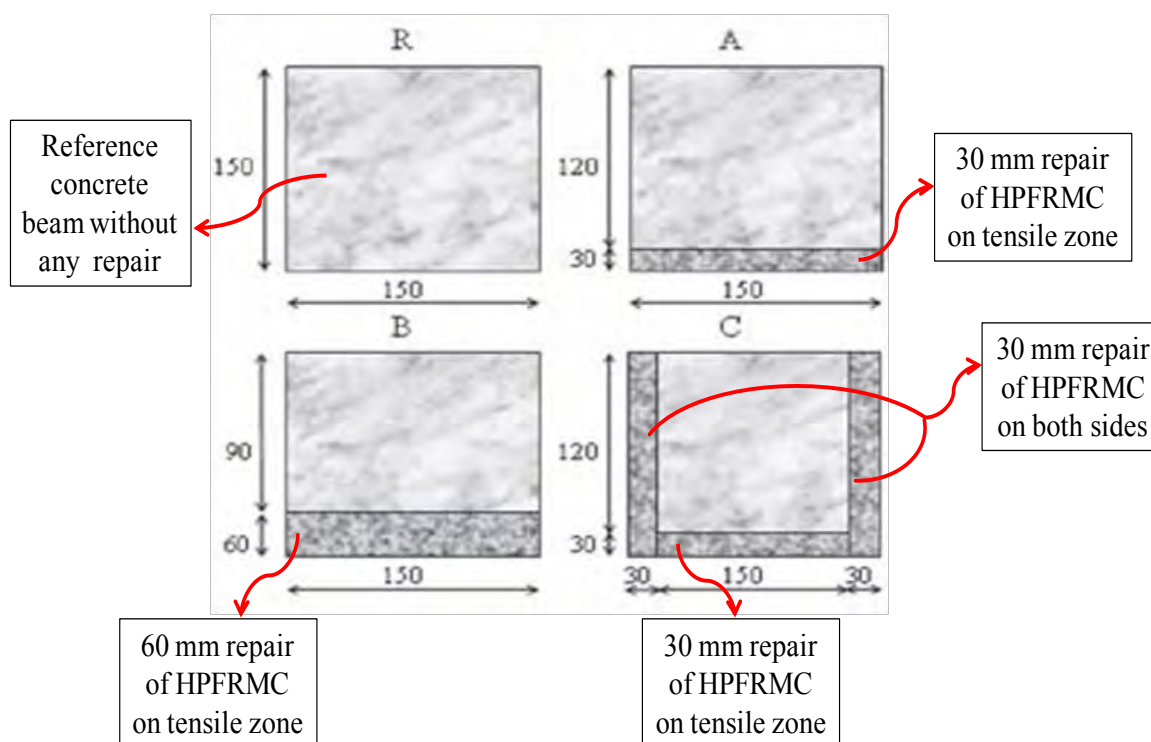


Figure I-6: Cross section of specimens (M. Skazlic et al., 2008)

An appreciable increase in flexure strength was observed in the concrete beams strengthened with HPFRMC repair as compared to concrete beam without any repair (R) as shown in Figure I-7. Among all types of beams, repaired beams B showed the best behavior under flexural loading. Since, concrete beams with 60 mm thick repair layer show the maximum flexural loading. And it can be concluded that this mode of reinforcing is the most optimum one.

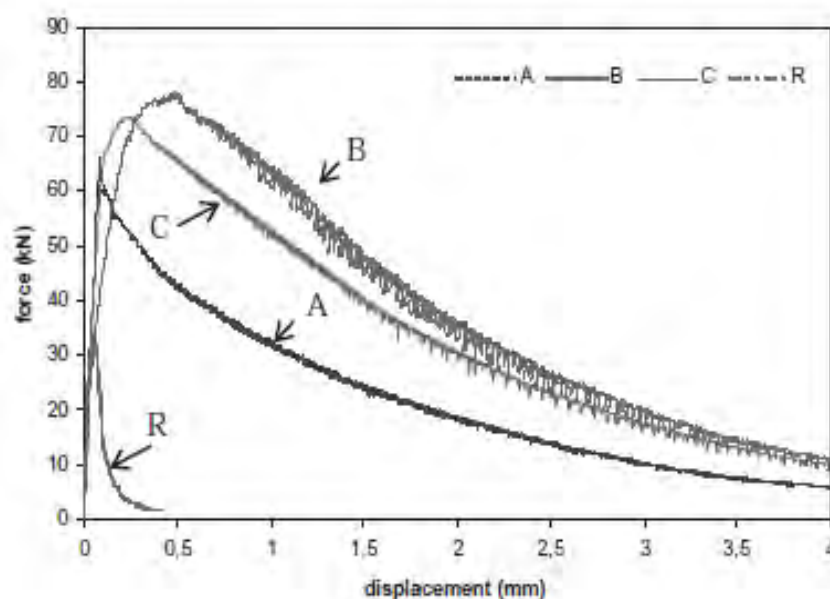


Figure I-7: Results of flexural loading test of concretes at 28 days (M. Skazlic et al., 2008)

Although, the incorporation of rubber aggregates and metallic fibers and can favorably modify the mechanical behavior of concrete in particular its strain capacity and residual post cracking strength. In this regard, a positive synergetic effect with material bridging is expected by using this composite as repair material. However, in actual cases, fatigue loading is more relevant for the repair system. Under these conditions, it is also necessary to understand the contribution of fiber-reinforced cement-based composites under fatigue loading. So, in this context, some studies related to the fatigue behaviour of fiber-reinforced concrete are presented below.

1.2.5 Behaviour of fiber-reinforced concrete under fatigue loading

Steel or fiber incorporation in concrete improves several of its properties like cracking resistance, ductility, wear resistance etc. It is well known fact that fiber-reinforcement is a suitable solution to control the cracking of concrete. For this reason fiber-reinforced concrete (FRC) is now being increasingly used in structures like highway overlays, pavements, bridge decks, machine foundations etc. However, most of these structures are subjected to cyclic loading. For example, the concrete overlays for highway or bridge decks are always subjected to cyclic loading because of traffic movement. Similarly, airport pavements are also expected to resist repeated loading during their service life. Therefore, it is necessary to investigate the

fatigue performance of FRCs and to study the effect of repeated cyclic loading on material characteristics (strength, durability, stiffness, toughness etc.)

Since, history of fatigue investigation in FRCs is not so long. Experimental fatigue performance of fiber reinforced concrete has been carried out in some previous researches (V. Ramakrishnan and G. Oberling., 1987; D.E. Otter and A.E. Naaman., 1988; M. Grzybowski and C. Meyer., 1993; J. Zhang and H. Stang., 1998). Mainly, empirical approaches have been conducted in order to predict and design the fatigue life of FRC structures. Processing of these types of empirical approaches requires certain data collection, which is time consuming and practically difficult to apply in real design cases. Keeping in view the above reason, a fatigue model was proposed by (V.C. Li and T. Matsumoto., 1998) which is equally capable of predicting fatigue life of FRC structure and designing FRC material for a given fatigue life.

In order to model the fatigue behaviour of FRC, it is necessary to understand the fatigue crack propagation mechanism in FRC. Generally for FRC material, fatigue loading causes microscopic changes, such as opening of crack at the interface between matrix, fiber and aggregate (A.M. Neville and J.J. Brooks., 1987). These microscopic changes, in turn produce some detrimental changes in macroscopic material properties. Particularly, the aggregate bridging force as well as the fiber bridging force decreases with the number of cycles, due to interfacial damage (J. Zhang and H. Stang., 1997) or by breaking of fibers due to surface abrasion (T. Matsumoto., 1998).

On the other hand, the fatigue life of normal concrete and FRC is also dependent upon fatigue crack growth. The fatigue crack growth process in FRC can be broadly divided in two parts. First is the crack initiation period and second is the development period. Some theoretical studies (B.N. Cox and L.R.F. Rose., 1994; A.G. Evans et al., 1995; J. Zhang and H. Stang., 1997; V.C. Li and T. Matsumoto., 1998) have revealed that rate of fatigue crack growth in different type of materials, which exhibit crack bridging, is highly dependent upon crack bridging law. More crack growth occurs if degradation of crack bridging happens with loading cycles. Normally, it can be assumed that this degradation in bridging strength is primarily due to interface bond degradation between fiber and matrix. Although, some other mechanisms can also happen, such as fatigue failure of fibers in tension/bending during opening of the crack. Similarly, fatigue loading also produces compression/bending in fibers during closing of the crack which subsequently produce buckling in non-metallic fibers (G. Bao and R.M. McMeeking., 1991; H.C. Wu et al., 1994)

J. Zhang (J. Zhang et al., 1999) used semi-analytical approach to model the fatigue behaviour of plain concrete and fiber reinforced concrete (FRC). This model relies on cyclic bridging law, the so-called stress-crack width relationship which is capable to simulate the development of fatigue damage. Three point bending fatigue tests were conducted on simple concrete beams and beams incorporated with smooth and hooked shaped steel fibers. Tests were carried out on the concrete beams having dimension $420 \times 100 \times 100$ mm and unsupported length 400mm. These fatigue tests were conducted at a constant frequency of 4.5Hz.

Monotonic three point bending tests were also conducted for making comparison between monotonic and fatigue behaviour of different types of concrete. Figure I-8 show the monotonic bending behaviour of plain concrete (PC) and two types of steel fiber reinforced concrete, i.e. straight shaped fiber reinforced concrete (SSFRC) and hooked shaped fiber reinforced concrete (HSFRC). Following important features can be highlighted from the load-CMOD curves for these three different types of concretes,

- ✚ In first branch, curves for all types of concrete beams show that the flexural strength is linearly proportional to the deformation (CMOD) until material stress of 5.0 MPa. In this branch, material behaviour is elastic and no crack produce.
- ✚ In second branch, flexural stress increases up to 7.0 MPa for plain concrete and 9.0 MPa for HSFRC and SSFRC. The deformation does not remain proportional to the stress in this branch. A crack was already developed and keeps on growing with the increase in load.
- ✚ In third branch, the increase in deformation is much more and also not proportional to flexural stress. In this branch, flexural stress of all types of concretes reached up to its maximum values, i.e. approximately 10.0 MPa for two FRCs. Also, in this branch the difference becomes significant in load-deformation behavior of HSFRC and SSFRC. Another noticeable thing is that hooked shaped fibers improve the material toughness more effectively as compared to straight fibers.

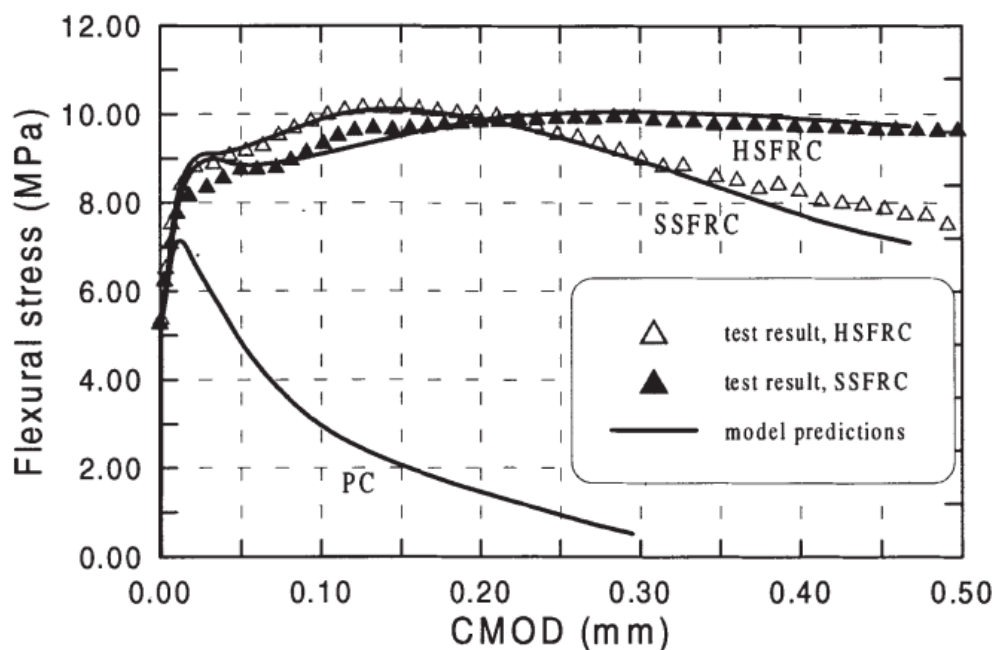


Figure I-8: Simulated flexure stress versus CMOD curves for plain concrete, SSFRC and HSFRC beams under three-point bending, shown together with experimental data (J. Zhang et al., 1999)

For evaluating the fatigue performance, these different types of concrete beams were subjected to flexural fatigue loading. Figure I-9 shows the typical S-N curves, the relationship between maximum flexural stress degradation with the number of cycles. In these curves, both experimental and theoretical are presented. Results show that model prediction is in good agreement with experimental results.

The S-N curve for plain concrete is almost linear, which is in agreement with some previous researches (JO. Holmen., 1979; J. Kim and Y. Kim., 1996; J. Zhang and H. Stang., 1998). For fiber reinforced concrete, the S-N curve is of curved shape. The present results show that fiber-reinforcement of concrete can significantly improve its fatigue performance, which is in agreement with some previous researches (V. Ramakrishan et al., 1987; D.E. Otter and A.E. Naaman., 1988; CD. Johnston and RW. Zemp., 1991; M. Grzybowski and C. Meyer., 1993; H. Stang and J. Zhang., 1994). These curves also show that reduction in material toughness is more pronounced in HSFRC as compared to SSFRC, under fatigue loading.

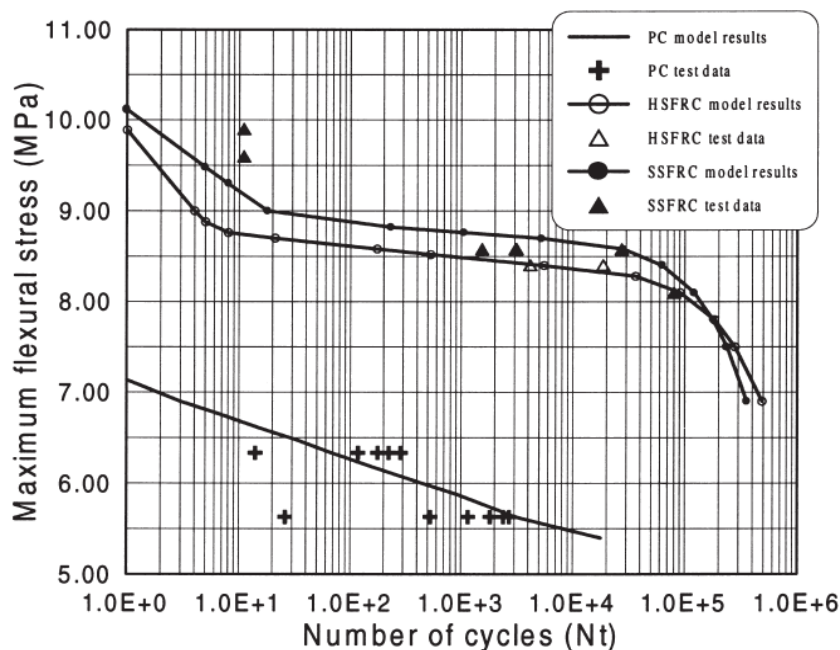


Figure I-9: Relationship of maximum flexure stress with fatigue life (J. Zhang et al., 1999)

The fatigue life of FRC, with maximum flexural stress between 9.0 to 10.0 MPa (third branch) is very small i.e. between 1 to 30 cycles. Since in this branch, the initial crack length and crack opening is more and significant bridging degradation occurred due to large crack opening. But in the second branch, fatigue life is considerably more and less reduction in residual flexure stress was observed. This longer fatigue life is due to shorter initial crack length and smaller crack opening. A good correlation was found between experimental and model predicted results. The basic analysis of results leads us to conclude that the fatigue performance of FRC is strongly dependent on cyclic stress-crack width relationship.

J. Zhang (J. Zhang et al., 2000) carried out the experimental study for investigating the crack bridging in steel fiber reinforced concrete (SFRC) under tensile fatigue loading. The uniaxial fatigue tension tests were conducted on the prismatic pre-notched specimens. These tests were controlled by deformation with a constant maximum and minimum amplitude of crack opening. Two types of steel fibers were used, i.e. straight shaped and hooked shaped for investigating the fatigue performance of SFRC.

Total six series of fatigue tension tests with different maximum crack width values were conducted on both types of SFRCs. The selected maximum crack width values were 0.05, 0.10, 0.20, 0.30, 0.40, and 0.50 mm. Figure I-10 shows typical bridging strength versus crack width curve for the SSFRC specimen under tensile fatigue loading controlled by crack

opening. This curve shows that the bridging strength corresponding to the maximum crack width decreases gradually with number of loading cycles.

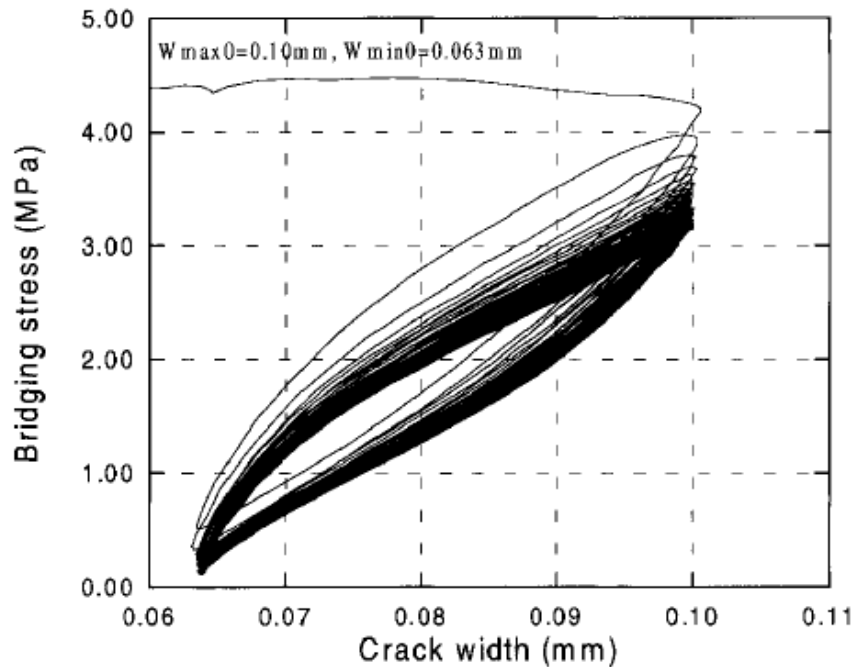
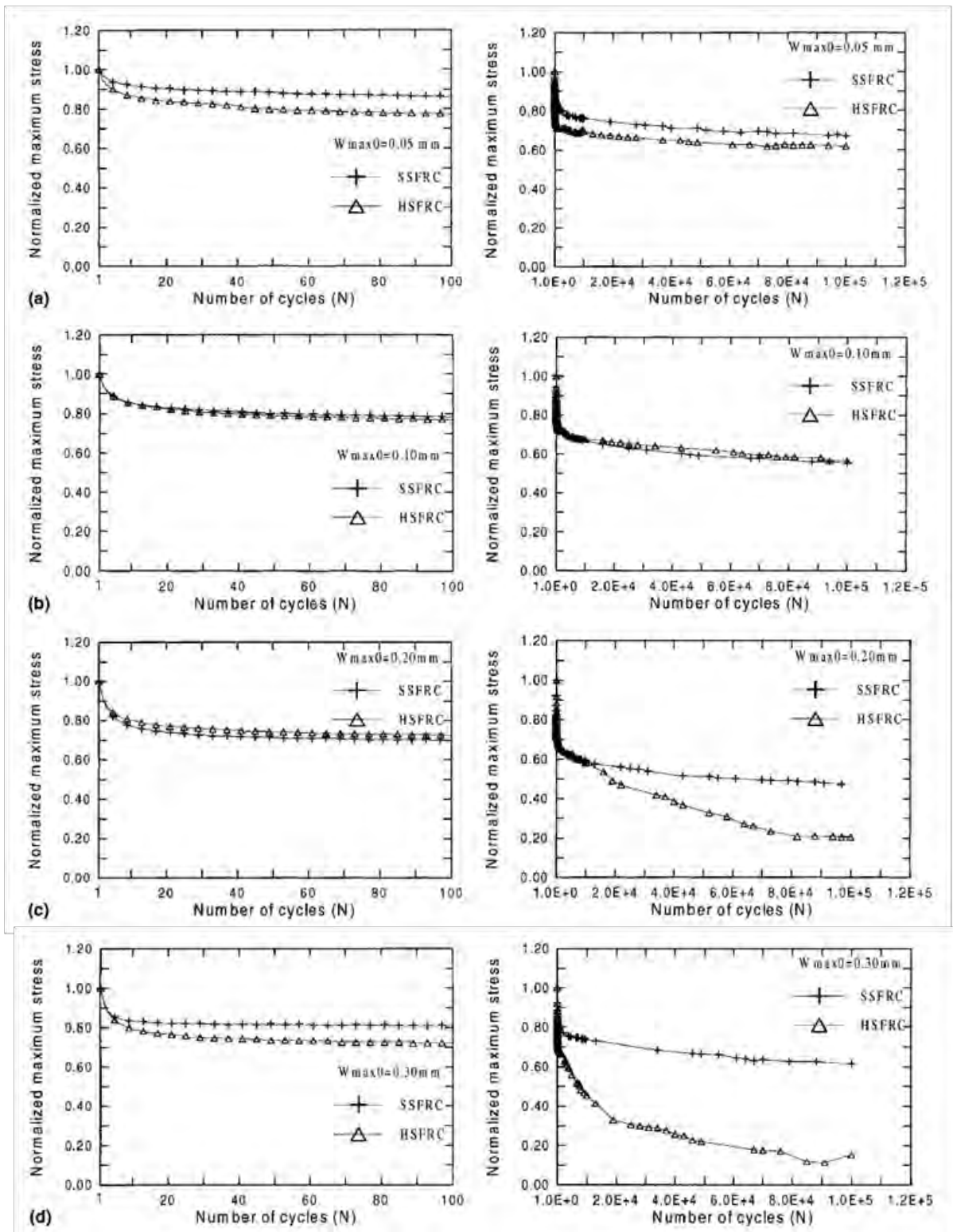


Figure I-10: Typical stress-crack width curve of fatigue tension test (J. Zhang et al., 2000)

The tensile fatigue test results of SSFRC and HSFRC are shown in Figure I-11. In Figure I-11(a-f), normalized bridging strength degradation curves at maximum crack width versus loading cycles are presented for different maximum crack widths (W_{max0}). Left side of figure represents the results for initial $1-10^2$ loading cycles, while on the right side of figure; results in the range of $1-10^5$ loading cycles are presented. In these curves, maximum bridging strength was normalized with reference to bridging strength at first cycle.



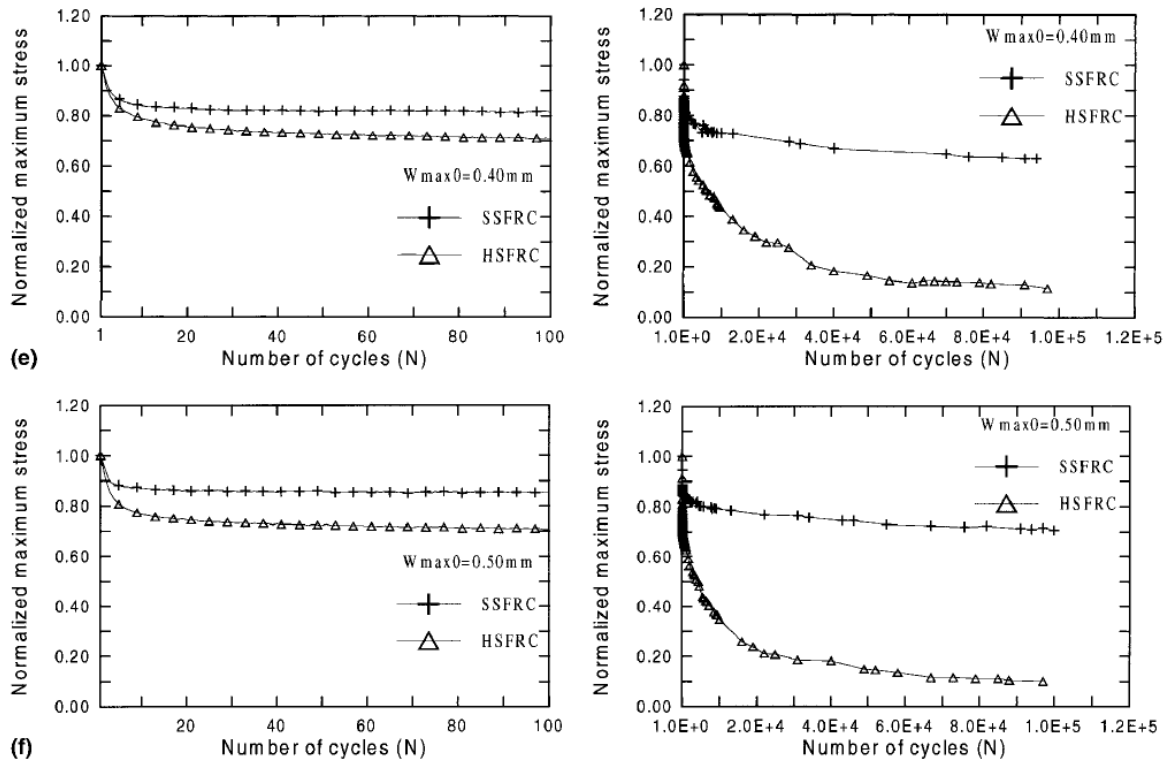


Figure I-11: Relationship between normalized maximum bridging strength and number of fatigue cycles (J. Zhang et al., 2000)

From results, it is evident that maximum bridging strength decreases with the number of fatigue cycles for both types of SFRCs. In case of SSFRC, rapid degradation of bridging strength was observed during the initial 10-15 cycles followed by a stable decreasing stage with almost constant degradation. For initial 10 fatigue loading cycles, the reduction in bridging strength increases with the increase of maximum crack width value. This indicates that the rate of bridging strength degradation is also affected by maximum crack width values as shown in Figure I-12.

Results presented in Figure I-12 show that maximum bridging strength degradation in SSFRC occurred upto maximum crack width value between 0.1 to 0.2 mm. But after this maximum crack width value behaviour becomes opposite. This strange behaviour is because of the pull-out mechanism of straight fiber. Since maximum reversible deformation (reversible slippage) occurs upto this maximum crack width (0.1mm to 0.2 mm) and after that it starts decreasing as a result of fiber pull-out. So, this behaviour is in accordance with the pullout mechanism theory of straight fiber. After 10^5 cycles, maximum reduction in crack bridging strength can be more than 50% of its original value for SSFRC.

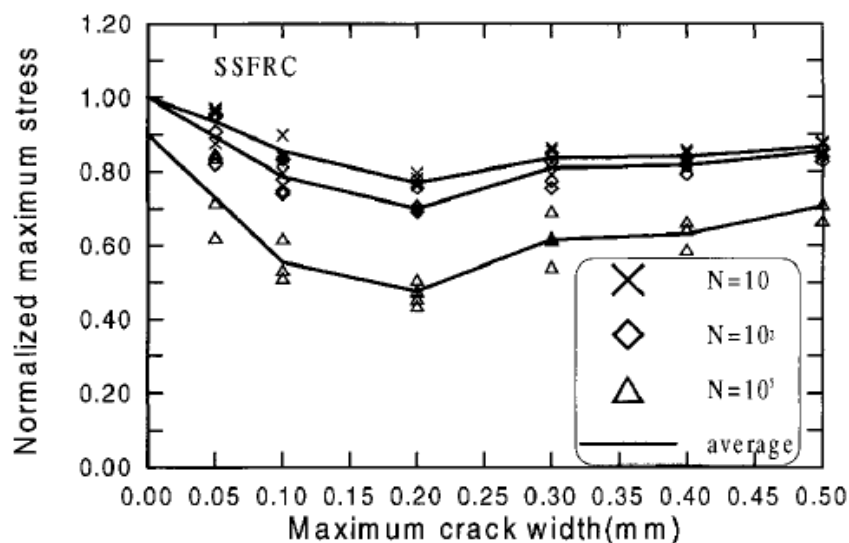


Figure I-12: Relations of normalized maximum bridging strength and maximum pre-cracked width for SSFRC, showing results after 10, 10^2 , and 10^5 cycles, respectively (J. Zhang et al., 2000)

The bridging strength degradation behaviour in HSFRC is different and always much higher than SSFRC. The difference in crack bridging degradation is almost negligible in both types of fibers upto maximum crack width value of 0.1mm. However, bridging strength degradation is more pronounced in HSFRC as compared to SSFRC when maximum crack width value is more than 0.1mm as evident in Figure I-11(c-f). This means, the reduction in material toughness is more significant in HSFRC as compared SSFRC under cyclic loading. In case HSFRC, maximum crack bridging degradation can be more than 80% of its original value, after 10^5 cycles. In addition to fatigue loading cycles, rate of bridging strength degradation is also dependent upon the maximum crack width as shown in Figure I-13.

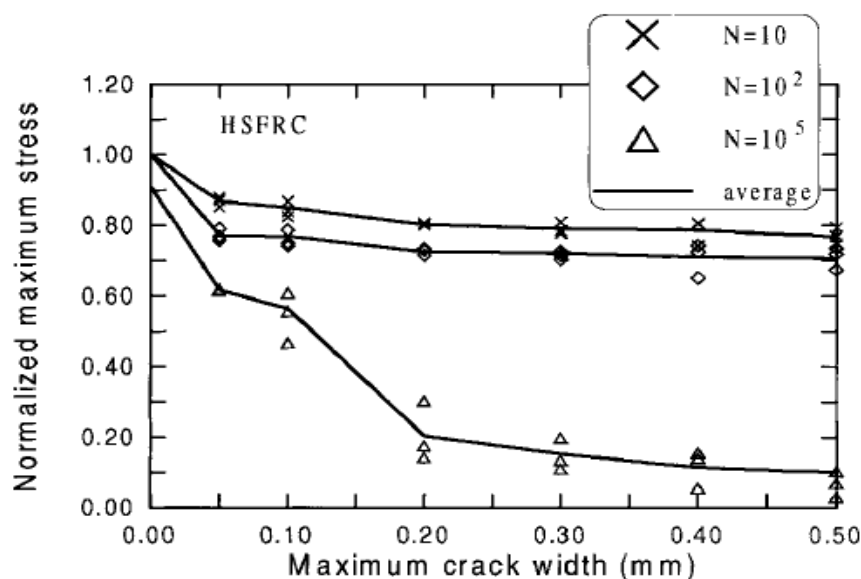


Figure I-13: Relations of normalized maximum bridging strength and maximum pre-cracked value of HSFRC, showing results after 10, 10^2 , and 10^5 cycles, respectively (J. Zhang et al., 2000)

A. Toumi (A. Toumi et al., 2015) carried out finite element modeling for predicting the debonding propagation of fiber reinforced and rubberized cement-based overlays under fatigue loading. The obtained model results were compared with the experimental results. Three point bending fatigue tests were conducted for experimentally determining the interface debonding propagation. A comparison shows a good agreement between experimental and modeling results.

Results show that the interface debonding in composite beams repaired with fiber reinforced mortar is almost half as compared to beams repaired with plain mortar. Also, restrained shrinkage between overlay material and substrate play a vital role to initiate debonding at the interface. It was noticed that use of material with high tensile strain capacity (rubberized mortar) as a repair material found helpful to delay the interface delamination. Minimum interface debonding propagation with number of fatigue cycles was observed in the composite beams repaired with fiber-rubberized mortar. This shows that the synergetic effect provided by the combine use of rubber aggregates and fibers remains valid under fatigue loading also.

In the light of above researches, it can be concluded that the durability of repair system is highly dependent on the mechanical characteristics of the repair material. Another important parameter that plays a vital role in order to develop a good bond between the old substrate and

new repair layer is the substrate surface roughness. Different surface preparation techniques are usually used to improve the substrate surface roughness. Several studies have been conducted in the past to evaluate the impact of substrate surface roughness on the bond behaviour of repair system. Out of those, some are presented below.

1.2.6 Impact of substrate surface preparation on bond behaviour between repair and substrate

For large concrete areas, thin bonded repairs are a suitable rehabilitation technique. The durability of these repairs is always a problem and one of its main reasons is debonding at interface with the substrate. The durability of repair system is directly dependent upon the adhesion quality, means the condition of bond between repair and substrate (J. Silfwerbrand and J. Paulsson., 1998). The quality of the bond depends upon various phenomena that take place at interfacial zone like: presence of bond-detrimental layers, saturation condition of substrate as compared to repair material and concrete surface geometry (L. Czarnecki and B. Chmielewska., 2005). In general the major objective of substrate surface preparation is to make it sound, cohesive, dust and oil free.

For surface preparation, the commonly used techniques are water blasting, sandblasting, shotblasting, etc. Each technique gives different level of roughness. Roughness is generally measured by a parameter called mechanical interlocking. This mechanical interlocking depends upon the waving condition of surface (L. Czarnecki et al., 2003). The waviness of the surface can be seen from the profile registered through mechanical profilometer presented in Figure I-14.

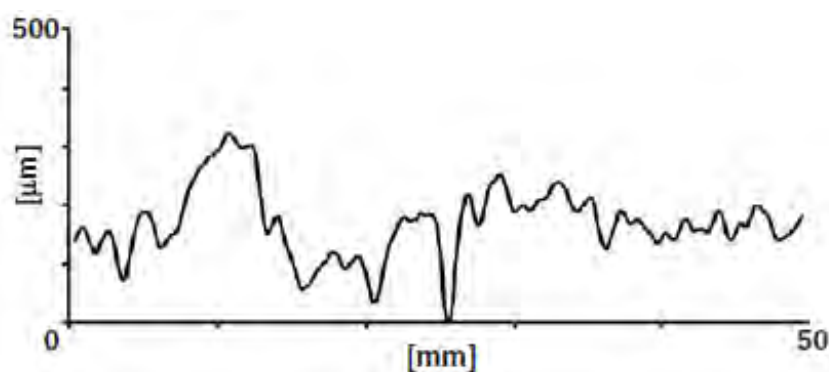


Figure I-14: Surface profile registered with mechanical profilometer (A. Garbacz et al., 2006)

Previous research shows that creation and durability of bond depends on several factors and each factor has its own degree of influence (J. Silfwerbrand and H. Beushausen., 2006) and can be divided into three main groups (J. Silfwerbrand., 1990) as shown in Figure I-15. From all of these factors, Silfwerbrand pointed out the following five major factors that have a great impact on bond tensile strength

- ✚ Micro-cracks on substrate surface
- ✚ Presence of laitance layer
- ✚ Cleanliness before placement of overlay
- ✚ Compaction
- ✚ Curing procedures

The first three parameters are directly related to the substrate characteristics and can be modified by substrate surface treatment. The substrate surface treatment is commonly done in order to improve surface roughness by removing the top weak laitance layer.

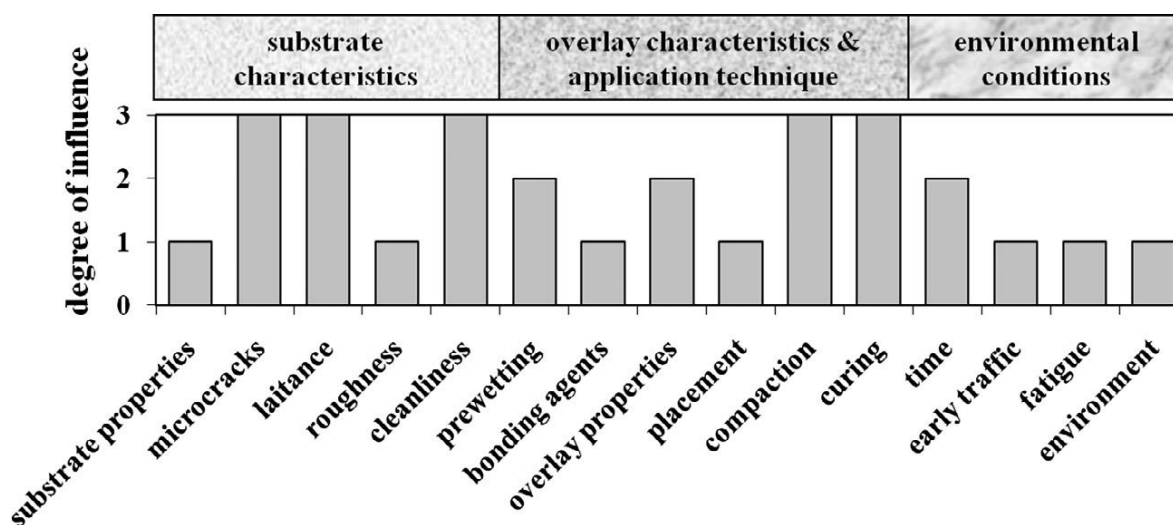


Figure I-15: Factors affecting bond between concrete substrate and repair material (J. Silfwerbrand., 1990)

A. Garbacz (A. Garbacz et al., 2006) performed characterization of concrete surface roughness and determine its relation to adhesion in repair system. In order to describe the surface roughness they developed different parameters and discussed the relationship between bond strength and these surface geometry parameters. For this purpose, concrete substrates of

dimensions (300×300×50 mm³) were used. Following four treatments were selected for the preparation of concrete substrates:

- ✚ Grinding method (GR)
- ✚ Sandblasting method (SB)
- ✚ Shotblasting method for time period of 35 sec and 45 sec (SHB)
- ✚ Hand and mechanical milling method (HMIL & MMIL)

For qualitative evaluation of concrete surface roughness, Scanning Electron Microscope (SEM) technique was used at various magnifications (20-500×), particularly for detecting possible cracks produced as a result of mechanical treatment on the substrate surface. In order to characterize the concrete surface geometry they used the following four different methods:

- ✚ Sand (macroscopic) method
- ✚ Microscopic method
- ✚ Mechanical profilometry
- ✚ Laser profilometry

First comparison was made on the basis of SEM observations. Figure I-16 shows SEM observations of concrete surfaces obtained from different techniques. Figure I-16(a) indicates that surface obtained from grinding technique show less but uniform roughness and without any sharp edges. Also at higher magnification, some narrow cracks are observed on the surface. The surface obtained by sandblasting technique is quite similar to the grinded surface as shown in Figure I-16(b). Sandblasted surface shows shallow irregularities with peak to valley height not exceeding 1mm. At higher magnification, some micro-cracks and sharp edges of aggregate grains are visible. The highest surface roughness was obtained after shotblasting for 45sec with peak to valley height upto 7mm as evident from Figure I-16(c). In shotblasting technique, an increase in treatment time shows the formation of dense cracking and surface deterioration due to chipping of aggregate particle. The surfaces obtained by hand and mechanical milling are similar to shotblasted surface as shown in Figure I-16(d) with alot of irregularities on the surface. It shows deep and wide cracking at higher magnification. Also at some places the removal of grains and loose concrete fragments were observed.

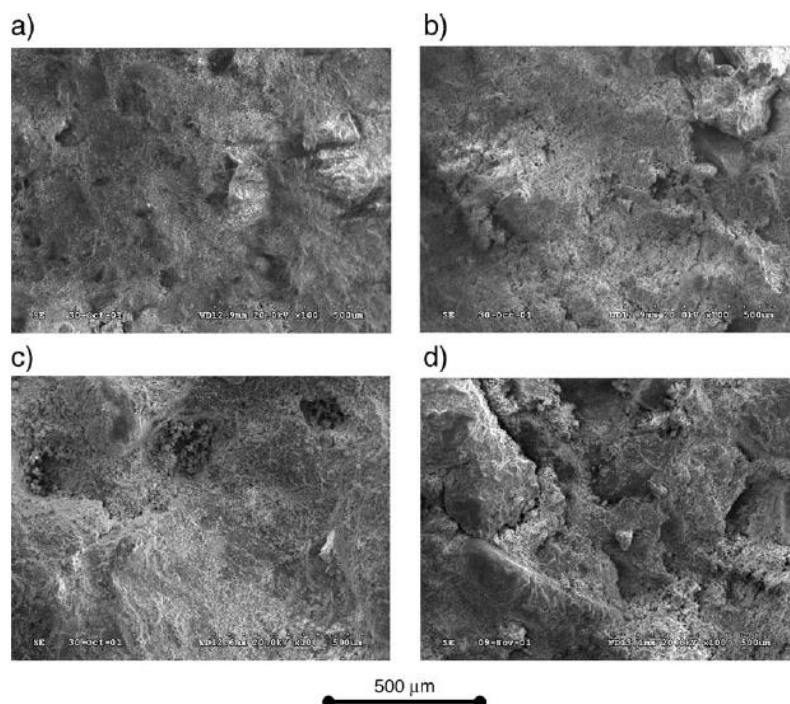


Figure I-16: Examples of concrete surface views after: (a) grinding; (b) sandblasting; (c) shotblasting; and (d) mechanical milling [magnification: 100×-SEM/SE] (A. Garbacz et al., 2006)

The second comparison was made on the basis of surface geometry characterization. The laser profilometry technique produces more detailed image of surface profile as compared to mechanical profilometry approach. The geometrical parameters determined at the microscopic or macroscopic level indicate that highest roughness was obtained after shotblasting treatment for 45 sec and lowest by grinding treatment.

The third comparison was made on the basis of pull-off strength between repair and substrate. Since, the roughness and presence of cracks on the substrate surface (normally generated during substrate surface preparation) have a direct influence on bond strength in repair system as shown in Table I-2. Test results indicate that without the use of bond coat in overlays a huge variation of pull-off strength was observed. Minimum pull-off strength was obtained for concrete surface prepared by mechanical milling and maximum for sandblasted surface. But pull-off strength in overlays prepared with bond coat was almost identical, varied between 1.4-2.0MPa. It means that application of bond coat significantly reduced the variation in pull-off strength. Results also show that the presence of this bond coat significantly improves the pull-off strength in the highly roughed surfaces like shotblasted surface. On the other hand, the effect of bond coat is significantly less on surfaces like sandblasted surface.

Moreover, the surface roughness and the use of bond coat have direct impact on failure type during pull-off test. In case of overlays with a bond coat, normally failure was observed in the concrete substrates while in the overlays without a bond coat, interfacial failure was dominant.

Table I-2: Results of pull-off strength tests (A. Garbacz et al., 2006)

Treatment type	Mean value (MPa)	Coefficient of variation (%)	Failure type (%)
<i>Overlays without bond coat</i>			
GR	1.16	50.9	21C+79C/R
SB	1.82	32.4	42C+58C/R
SHB35	1.25	28.8	46C+54C/R
SHB45	0.83	25.3	50C+50C/R
HMIL	1.01	40.6	29C+71C/R
MMIL	0.49	57.1	31C+69C/R
<i>Overlays with bond coat</i>			
GR	1.82	15.9	100 C
SB	1.93	11.4	100 C
SHB35	1.94	11.3	100 C
SHB45	1.96	32.7	100 C
HMIL	1.42	12.7	100 C
MMIL	1.60	24.4	100 C

C= cohesive failure in concrete substrate; C/R=interfacial failure between overlay and concrete.

L. Courard (L. Courard et al., 2014) studied different properties near to the concrete substrate surface which affect the bond strength in repair system. The primary objectives of this research were the characterization of the surface roughness of substrates prepared through different techniques, the description of micro-cracks near-to-surface layer and the assessment of pull-off bond strength between repair and base.

For this research program, they conducted tests on several repair systems having different qualities of concrete substrates. The research program was divided in two groups. The first group performed research at the University of Liege (Group A). They used four different types of surface treatment techniques in order to obtain different profiles, surface roughness and level of micro-cracking near-to-surface layer. Following, four different types of surfaces were used: polished smooth surface (PL) as a reference surface, dry sandblasted surface (SB-D), jack hammered surface (JH) and high pressure water jetted surface called “hydrodemolition” (HD) with pressure (250 MPa). In Jack hammering technique, a hammer

with a special head was used for surface roughening, it is also called as "scrabbling" in ACI repair manual (ACI 546R-04., 2013).

The second group performed research at the Warsaw University of Technology (Group B). They used concrete substrate having different compressive strengths as compared to the first group. They choose less aggressive surface treatment techniques in order to attain low-level micro-cracking. Following surface preparation techniques were used: brushing (BR) with a metallic brush, wet sandblasting (SB-W), scarification (SC) and water jetting with a low pressure of 12 MPa (LC).

Several approaches are available to quantify the surface roughness (PMD. Santos et al., 2007; A. Garbacz et al., 2006; L. Courard., 2005). But European standard (EN 1504., 2003) recommends visual observation, either by using profilometry method or by the volumetric sand patch method. In profilometry method, a surface profile can be obtained by means of profilometers (laser/mechanical) or by digitalization of cross-section images (PMD. Santos et al., 2007; A. Garbacz et al., 2006). While, in the case of sand patch technique, a constant volume of specific sand is poured on top of concrete surface and spread it in circular format and measures the average diameter of this circle as shown in Figure I-17. Surface Rough Index (SRI) can be computed by using the following equation:

$$SRI = V/d^2 \cdot 1272 \text{ (mm)}$$

Where d is the average diameter of sand patch in (mm), V is the volume of sand used in (ml).



Figure I-17: Sand test for surface roughness evaluation (L. Courard et al., 2014)

In this research, the substrate surface roughness was measured by using sand patch method and the results obtained by both groups are presented in Table I-3. Smaller value of SRI indicates that the concrete surface is smooth.

Table I-3: Results of Surface Roughness Index (SRI), surface tensile strength and pull-off bond strength vs. surface treatment technique (L. Courard et al., 2014)

Sample	SRI (mm)	Surface tensile strength (f_{ts})		Self defined failure modes			Pull-off bond strength (f_b)		Failure modes		
		Mean (MPa)	COV (%)	A1 (%)	A2 (%)	A3 (%)	Mean (MPa)	COV (%)	A (%)	A/B (%)	B (%)
<i>Group A</i>											
C30-PL	0.25	4.29	8.5	0	0	100	1.91	29.7	0	100	0
C40-PL	0.20	4.07	15.0	0	40	60	2.04	24.7	0	100	0
C45-PL	0.14	3.71	7.8	0	0	100	0.86	29.0	0	100	0
C30-SB-D	0.29	3.70	7.1	0	0	100	2.04	5.3	0	80	20
C40-SB-D	0.28	3.93	19.4	0	0	100	2.19	15.5	0	100	0
C45-SB-D	0.31	3.76	15.0	0	0	100	2.16	25.2	20	40	40
C30-JH	0.89	3.39	20.0	60	0	40	1.02	48.9	0	0	100
C40-JH	0.89	3.51	17.2	60	0	40	1.42	22.7	0	0	100
C45-JH	0.80	3.58	10.8	100	0	0	1.66	13.1	0	0	100
C30-HD	2.22	3.53	11.1	40	0	60	2.51	16.7	0	20	80
C40-HD	5.00	3.54	10.6	20	20	60	2.54	30.4	40	20	40
C45-HD	3.20	3.59	14.0	20	0	80	2.30	22.3	0	100	0
<i>GROUP B</i>											
C25-LC	0.37	3.02	18.1	33	0	67	2.20	9.3	25	25	50
C35-LC	0.39	3.99	2.1	0	33	67	1.42	40.4	0	100	0
C50-LC	0.16	4.98	9.1	0	0	100	0.00	-	0	100*	0
C25-BR	0.39	3.10	12.1	67	0	33	1.60	25.3	0	100	0
C35-BR	0.39	3.37	3.6	17	50	33	0.13	-	0	100	0
C50-BR	0.41	4.71	3.5	28	28	44	0.00	-	0	100*	0
C25-SB-W	0.50	3.15	21.3	50	17	33	2.46	43.1	25	0	75
C35-SB-W	0.61	2.66	7.7	66	17	17	2.08	25.9	0	50	50
C50-SB-W	0.41	4.48	7.2	100	0	0	0.14	-	0	100	0
C25-SC	0.66	2.95	16.2	100	0	0	1.55	41.5	0	0	100
C35-SC	0.88	3.39	11.2	83	0	17	1.81	29.0	50	0	50
C50-SC	0.50	4.09	6.5	67	17	17	0.56	26.6	0	100	0

* Total delamination.

In order to evaluate the substrate quality, a surface tensile strength is determined by conducting pull-off test according to the European standard (EN 1542., 1999). Along with pull-off strength measurement, the failure modes were also registered (B1 - superficial, B2 - middle, B3 - deep) as presented in Figure I-18. Results presented in Table I-3 indicate that concrete samples of Group A show no influence on surface tensile strength after surface treatment. Moreover, for surfaces treated by scarification and jack hammering, mostly failure appeared in the superficial zone (type B1) as shown in Figure I-18. Similar kind of observation was also reported by some previous researchers (B. Bissonnette et al., 2006; E. Bonaldo et al., 2005) who also used jack hammering technique for substrate surface preparation. The simple reason for this superficial failure is micro-cracking, which are generally induced on the substrate surface as a result of surface treatments like jack hammering.



Figure I-18: Failure modes on pull-off test scheme for surface tensile strength evaluation and examples of type B1 [superficial], B2 [middle] and B3 [deep] self defined failure modes (L. Courard et al., 2014)

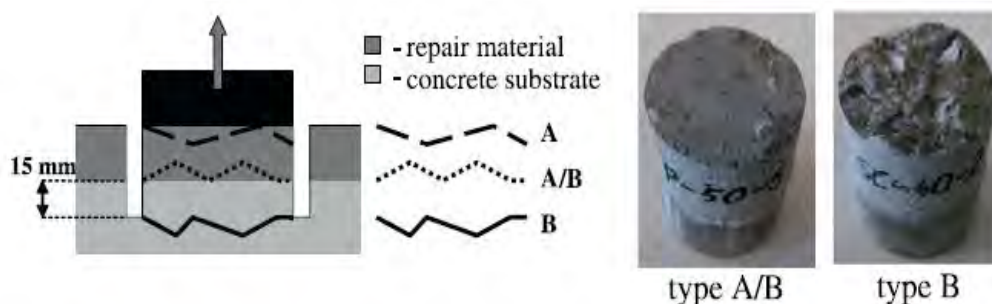


Figure I-19: Failure modes on pull-off test scheme for bond strength evaluation and examples of type A/B and B failure modes (L. Courard et al., 2014)

Pull-off tests were conducted for evaluating the bond strength between repair and substrate. Pull-off bond strengths and failure modes are also presented in the above Table I-3. During pull-off test, failure can occur at different locations as shown in Figure I-19, where A represents the failure in repair material, B represents concrete substrate failure and A/B is the failure at the interface between repair and substrate. In order to show the effect of substrate surface preparation on bond strength and failure modes, results of Group A and Group B can be summarized as follows.

- ✚ Improvement in bond strength was observed for substrates prepared by sandblasting and hydrodemolition technique.
- ✚ Bond strengths of surface treated by jack hammering technique are quite similar to bond strength of polished surface (reference surface); rather some reduction in bond

strength was observed. This decrease in bond strength is due to the development of micro-cracks on the surface of substrate while performing jack hammering.

- ✚ For polished surface (reference surface), all failures occurred at interface location (type A/B), probably due to insufficient mechanical interlocking between repair layer and substrate and lower effective surface of contact.
- ✚ A total delamination was observed in case of substrate surfaces prepared by water jetting and brushing method.
- ✚ Generally, it is desirable that failure should not occur at interface location (type A/B), which shows that the bond between repair material and substrate is not strong enough. But for Group B, almost all failures occurred at interface location (type A/B) except in substrates treated with aggressive treatments like scarification (SC). This shows that insufficient bond was achieved between repair material and substrate through surface preparation techniques used in Group B.

Finally, it can be concluded that the selection of surface preparation technique depends upon the quality of concrete substrate. The substrates with higher strengths require more aggressive treatment and the substrate surfaces with lesser strengths require less aggressive surface preparation technique. However, the surface treatment can produce micro-cracking if it is not well operated with regard to the quality and the strength of concrete (A. Garbacz et al., 2006; L. Courard et al., 2006; PMD. Santos et al., 2007).

1.2.7 Detection and measurement of cracking by using Digital Image Correlation technique

Digital image correlation (DIC) is an optical and non-contact measurement technique which is used to measure displacements on the surface of an object of interest. This displacement is then used to calculate the surface strain of the object. This technique was used in the past for studying cracking in concrete members. It provides a freedom to monitor cracking under wide range of loading conditions. DIC technique is very much helpful to detect early cracking and also provide us an opportunity to mark and measure the cracks under fatigue loading. Also, there is no need to pause the test for crack measurement.

M. Mahal (M. Mahal et al., 2015) used this DIC technique for evaluating the fatigue behavior of externally strengthened reinforced concrete beams. Displacement fields obtained from images recorded after specific load cycles were analyzed. This analysis provides information about crack width, beam deflection and major principal strain to detect crack initiation. Obtained DIC results were compared with the results gathered by using conventional sensors. Comparison revealed that the DIC technique provides more detailed and accurate information as compared to conventional techniques.

From the last decade, the use of this non-contact optical technique is also increasing for asphalt materials. E. Romeo (E. Romeo., 2013) used 2D DIC technique for investigating fracture phenomena and characterization of asphalt mixtures. In the past, Hartman and Gilchrist (AM. Hartman and MD. Gilchrist., 2004) used this DIC technique for measuring the length of cracks developed while conducting four point bending fatigue tests on asphalt specimens.

W.G. Buttlar (W.G. Buttlar et al. 2014) used this DIC technique to investigate the strain fields and cracking phenomena in asphalt materials. They concluded that this image processing technique appeared as a suitable solution to monitor fracture phenomena and debonding in asphalt mixtures. One can measure displacements/strains precisely without using traditional LVDTs and strain gauges. This image analysis provides an opportunity to pinpoint the location of crack initiation. Also, this technique provides a flexibility to do a back analysis of the resulting strain fields in selected area of extent.

In the light of above studies, one can say that this DIC technique is very much effective to detect the cracking phenomena. So, it is decided to use this DIC technique in this research for monitoring the cracking pattern and determining the interface debonding propagation in thin bonded cement-based overlays, under monotonic and fatigue loading.

I.3 CONCLUDING REMARKS

Keeping in view the main objectives of research program, a comprehensive literature review was carried out in order to get some guidelines about thin bonded cement-based overlays. The main objective of this chapter is to highlight the different mechanical aspects of fiber reinforced and rubberized mortars, the impact of substrate surface preparation on bond behaviour, the fatigue performance of fiber reinforced concrete, the benefits of using

rubberized and fiber reinforced mortar as a repair material and the durability of thin bonded cement-based overlays subjected to monotonic and fatigue loading.

Previous studies show that with the incorporation of rubber aggregates in mortar, reduction in compressive and tensile strengths and modulus of elasticity was observed. Although, incorporation of rubber aggregates in mortar is detrimental to tensile and compressive strengths, but along with that improvement in strain capacity before the macro-crack localization was also observed. These rubber particles in mortar act like a micro-crack arrestor and also found helpful to limit the propensity for shrinkage cracking. By the incorporation of metallic fibers in mortar, significant improvement in residual post cracking strength was observed. Further, it can be concluded that the combine use of rubber aggregates and fibers in mortar produced a positive synergetic effect by improving the strain capacity and the residual post cracking strength simultaneously.

The durability of a thin bonded repair system depends upon the sustainability of repair material. The sustainability of repair material means its ability to withstand the loads without any cracking, which is highly dependent upon its mechanical characteristics. The durability of a thin bonded repair system also depends upon its ability to resist debonding at interface. The debonding at interface is mainly induced due to externally applied loads and differential shrinkage between overlay and substrate.

The combined use of rubber aggregates and fibers in the repair material of thin bonded cement-based overlays appeared as a suitable solution to improve the durability of repair system. Since, rubber aggregates incorporation in repair material control the first micro-cracking and fibers control the opening of crack which as a result delay the debonding initiation and also limit the interface debonding propagation. A similar kind of behaviour was observed under fatigue loading also. The interface debonding propagation with the number of fatigue cycles was very much limited in composite beams repaired with fiber-rubberized mortar. Further, use of rubber aggregates obtained by grinding end-of-life tyres in cement-based materials can be considered as a solution to maintain a clean environment by limiting the landfill for residual waste.

In the light of previous research, one can conclude that material bridging degradation was observed with the number of fatigue cycles. The fatigue performance of FRC is strongly dependent on cyclic stress-crack width relationship. Along with the number of fatigue cycles,

the rate of bridging strength degradation is also dependent upon the maximum crack width and type and content of metallic fibers.

The substrate surface roughness has a great impact on the bond behaviour between repair material and substrate. Each surface preparation technique has its own influence on bond strength. Generally, an improvement in bond strength was observed with substrate surface preparation due to the removal of top weak laitance layer or dirt deposit. The selection of surface preparation technique depends upon the quality of concrete substrate. The substrates with higher strengths require more aggressive treatment and the substrate surfaces with lesser strengths require less aggressive surface preparation technique. However, the surface treatment can produce micro-cracking, if it is not well operated with regard to the quality and the strength of concrete, which as a result cause reduction in bond strength.

In order to mechanically characterize the mortar mix composites used in this study (fiber reinforced and/or rubberized mortar), different tests were conducted. The results of these tests along with the discussion will be presented in the next chapter.



Chapter # II

MECHANICAL CHARACTERIZATION

OF STUDIED CEMENTITIOUS COMPOSITES

II. MECHANICAL CHARACTERIZATION OF STUDIED CEMENTITIOUS COMPOSITES

II.1 INTRODUCTION

In this chapter, the experimental methodology is explained, for characterizing different mortar mixes used as repair material and substrate material in thin bonded cement-based overlays. Also, the complete procedural steps for sample preparation and testing of specimens are explained.

It has been confirmed from the previous researches (T-H. Nguyen et al., 2010; T-H. Nguyen et al., 2012; A. Toumi et al., 2013; A. Turatsinze et al., 2016; S. Asad Ali Gillani et al., 2016), that the incorporation of rubber aggregates in mortar is a suitable solution to improve its strain capacity. On the other hand, it is a well known fact that fiber-reinforcement can favorably modify the residual post cracking strength of cement-based materials. These two properties are without any doubt essential in the durability of bonded cement-based overlays. Moreover, it is also concluded that the combined use of rubber aggregates and of fiber-reinforcement in mortar produces a positive synergetic effect by improving the strain capacity and post cracking residual tensile strength simultaneously (Nguyen et al., 2010; A. Toumi et al., 2013; S. Asad Ali Gillani et al., 2016). In order to study the effectiveness of rubber aggregates and fiber-reinforcement in overlays repair material a comprehensive experimental program was designed and carried out to investigate following mechanical properties:

- ✚ Compressive strength
- ✚ Modulus of elasticity
- ✚ Direct tensile strength
- ✚ Shrinkage and mass loss

II.2 SELECTION OF MATERIALS

II.2.1 Mortar Constituents

Ordinary Portland cement (CEM I 52.5R), sand (fine river rounded aggregates 0/4 mm), super-plasticizer (BASF Glenium 27) for required workability and viscosity agent (BASF Rheomac 890F) for avoiding segregation of rubber aggregates were used in different mortar mixes.

II.2.2 Fibers

Commercially available amorphous metallic fibers of 30 mm in length were used. This length of fiber also satisfies the condition for effective bridging action, i.e. the length of fiber should be equal or greater than two times the maximum aggregate particle size (S-U. Balouch and J-L. Granju., 1999). Illustration of metallic fibers used is shown in Figure II-1. According to previous research, these types of fibers didn't show any corrosion when immersed in FeCl_3 and HCl for a period of 24 hour (P. Rossi., 1998). So, the mix containing this type of metallic fibers can also be used in aggressive environment. Due to large surface area and rough surface, these types of fibers make a good bond with cement matrix. Also, these fibers are flexible and straight. Characteristics of these metallic fibers are presented in Table II-1 (Fibraflex saint-gobain).



Figure II-1: Amorphous metallic fibers of 30mm length

Table II-1: Characteristics of amorphous metallic fibers (Fibraflex saint-gobain)

Fiber Properties	Metallic Fibers
Length	30 mm
Least dimension	29 μm
Density	7200 kg/m^3
Elastic modulus	140 GPa
Tensile strength	> 1400 MPa
Raw material	Amorphous metal (Fe,Cr)80, (P,C,Si)20

II.2.3 Rubber Aggregates

In this study, rubber aggregates were used as a partial replacement of sand by an equivalent volume in order to increase the mortar straining capacity. These rubber aggregates were obtained by grinding end-of-life tyres. The density of these rubber aggregates is 1.2 which is very less as compared to sand, i.e. 2.7. Also, one can notice that these rubber aggregates have a slightly different particle size distribution as compared to sand as shown in Figure II-2, but maximum dimensions of grains do not exceed 4 mm as shown in grading curve Figure II-3.

**Figure II-2: Rubber aggregates and sand**

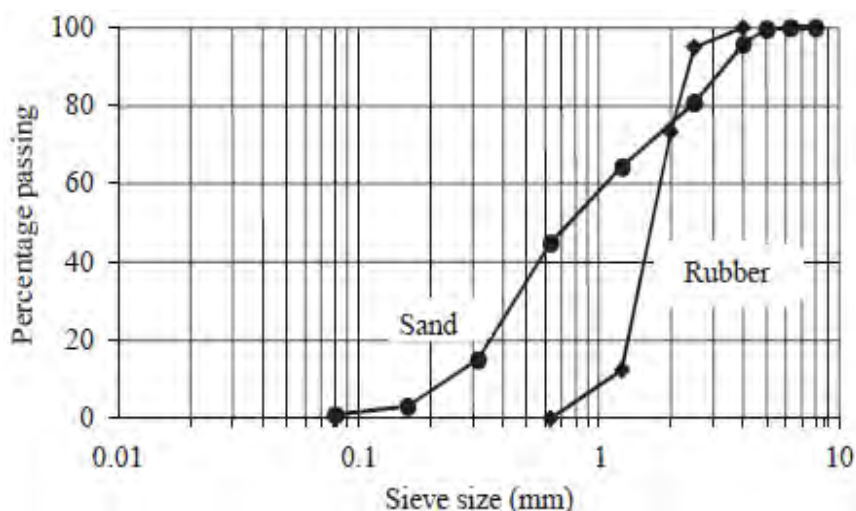


Figure II-3: Grading curves of sand and rubber aggregates

II.3 MORTAR MIX COMPOSITIONS

Taking into account the workability problem of mix composites associated with the addition of fibers, rubber aggregates and also the cost effectiveness, maximum dosage of fibers and rubber aggregates was kept limited. In the light of previous research (T-H. Nguyen et al., 2010), maximum dosage of fibers used was 30 kg/m^3 and rubber aggregates was 30% as partial replacement of natural aggregates. Total four mortar mixes were tested: one control mortar (without rubber aggregates and fibers), second with fibers at a dosage of 30 kg/m^3 , third containing rubber aggregates replacing 30% sand by equivalent volume and fourth one containing 30 kg/m^3 fibers and 30% sand replacement by rubber aggregates. Using similar water to cement ratio, the super-plasticizer dosage was adjusted in order to maintain almost identical workability having a slump (10 ± 2) mm. For this purpose, dosage of super-plasticizer needs to be increased in rubberized and/or fiber reinforced mortars. The quantity of each constituent of mortar is shown in Table II-2.

Table II-2: Mix design and proportioning (Values in kg/m³)

Sr. No	Mix Designation	Cement	Sand	Water	Rubber	Fibers	Super-	Viscosity
					Aggregates		Plasticizer	Agent
1	0R0F (CC)	500	1600	250	0	0	1.2	0
2	0R30F	500	1600	235	0	30	5	0
3	30R0F	500	1120	235	215	0	4.5	2.5
4	30R30F	500	1120	235	215	30	10	2.5

Mix designations:

- ✚ **30R30F:** 30R refers to the mix containing 30% sand replacement with rubber aggregates by equivalent volume and 30F indicates 30 kg/m³ of metallic fibers.

II.4 MECHANICAL CHARACTERISTICS**II.4.1 Compressive Strength****II.4.1.1 Testing Procedure**

The compressive tests were carried out on cylindrical specimens of size 110 mm in diameter and 220 mm in height. The compressive test was conducted according to European Standard NF EN 12390-3. For each mortar mix composition, minimum three samples were tested. Also, before conducting these types of tests rectification of both ends of cylindrical test specimens was done.

II.4.1.2 Results and Discussion

Compressive strength results of all mortar mixes containing rubber aggregates, fibers, combination of fibers and rubber aggregates and control mortar are presented in Figure II-4.

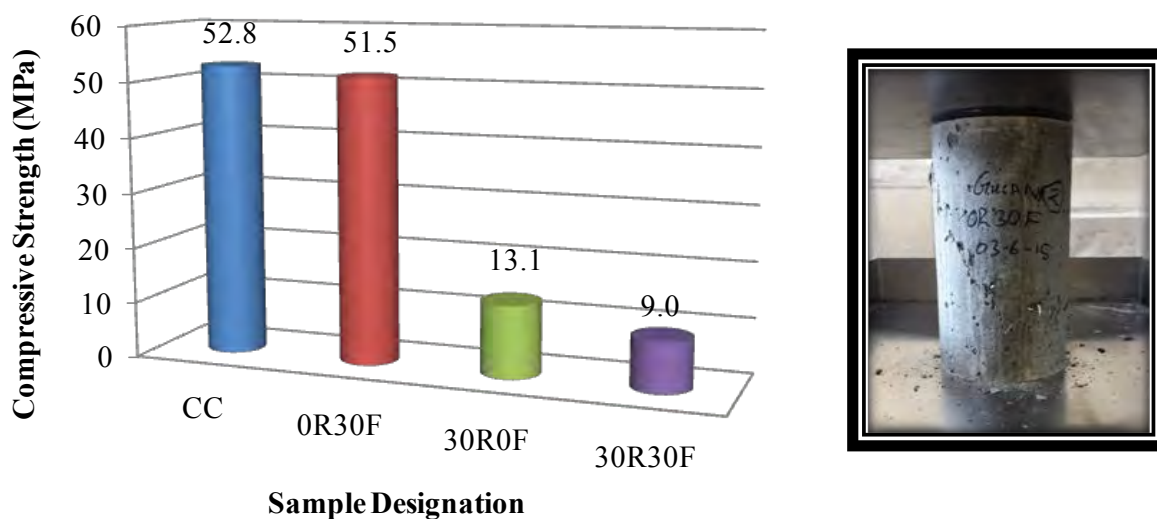


Figure II-4: Compressive strength of different mortar mixes

Experimental results indicate that with the addition of rubber aggregates in mortar, a significant reduction of 28 days compressive strength is observed as compared to reference control mortar as shown in Figure II-4. This shows that the obtained results are in good agreement with the previous researches (A. Turatsinze et al., 2005; T-H. Nguyen et al., 2010), who also used rubber aggregates in mortar as a partial replacement of mineral aggregates. Results also show that the fiber-reinforcement of mortar does not show any significant change in compressive strength as compared to control mortar.

II.4.2 Modulus of Elasticity in Compression

II.4.2.1 Testing Procedure

The modulus of elasticity tests were conducted on cylindrical specimens of size 110 mm in diameter and 220 mm in height. These tests were conducted by following RILEM recommendations (RILEM CPC8., 1972). For each mortar mix composition, minimum three samples were also tested. To measure the longitudinal deformation, a strain cage was used as shown in Figure II-5. Three extensometers are attached at the base of this cage at an angle of

120° from each other. Average of longitudinal deformation measured by these extensometers is used to calculate modulus of elasticity.



Figure II-5: Testing set-up for compressive modulus of elasticity

First step is to fix the specimen in this strain cage and adjust it under 4000 kN compression testing machine. Second step is to apply the initial stress (pre-stress) of 0.5 N/mm² (f_b) and also record the strain accordingly. Subsequently, increase the stress amplitude uniformly without jarring upto $f_a = 1/3f_{cc}$ (33% of the compressive strength). The test comprises of 5 continuous increasing and decreasing loading cycles ranging between f_a and f_b stresses. The modulus of elasticity is calculated from the strain value at the end of 5th unloading cycle (at value f_b) and the strain value of 6th loading cycle (at value f_a) as follows

$$E_c = \frac{\Delta f}{\Delta c} = \frac{f_a - f_b}{\varepsilon_a - \varepsilon_b} \quad \text{in N/mm}^2$$

Where:

E_c = Modulus of elasticity

$f_a = 1/3 f_{cc}$ in N/mm²

f_b = Initial Stress = 0.5 N/mm²

ε_a = Strain under stress f_a

ε_b = Strain under stress f_b

II.4.2.2 Results and Discussion

The results of modulus of elasticity in compression for all mortar mixes containing rubber aggregates, fibers, combination of fibers and rubber aggregates and control mortar are presented in Figure II-6.

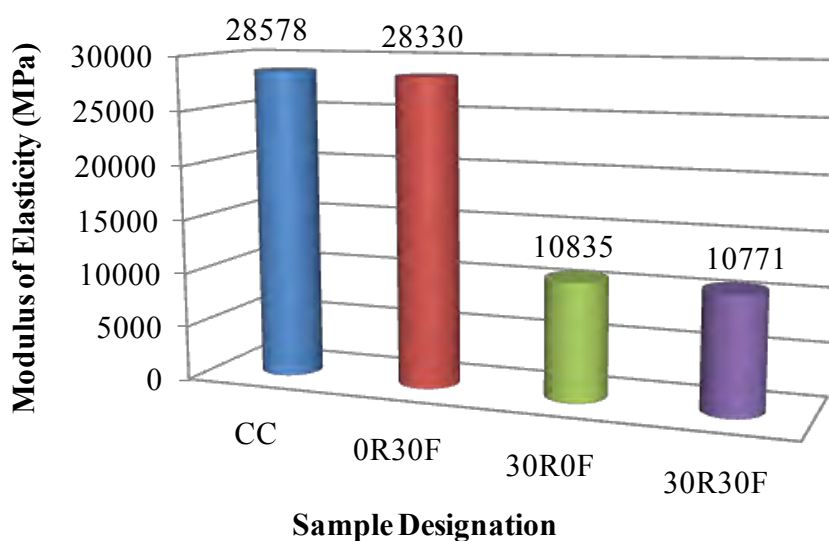


Figure II-6: Modulus of elasticity in compression

From the results, it is evident that with the addition of rubber aggregates in mortar, a significant reduction in modulus of elasticity was observed as compared to control mortar. A similar reduction of modulus of elasticity with rubber aggregates incorporating has been observed in the previous research (A. Turatsinze et al., 2005). Along with the reduction of modulus of elasticity, the strain capacity of mortar is also enhanced which in turn is helpful to restrain micro-cracking. This decrease in compressive strength and modulus of elasticity by incorporating rubber aggregates in mortar is mainly because of low stiffness of rubber aggregates and also due to some other reasons like poor bonding between rubber aggregates and cement paste etc. Results also show that the presence of metallic fibers has no significant impact on modulus of elasticity as shown in Figure II-6.

II.4.3 Direct Tensile Strength

Direct tension tests were conducted in order to access the effect of incorporating metallic fibers and of rubber aggregates in mortar matrix. These tests show the deformation capacity at peak load (named strain capacity) and also give an idea about the residual strength beyond peak load. So by conducting these tests, one can get an idea that how strain capacity and residual post peak strengths are improved by incorporating rubber aggregates and fibers in mortar matrix.

II.4.3.1 Testing Procedure

The direct tension tests were conducted on the notched prismatic specimens as shown in Figure II-7.

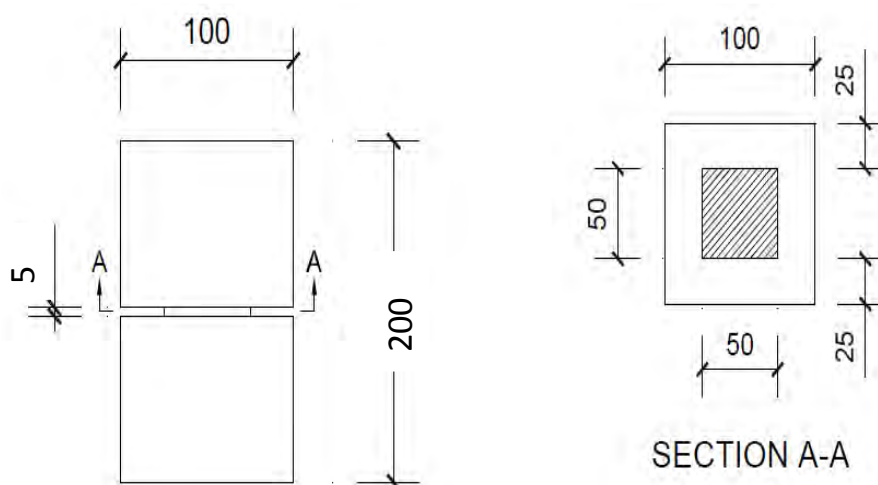


Figure II-7: Notched test specimen for direct tension tests (dimensions are in mm)

In order to ensure proper alignment of the test specimen, a specially designed testing assembly was used containing interchangeable steel blocks. The specimen is first glued to the aluminium blocks. Both glued surfaces of a specimen were prepared before gluing by making small notches on surface for enhancing a bond between specimen and aluminium block. A special fast curing polymer was used for gluing the specimen. This polymer gains its strength in about 5 minutes. The test was conducted on an MTS machine with 100kN capacity and was controlled by Crack Mouth Opening Displacement (CMOD) by using clips which are called as COD attached on two faces as shown in Figure II-8 and Figure II-9. These clips (COD)

can easily be attached with the sample by using metallic supports which were firstly glued on the sample. These metallic supports were glued on the specimen face exactly at notched location at a distance of 5 mm from each other. The COD can easily be placed between these two supports in order to measure the opening at notched cross section during tension test. Minimum three samples were tested for each mix composition. The loading rate was same as proposed by RILEM recommendation (RILEM TC 162-TDF., 2001). The test was controlled by using this sensor called COD clip at the following rates:

- ✚ 0 to 0.1 mm: speed equal to 5 microns / min,
- ✚ 0.1 to 1 mm: speed equal to 100 microns / min.

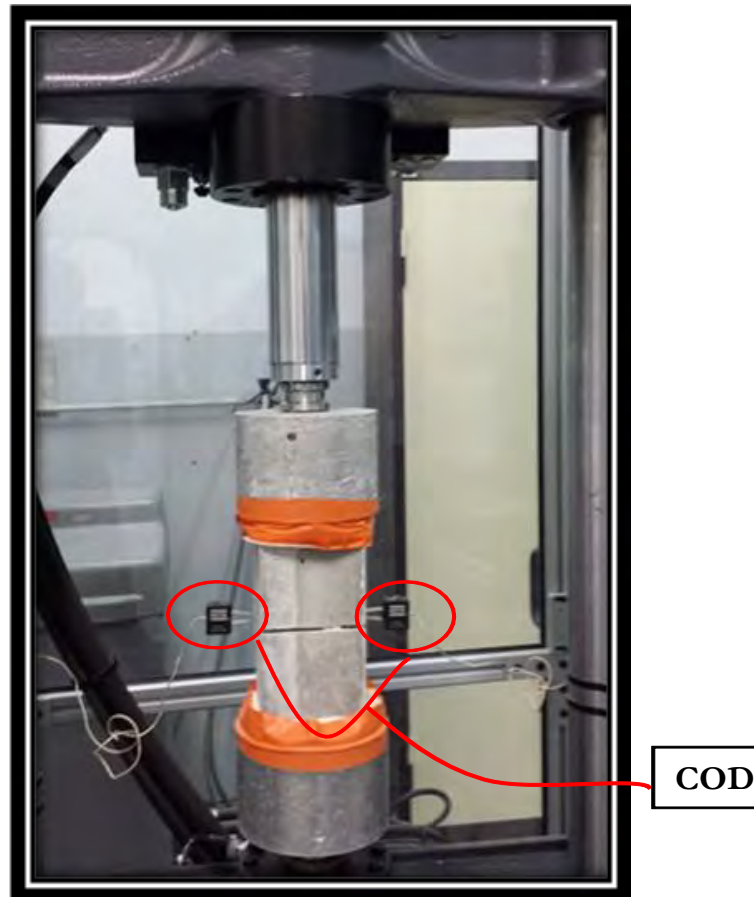


Figure II-8: Complete experimental testing set-up for tension test

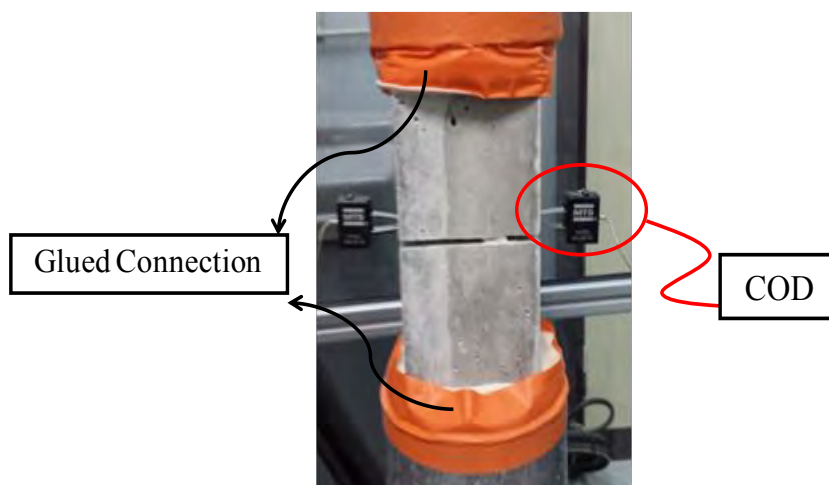


Figure II-9: COD attached at notch (direct tension test)

II.4.3.2 Results and Discussion

Results of direct tension tests for all mortar mixes are presented in Figure II-10. It is evident that with the addition of 30% rubber aggregates, a significant reduction in tensile strength is observed, but strain capacity is also improved about 1.5 times with reference to control mortar as shown in Figure II-11. Figure II-12 represents the enlarged view of the graph shown in Figure II-11, in order to exhibit the improvement in strain capacity by rubber aggregates incorporation in mortar as compared to reference control mortar. With the only fiber-reinforcement, a significant improvement in residual post peak strength is observed as evident from Figure II-12. The combine incorporation of metallic fibers and rubber aggregates in mortar (30R30F) produce a positive synergetic effect, not only improves the residual post peak strength, but also enhances the strain capacity upto 3.5 times with reference to control mortar. This synergetic effect is also observed from energy analysis presented in annexe B. The fracture energy (G_f) for all of our studied mortar mixes is calculated from the direct tension curves shown in Figure II-11.

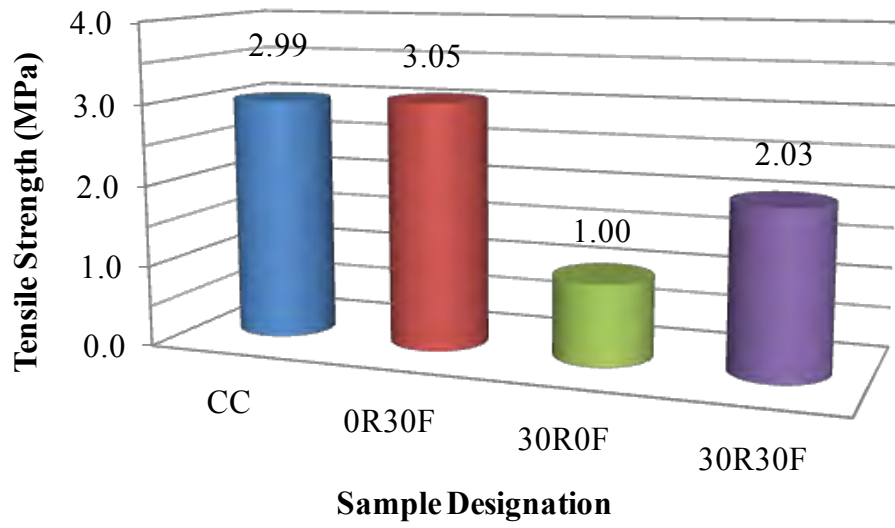


Figure II-10: Tensile strength of different mortar mixes

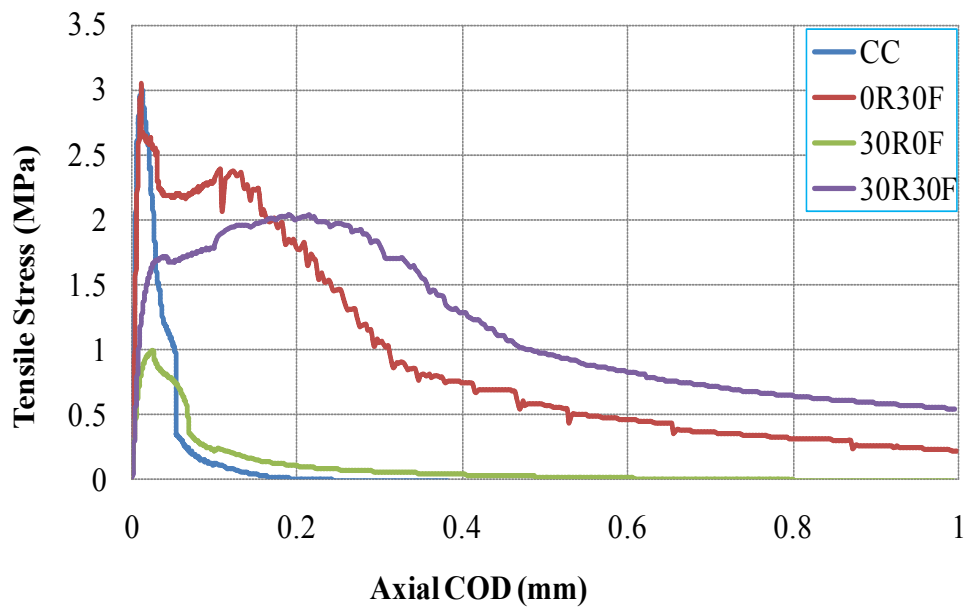


Figure II-11: Effect of rubber aggregates and fibers on straining capacity

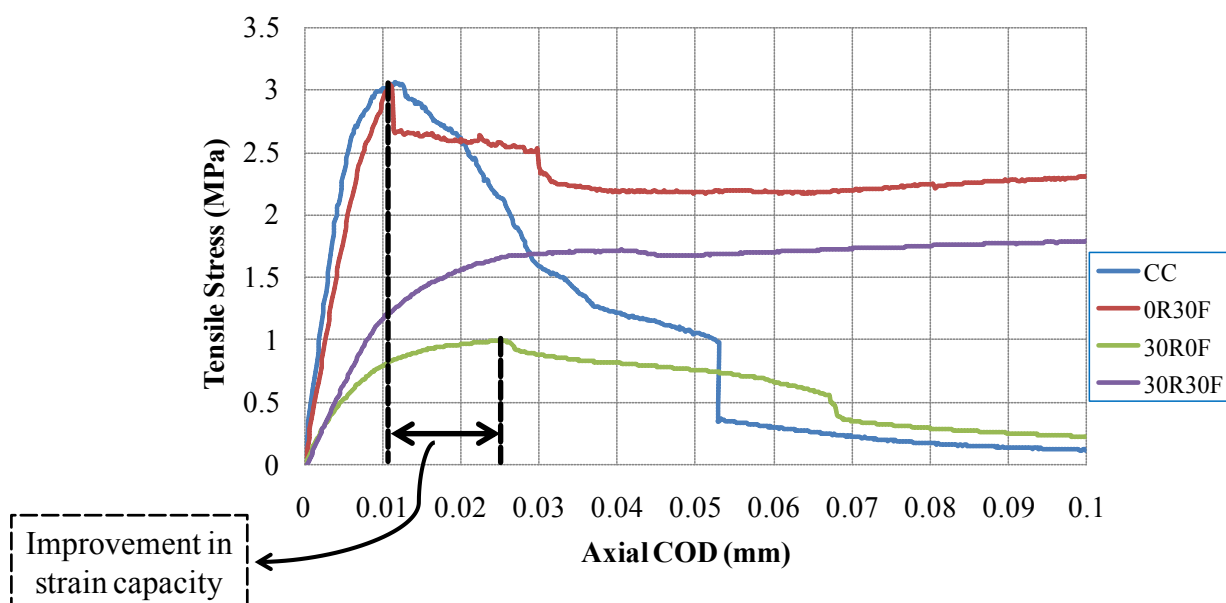


Figure II-12: Effect of rubber aggregates and fibers on strain capacity (enlarged view)

Softening Behavior:

The softening behavior of the material can be obtained by conducting direct tension test on a notched specimen. Generally, the tensile behavior of a cementitious material includes two phases: an elastic behavior (zone A-B) and a softening behavior (zone C-D-E) as shown in Figure II-13.

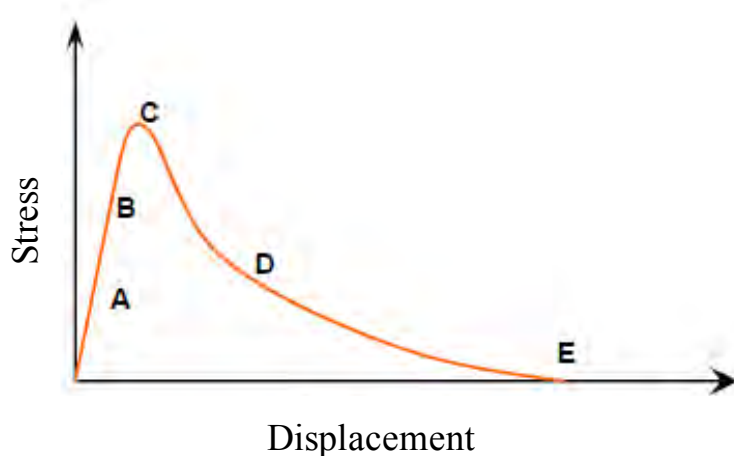


Figure II-13: Material behaviour in direct tension test

Initially, the behaviour of material is linear (zone A-B) than a slight change of slope is observed just before the peak stress value (zone B-C). During loading, pre-existing micro-cracks first propagate at matrix-aggregates interface (zone AB) and then in the mortar (Zone BC). After reaching the ultimate peak load (point C), the force required to increase the material deformation gradually starts decreasing (zone CDE). This behavior is called as softening of the material. At point E, the two sides of the specimen are separated distinctly. The exact location of point E generally represents the crack opening limit beyond which the residual strength can be considered as zero.

The (σ -w) curves of studied mortar mix compositions are presented in Figure II-14. These curves are obtained by following the RILEM method (RILEM TC 162-TDF., 2002). This RILEM method is explained in annexe A.

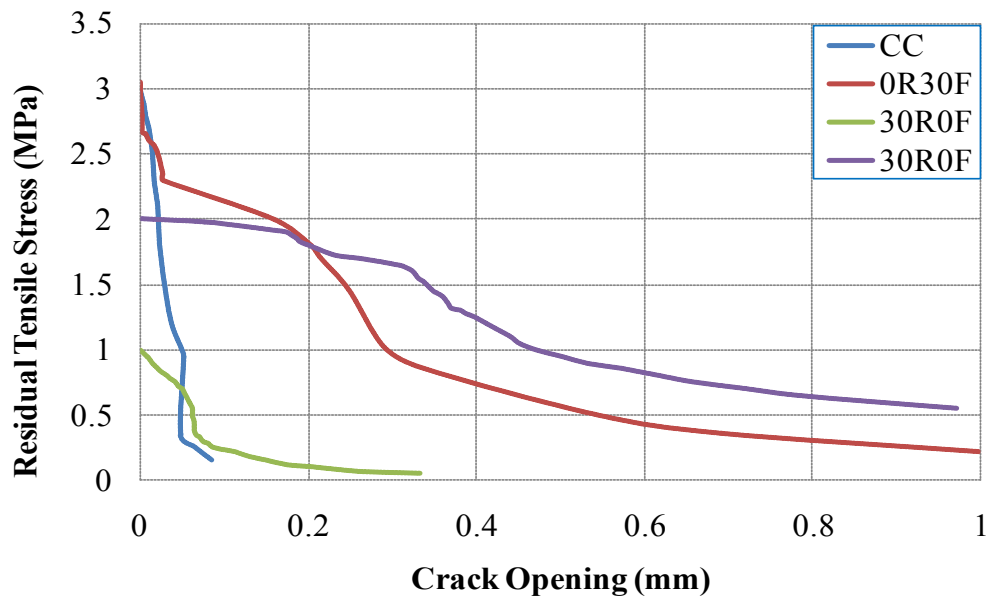


Figure II-14: Softening behaviour of different type of mortar mixes

II.4.3.3 Highlights

From the experimental results, it can be summarized that with the addition of rubber aggregates in mortar, a significant reduction in tensile strength of mortar is observed as compared to control mortar but along with that improvement in strain capacity of mortar is

also observed. Also, the addition of metallic fibers in mortar improves significantly post peak residual tensile strength. It can also be concluded that the combine use of rubber aggregate and fibers produce a positive synergetic effect, not only improves post peak residual tensile strength, but also improves the strain capacity which in turn is helpful to delay micro-cracking phenomena. Moreover, this combination also improves the softening behavior significantly. Further, it can be concluded that the presence of rubber aggregates didn't affect the role of fiber-reinforcement.

II.4.4 Mass Loss and Shrinkage

Shrinkage is a phenomenon which imposed deformations in cementitious materials and these deformations in turn produce cracking. Shrinkage is a complex phenomena that normally occurs due hydration of cement and loss of moisture from inside of concrete. Generally, this shrinkage phenomenon occurs at the early age of concrete. In case of thin bonded cement-based overlays, concrete substrate absorbs moisture from newly cast repair layer and causes a differential shrinkage at the interface between substrate and repair layer. This differential shrinkage in repair system causes micro-cracking, which as a result initiates debonding at the interface. Shrinkage of cementitious materials depends upon many factors, but the intensity of shrinkage majorly depends upon elastic modulus of aggregates. In this section, the shrinkage and mass loss phenomena of our studied mix compositions are presented.

In order to determine mass loss and shrinkage in different type of mortar mixes, specimens of $(40 \times 40 \times 160)$ mm³ in size were manufactured. After casting, these specimens were demoulded in 21h and than kept in a room specially dedicated for shrinkage tests. The temperature of this room is 20°C and relative humidity is 55%. Minimum, six samples were manufactured for each mix composition (control mortar, rubberized mortar, fiber reinforced mortar and mix containing both rubber aggregates and fibers) in order to determine total and autogenous shrinkage. The autogenous shrinkage is the shrinkage that occurs without any moisture exchange. In order to ovoid moisture exchange with the external environment, the specimens are properly wrapped in an adhesive aluminium scotch. Weighing balance was used to determine the mass loss as shown in Figure II-15. The apparatus used to determine autogenous and total shrinkage in different mortar mixes is shown in Figure II-16.



Figure II-15: Weighing balance for mass loss determination



Figure II-16: Apparatus for shrinkage measurement

II.4.4.1 Total Shrinkage

The maximum volume change that occurs in a cementitious material is called as total shrinkage. Most common phenomena's that cause shrinkage in cementitious material is moisture loss and cement hydration. The curves presented in Figure II-17 show the total shrinkage values in different mortar mixes during period of 150 days from date of casting.

Results show that there is a significant increase in total shrinkage by incorporating rubber aggregates in mortar. The maximum total shrinkage was observed in a mortar mix with 30 percent rubber aggregates substitution (30R0F). These results are in good agreement with the previous researches (D.W. Hobbs., 1971; S. Bonnet., 2004; T-H. Nguyen., 2010), who also concluded that aggregate properties have significant impact on shrinkage of the cement-based matrix. Figure II-17 also shows that least total shrinkage was observed in a mix containing 30kg/m^3 of metallic fibers. Another noticeable thing is that the incorporation of these types of metallic fibers in mortar does not substantially reduce the shrinkage as compared to control mortar. Curves presented in Figure II-18 and Figure II-19 show that the mass loss due to water evaporation is an important factor in total shrinkage. But in case of rubberized mortar, along with the mass loss, low stiffness of rubber aggregates also play a vital role in order to enhance the shrinkage phenomena.

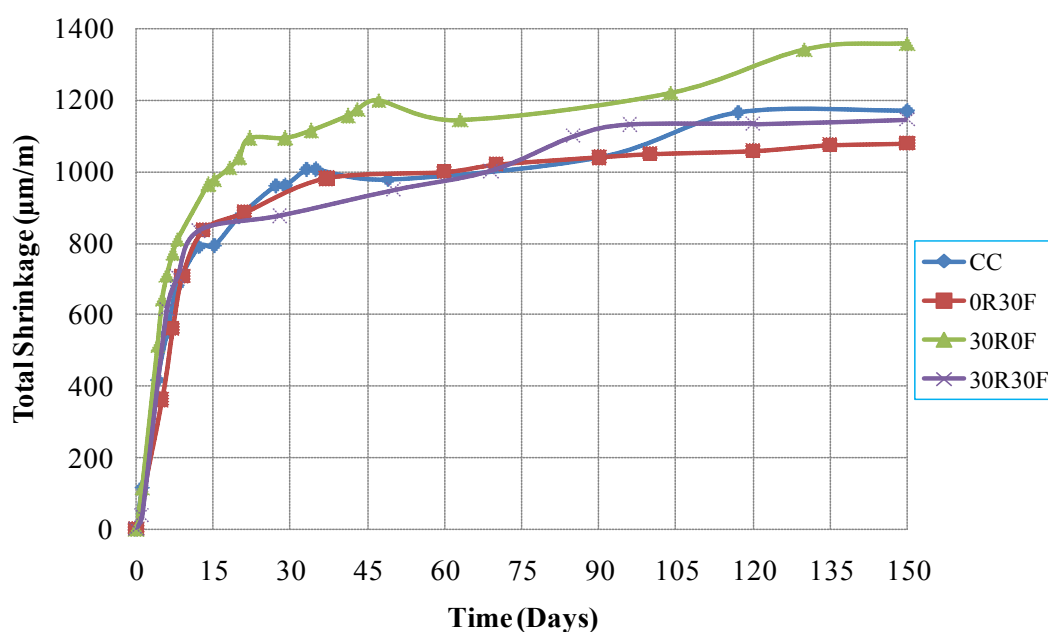


Figure II-17: Evolution of total shrinkage in different mortar mixes during period of 150 days

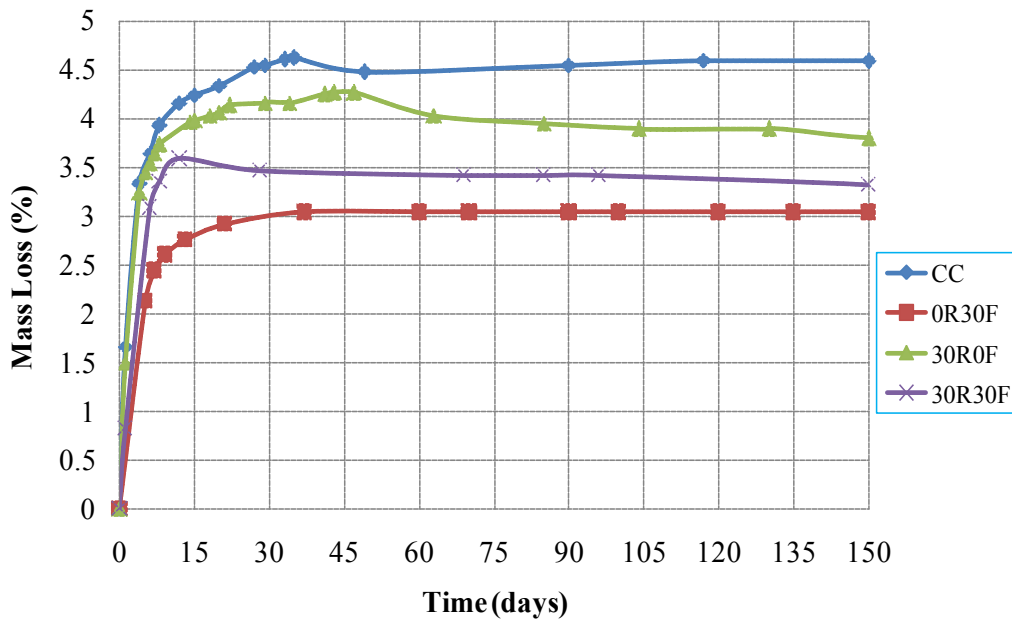


Figure II-18: Evolution of mass loss in different mortar mixes during period of 150 days

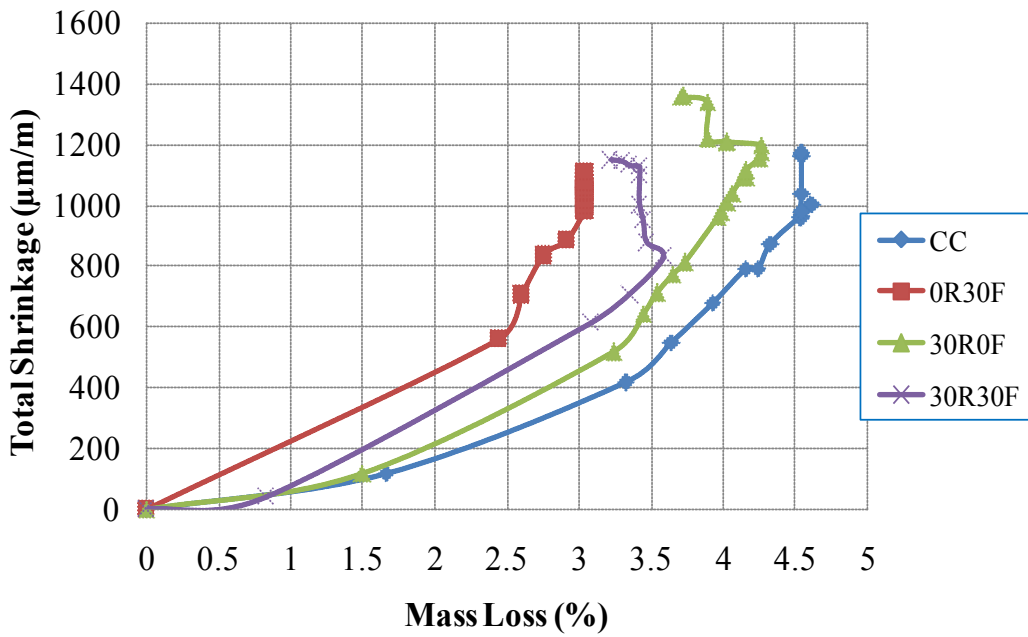


Figure II-19: Total shrinkage vs. mass loss curves for different mortar mixes

II.4.4.2 Autogenous Shrinkage

Autogenous shrinkage is defined as volume change occurring without moisture exchange to the exterior surrounding environment. This phenomenon occurs as a result of internal chemical reactions in mortar mix components majorly due to hydration of cement particles. Figure II-20 shows the autogenous shrinkage values in different mortar mixes during initial 150 days from day of casting.

Results show that fiber-reinforcement of mortar does not reduce the autogenous shrinkage. On the contrary, fiber-reinforcement in mortar leads to a slight increase in autogenous shrinkage. A similar trend was found in some previous studies (F. Grandhaie., 1993; S. Bonnet., 2004). Also, some reduction in autogenous shrinkage was observed by rubber aggregates substitution in mortar. In rubberized mortar this early reduction in autogenous shrinkage is not because of rubber particles, but due to the high dosage of viscosity modifying agent (VMA). Since, it is necessary to add these VMAs in rubberized mortar for avoiding segregation of rubber particles. It was also reported in previous research (C. Ciobanu, et al., 2013) that by addition of these VMAs, small proportion of $\text{Ca}(\text{OH})_2$ produce which as a result delay the cement hydration process.

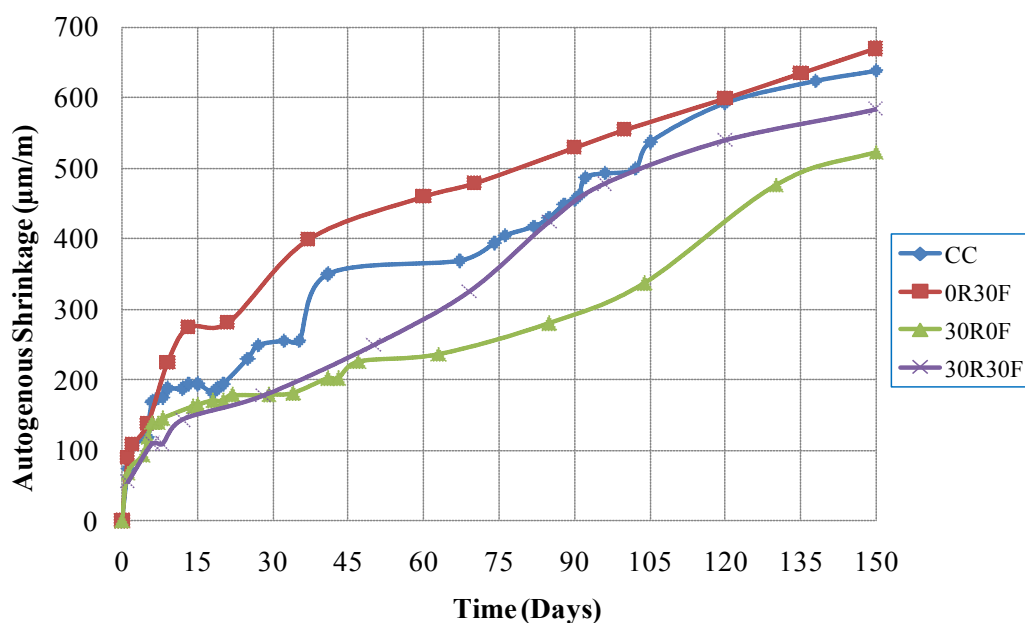


Figure II-20: Evolution of autogenous shrinkage in different mortar mixes during period of 150 days

II.4.4.3 Drying Shrinkage

Drying shrinkage is defined as a combination of all types of shrinkage without taking into account autogenous shrinkage and any thermal shrinkage (AS3600., 2009; EN 1992., 2004). Drying shrinkage occurs under drying conditions, which are not associated with chemical or autogenous self-desiccation of a concrete test specimen, and takes place through the exposed surfaces of the concrete. The rate of drying depends upon several factors such as the concrete member's size and shape as well as the exposed surface conditions (temperature, air speed and relative humidity) and the permeability of the concrete. The easiest way to compute drying shrinkage is to take the simple difference between total shrinkage and autogenous shrinkage value assuming that these phenomena's are not coupled.

Figure II-21 shows the drying shrinkage values in the studied mortar mixes. The graphs show that there is a significant increase in drying shrinkage by incorporating rubber aggregates in mortar. In rubberized mortar almost 30% increase in drying shrinkage is observed as compared to control mortar. As far as the influence of fibers on drying shrinkage is concerned, results show some reduction in drying shrinkage as compared to control mortar. Also, it is evident from Figure II-21 and Figure II-22 that the combine use of rubber aggregates and fibers (30R30F) in a mortar is helpful to limit the shrinkage phenomena, especially the shrinkage induced due to low stiffness of rubber aggregates. And fiber-reinforcement of rubberized mortar try to counter balance the shrinkage additionally induced by the aggregates with low stiffness (rubber aggregates).

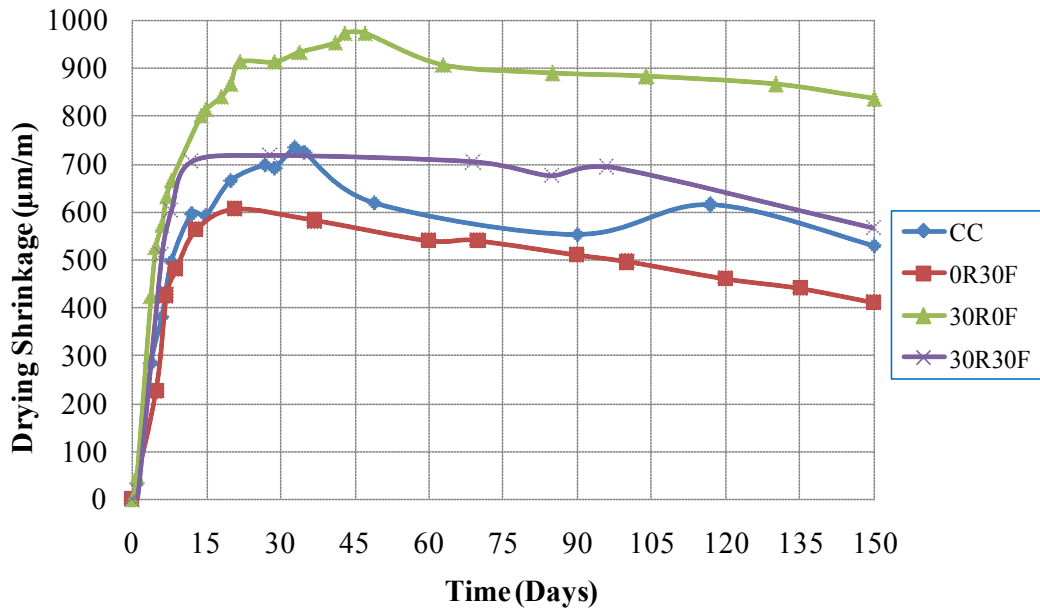


Figure II-21: Evolution of drying shrinkage in different mortar mixes during period of 150 days

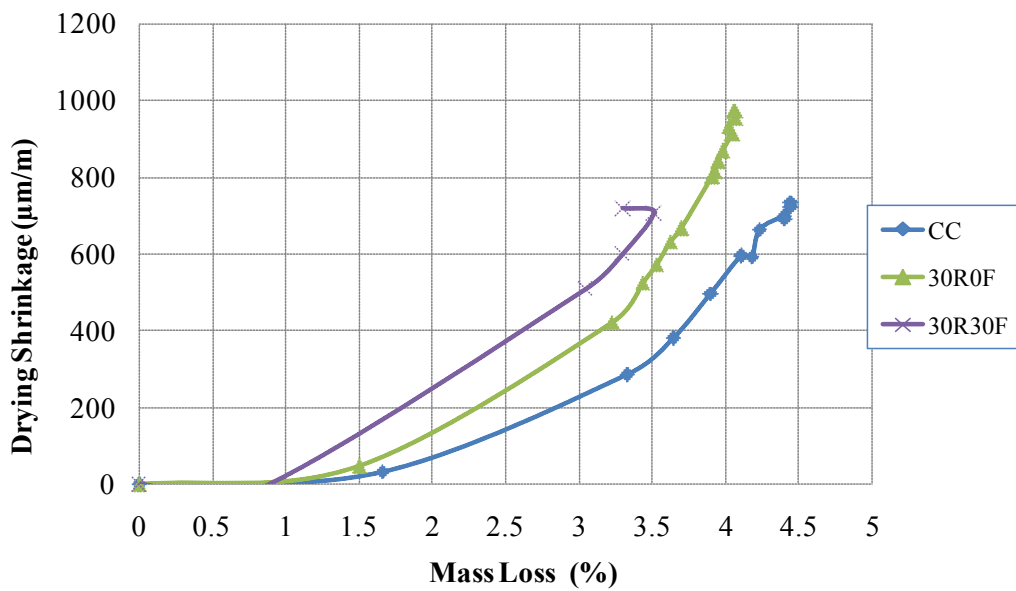


Figure II-22: Drying shrinkage vs. mass loss curves for different mortar mixes

II.5 CONCLUDING REMARKS

In the light of mechanical testing and shrinkage test results, following conclusions can be drawn:

- ✚ Incorporation of rubber aggregates in mortar is a detrimental to its mechanical strengths (compressive and tensile strengths) and reduces the modulus of elasticity as compared to reference control mortar. Along with the reduction in mechanical strengths, an improvement in strain capacity of mortar is also observed before macro-crack localization. And one believes that the incorporation of rubber aggregates in mortar tries to arrest a micro-cracking phenomenon which as a result is helpful to delay macro-crack propagation.
- ✚ Metallic fiber-reinforcement of mortar does not show noticeable change in mechanical characteristics before cracking. But after cracking, residual post cracking tensile strength is significantly enhanced.
- ✚ The combine use of rubber aggregates and fibers in mortar not only improves the strain capacity, but also improves the residual post peak strength, which is a solution to control the crack opening and debonding propagation specially in thin bonded overlays. Also, it can be said that the presence of rubber aggregates didn't change the role of fiber-reinforcement. However, the combination of both rubber aggregates and fibers in mortar produce a positive synergetic effect.
- ✚ Significant increase in total shrinkage was observed in a mortar mix with rubber aggregates substitution (30R0F). Along with the mass loss, the low stiffness of rubber aggregates also play a vital role in order to enhance shrinkage phenomena in rubberized mortars.
- ✚ As far as the influence of fiber-reinforcement on shrinkage is concerned, some reduction in total and drying shrinkage is observed as compared to control mortar at the age of 150 days. Also, the combine use of rubber aggregates and fibers (30R30F) in a mortar is helpful to limit the shrinkage additionally induced due low stiffness of rubber aggregates.

- ✚ The use of rubber aggregates obtained by grinding end life of tyres in cement-based materials can be considered as a solution to maintain a clean environment by limiting the landfill for residual waste. Incidentally, this approach helps to the development of a circular economy.

This chapter highlights the different benefits which can be attained by incorporating rubber aggregates and fibers in cement-based composites. And the application of these types of composite mortars as repair material in thin bonded cement-based overlays is helpful to control crack opening and debonding propagation. The bond behaviour of repair system is also dependent upon the substrate surface roughness. In order to improve surface roughness of substrate, different surface preparation techniques are used. So, in the next chapter impact of substrate surface preparation on bond tensile strength between repair material and substrate will be presented.



Chapter III



IMPACT OF SUBSTRATE SURFACE PREPARATION ON BOND STRENGTH

III. IMPACT OF SUBSTRATE SURFACE PREPARATION ON BOND STRENGTH

III.1 INTRODUCTION

As concluded in some previous research works (J. Silfwerbrand., 1990; J. Silfwerbrand and H. Beushausen., 2006; L. Courard et al., 2014), the bond between substrate and repair material depends upon many factors and each factor has its own influence. In order to achieve a good bond between the substrate and repair material, surface roughness of substrate plays a vital role (Dinis et al. 2012, Pedro and Eduardo 2013, Hindo1990, Silfwerbrand 1990). So, substrate surface should be rough and top laitance or dirt deposit layers should be removed before casting new repair layer. For making the substrate surface rough, there can be different surface preparation techniques as discussed in chapter I (A. Garbacz et al. 2005; A. Garbacz et al. 2006) in order to enhance mechanical interlocking between substrate and overlay repair material. Each technique has a different impact on bond behavior between substrate and repair material. Regardless of mechanical interlocking, this surface preparation makes accessible certain un-hydrated or insufficiently hydrated cementitious particles, which as a result, is helpful in promoting an epitaxial growth on this treated surface (W. Zhong and Wu. Yao., 2008). However, the surface treatment can produce micro-cracking, if it is not well operated with regard to the quality and the strength of concrete, which as a result, cause reduction in bond strength (A. Garbacz et al., 2006; L. Courard et al., 2006; PMD. Santos et al., 2007).

Keeping in view the already conducted research work, two surface preparation techniques were used here in this research, which are not very aggressive and by opting them there is less risk to induce micro-cracks. Bond tensile strengths were evaluated by conducting the direct tension tests. Following, two techniques were used for surface treatment and their results were compared with the reference substrate surface (RS i.e. without any treatment).

-  Cutting/Sawing of substrate (SS)
-  Sandblasting of substrate (SB)

Control mortar (CC) was used as repair material in all types of substrates (prepared substrates or substrates without any preparation), in order to study the effect of surface roughness only.

III.2 SUBSTRATE SURFACE PREPARATION

III.2.1 Cutting/Sawing Method

The substrate used is of size (100×100×500) mm as shown in Figure III-1. These substrates were manufactured by using control mortar (CC). After casting, these substrates were cured for 3 months under controlled environment at temperature of 20°C and 100 % RH. In order to remove the weak thin layer of laitance (mortar slurry) from the top of substrate, 10 mm layer has been removed by a saw cut. After removing 10mm thickness, the total depth of substrate left is 90 mm. Then on top of it, control mortar repair of 40 mm was cast in order to check the bond behaviour after removing this weak laitance layer.

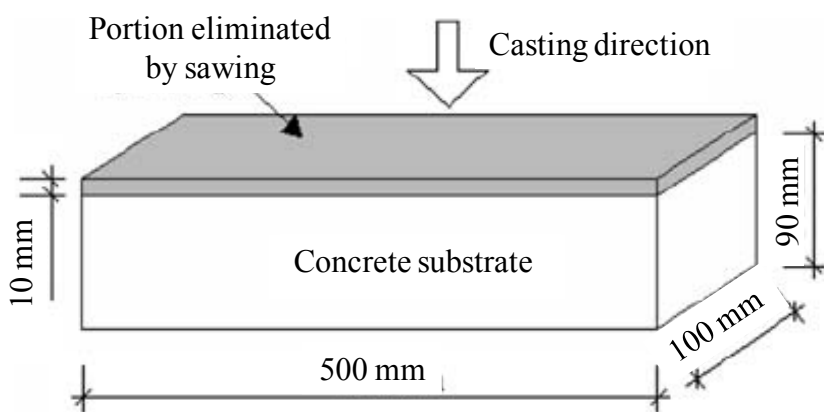


Figure III-1: Substrate surface prepared with sawing method

III.2.2 Wet Sandblasting Method

In wet sand blasting method, the substrates used are also of the same size (100×100×500) mm. In this method of surface preparation, a top weak layer was removed by blasting of sand along with water with the help of a machine at high pressure as shown in Figure III-2. After that, control mortar repair of same depth 40 mm was cast on top of it in order to check the bond behaviour. Surfaces textures obtained from different surface preparation techniques are

shown in Figure III-3. Figure III-4, Figure III-5 and Figure III-6 show the enlarged zoom view of reference surface (RS), sandblasted surface (SB) and cut surface (CS) respectively.



Figure III-2: Substrate surface prepared by sandblasting

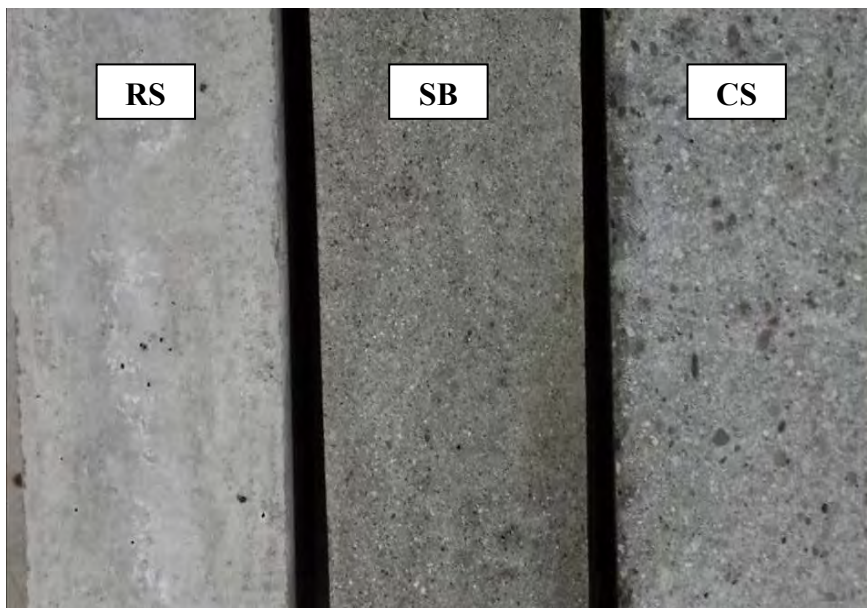


Figure III-3: View of surfaces obtained after different preparation techniques

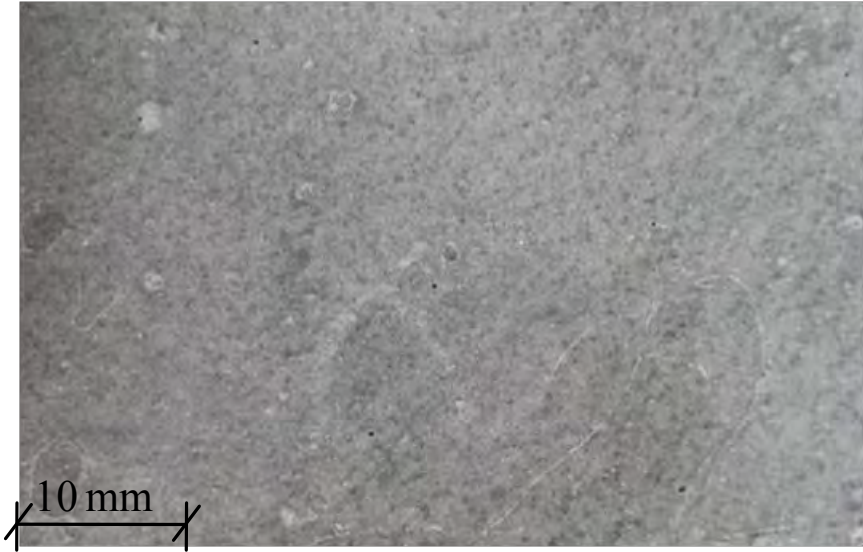


Figure III-4: Enlarged view of reference surface (RS) without any treatment

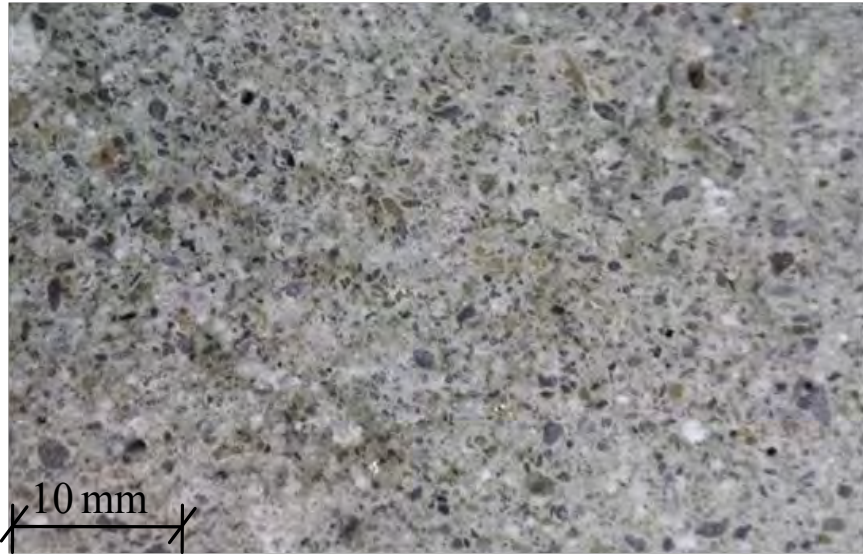


Figure III-5: Enlarged view of sandblasted surface (SB)



Figure III-6: Enlarged view of cut surface (CS)

III.3 BOND TENSILE STRENGTH

The direct tension tests have been carried out in order to check the impact of substrate surface preparation on the bond between prepared substrate surfaces and without any preparation with the control mortar repair material. These tests point out the loading at which the debonding is initiated, deformation at peak load (named strain capacity) and also give an idea about residual post peak strength.

III.3.1 Testing Procedure

The direct tension tests were carried out on notched prismatic specimens as shown in Figure III-9 by following the RILEM recommendation (RILEM TC 162-TDF., 2001). This notch was created while casting of overlay with the help of an adhesive tape as reservation as shown in Figure III-7.



Figure III-7: Notch created by adhesive tape before casting repair



Figure III-8: Specimen after repair casting

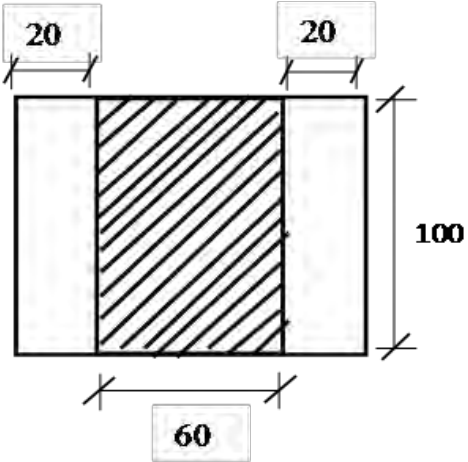
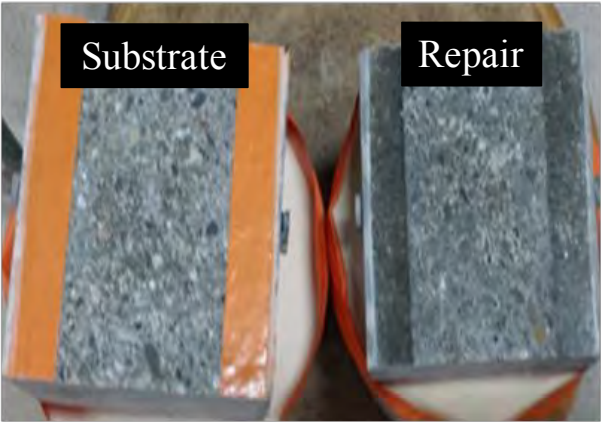


Figure III-9: Notched specimen for bond tensile strength test (dimensions are in mm)

A similar procedure was adopted for sample fixation on interchangeable aluminium blocks by using fast curing glue as previously done for simple direct tension test. These tests were carried out on machine MTS 100kN and were controlled by Crack Mouth Opening Displacement (CMOD) by using clips (COD) attached on two faces as shown in Figure III-10. This COD can easily be attached with the sample by using metallic beveled ends supports. These metallic supports were firstly glued on specimen face exactly at notched location at a distance of 5mm from each other and then COD can easily be placed between these two supports in order to measure the opening at notched cross section during tension test. These tests were controlled by using these COD clips according to the RILEM recommendation (RILEM TC 162-TDF 2001) at the following rates:

- 0 to 0.1 mm: speed equal to 5 microns / min,
- 0.1 to 1 mm: speed equal to 100 microns / min.

Minimum three samples were tested for each surface preparation technique.



Figure III-10: View of notched specimen for bond tensile tests controlled by COD

III.3.2 Results and Discussion

The results of direct tension tests controlled by Crack Mouth Opening Displacement (CMOD) for all types of substrate surfaces are presented in Figure III-11. From the results, it is evident that with surface preparation there is a significant increase in bond tensile strength perpendicular to the interface. An improvement in strain capacity is also observed with surface preparation as compared to substrate surface used in its original condition as shown in Figure III-12. Cut surface show maximum bond tensile strength and strain capacity. The reason for having more bond strength in cut surface is that after sawing the top surface, small grooves come on top of substrate surface as shown in Figure III-6. When new repair layer is cast on this top surface, a mortar goes inside these grooves and creates bridging material between substrate and repair layer. These small grooves already present inside the substrate due to the air void entrapped during substrate casting and after sawing these grooves come to the top surface. Figure III-13 shows the post peak behaviour obtained by following the RILEM method (RILEM TC 162-TDF., 2002) of curves shown in Figure III-12 of overlays with different substrate surfaces.

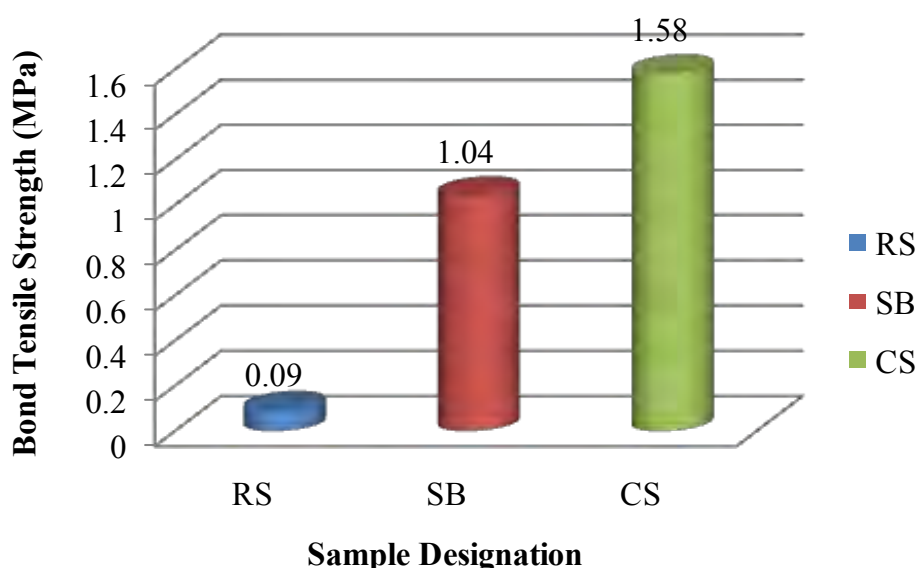


Figure III-11: Bond tensile strength variation with different surface preparation techniques

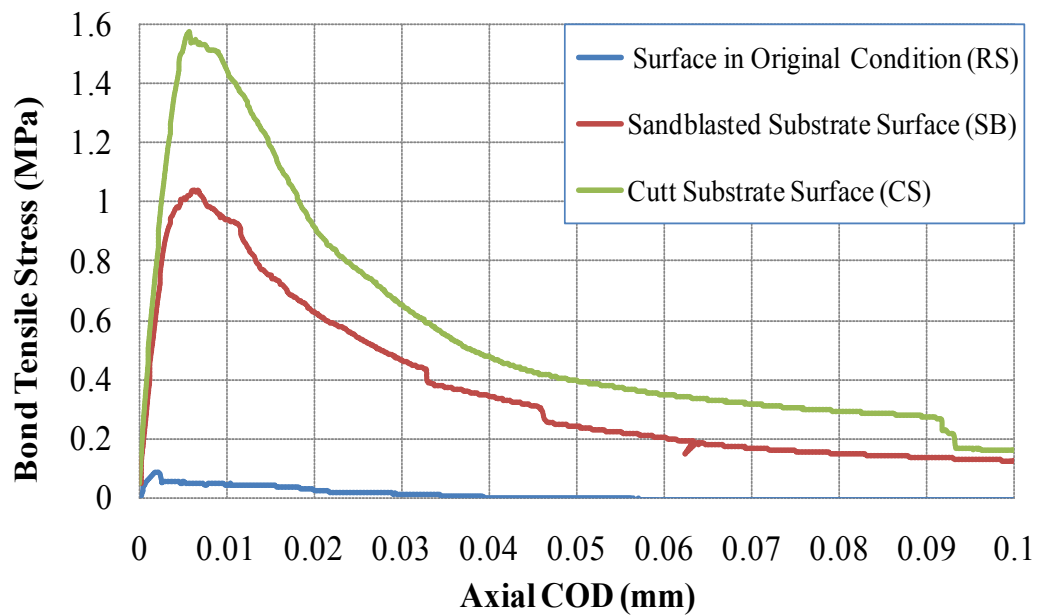


Figure III-12: Strain capacity behavior of overlays with different substrate surface textures

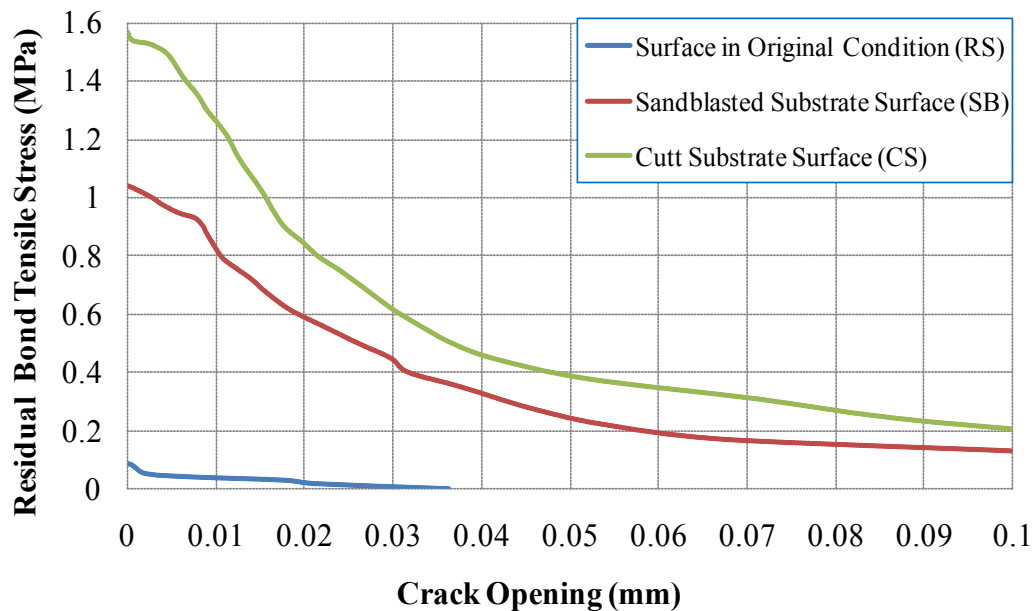


Figure III-13: Post Peak Bond Softening Behavior of overlay with different substrate surface textures

III.3.3 Summary

From the experimental results, it can be summarized that the surface roughness of substrate is a key parameter that can significantly increase the bond tensile strength perpendicular to the interface. For improving the substrate surface roughness, two surface preparation techniques are evaluated here. Although, maximum of this strength was obtained with the cut substrate surface, but it was decided to use sandblasted one in this research work. Since, sand blasting surface preparation technique is easy to implement in actual conditions instead of cutting the whole surface. So, keeping in view the improvement observed with the substrate surface preparation, it is also necessary to investigate the bond behaviour by using reference substrates (without any surface preparation) and sandblasted substrates with different types of repair mortar mixes.

III.4 BOND TENSILE STRENGTH BETWEEN UNTREATED SUBSTRATES AND DIFFERENT TYPE OF REPAIR MATERIALS

All types of studied mortar mix compositions (control mortar, rubberized mortar, fiber reinforced mortar and mortar containing both fibers and rubber aggregates) were cast as a repair material on top of these untreated substrates (reference substrates). Direct tension tests were carried out in order to evaluate the bond tensile strength between these untreated substrates and different type of repair materials. These tests show the bond tensile strength, strain capacity and also give an idea about the residual post peak strength. Also, one can get an idea that the incorporation of metallic fibers and rubber aggregates in the repair matrix has some impact on bond strength or not.

III.4.1 Results and Discussion

Results of the bond tensile test controlled by Crack Mouth Opening Displacement (CMOD) for different types of repair mortar mixes are presented in Figure III-14. This Figure III-14 indicates that bond tensile strength between untreated substrate and control mortar repair (CC) is very less than the one obtained with another type of repair materials. This negligible bond tensile strength between the untreated substrate and control mortar repair is caused by the presence of laitance (weak layer) on top of the substrate. And this improved bond strength with the other type of repair materials (rubberized and/or fiber reinforced mortar) is not due to the presence of rubber aggregates or fibers. Actually, this improvement in bond tensile

strength is an artifact, due to the necessity of using super-plasticizers (SP) and viscosity modifying agents (VMAs) in the mortars incorporating rubber aggregates and metallic fibers for ensuring proper workability and preventing the segregation of rubber aggregates. The high dosage of SP and VMAs in these repair materials impacts the material compatibility with the surface of the substrate. These repairs have a modified contact with the substrate and also cement slurry of these repair materials penetrate into porous substrate surface, which as a result, produces an enhanced bond between substrate and repair material.

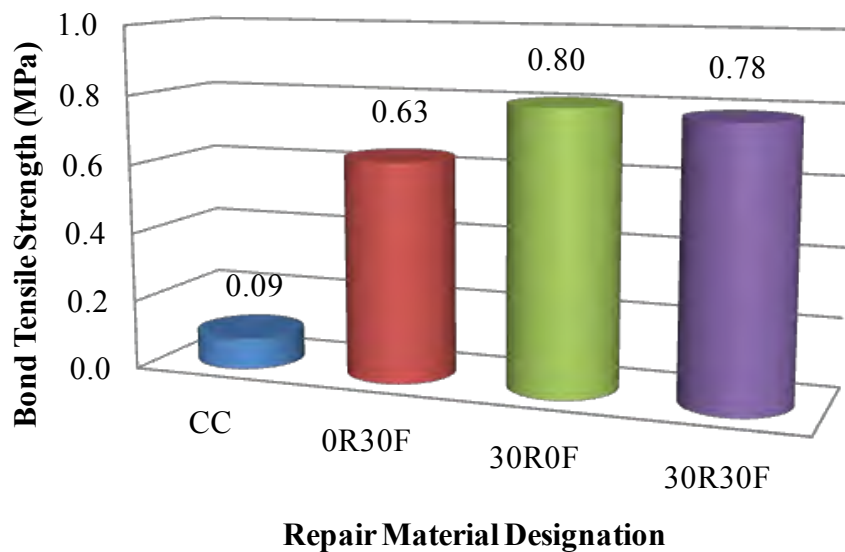


Figure III-14: Bond tensile strength variation with different repair materials

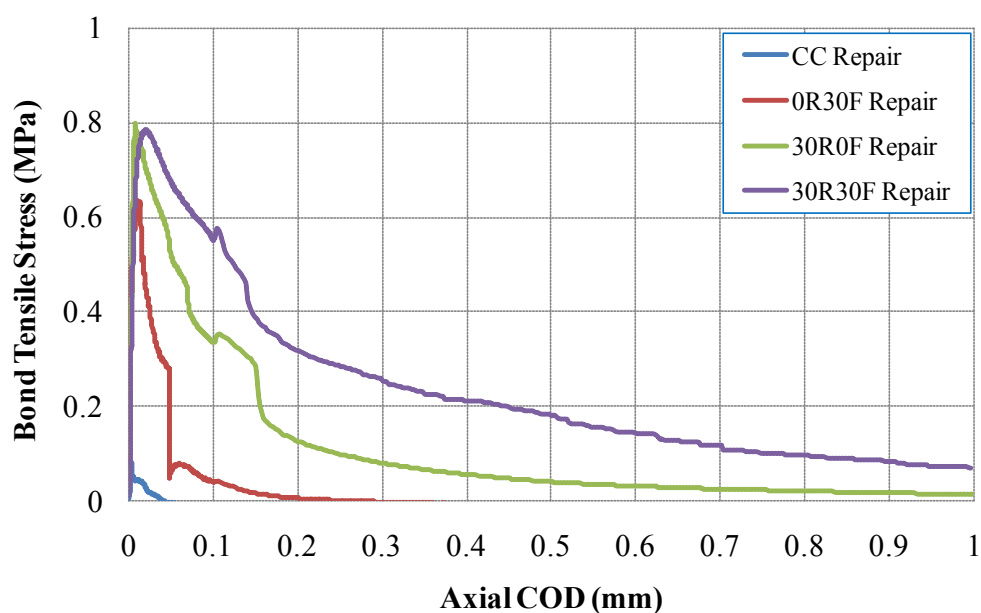


Figure III-15: Strain capacity behavior with different overlay repair materials

When tension tests were conducted on the specimens repaired with rubberized mortar (30R0F) or fiber-rubberized mortar (30R30F), it was noticed that failure started from interface location between repair and substrate, but the major damage occurs in the repair material as indicated in Figure III-16 and Figure III-20. This means that the bond tensile strength is more than the one of repair material. Results also show that the incorporation of metallic fibers along with the rubber aggregates in the repair material didn't significantly affect the bond tensile strength. Since, fibers didn't play their role effectively, because these fibers have no bond with the substrate mortar. The bond tensile strengths are almost same in specimens repaired with rubberized mortar (30R0F) and fiber-rubberized mortar (30R30F).

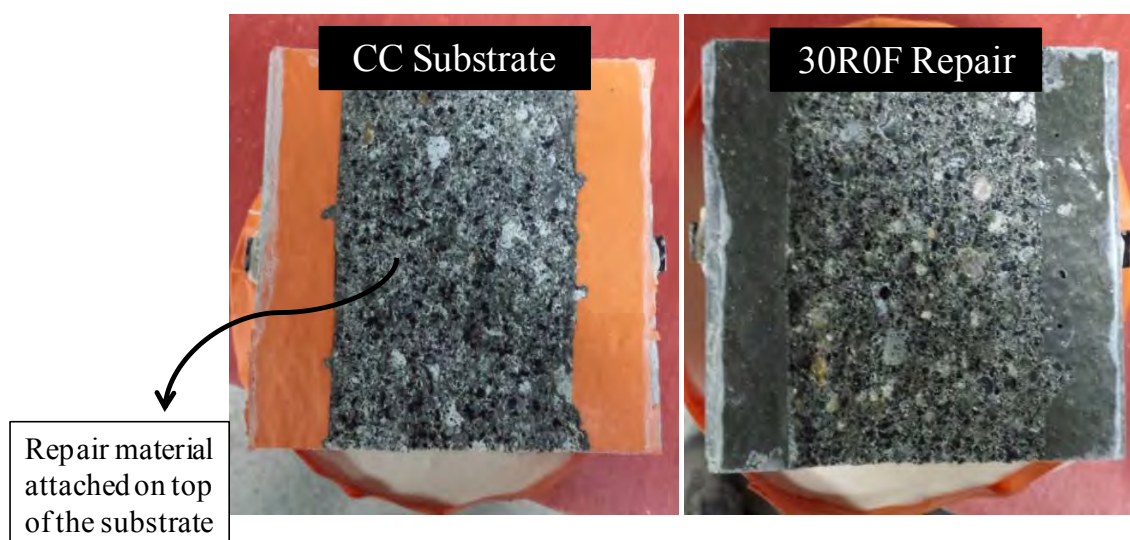


Figure III-16: View of broken sample with 30R0F repair, showing the fracture mainly occurred in the repair material

III.4.2 Summary

From the experimental results, it can be summarized that the improvement in bond tensile strength with fiber-reinforced and/or rubberized repair mortar is due to the addition of SP and VMAs, which are the necessary ingredients for these types of mortars in order to maintain required workability and to avoid segregation. Another noticeable thing is that the bond between control mortar repair and untreated substrate is almost negligible. Since, in the case of control mortar repair, high dosage of these admixtures was not used. And the poor bonding of control mortar repair with the untreated substrate is due to the presence of weak thin layer

of laitance (mortar slurry) on top of the substrate. In order to enhance the bond between repair and substrate, it is necessary to remove this weak portion from top of the substrate. There are different techniques available for removing this weak laitance layer from top of the substrate and to improve the substrate surface roughness. Sand blasting surface preparation technique is selected for improving the surface roughness. The bond behaviour between sandblasted substrates and different types of repair mortar mix compositions is described below.

III.5 BOND TENSILE STRENGTH BETWEEN SANBLASTED SUBSTRATES AND DIFFERENT TYPE OF REPAIR MATERIALS

In this section, the bond behaviour between sandblasted substrates and different types of repair materials has been investigated. The direct tension tests were conducted in order to evaluate the effectiveness of sand blasted substrates towards the bond improvement. Similar testing procedure as prescribed in section III.3 has been adopted for investigating the bond tensile strength.

III.5.1 Results and Discussion

The results of bond tensile tests for different repair mortar mixes laid on sandblasted substrates are presented in Figure III-17. Results show significant improvement in bond tensile strengths with prepared substrates (sandblasted substrates) as compared to the substrates used in original condition (untreated substrates). This improvement in bond tensile strength is due to enhanced mechanical interlocking between the repair material and the substrate. And this mechanical interlocking improves due to removal of top weak laitance layer through sandblasting technique. Also, a similar kind of failure pattern is observed in sandblasted substrates repaired with rubberized or fiber-rubberized mortar, as previously observed with untreated substrates. In these specimens, the failure initiated from the interface location between repair and substrate, but significant damage occurs in the repair material as shown in Figure III-16 and Figure III-20. It means, the obtained bond tensile strengths with these two types of repair materials is less than the actual bond strength at the interface. While conducting a tension test with these two types of repair materials, tensile strength of repair material arrived first as evident from Figure III-17 (0.98 MPa is equivalent to the tensile strength of rubberized mortar). And bond tensile strength at the interface is evidently more than repair material tensile strength. Due to this reason, the failure didn't occur exactly at interface location. This behaviour can also be verified from strain capacity curves shown in

Figure III-18 and Figure III-19. This improvement in strain capacity behaviour with 30R0F and 30R30F overlays is due to the fact that the failure occurs in repair material and rubber aggregates present in repair material play their role.

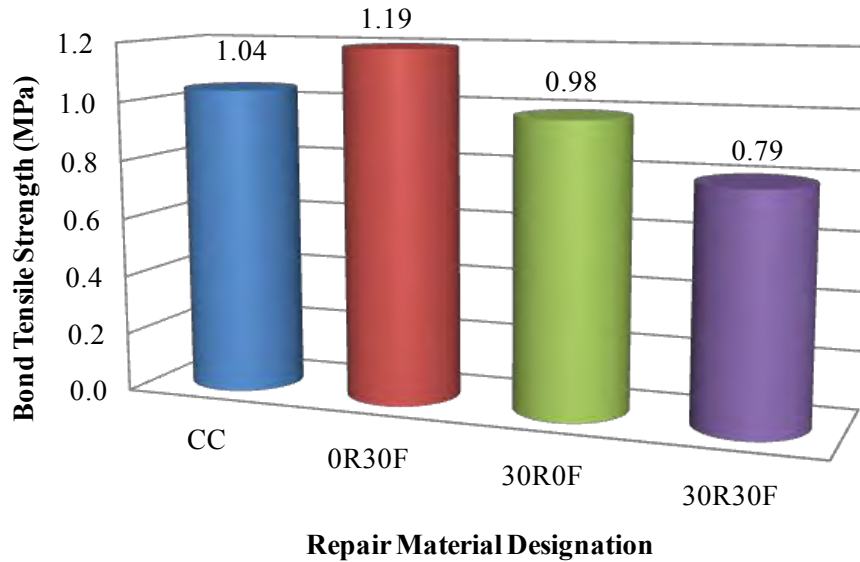


Figure III-17: Bond Tensile strength variation with different repair materials on sandblasted substrates

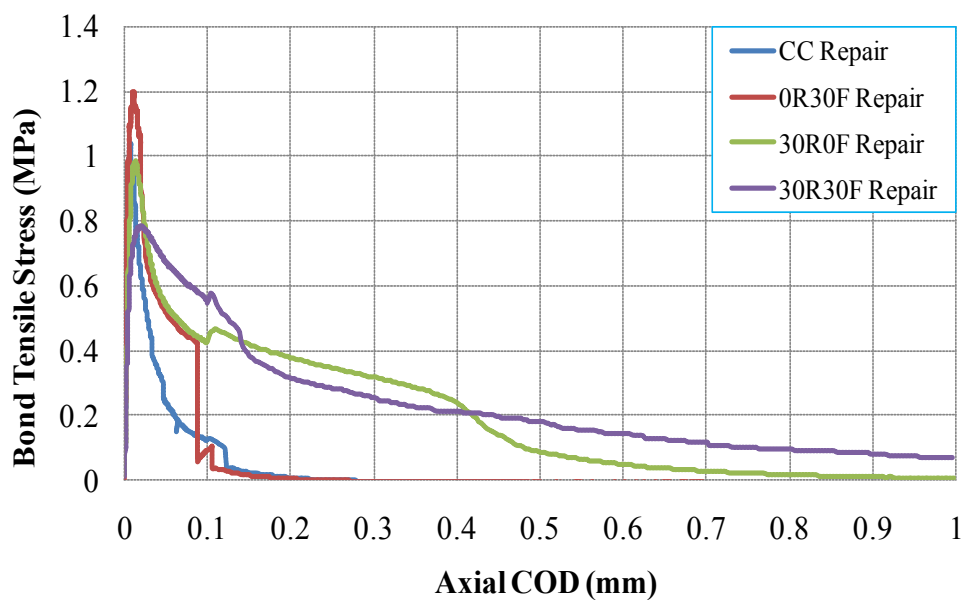


Figure III-18: Strain capacity behavior with different overlay repair materials on sandblasted substrates

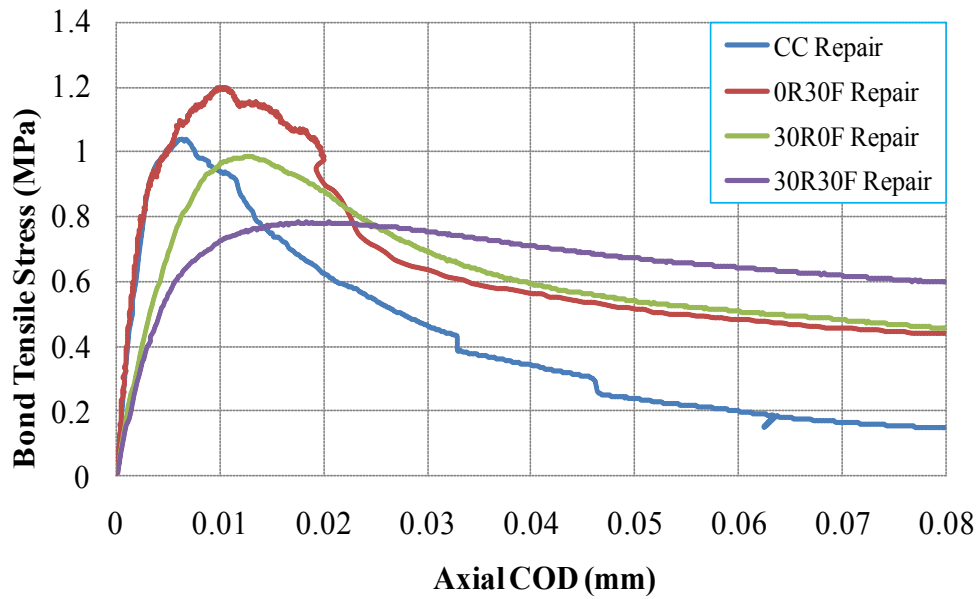


Figure III-19: Strain capacity behavior with different overlay repair materials on sandblasted substrates (enlarged view)

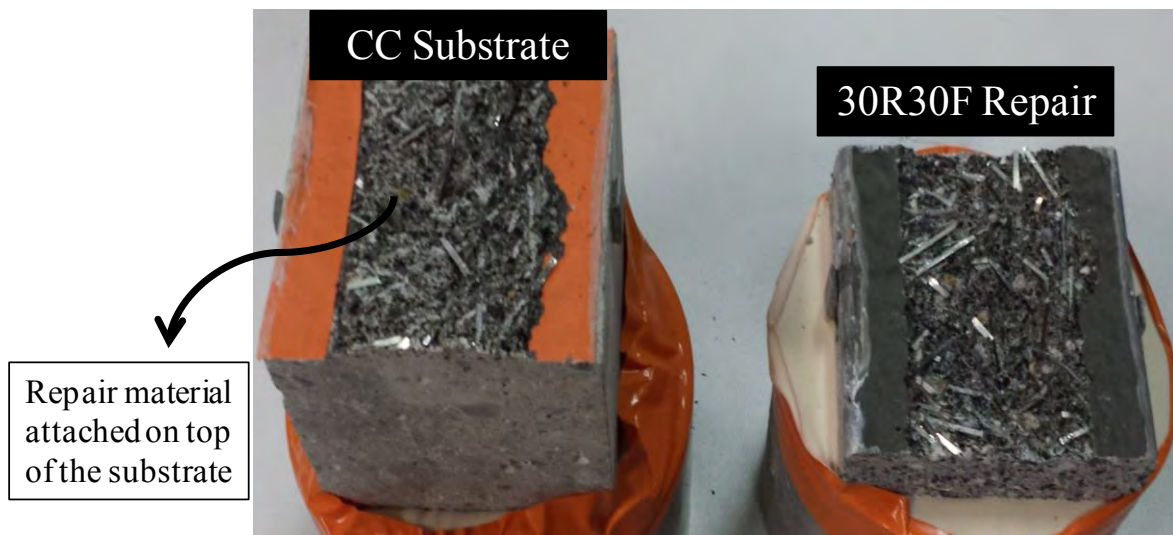


Figure III-20: View of broken sample with 30R30F repair, showing the fracture mainly occurred in the repair material

III.5.2 Summary

From the experimental investigation, it can be summarized that a significant improvement in bond tensile strength is observed by surface preparation of substrate as compared to the substrate used without any preparation (untreated substrates). This improvement in the bond tensile strength is because of enhanced mechanical interlocking between repair material and substrate. Results also show that the presence of metallic fibers alone or in combination with rubber aggregates in repair material has no significant impact on the bond tensile strength. Since, these fibers didn't play their role effectively, because these fibers have no bond with the substrate mortar.

III.6 CONCLUDING REMARKS


This chapter reports the impact of substrate surface preparation on its bond with thin bonded cement-based repairs. Tension tests were conducted to quantify the bond strength. The following conclusions can be drawn from the experimental program:

- ✚ The bond strength improvement in repair system by substrate surface preparation depends upon the selection of surface preparation technique, since each technique has its own efficiency level notably with regard to the surface roughness. Among the selected surface preparation techniques, more bond strength improvement is observed with sawed substrates in comparison with the sandblasted one.
- ✚ Repairs cast on top of sawed or sand blasted surfaces also show some improvement in strain capacity. This improvement in strain capacity is due to the creation of small grooves on treated surface while operating these techniques. Actually, while removing the top weak layer, some particle may also be chipped-off from the top surface and create grooves. Also, by removing the top layer of substrate, internal air voids which already present within the substrate come on top of the substrate surface. So, after casting repair on top of these treated substrates, repair material penetrates inside of these grooves with additional epitaxial growth and creates an anchorage between repair and substrate surface and improves post peak strain capacity.
- ✚ Sudden drop of post peak residual tensile strengths occurs in specimens with control mortar (CC) and 0R30F repair material. Also, brittle failure is observed with these two

types of repair materials. However, an improvement in the softening behaviour is observed with 30R0F and 30R30F overlays.

- ✚ Sand blasting surface preparation technique can be easily employed in practical field conditions as compared to sawing. Since, it is difficult to saw a complete top portion in large area application. Due to this reason, the sandblasted substrates are selected for evaluating the durability of thin-bonded cement-based repairs.

The effect of using rubber aggregates and fibers on mechanical characteristics has been described in chapter II. The impact of substrate surface preparation on bond behaviour is discussed in this chapter. In order to utilize the rubberized and/or fiber-reinforced mortar as a repair material in thin bonded cement-based overlays, it is also necessary to investigate the behaviour of these mortar mix compositions in fatigue. Since, overlay structures are always subjected to fatigue loading in actual conditions. So, in the next chapter, the behaviour of fiber-reinforced and/or rubberized mortar is evaluated under tensile fatigue loading. The cyclic bridging degradation of residual post cracking strengths is determined for the studied mortar mix compositions.



Chapter IV
FIBER REINFORCED AND
RUBBERIZED MORTAR UNDER
TENSILE FATIGUE LOADING

IV. FIBER REINFORCED AND RUBBERIZED MORTAR UNDER TENSILE FATIGUE LOADING

IV.1 INTRODUCTION

Fiber-reinforcement and rubber aggregates incorporation can favorably modify the mechanical behavior of concrete in particular its residual post cracking strength and strain capacity. In this regard, a positive synergetic effect with material bridging can be expected. However, in actual cases, fatigue loading is more relevant. Under these conditions, understanding the contribution of fiber-reinforcement and of rubber aggregates necessarily involves knowledge of the degradation of the residual post-cracking resistance under fatigue loading.

Some previous theoretical studies (D.H. Dauskardt et al., 1993; T. Matsumoto and V.C. Li., 1996) revealed that fatigue crack growth in fiber-reinforced cement-based materials seems to be governed by two mechanisms. First, is the fatigue law governing the growth of the matrix crack tip as a function of the variation of an effective stress intensity factor. Second is the fiber bridging law governing the zone behind the matrix crack and also on the law governing the degradation of the crack bridging with the number of loading cycles. With respect to the fatigue law governing the growth of the matrix crack tip, the traditional formulation of Paris law (P. Paris and F. Erdogan., 1963) has been used in previous works on cementitious materials. At present, data to describe the degradation of the fiber or rubber particle bridging with matrix under cyclic loading is insufficient. Normally, it can be assumed that this degradation in bridging strength is primarily due to interface bond degradation between fiber and matrix. Although, some other mechanisms can also happen, such as fatigue failure of fibers in tension/bending during opening of crack. Similarly, fatigue loading also produces compression/bending in fibers during closing of crack which subsequently produce buckling in non-metallic fibers (G. Bao and R.M. McMeeking., 1991; H.C. Wu et al., 1994).

Experimental fatigue performance of fiber-reinforced materials has been carried out in some recent researches (V. Ramakrishan and G. Oberling., 1987; D.E. Otter and A.E. Naaman.,

1988; M. Grzybowski and C. Meyer., 1993; J. Zhang and H. Stang., 1998). Mainly empirical approaches have been conducted in order to predict and design the fatigue life of FRC structures. Processing of these types of empirical approaches requires certain data collection, which is time consuming and practically difficult to apply in real design cases. J. Zhang (J. Zhang et al., 2000; J. Zhang., 2001) carried out experimental studies on FRCs for evaluating bridging behaviour under uniaxial fatigue tension. The experimental results show a reduction in bridging strength with the number of loading cycles.

In this chapter, the primary objective is to establish the cyclic bridging law, the so-called stress-crack width relationship under tensile fatigue load, which is capable to predict cyclic crack bridging behaviour of composite materials, especially for fiber-reinforced and/or rubberized mortar.

IV.2 CRACK BRIDGING DEGRADATION OF FIBER REINFORCED AND RUBBERIZED MORTAR UNDER FATIGUE TENSION

In order to investigate the cyclic crack bridging behaviour of fiber reinforced and/or rubberized mortar, uniaxial tensile fatigue tests controlled by crack mouth opening displacement method (CMOD) were conducted. The uniaxial tensile fatigue tests were conducted on prismatic pre-notched specimens as shown in Figure IV-1. The crack opening was measured by using two standard MTS COD clips attached on two faces as shown in Figure IV-3. The test was carried out on MTS 100 kN testing machine equipped with closed-loop testing. The complete experimental testing set-up is shown in Figure IV-2.

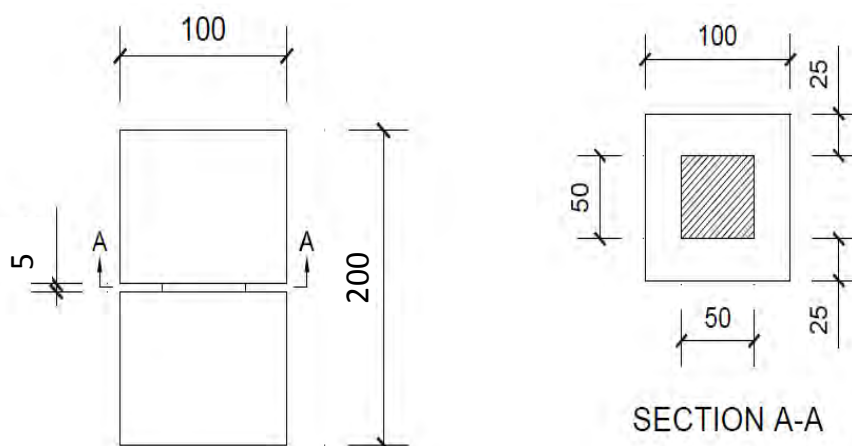


Figure IV-1: Notched test specimen for uniaxial tensile fatigue tests (dimensions are in mm)

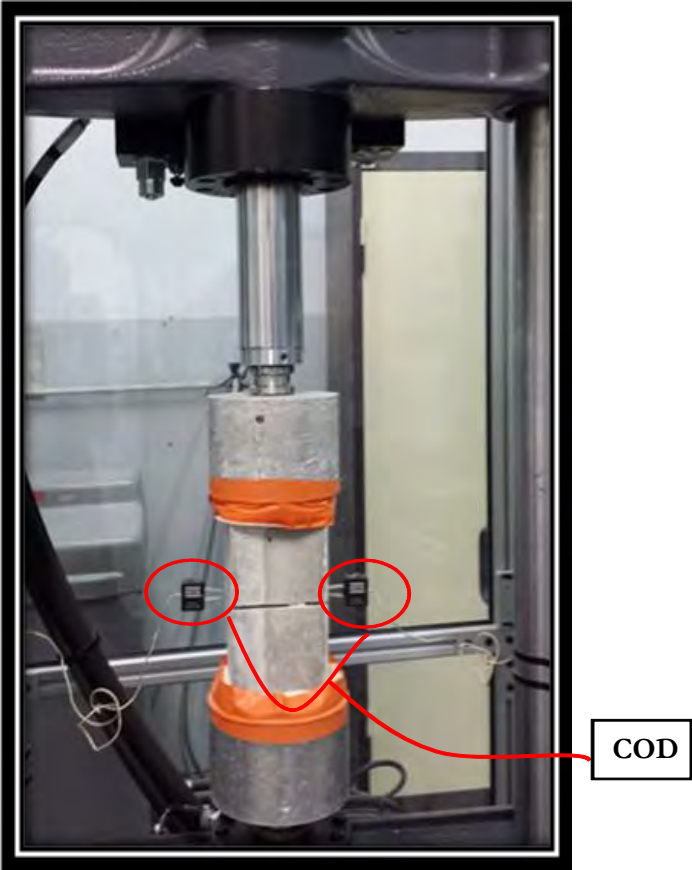


Figure IV-2: Complete experimental testing set-up for conducting uniaxial fatigue tension test

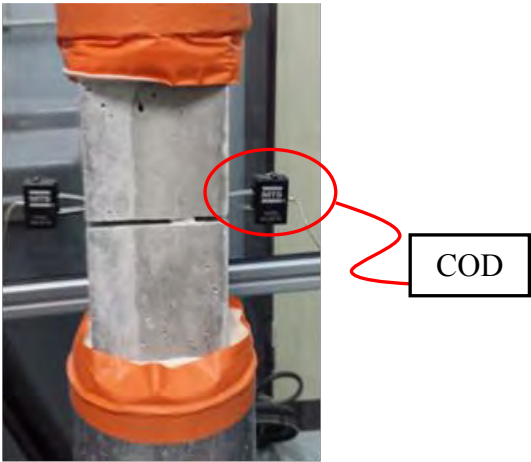


Figure IV-3: COD attached at notch

IV.2.1 Testing Procedure

The uniaxial tensile fatigue tests were conducted on the prismatic pre-notched specimen shown in Figure IV-2. Similar procedure was adopted for sample fixation on interchangeable steel blocks by using fast curing glue as previously done in simple direct tension test. Firstly, the direct tension tests were conducted for each mix composition in order to access the peak load and the corresponding crack opening value. After that, control mortar (CC) is taken as a reference as shown in Figure IV-4. With reference to peak COD of control mortar, two COD values were selected as pre-cracked width (COD_{max}) for fatigue loading. One before peak COD and second after peak COD. A uniaxial tensile fatigue test was conducted between this maximum pre-cracked width (COD_{max}) and zero load. The above selected two COD_{max} values for control mortar (reference mortar) was used not only for control mortar but also for other mortar mixes in order to make comparison in degradation of bridging strength under tensile fatigue load. A fatigue loading with 5Hz frequency is conducted between this COD_{max} value and zero load.

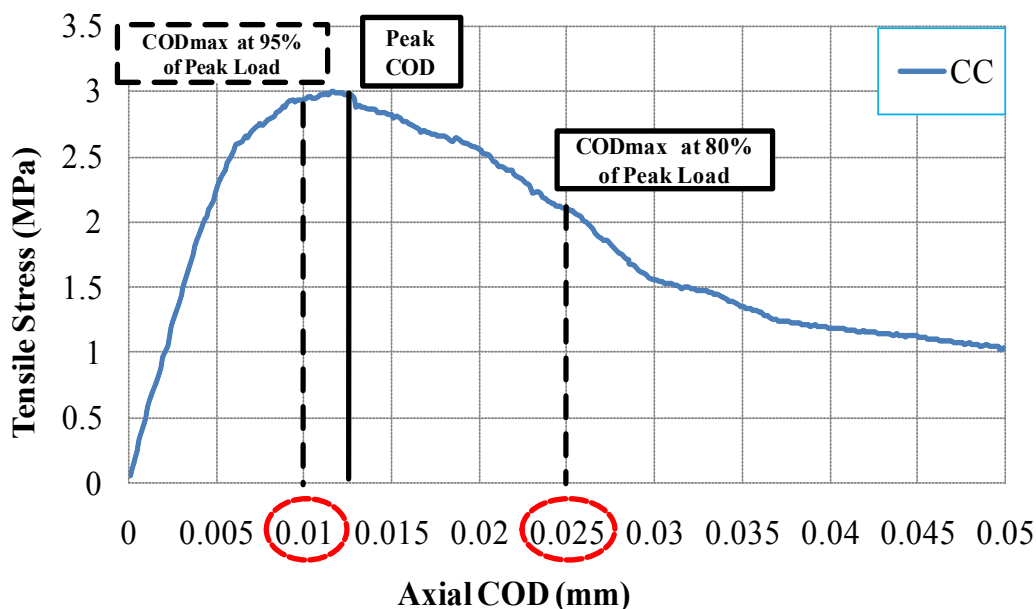


Figure IV-4: Selection of COD_{max} for tensile fatigue loading corresponding to control mortar

Here, two maximum crack widths, i.e. 0.010 mm and 0.025 mm were analyzed. An example of the testing procedure for COD_{max} equal 0.025 mm with control mortar is described below: Firstly, control mortar sample was loaded upto pre-defined crack width value (0.025mm) in direct tension as shown in Figure V-5. After reaching this predefined crack width value (COD_{max}), fatigue loading with a constant frequency of 5 Hz was applied between COD_{max} value and zero load for 10000 number of cycles. Figure IV-6 shows the typical loading-unloading loops of control mortar under uniaxial tensile fatigue loading. Figure IV-7 shows the maximum bridging strength degradation of control mortar under fatigue loading. In Figure IV-8, the maximum bridging strength corresponding to the maximum crack width is normalized to the strength level at first cycle.

The similar approach is adopted for the other mortar mixes with the two maximum CODs, i.e. 0.01 and 0.025 mm.

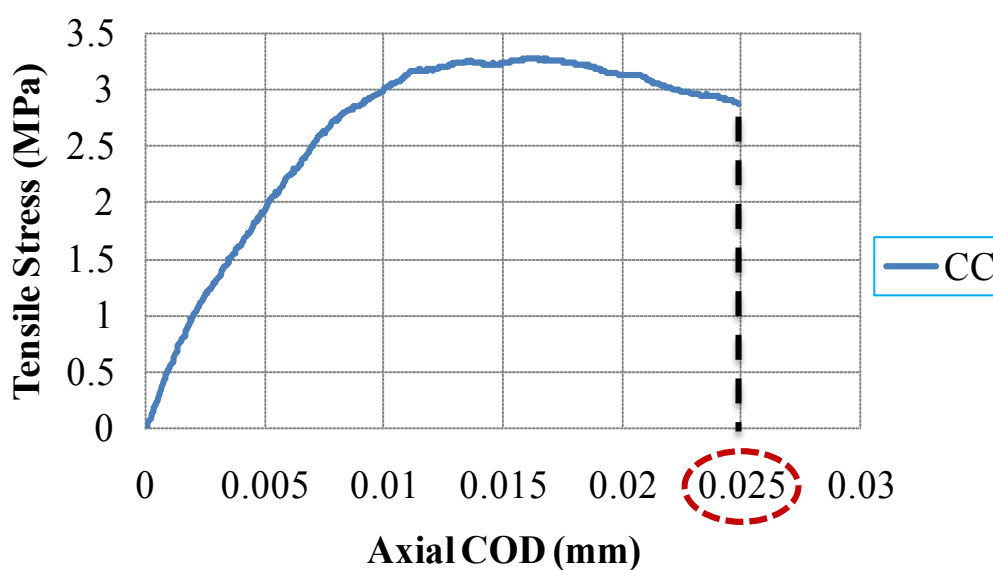


Figure IV-5: Direct tension test upto $COD_{max} = 0.025$ mm

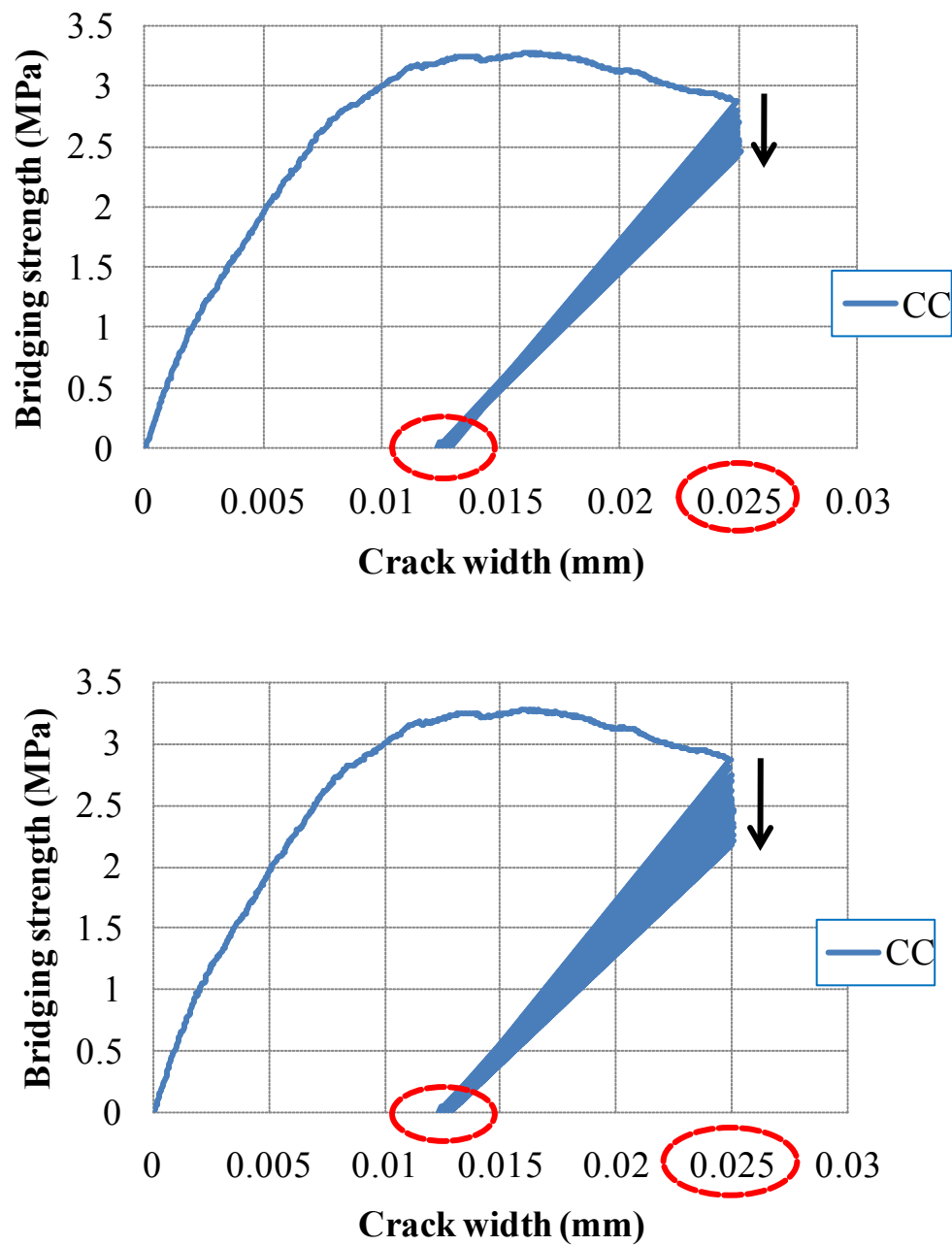


Figure IV-6: Typical loading - unloading loops of crack bridging strength under cyclic loading for control mortar

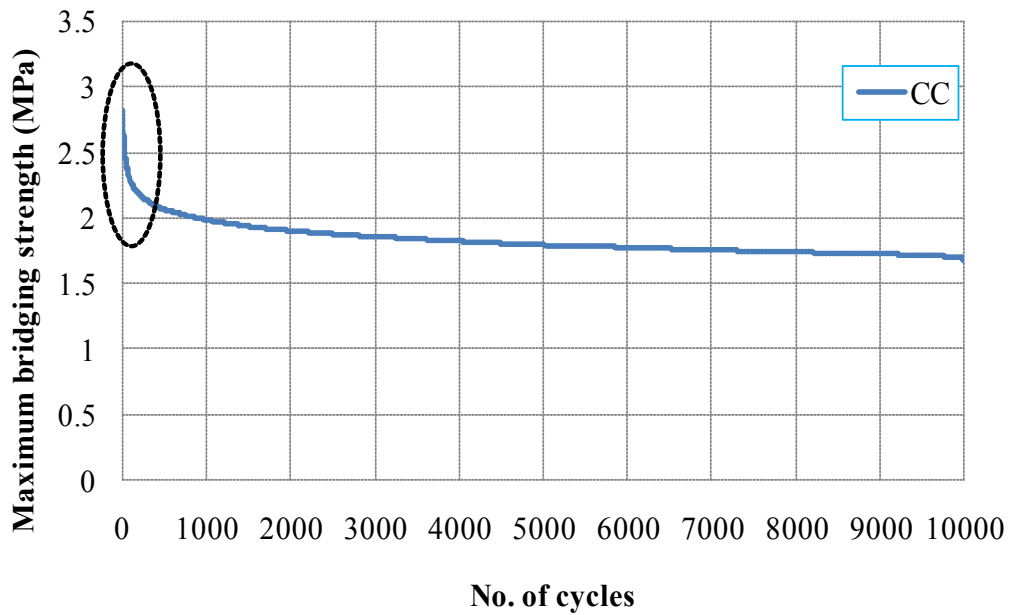


Figure IV-7: Test results of maximum bridging strength vs. number of cycles for control mortar corresponding to $COD_{max} = 0.025$ mm

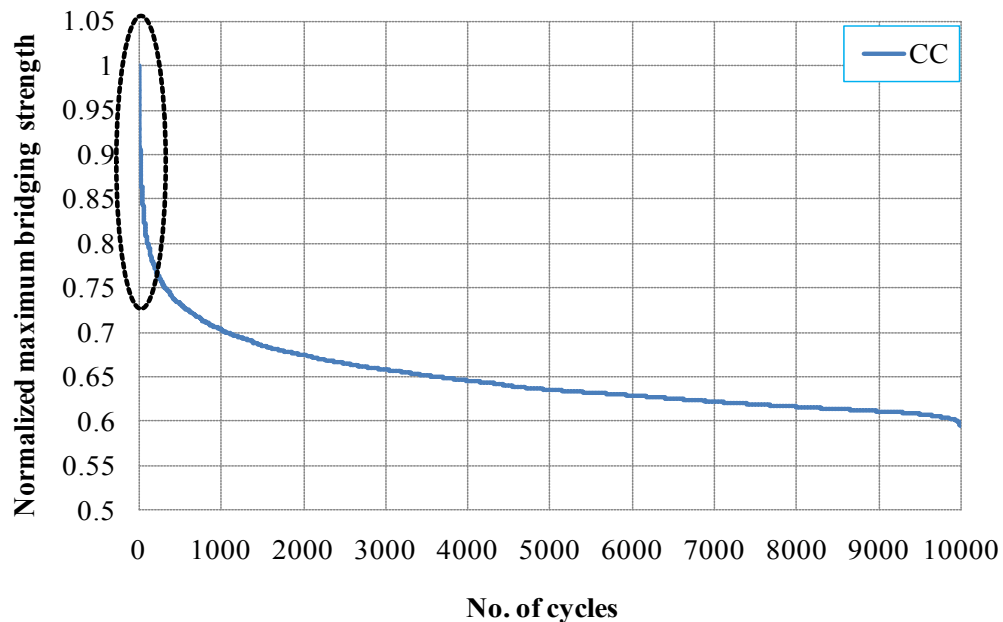


Figure IV-8: Test results of normalized maximum bridging strength vs. number of cycles for control mortar corresponding to $COD_{max} = 0.025$ mm

IV.2.2 Results and discussion

Results show that the maximum material crack bridging degradation occurs in control mortar (0R0F), whatever the value of maximum crack width. The same trend is observed in mortar with rubber aggregates only, i.e. 30R0F for large pre-cracked width value which is also evident from Figure IV-9. However, for less maximum crack width, i.e. 0.01mm, cyclic bridging strength degradation seems to be limited as shown in Figure IV-12. Since, the rubber aggregates incorporation in a mortar improves significantly the strain capacity and at less pre-cracked width value the load is always less than the peak load. So, this extra margin before peak load provides more bridging under cyclic loading.

The incorporation of metallic fibers in the mortar (0R30F) tends to limit the cyclic bridging strength degradation for large crack widths. The reason behind is that these types of metallic fibers require certain crack opening in order to play their role. That's why at less pre cracked width value, i.e. 0.01mm, more cyclic bridging strength degradation is observed as compared to large pre-cracked width value (0.025mm). Since, crack width opening of 0.010 mm is a bit less for this type of metallic fibers in order to play their role.

Moreover, a mortar mix incorporating both rubber aggregates and metallic fibers (30R30F) appeared as a suitable mix composite to limit the cyclic bridging strength degradation at a wide range of pre-cracked width values. This is due to the double bridging action provided by rubber aggregates as well as fibers. At less pre-cracked width value, rubber aggregates provide bridging and at large pre-cracked width value, fibers play their role. So, the composite matrix containing both rubber aggregates and fibers is found helpful to limit bridging strength degradation at different pre-cracked widths. Figure IV-11 and Figure IV-14 show the normalized maximum bridging strength degradation values in different mortar mixes at 10^4 cycles, corresponding to maximum crack widths of 0.010 mm and 0.025 mm respectively. Figure IV-10 and Figure IV-13 represent the relationship between normalized maximum bridging strength and number of fatigue load cycles on a logarithmic scale corresponding to the maximum crack width of 0.010 mm and 0.025 mm respectively. Figure IV-15 shows the comparison of normalized maximum bridging strength degradation values in different mortar mixes corresponding to different pre-cracked width values at 10^4 cycles.

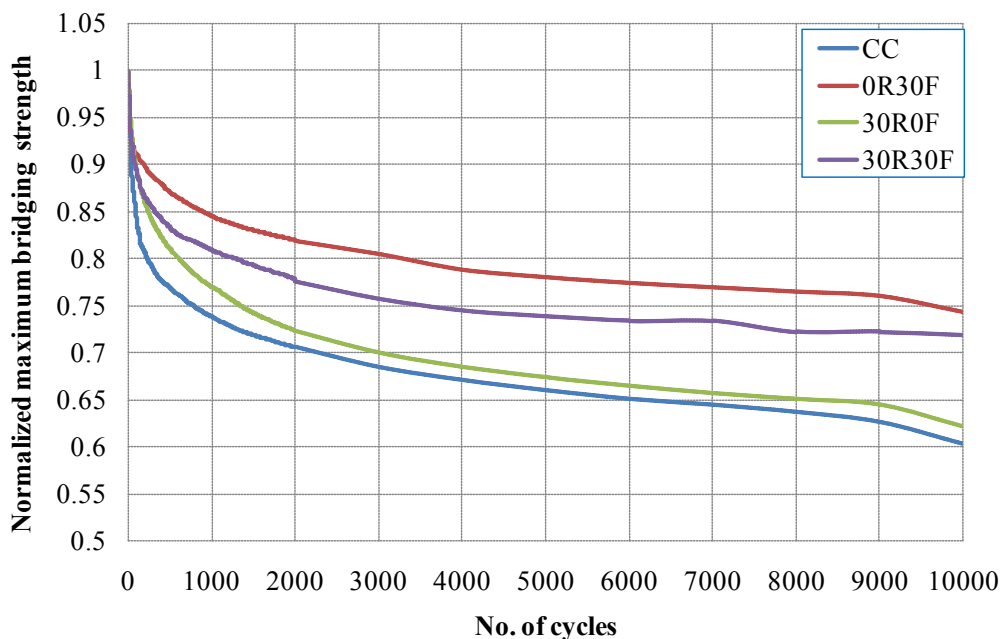


Figure IV-9: Relationship between normalized maximum bridging strength and number of fatigue cycles corresponding to $COD_{max} = 0.025$ mm

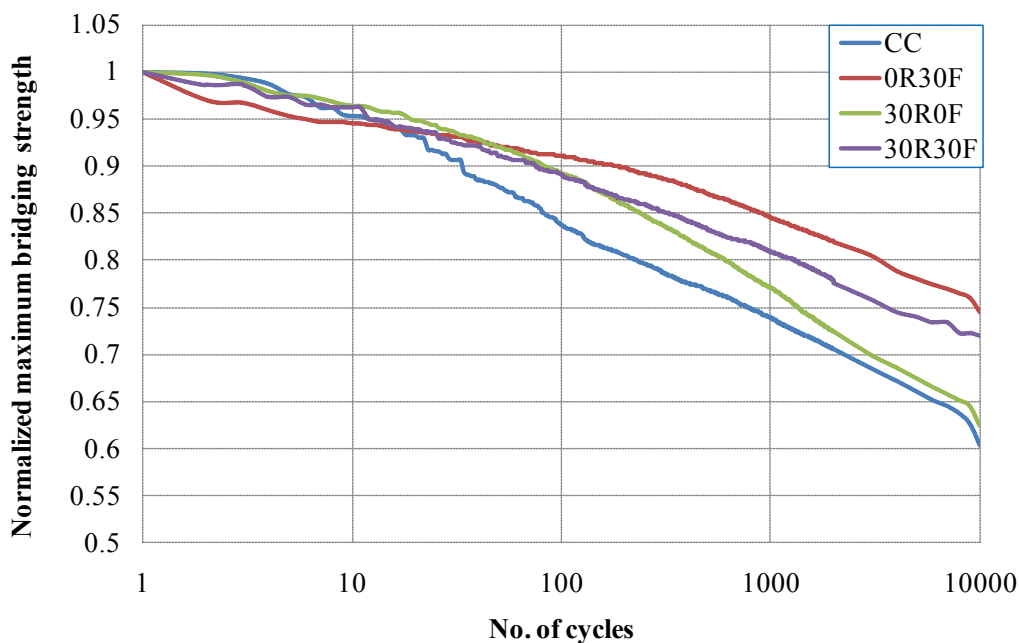


Figure IV-10: Relationship between normalized maximum bridging strength and number of fatigue cycles corresponding to $COD_{max} = 0.025$ mm on logarithmic scale

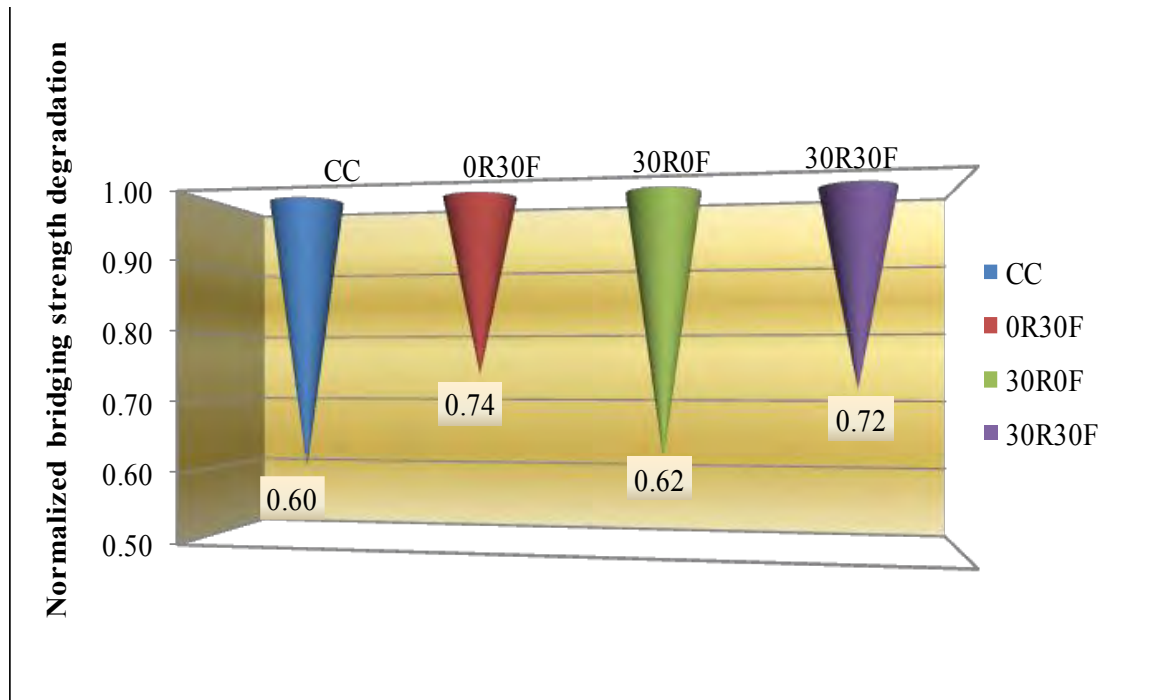


Figure IV-11: Normalized maximum bridging strength degradation values in different mortar mixes corresponding to $COD_{max} = 0.025$ mm at 10^4 cycles

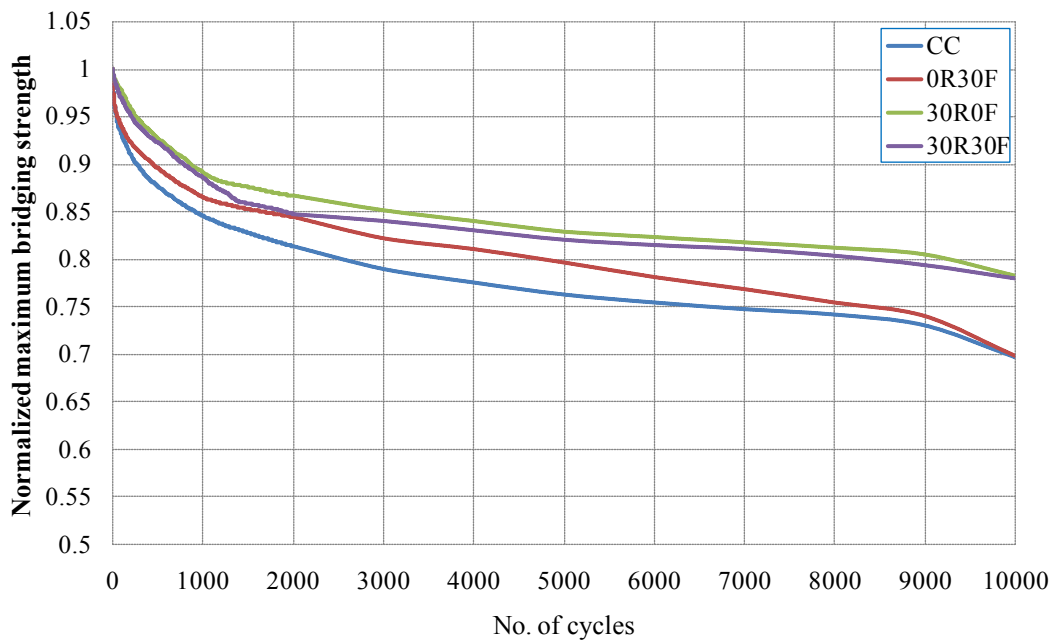


Figure IV-12: Relationship between normalized maximum bridging strength and number of fatigue cycles corresponding to $COD_{max} = 0.010$ mm

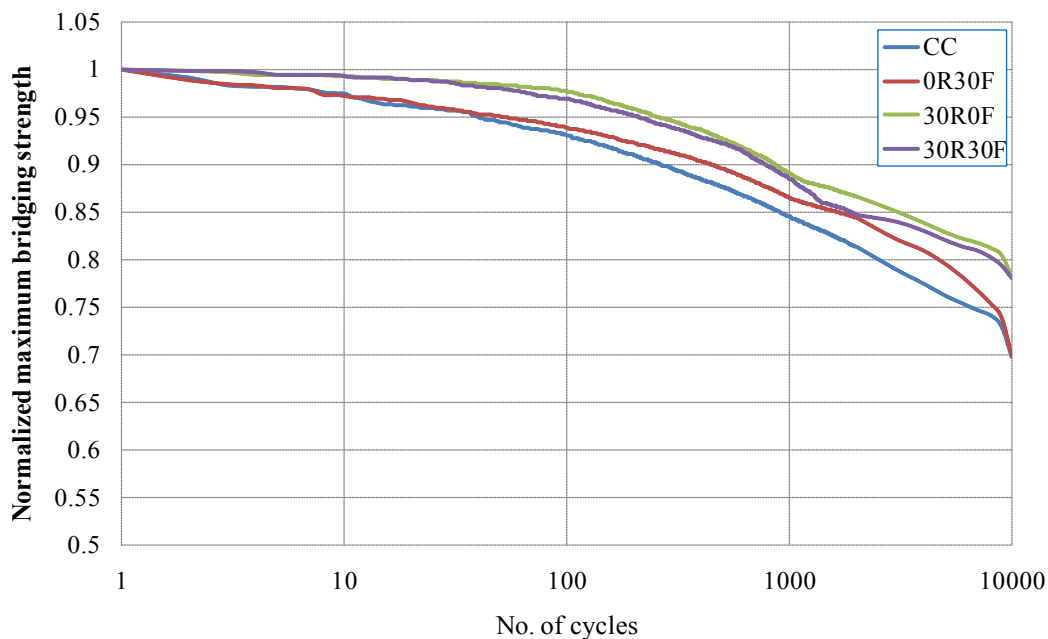


Figure IV-13: Relationship between normalized maximum bridging strength and number of fatigue cycles corresponding to $COD_{max} = 0.010$ mm on logarithmic scale

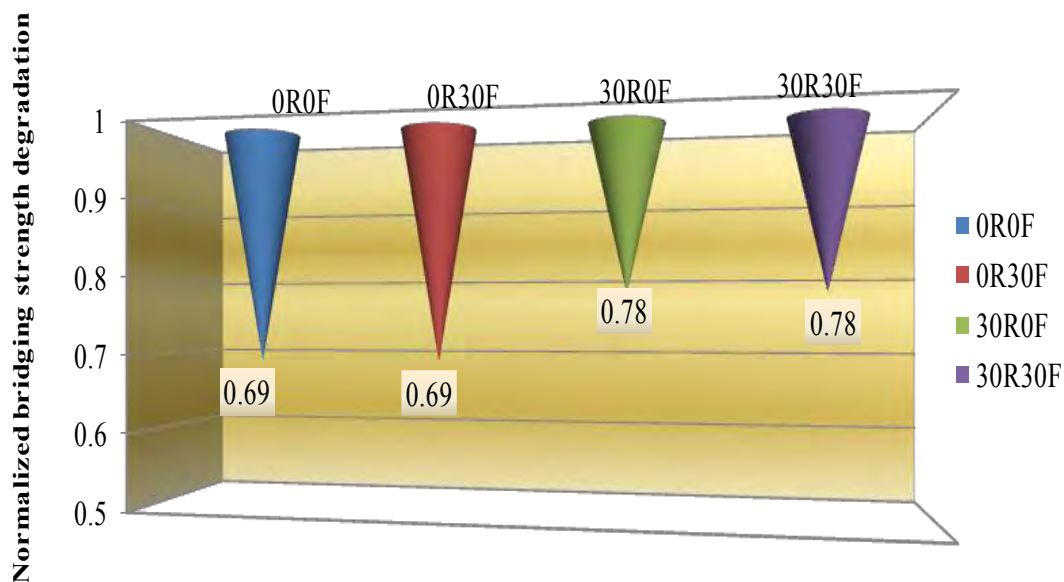


Figure IV-14: Normalized maximum bridging strength degradation values in different mortar mixes corresponding to $COD_{max} = 0.010$ mm at 10^4 cycles

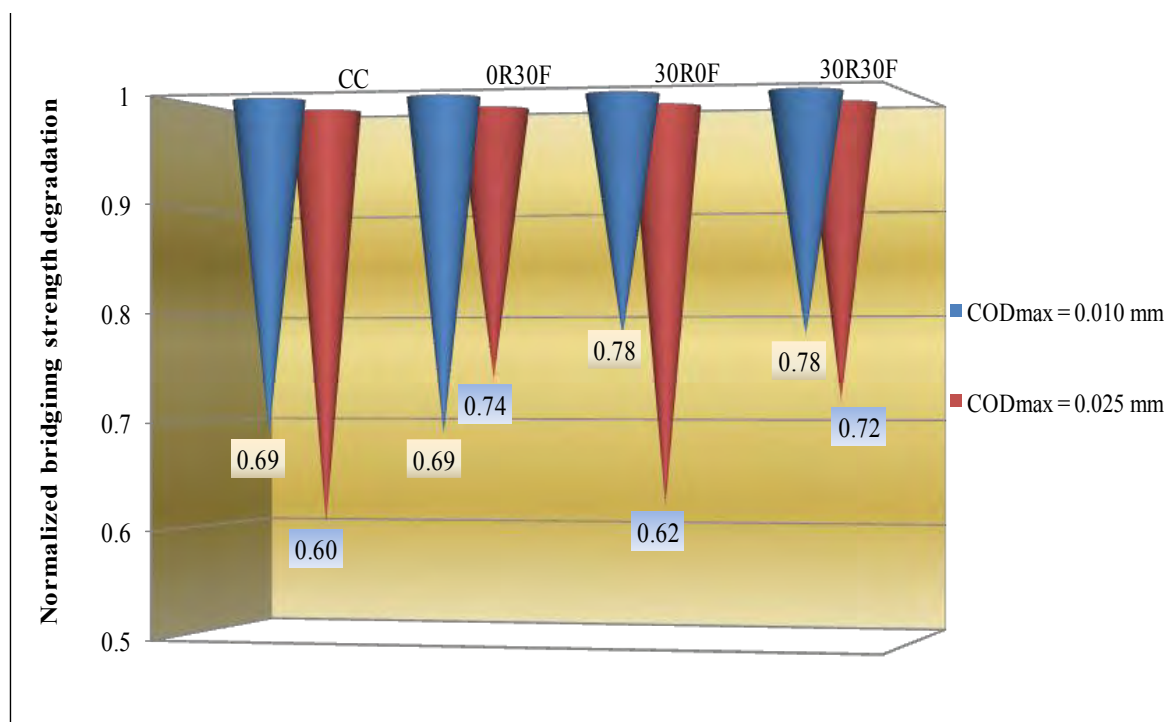


Figure IV-15: Comparison of normalized maximum bridging strength degradation values in different mortar mixes, corresponding to different pre-cracked widths (COD_{max}) at 10^4 cycles

The degradation curves of different mortar mixes are presented in Figure IV-16, where the maximum bridging strength corresponding to the maximum crack width is normalized to the strength level at first cycle. Experimental results of uniaxial tensile fatigue tests on pre-cracked plain mortar and fiber-rubberized ones show that the bridging strength decreases with the number of load cycles for the same maximum crack openings.

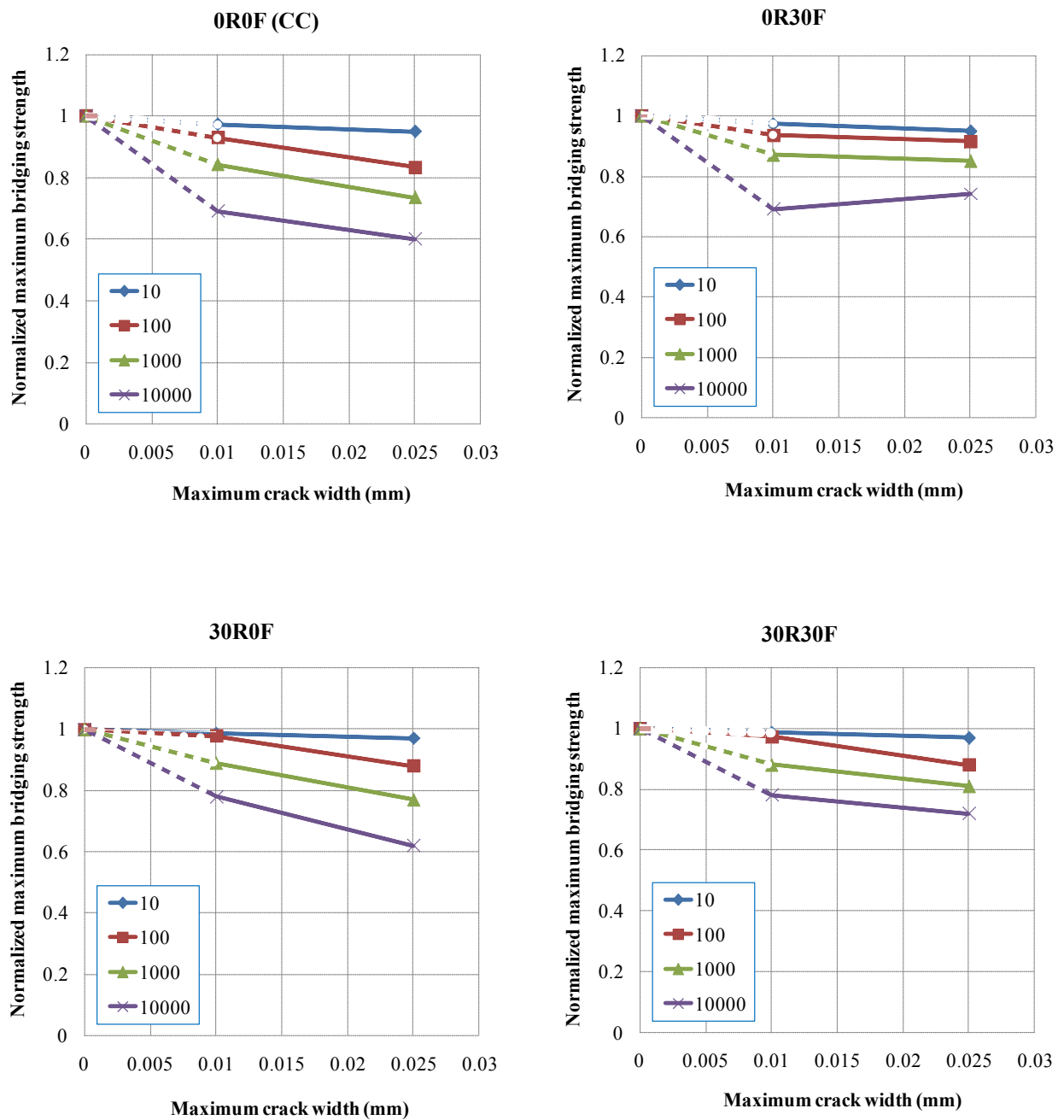


Figure IV-16: Relationship between normalized maximum bridging strength and maximum crack width for different mortar mixes, showing results after 10, 10², 10³ and 10⁴ cycles, respectively

IV.2.3 Highlights

This experimentation is focused on the development of cyclic bridging law which is capable to predict the fatigue degradation behaviour of composite materials, especially for fiber-reinforced and/or rubberized mortar. Based on the experimental results, the following conclusions can be drawn:

- ✚ Bridging strength decreases with the number of fatigue cycles for the same maximum crack width, whatever the nature of the composite.
- ✚ The maximum material crack bridging degradation occurs in plain mortar.
- ✚ The cyclic bridging strength degradation for large pre-cracked widths is limited for mortar with metal fibers.
- ✚ In case of rubberized mortar, cyclic bridging degradation is limited at less pre-cracked width value.
- ✚ A combine use of rubber aggregates and metallic fibers in mortar appeared to be a suitable solution to limit the cyclic bridging strength degradation for a wide range of pre-cracked widths.

IV.3 INTERFACIAL BOND DEGRADATION IN THIN BONDED CEMENT-BASED OVERLAYS UNDER FATIGUE TENSION

In order to investigate the interfacial bond degradation under fatigue loading, similar types of specimens are selected as used in bond tensile strength evaluation. Four different mortar mix compositions were selected to use as a repair material; reference mortar (0R0F), mortar containing fibers only (0R30F), mortar with rubber aggregates only (3R0F) and mortar mix containing both rubber aggregates and fibers (3R30F). The objective of conducting these tests is to study the influence of using different type of repair materials on interfacial bond strength degradation under fatigue tension.

IV.3.1 Testing Procedure

For interfacial bond strength degradation, similar testing procedure was adopted as conducted above for determining the material cyclic bridging strength degradation. The tensile fatigue

tests were conducted on the prismatic pre-notched specimen as shown in Figure IV-17. Also, the procedure for sample fixation on interchangeable steel blocks by using fast curing glue is the same as previously described in simple bond tensile strength evaluation. The complete experimental testing set-up is shown in Figure IV-18.

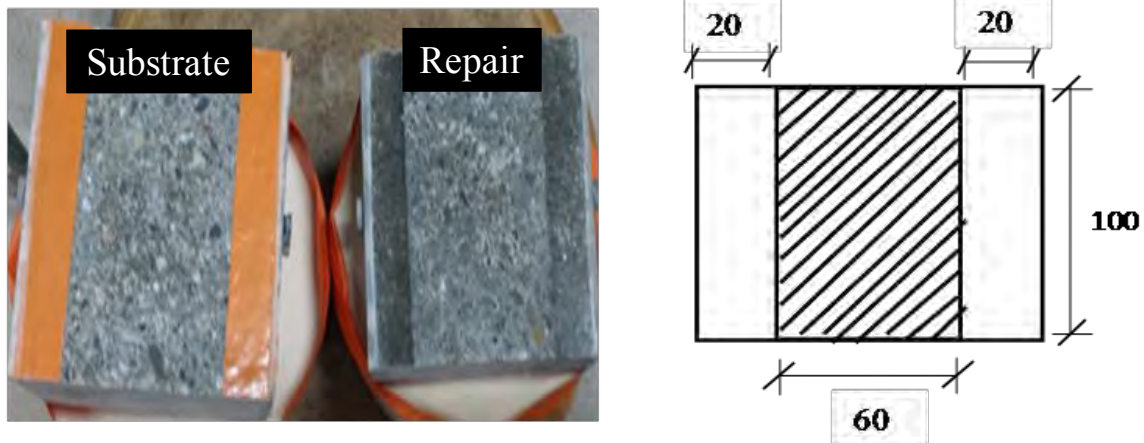


Figure IV-17: Notched specimen for interfacial bond strength degradation (dimensions are in mm)



Figure IV-18: Complete experimental testing set-up for determining interfacial bond strength degradation

Minimum three bond tensile tests were conducted for each type of overlaid composite specimen in order to access the peak load and the corresponding crack opening value. After that, overlaid specimen with control mortar repair is taken as a reference as shown in Figure IV-19. With reference to peak COD, two COD values, i.e. 0.010 mm and 0.020 mm were selected as pre-cracked opening width (COD_{max}) for fatigue loading. A uniaxial tensile fatigue test was conducted between this maximum pre-cracked opening (COD_{max}) and zero load. The above selected two COD_{max} values were not only used for specimens with control mortar repair, but also used for other overlaid composite specimens with different repair mortar mixes in order to make a comparison in interfacial bond strength degradation. Fatigue loading with a constant frequency of 5 Hz was applied between COD_{max} value and zero load for 10000 number of cycles.

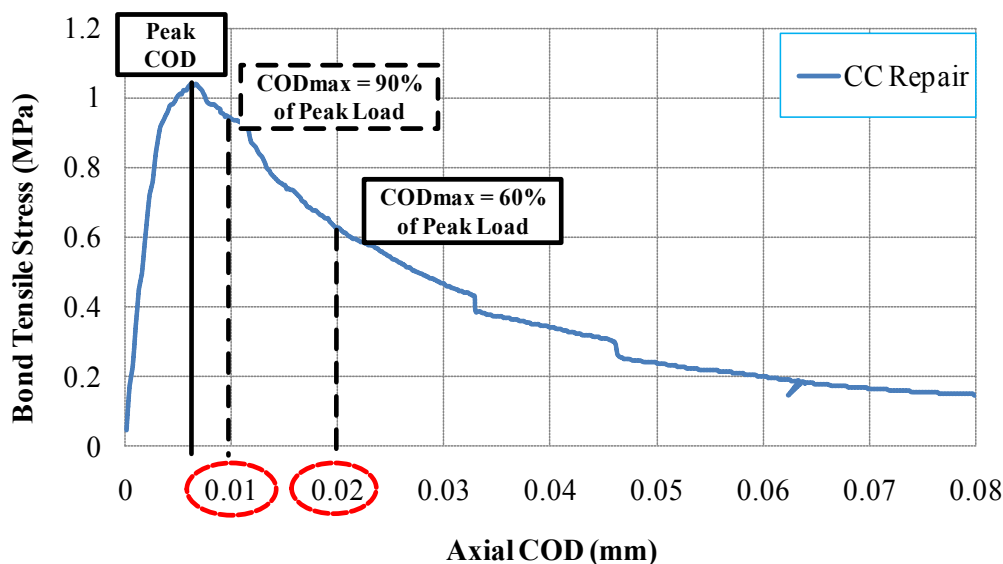


Figure IV-19: Selection of COD_{max} for tensile fatigue loading corresponding to control mortar repair

IV.3.2 Results and discussion

Results show that the maximum interfacial bond strength degradation occurs in specimens with control mortar (CC) repair, whatever is the value of maximum crack width. The same trend is observed in specimens with fiber reinforced repair material (OR30F) for both pre-cracked width values as shown in Figure IV-21 and Figure IV-24.

However, the cyclic bond strength degradation seems to be limited for rubberized repair (30R0F), where failure didn't occur exactly at the interface. Indeed, the crack initiated from notch, but major failure occurs in the repair material as it is also evident from the broken sample as shown in Figure IV-20. So, due to this reason, the failure at interface with rubberized repair is not as brittle as in case of control mortar and fiber reinforced repairs.

Moreover, the cyclic bond degradation behaviour of specimens repaired with material containing both rubber aggregates and fiber-reinforcement (30R30F) is quite similar to the behaviour of specimens repaired with rubberized mortar (30R0F). This shows that the presence of metallic fibers alone or in combination with rubber aggregates in repair material has no significant impact on bond behaviour. Since fibers didn't play their role because these fibers have no bond with the substrate. Figure IV-23 and Figure IV-26 show the normalized maximum bond strength degradation values in specimens with different repair materials at 10^4 cycles, corresponding to maximum crack widths of 0.010 mm and 0.020 mm, respectively. Figure IV-22 and Figure IV-25 represent the relationship between normalized maximum bond strength and number of fatigue cycles on a logarithmic scale corresponding to the maximum crack width of 0.010 mm and 0.020 mm, respectively. Figure IV-27 shows the comparison of normalized maximum bond strength degradation values in specimens repaired with different mortar mixes corresponding to different pre-cracked width values at 10^4 cycles.

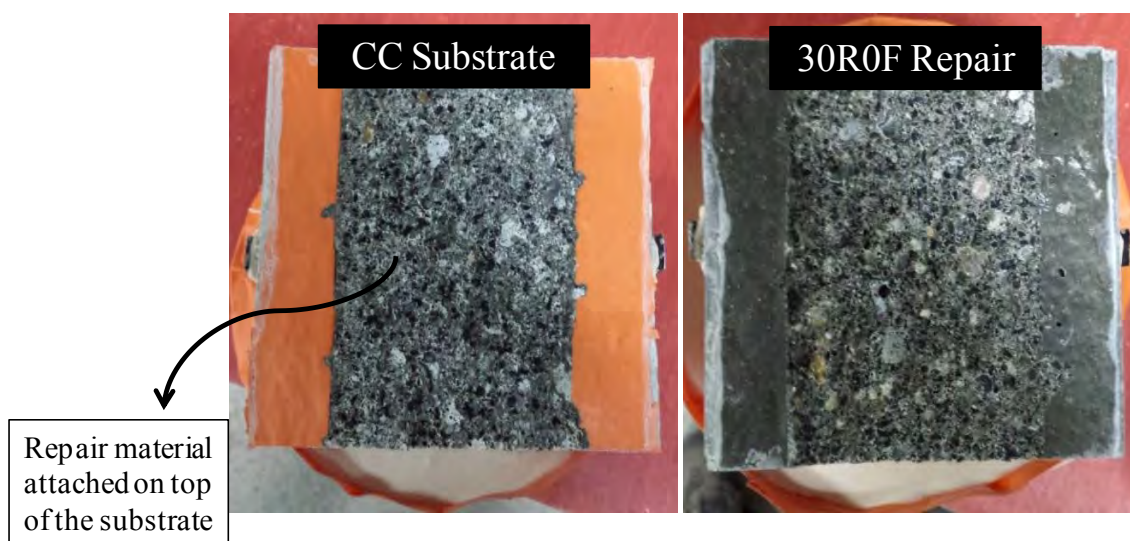


Figure IV-20: View of broken sample with 30R0F repair after conducting bond tension test

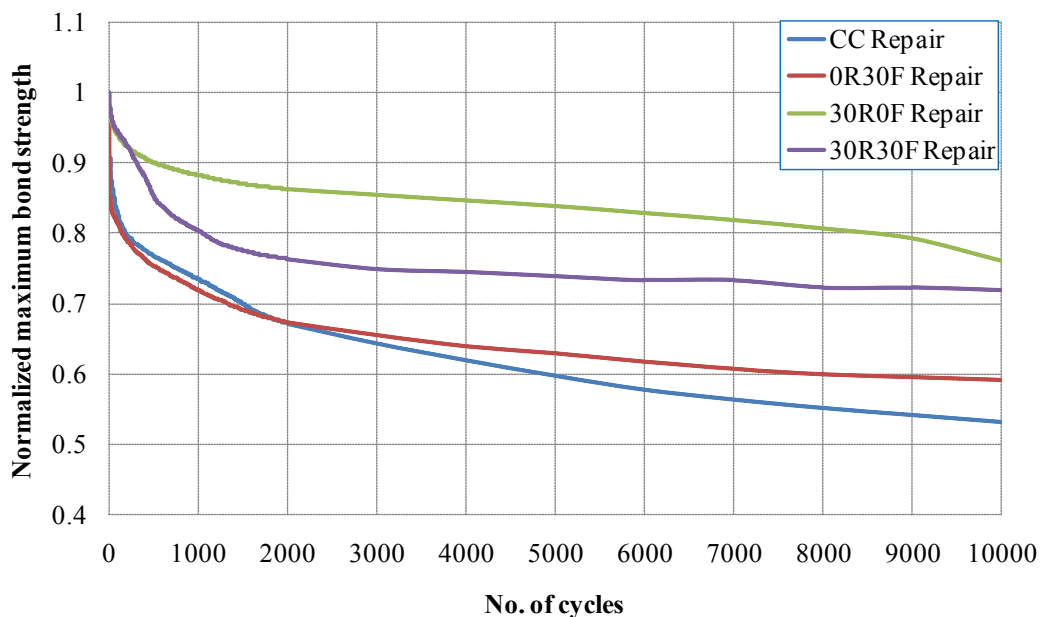


Figure IV-21: Relationship between normalized maximum bond strength and number of fatigue cycles corresponding to $COD_{max} = 0.010$ mm

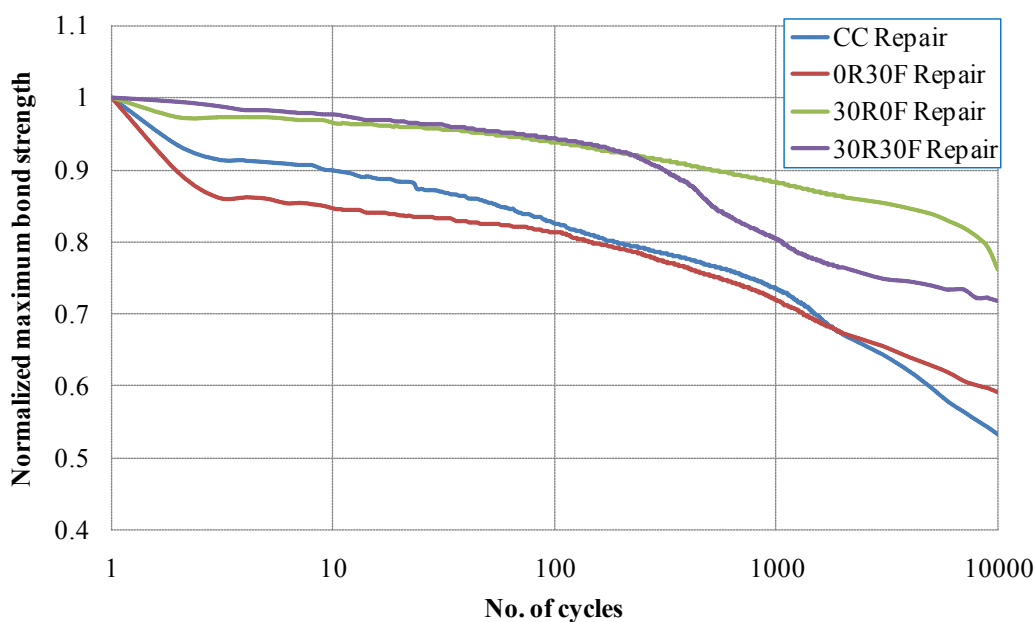


Figure IV-22: Relationship between normalized maximum bond strength and number of fatigue cycles corresponding to $COD_{max} = 0.010$ mm on logarithmic scale

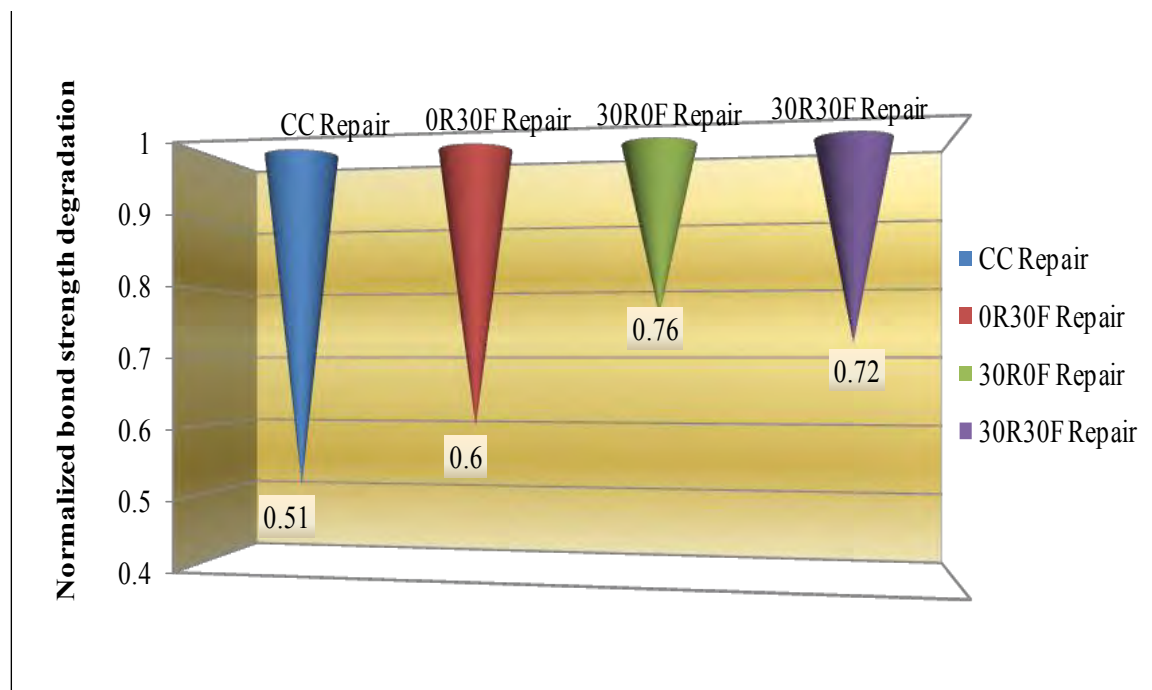


Figure IV-23: Normalized maximum bond strength degradation with different repair mortar mixes corresponding to $COD_{max} = 0.010$ mm at 10^4 cycles

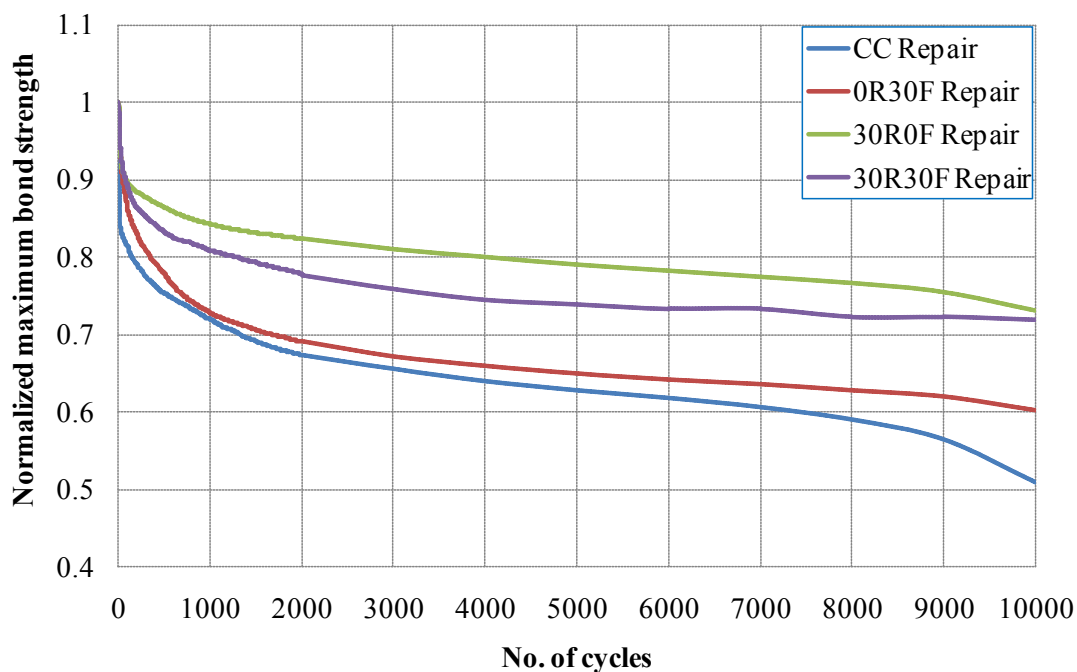


Figure IV-24: Relationship between normalized maximum bond strength and number of fatigue cycles corresponding to $COD_{max} = 0.020$ mm

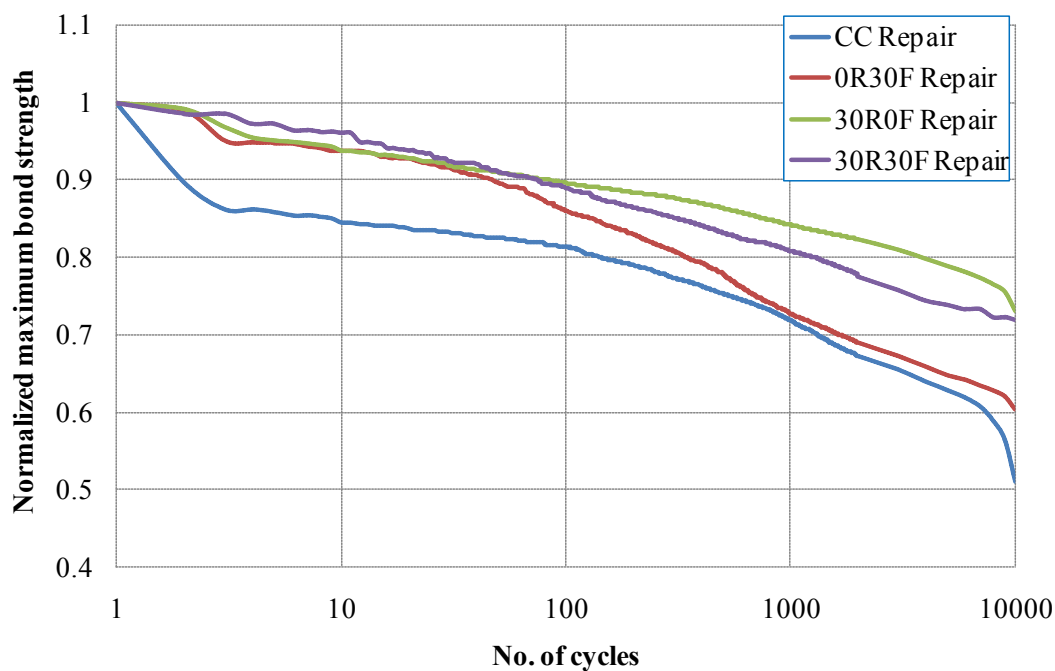


Figure IV-25: Relationship between normalized maximum bond strength and number of fatigue cycles corresponding to $COD_{max} = 0.020$ mm on logarithmic scale

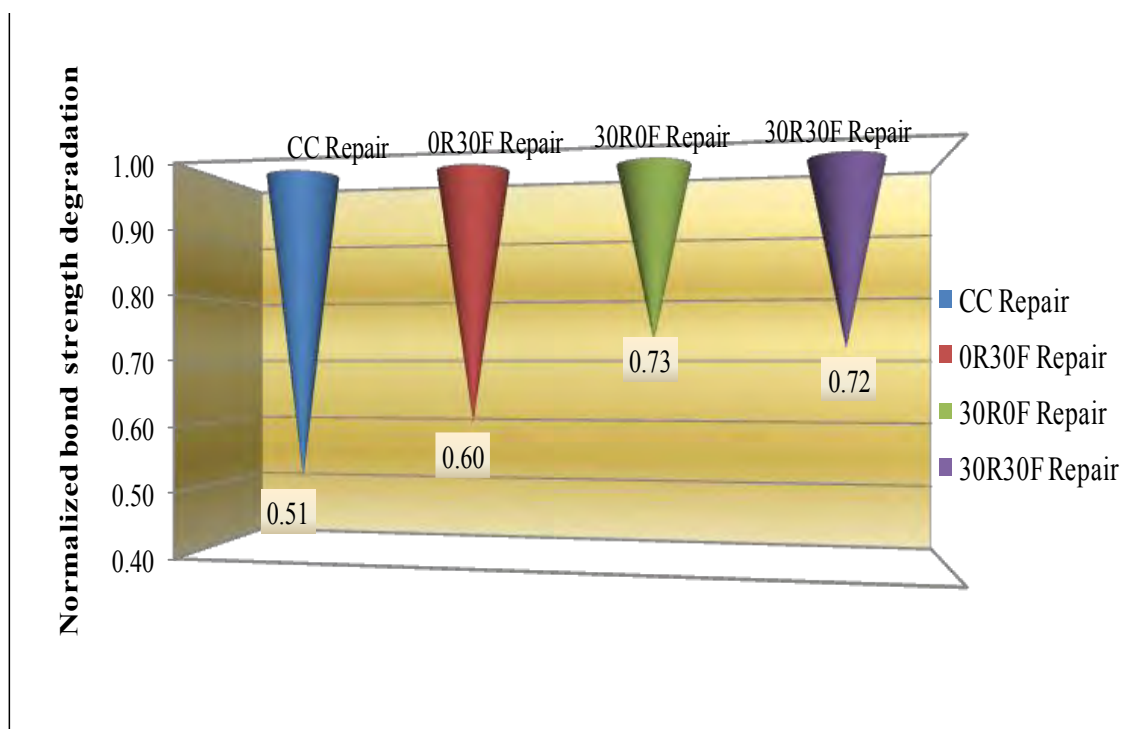


Figure IV-26: Normalized maximum bond strength degradation with different repair mortar mixes corresponding to $COD_{max} = 0.020$ mm at 10^4 cycles

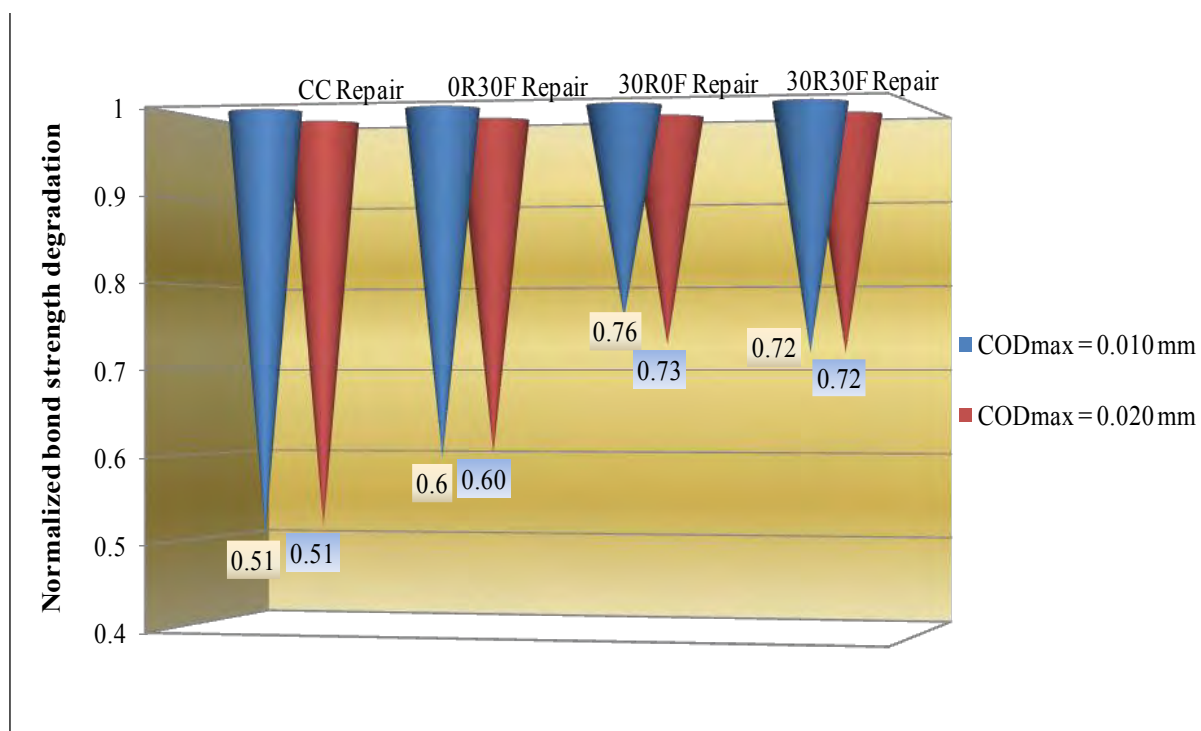


Figure IV-27: Comparison of normalized maximum bond strength degradation for different repair material, corresponding to different pre-cracked widths (COD_{max}) at 10^4 cycles

The interfacial bond degradation curves for specimens with different repair materials are presented in Figure IV-28, where the maximum bond strength corresponding to the maximum crack width is normalized with respect to the strength level at first cycle. Experimental results show that the bond strength decreases with the number of load cycles for given maximum cracked width value. Also, no significant change in bond strength degradation is observed by varying the maximum pre-cracked width value.

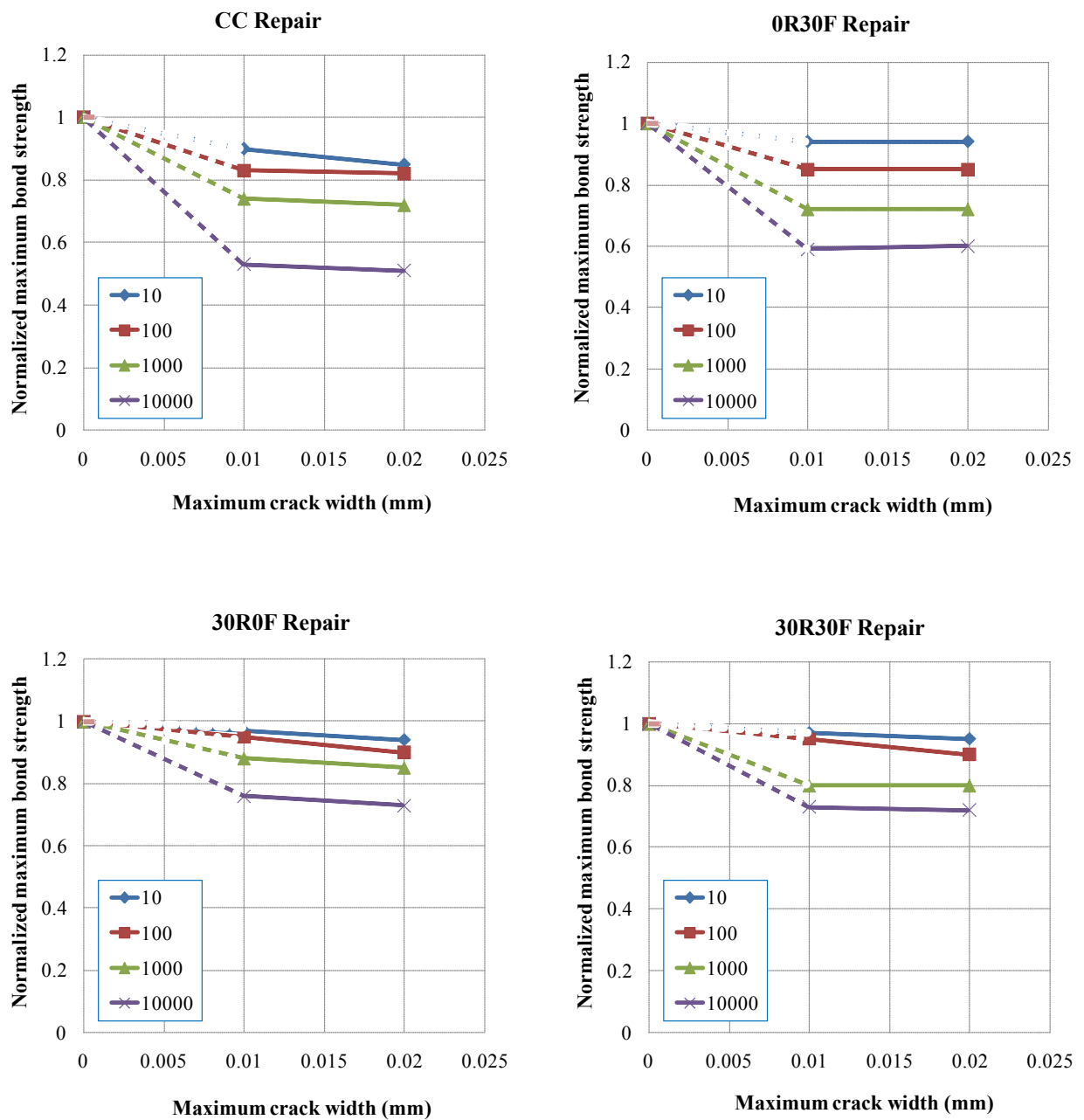


Figure IV-28: Relationship between normalized maximum bond strength and maximum crack width with different repair mortar mixes, showing results after 10, 10^2 , 10^3 and 10^4 cycles, respectively

IV.3.3 Highlights

Experimental investigation shows that the cyclic bond strength degradation behaviour can be influenced upto certain extent by repair material composition, especially with rubberized repairs, but didn't show any significant change by varying maximum pre cracked width value. It means, even at different pre-cracked width values, interfacial bond strength degradation is almost identical. Based on the experimental results, the following remarks can be drawn:

- ✚ The interfacial bond strength decreases with the number of fatigue cycles irrespective of the nature of the composite used as a repair material.
- ✚ The maximum interfacial bond strength degradation occurs in composite specimens repaired with control mortar and fiber reinforced mortar.
- ✚ Cyclic bond strength degradation seems to be limited upto certain extent in composite specimens repaired with mortar containing rubber aggregates.
- ✚ Fiber-reinforcement of repair material didn't show any impact on the cyclic bond stress degradation.


IV.4 CONCLUDING REMARKS

This chapter reports the cyclic crack bridging behaviour of fiber reinforced and/or rubberized mortar and also the impact of using these composites as repair material on the interfacial bond degradation in thin bonded overlays. Experimental investigation shows that the cyclic bridging behaviour of fiber reinforced and/or rubberized mortar is quite complicated phenomena and can be influenced by many parameters like material composition, loading conditions, maximum pre-crack width value etc. Based on the experimental results, the following conclusions can be drawn

- ✚ Degradation in cyclic bridging strength and in interfacial bond strength was observed with the number of fatigue cycles for the same maximum crack width, irrespective of the nature of the composite material.
- ✚ Maximum crack bridging degradation occurs in control mortar and similarly maximum interfacial bond degradation was observed in the specimens repaired with control mortar.

- ✚ Metallic fiber-reinforcement of mortar tends to limit cyclic bridging strength degradation at large crack opening widths, but the use of this fiber-reinforced material as repair material didn't show any impact on the interfacial bond strength degradation.
- ✚ Rubberized mortar tends to limit the cyclic crack bridging degradation at less pre-crack widths and the use of rubberized mortar as a repair material also try to limit the bond strength degradation.
- ✚ A combine use of rubber aggregates and of metallic fibers in mortar appeared to be a suitable solution to limit the cyclic bridging strength degradation. It confers to the composite an interest for durable application such as cement-based thin bonded overlays.

In this chapter, the cyclic bridging behaviour of fiber reinforced and/or rubberized mortar is investigated. Also, the impact of using plain and fiber-rubberized mortar on bond strength degradation is studied here. In the next chapter, the structural performance of repaired beams under flexure loading is presented. For this purpose, composite beams consisting of a thin repair layer on top of the substrate (simulating repaired structure) are tested in bending (monotonic and fatigue). In order to monitor the evolution of crack in the repair layer and of debonding at interface digital 3D image correlation technique is used.



Chapter # V
STRUCTURAL BEHAVIOUR OF
REPAIRED BEAMS UNDER
FLEXURAL LOADING

V. STRUCTURAL BEHAVIOUR OF REPAIRED BEAMS UNDER FLEXURAL LOADING

V.1 INTRODUCTION

The effect of incorporating rubber aggregates and fiber-reinforcement in mortar has been explained in previous chapters. Although, rubber aggregates incorporation in mortar is detrimental to compressive and tensile strengths, but some other benefits can also be achieved e.g. improvement in strain capacity, control of micro-cracking and less cyclic bridging degradation, especially at small crack openings. Similarly, the fiber-reinforcement of mortar improves the post cracking residual strength. Also, the combine use of rubber aggregates and fibers in mortar produces a positive synergetic effect by enhancing the strain capacity and improving the post cracking residual strength simultaneously. Moreover, the mortar mix incorporating both rubber aggregates and fibers exhibits a good cyclic bridging under tensile fatigue loading. So, these benefits encourage the use of rubber aggregates and fibers in the repair material of thin bonded cement-based overlays.

Taking into account the main problems arising in thin bonded cement-based overlays, i.e. cracking of repair layer and interface debonding, one can suggest that the use of repair material incorporating rubber aggregates and metallic fibers can be a promising solution. Based on the results presented in Chapter II, four mortar mix compositions, i.e. 0R0F (CC), 0R30F, 30R0F, 30R30F were selected as repair materials and cast on top of control mortar substrate. Before casting the repairs, the substrate surfaces were properly prepared by using the sandblasting technique for ensuring the proper bond between substrate and repair material.

The use of above mentioned mortar mixes as repair materials allow us to highlight the effect of incorporating fibers, rubber aggregates and their combination on the structural behavior of repaired beams. A thin layer of above mentioned mix composites is used as a repair material on top of the sandblasted substrates which simulates that the beams are structurally repaired. In order to study the structural behaviour of repaired beams, firstly these beams are subjected

to monotonic three point bending test. From these tests, one can determine the following parameters:

- ✚ Relationship between the force and opening of notch (COD).
- ✚ Relationship between force and deflection.
- ✚ Detection of load at which crack reach at interface location by using digital image correlation technique (DIC). This load will be used for carrying out the flexural fatigue test.

In the second step, the behaviour of these repaired beams is evaluated under flexure fatigue loading. The following two parameters are determined and discussed:

- ✚ Evolution of notch opening with the number of cycles.
- ✚ Interface debonding propagation with the number of cycles.

V.2 MANUFACTURING OF COMPOSITE SPECIMENS

The composite specimens consist of thin repair layer on top of the substrate which simulates that the beam is repaired. Cement-based substrates were used in this study for making condition closer to real application. These substrate bases were manufactured by using control mortar (CC) mix composition. The dimensions of these prismatic substrate bases are $(100 \times 100 \times 500)$ mm³. After casting, these substrate bases were properly cured for 3 months under control temperature of 20 °C and at 100% relative humidity.

The results presented in chapter III and also in some previous researches (J. Silfwerbrand., 1990; F. Grandhaie., 1993; H. Chausson., 1997; H. Farhat., 1999; Q-T. Tran., 2006; A. Garbacz et al., 2006; L. Courard et al., 2014) show that substrate surface preparation has a direct impact on the durability of repair system. So, keeping in view the impact of substrate surface preparation on the bond behaviour of repair system, the sandblasted substrates were used in this study. In the light of previous researches (Q-T. Tran., 2006; T.H. Nguyen., 2010), the thickness of repair layer used was 40 mm. So, on top of the sandblasted substrates, a 40 mm thick repair layer was cast. Complete dimensions and details of the composite specimen are presented in Figure V-2 and Figure V-3. After casting repair layer on top of

these sandblasted substrates, these repaired beams are cured for 28 days at a temperature of 20 °C and relative humidity of 100%. In order to localize crack initiation under mechanical loading, a notch is created at mid-span of each repair layer. This notch is created during casting of the repair layer on top of substrate by providing a simple reservation in the formwork as shown in Figure V-1. The depth of this notch is 10 mm.

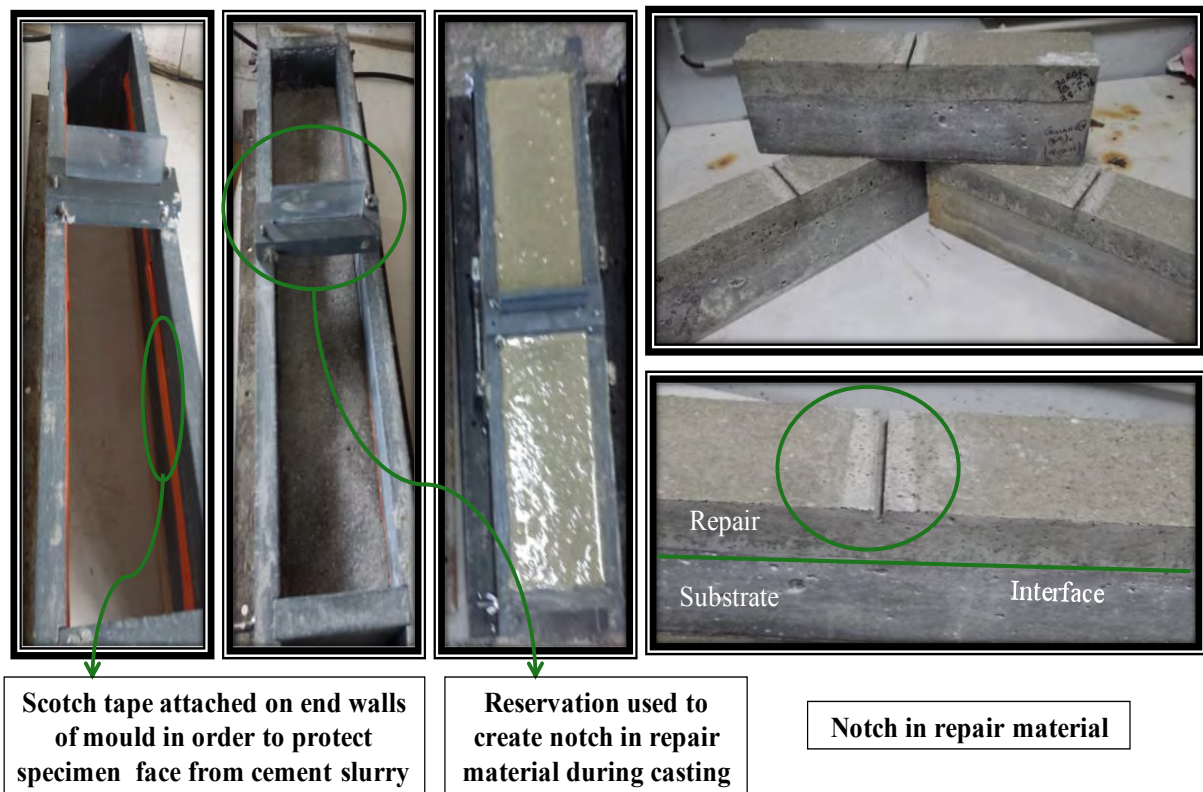


Figure V-1: Casting of repair on top of substrate

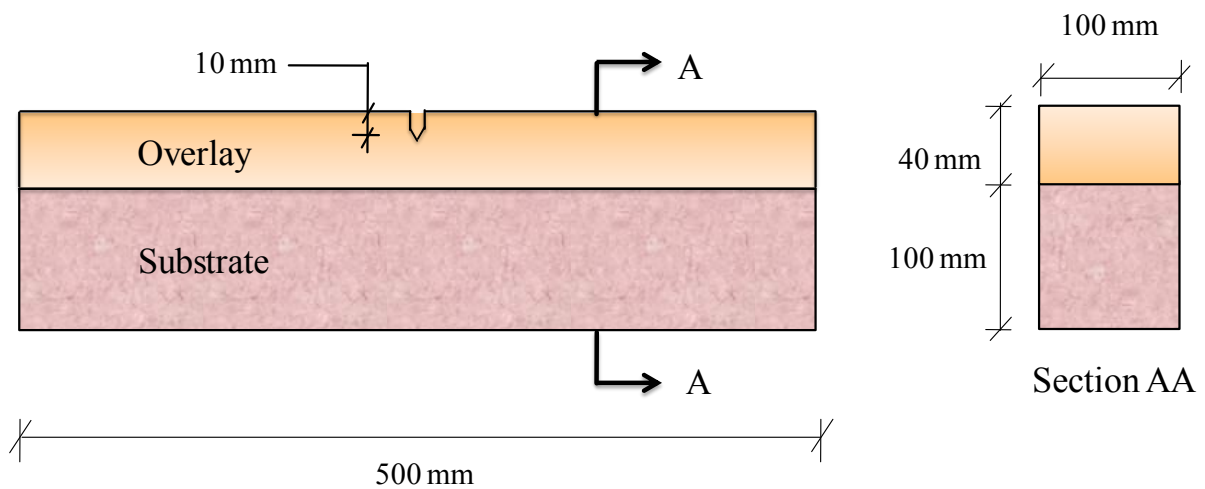


Figure V-2: Complete dimensions of composite specimen

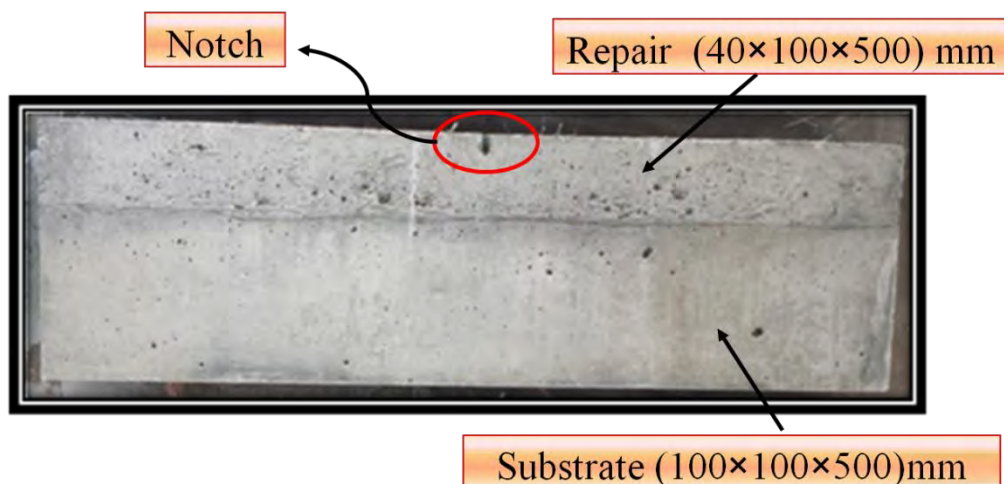


Figure V-3: Detail of a composite specimen

V.3 THREE POINT BENDING TEST UNDER MONOTONIC LOADING

Monotonic three point bending tests were carried out on MTS machine having loading capacity of 100 kN. Schematic diagram of the composite specimen under three point bending test is presented in Figure V-4. Figure V-5 shows the complete testing setup for three point bending tests. Under mechanical loading, the crack initiates from the notched tip in repair layer, that subsequently cause the debonding when this crack reaches the interface between the substrate and the repair layer.

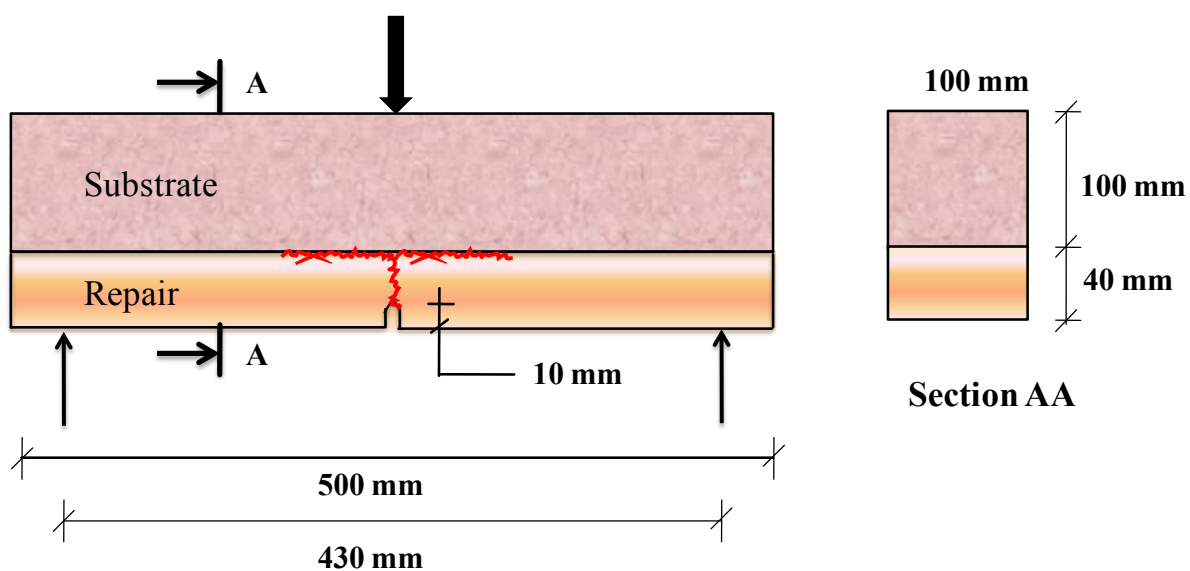


Figure V-4: Schematic diagram of a composite specimen under three point bending test

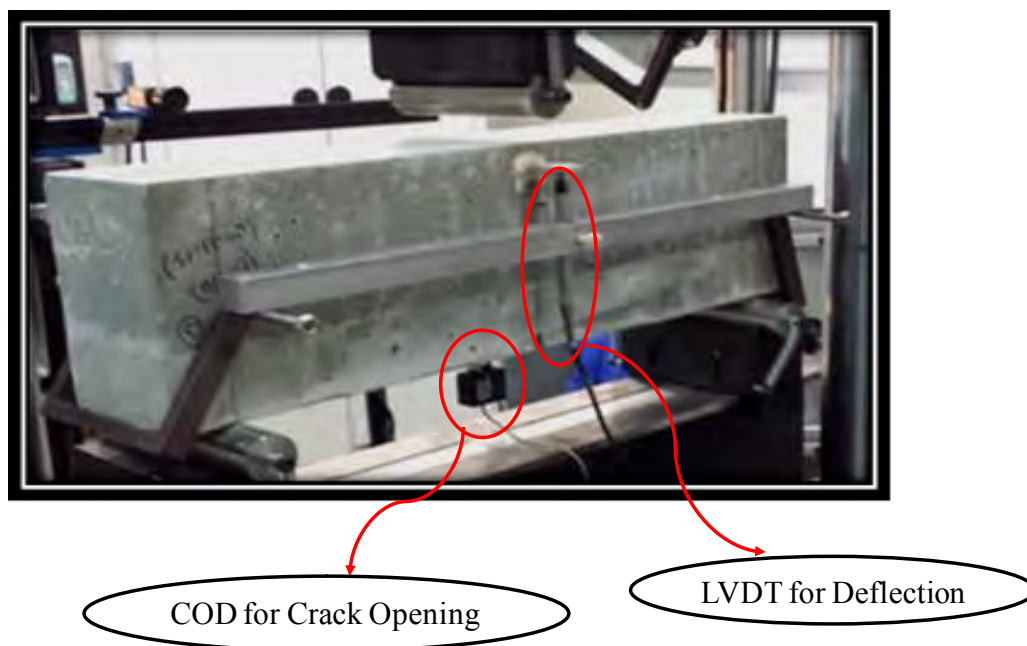


Figure V-5: Complete testing setup for three point bending test

These tests were controlled by Crack Mouth Opening Displacement (CMOD) using a sensor called COD. These tests were conducted by using the loading rate of 0.05mm/min up to 0.1 mm notch opening and then increased to 0.2 mm/min until completion of the test (when resisting load is approximately equal to zero). Mid span deflection of the composite specimen was also measured by using LVDT sensor according to RILEM recommendations (RILEM CPC 7., 1994). The values of force, deflection, and opening of the notch (COD) are automatically recorded by the data acquisition system of MTS 100 kN machine. This data is also synchronized with 3D digital image correlation (DIC) equipment. Since, this 3D image correlation technique is used to trace the crack propagation and to do determine the interface debonding length. By using this technique, one can also detect the load at which interface debonding initiates. In the previous studies conducted in LMDC (Q-T. Tran., 2006; T.H. Nguyen., 2010), video-microscope was used to monitor crack propagation and debonding length. According to these authors, the interface debonding has a close relationship with the opening of notch.

V.3.1 Mechanical behaviour of composite beams

The aim of conducting three point bending tests on composite beams is to evaluate the following parameters under monotonic loading:

- ✚ Relationship between the force and opening of notch (COD)
- ✚ Relationship between force and deflection

V.3.1.1 Relationship between force and opening of notch

The curves presented from Figure V-6 to Figure V-9 show the relationship between force and opening of the notch (COD) of the composite specimens having four different repair materials i.e. 0R0F (CC), 0F30F, 30R0F and 30R30F. In order to make comparison, the average curve of each repair mix composition is presented in one graph shown in Figure V-10.

As far as the effect of fiber-reinforcement of repair material is concerned, it is observed that at any notch opening value the corresponding force is always higher with 0R30F and 30R30F repair material in comparison with a control mortar repair. Results also confirm that the fiber-reinforcement of repair material controls the opening of notch under flexural loading by restraining the crack opening.

The obtained results also show that incorporation of rubber aggregates in repair material has no significant impact on the opening of notch. The force versus opening of notch curve is almost identical with 0R0F (CC) and 30R0F repair material. The only difference which is observed among these two composite specimens is the notch opening before the peak load. The notch opening at which crack reach at the interface location is little bit more in rubberized repairs as compared to the control mortar repair. This behaviour is due to the enhanced strain capacity of rubberized mortar. However, after the peak load the behaviour of these two composite beams is almost identical.

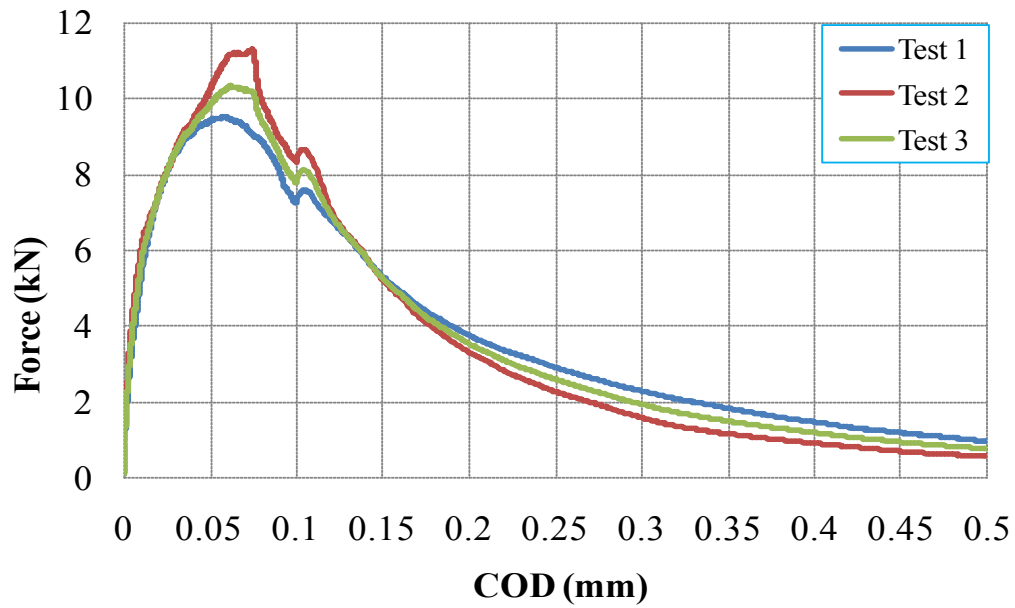


Figure V-6: Load versus opening of notch (COD) curves for 0R0F (CC) repair

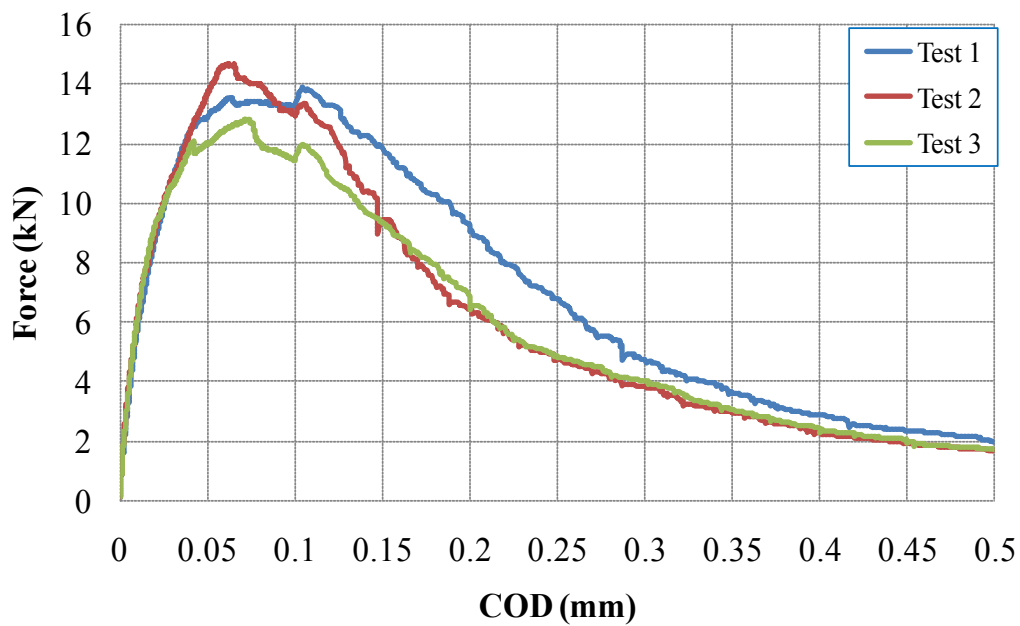


Figure V-7: Load versus opening of notch (COD) curves for 0R30F repair

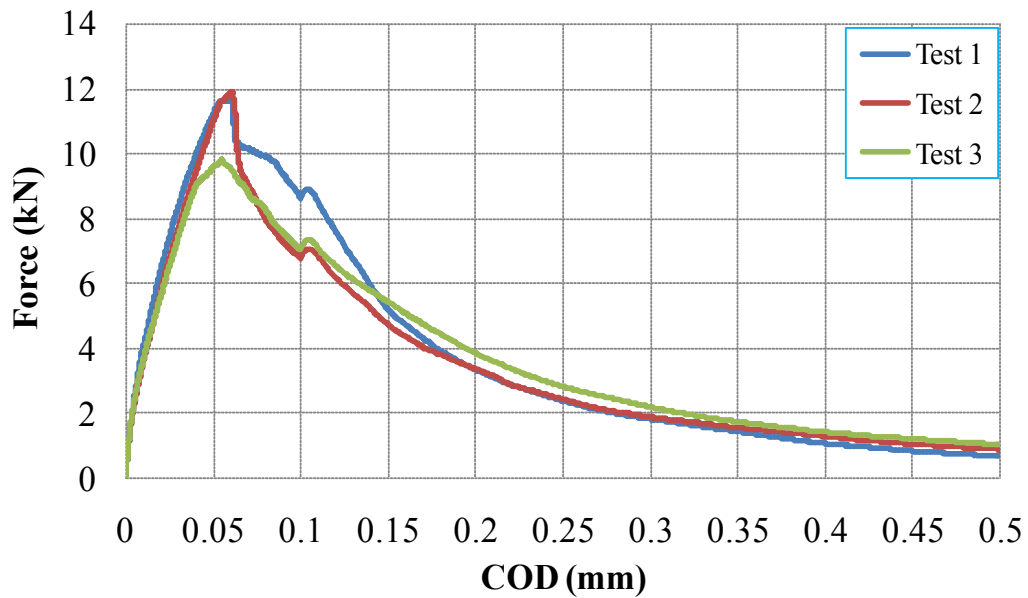


Figure V-8: Load versus opening of notch (COD) curves for 30R0F repair

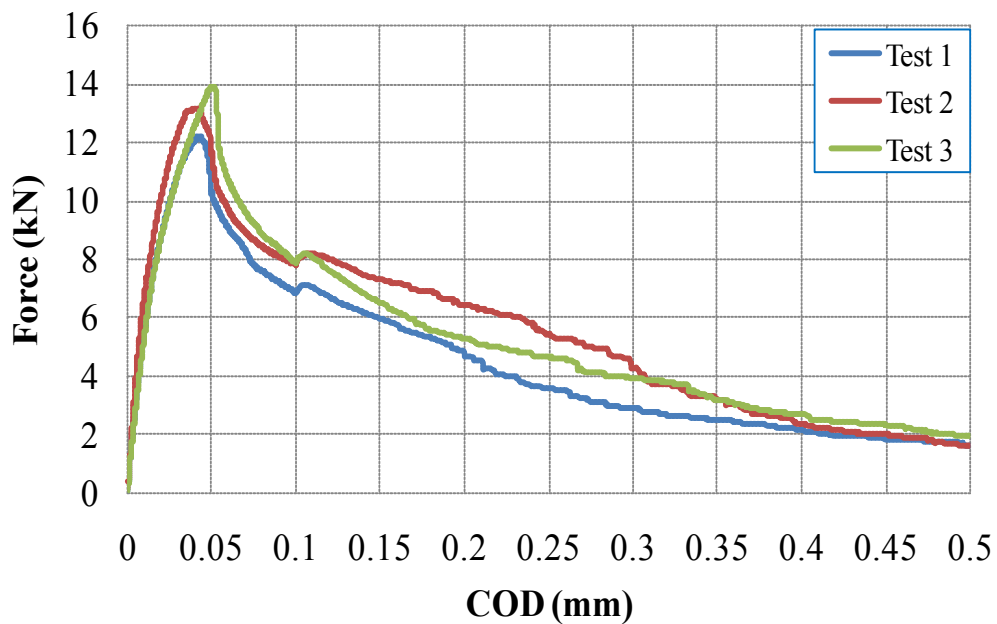


Figure V-9: Load versus opening of notch (COD) curves for 30R30F repair

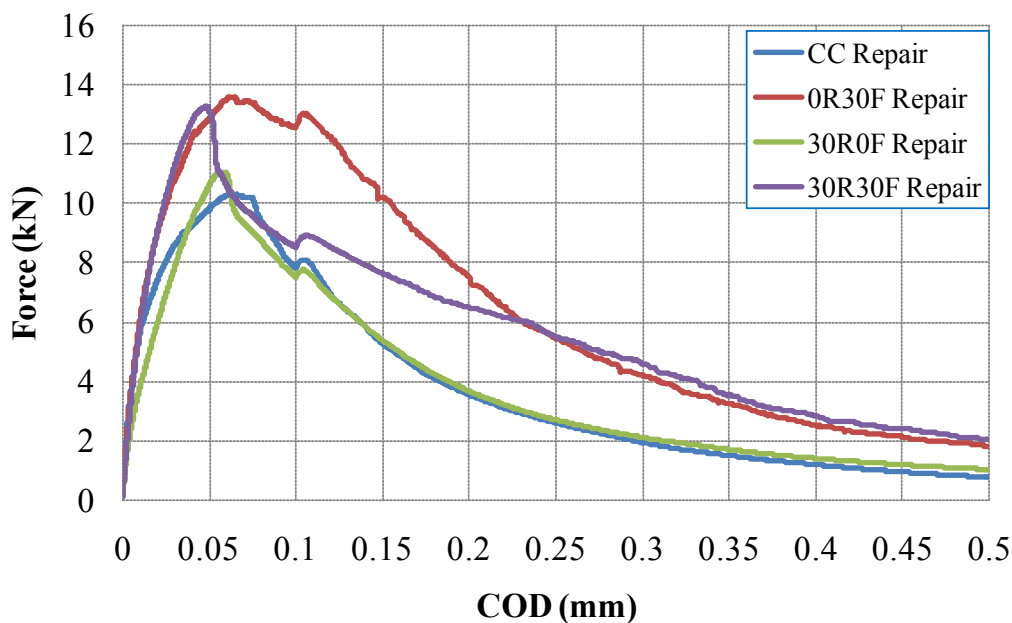


Figure V-10: Load versus opening of notch (COD) curves for composite repaired beams with different repair mix compositions

V.3.1.2 Relationship between force and deflection

The curves presented from Figure V-11 to Figure V-14 show the relationship between force and deflection of the composite specimens having four different repair materials. In order to make comparison among composite beams with different repair material, the average curve of each repair mix composition is presented in one graph shown in Figure V-15. Results show that fiber-reinforcement of repair material increases the peak load as well as corresponding deflection. The increase in deflection in specimens repaired with fiber-reinforced material is due to the additional restriction, provided by these fibers against crack opening.

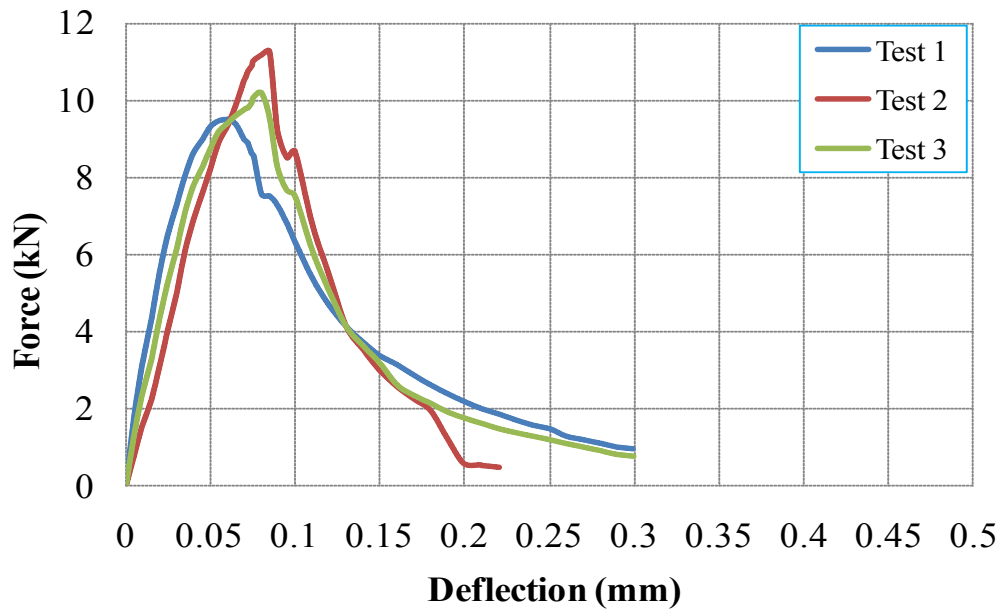


Figure V-11: Load versus deflection curves for CC repair

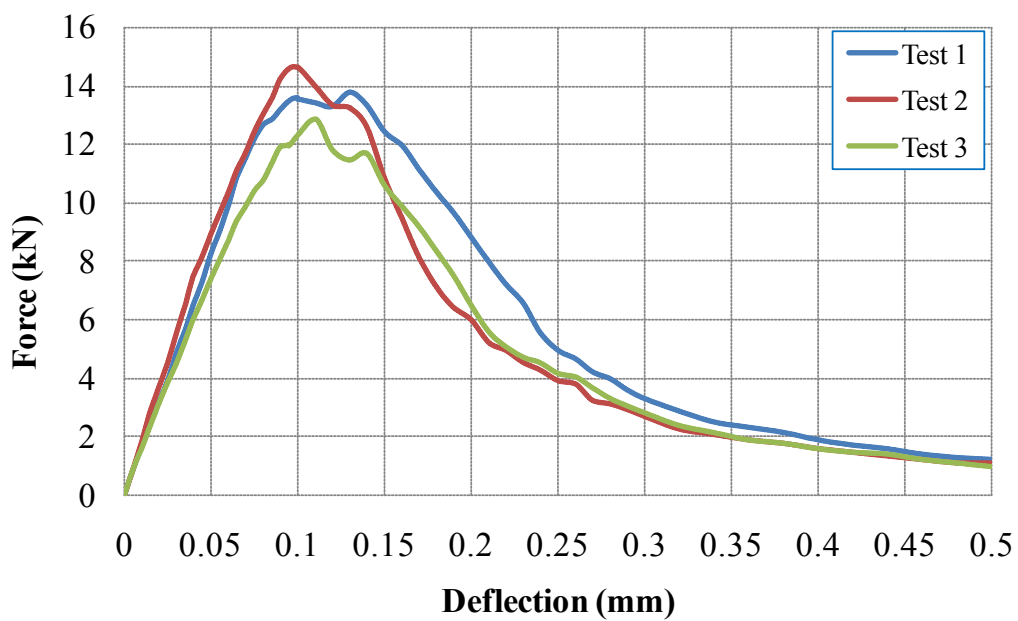


Figure V-12: Load versus deflection curves for OR30F repair

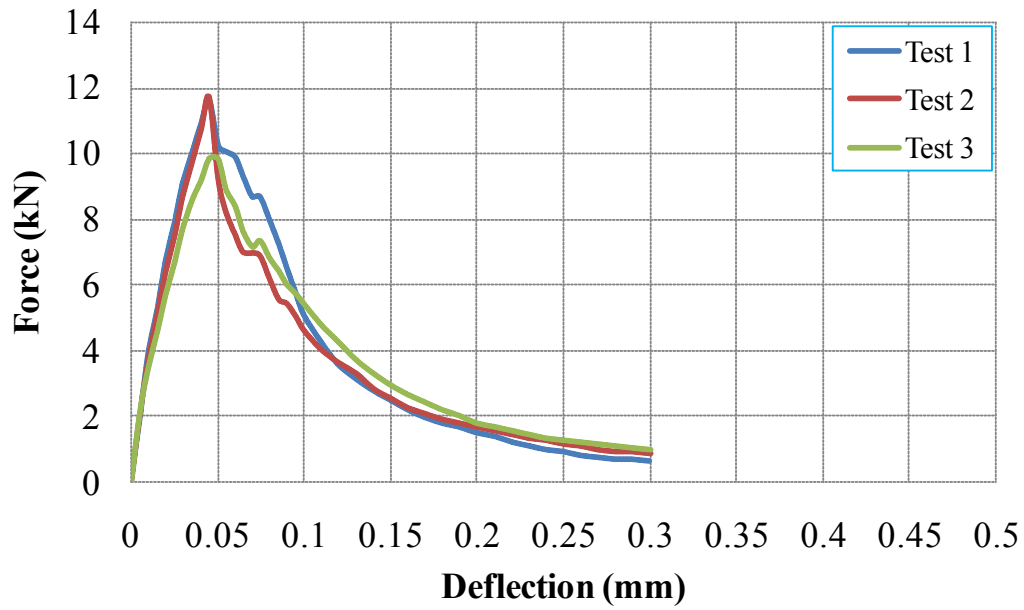


Figure V-13: Load versus deflection curves for 30R0F repair

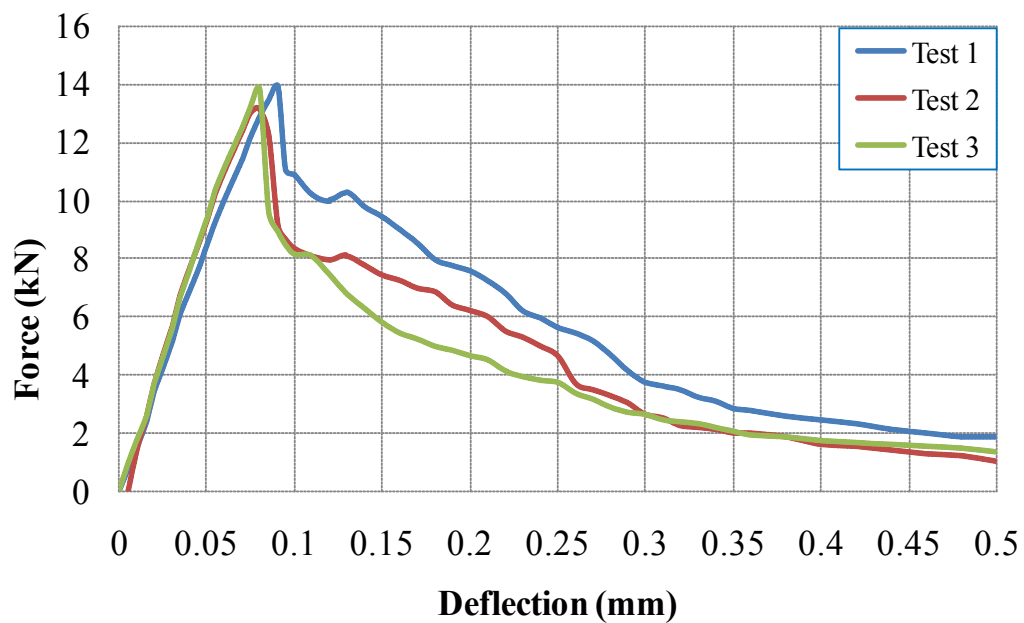


Figure V-14: Load versus deflection curves for 30R30F repair

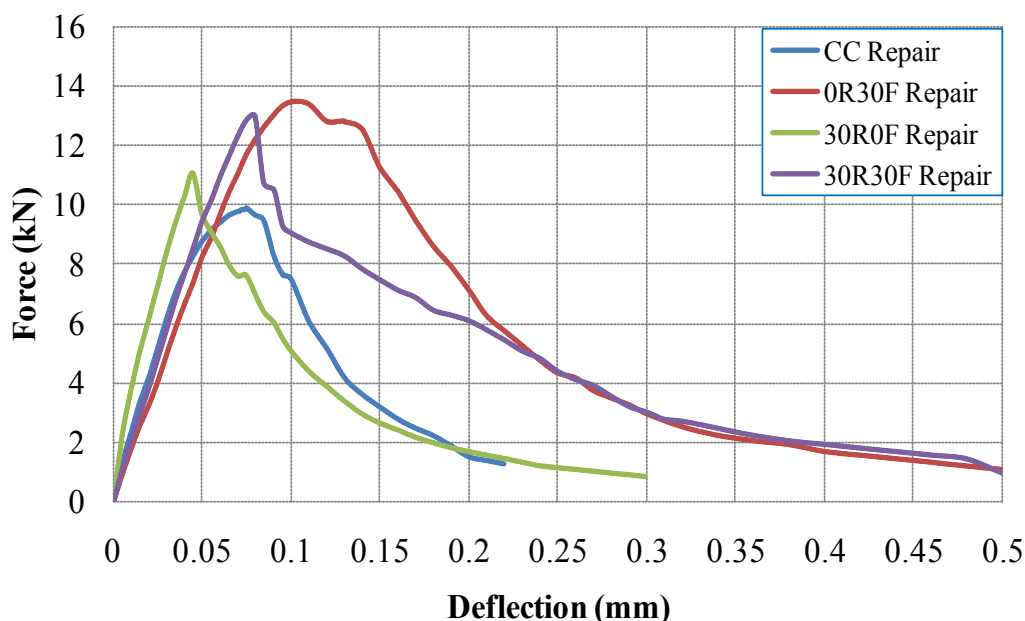


Figure V-15: Load versus deflection curves for composite repaired beams with different repair mix compositions

V.4 FLEXURE TESTING ALONG WITH DIGITAL 3D IMAGE CORRELATION TECHNIQUE

V.4.1 *Digital image correlation Technique*

Digital image correlation (DIC) is an optical and non-contact measurement technique that is used to measure displacements on the surface of an object of interest. This displacement is then used to calculate the surface strain of the object. DIC involves comparing a series of images taken in sequence over a period of time by a digital camera with specific resolution. The distributions of grey scale values in successive images are compared, and their differences are used to characterize the deformation of the surface. For the process to be most effective, the area of interest should be painted with a random speckle pattern prior to the start of the process (B. Gencturk et al., 2014).

3D digital image correlation technique requires two sets of images of the object taken from separate camera angles at the same time. The system must be calibrated to define the 3D space in which the event or process to be studied will occur. The results of this calibration process are then used to correlate the images from the two cameras to enable the

determination of the studied deflection and strain of the material (V. Pickerd., 2013). In order to carry out 3D image correlation, sample preparation is necessary like painting it white and then black spot on this white painted surface as shown in Figure V-16. Figure V-17 shows the complete experimental testing arrangements (lights, cameras, etc.) necessary to use this digital image correlation technique. The purpose of conducting three point bending test along with this DIC technique is to follow the crack initiation and propagation and to determine the point at which crack reached at interface location.

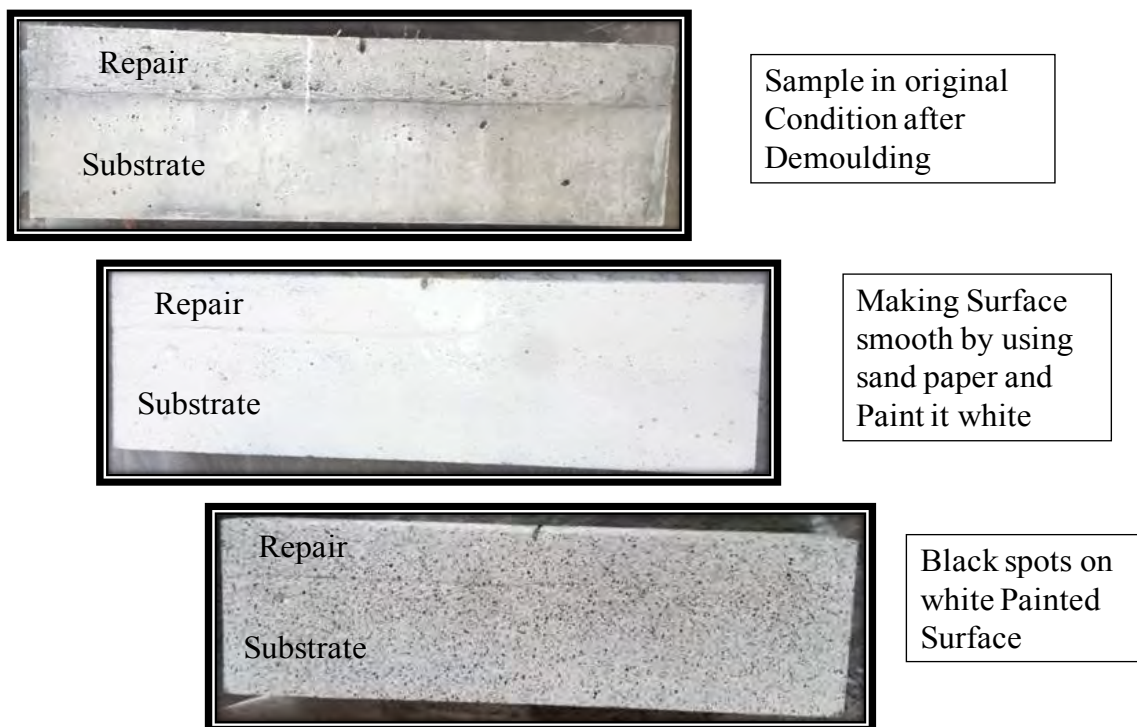


Figure V-16: Sample preparation for bending test along with 3D digital image correlation technique

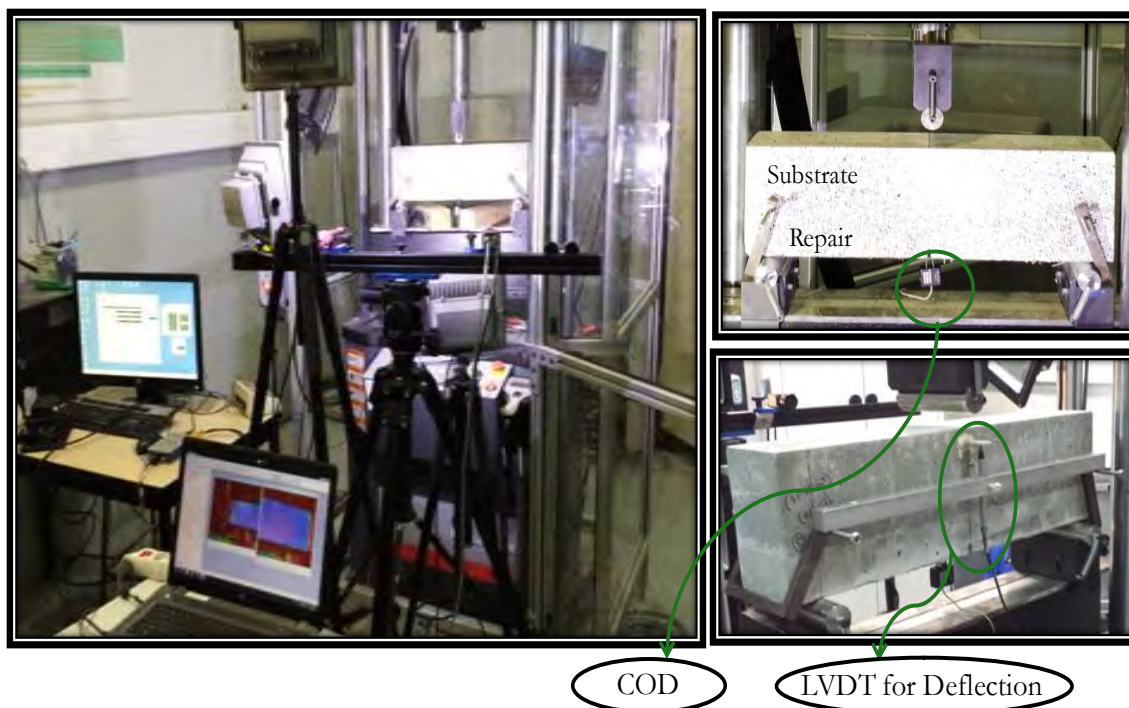


Figure V-17: Complete experimental testing setup for three point bending test along with 3D digital image correlation technique

V.4.2 Detection of interface debonding initiation through 3D digital image correlation technique

The primary purpose of conducting three point bending test along with this DIC technique is to follow the cracking pattern and to determine the load at which interface debonding starts. For image processing, all recorded images were treated on the software Vic-3D, 2010. Post treatment of images indicates displacements and strains that occur on surface of the repaired beam during bending test from first image to last image.

This post treatment analysis shows the complete cracking pattern, the image at which crack initiates from tip notch, the load at which crack reached at interface location, etc. Also, it indicates that either debonding at interface occurs or not under flexure loading. In order to identify the load at which crack reaches at interface, an artificial extensometer is used at interface location in post treatment. This artificial extensometer is placed perpendicular to the

direction to crack propagation as shown in Figure V-18. This DIC technique provides the flexibility to do back analysis of resulting strains obtained by post processing of images. So, after tracing the crack path one can place the artificial extensometer at an exact crack location in order to precisely identify the load at which interface debonding initiates. When crack crosses this artificial extensometer, there is a sudden change in D1 value as shown in Figure V-19. This D1 is the elongation that occurs in this artificial extensometer due to the opening of the crack. The load corresponding to the point at which there is a sudden change in D1 value is considered as a load at which crack reach at interface location and initiates the interface debonding. For each repair mix composition, minimum three samples were tested in monotonic loading along with DIC technique. Image processing results also lead us to conclude that interface debonding initiates on the spot when crack reaches the interface level.

The load calculated from the average of three specimens was not used exactly as maximum load (P_{max}) in fatigue testing. Since, scattering among load values was observed in different composite specimens repaired with the same mortar mix. So, it was decided to use 85% of the average load as maximum load (P_{max}) in fatigue tests. This reduction of load was done in order to ensure that the crack should not cross the interface location before applying cyclic loading.

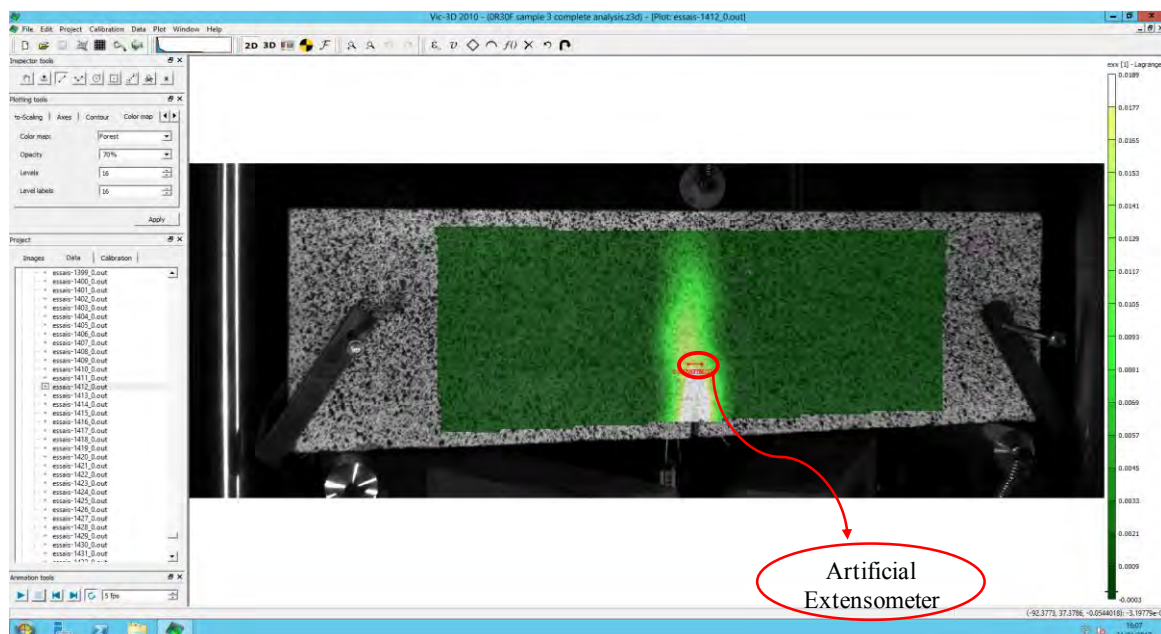


Figure V-18: Selected strain visualizations for crack observation and use of artificial extensometer for detecting the load at which crack reach at interface location

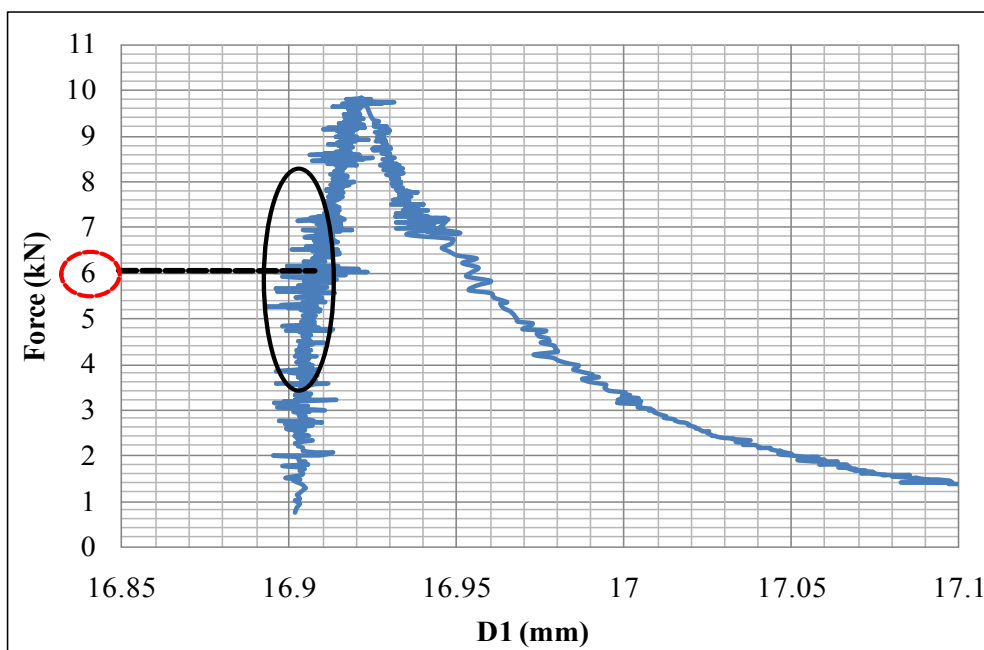


Figure V-19: Force vs. opening of artificial extensometer (D1): detection of load at which crack reach at interface location and debonding initiated

Debonding initiation force for composite specimens having different repair mix compositions are listed in Table V-1. The results show that these loads are different for each repair mix composition. It may also be noticed that the opening of the notch at which crack reached at interface location is also variable for each repair mix. In the case of non-fiber repair mortars, i.e. 0R0F and 30R0F, the average initiation force at which interface debonding starts is less as compared to repairs reinforced with fibers (with or without rubber aggregates, i.e. 0R30F and 30R30F). Since, the presence of fibers in repair material provides bridging at the crack location and also limits the opening of the crack. In the case of 30R0F repairs, some improvement in debonding initiation force is also observed as compared to control mortar repair. Since, rubber aggregates incorporation in repair material tries to limit micro-cracking phenomena. Also, the debonding initiation force is significantly increased for specimens repaired with 30R30F material. This increase in load is due to the combined synergetic effect provided by rubber aggregates and fibers.

Table V-1: Load at which crack reached at interface and debonding at interface started

Mix Composition	Sample No.	Interface debonding initiation force (kN)	Average Value (kN)	Force (P_{max}) used for fatigue testing (kN)
0R0F (CC)	1	7.0	6.6	5.6
	2	6.6		
	3	6.1		
0R30F	1	8.4	7.9	6.7
	2	8.0		
	3	7.6		
30R0F	1	7.0	6.9	5.8
	2	6.7		
	3	6.6		
30R30F	1	8.8	9.0	7.6
	2	9.0		
	3	9.2		

The curves presented from Figure V-20 to Figure V-23 show the interface debonding length versus load for the composite beams. For an easy comparison, the set of average curves is grouped in Figure V-24. The results show that the interface debonding propagation is least controlled in beams repaired with 0R0F and 30R0F mortar. It can be noticed that interface debonding is limited in beams repaired with 0R30F and 30R30F mortar. The interface debonding propagation is closely related to the opening of the crack in repair layer. So, the fiber-reinforcement of repair layer controls the crack opening and thus limits the initiation and propagation of interface debonding.

Figure V-24 also shows that at any debonding length the corresponding force is always higher for beams with 30R30F repair. For example, in order to achieve 20 mm interface debonding, the force required is 6.5 kN for 0R0F repair, 10 kN for 0R30F and 10.8 kN for 30R30F.

Similarly, the interface debonding initiation force is also higher with 30R30F repair material. One can also notice the positive synergetic effect of the combine use of rubber aggregates and fibers to limit the debonding initiation and its propagation.

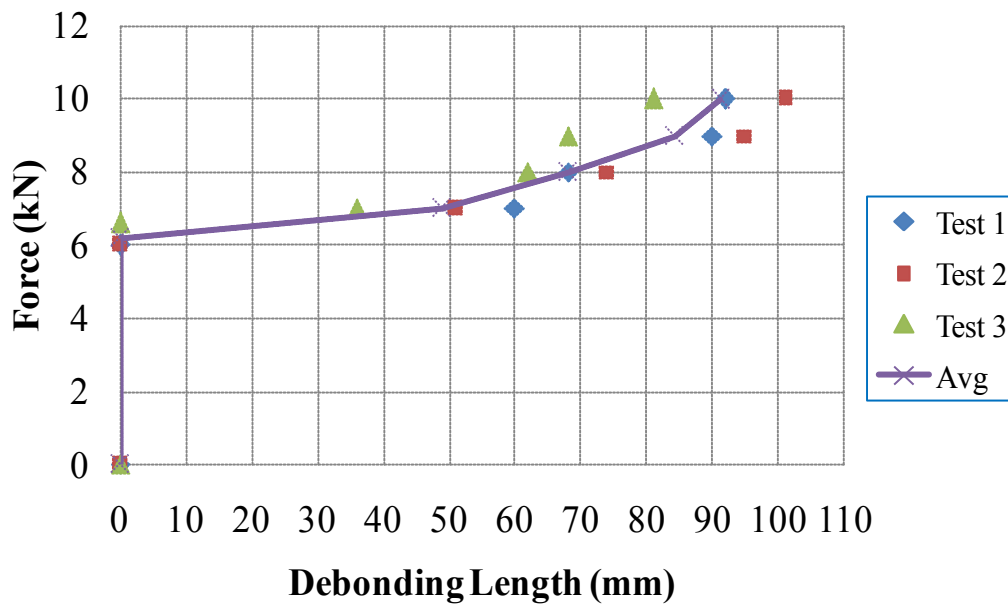


Figure V-20: Force vs. debonding length at interface for 0R0F (CC) repair

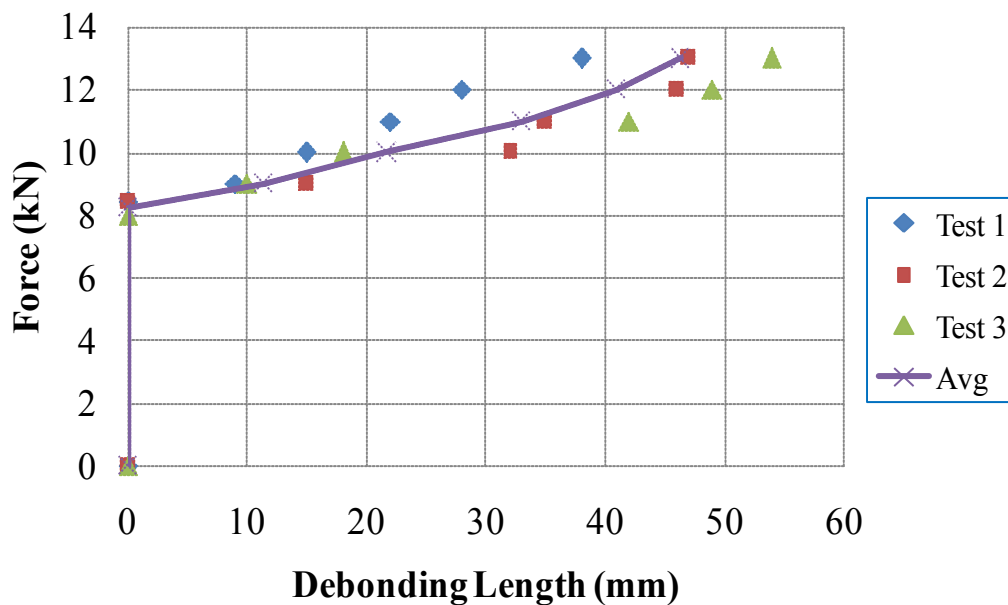


Figure V-21: Force vs. debonding length at interface for 0R30F repair

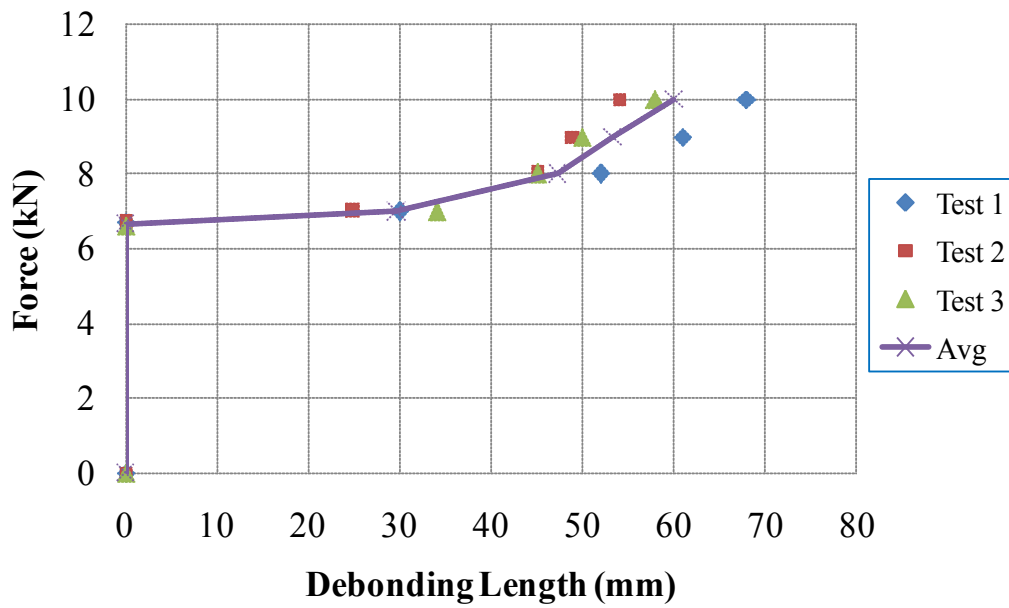


Figure V-22: Force vs. debonding length at interface for 30R0F repair

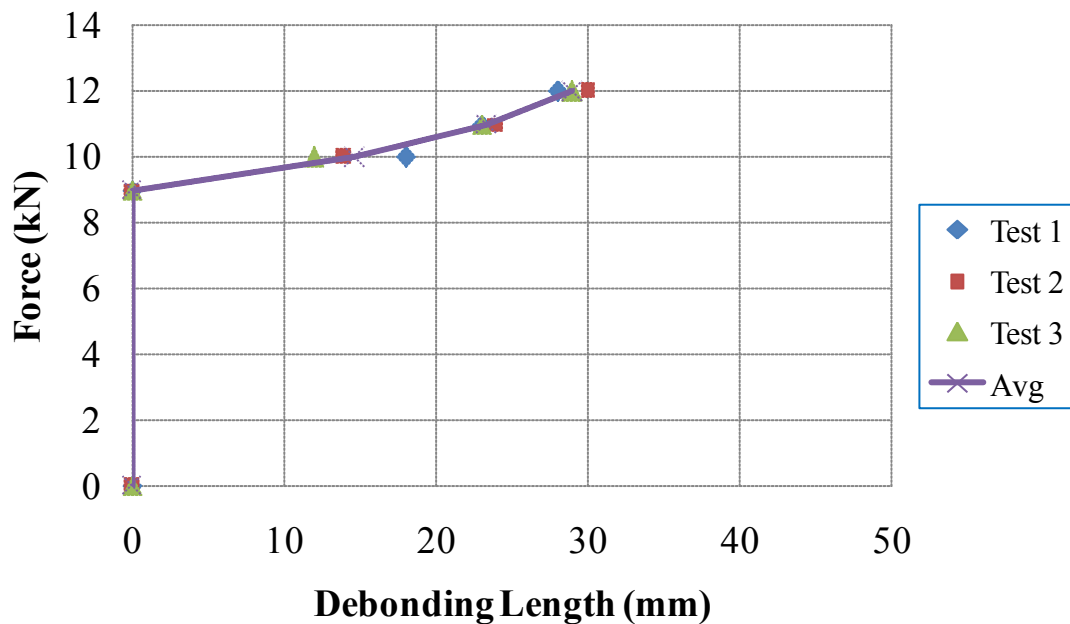


Figure V-23: Force vs. debonding length at interface for 30R30F repair

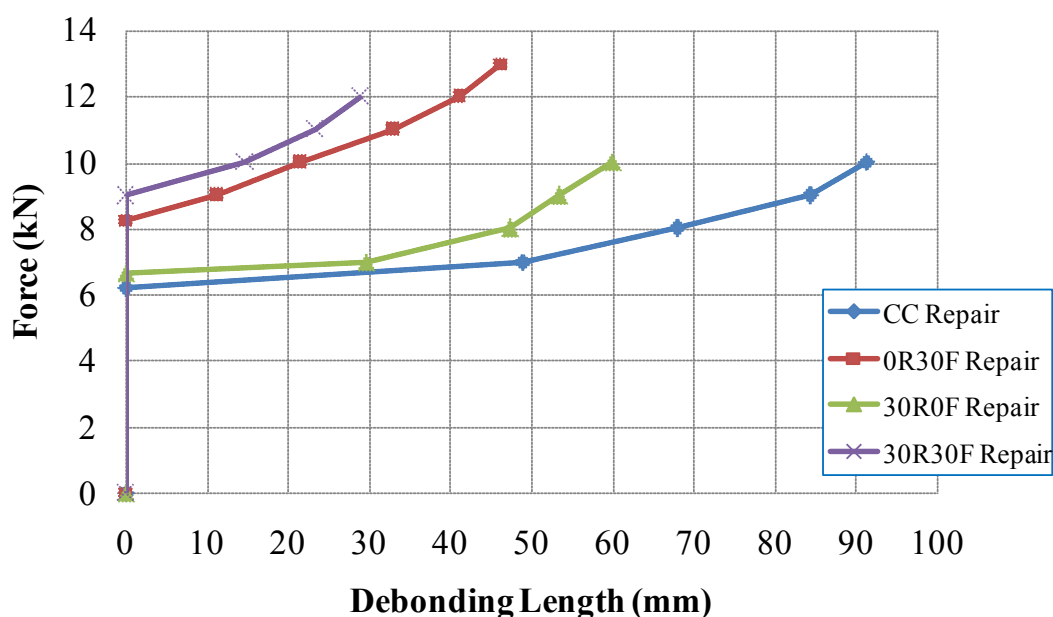


Figure V-24: Force vs. debonding length at interface for different repair layers

The propagation of debonding along the interface between substrate and repair is a function of the opening of the notch as shown in Figure V-25. The specimens with control mortar repair (CC) show a maximum notch opening and the corresponding debonding length is also maximum. On the other hand, opening of notch and debonding length is limited in composite beams repaired with 30R30F mortar.

The notch openings at which debonding initiate in beams repaired with mix compositions 0R0F (CC), 0R30F, 30R0F and 30R30F are $15\mu\text{m}$, $16\mu\text{m}$, $21\mu\text{m}$ and $22\mu\text{m}$, respectively. This shows that incorporation of rubber aggregates in repair material does not only control the cracking, but also helpful to delay the peeling initiation along the interface.

As far as the effect of fiber-reinforcement on the peeling initiation is considered, it is not so significant. Since, the crack opening at which debonding initiates is quite less. Indeed, these types of metallic fibers require a certain crack opening in order to play their role effectively. The debonding lengths are limited in specimens with 0R30F and 30R30F repair materials. So, it can be concluded that fiber-reinforcement of repair material not only control the crack opening but also limit the interface debonding.

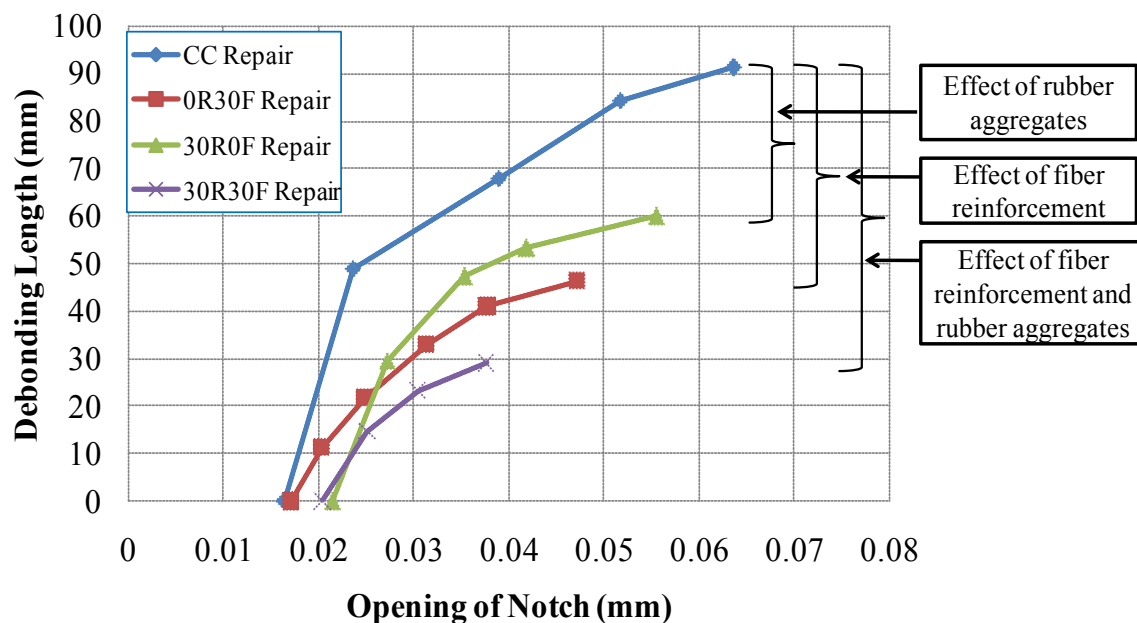


Figure V-25: Debonding length vs. opening of notch for different repair layers under monotonic loading

V.5 BENDING TESTS UNDER FATIGUE LOADING

In real conditions, every civil engineering structure is subjected to fatigue loading. In order to carry out fatigue tests in the laboratory setup, a sinusoidal loading is applied as fatigue loading.

V.5.1 Experimental protocol of fatigue testing

Three point bending fatigue tests were also carried out on the same MTS 100 kN machine that was used in monotonic bending tests. A sinusoidal loading with the constant amplitude between maximum (P_{\max}) and minimum (P_{\min}) loads is applied. An example of cyclic loading for 30R0F repair is illustrated in Figure V-26.

The maximum load (P_{\max}) values for composite specimens with different repair layers have already been determined in previous section V.4.2 by using DIC technique. These fatigue tests are conducted at a constant frequency of 10 Hz. This frequency of fatigue loading is selected in the light of previous research (M. T. Do., 1989), who concluded that fatigue loading frequency ranging between 1 to 20 Hz has very little impact on the mechanical behaviour of concrete. The P_{\max} values for our selected repair mix compositions are presented

in Table V-1. However, minimum load (P_{\min}) of 0.5 kN is selected as a pre-load for assuring that the specimen always remains in contact with the jack in order to avoid mechanical shock at each step of the load increase cycle (at every loading cycle). Figure V-30 shows the Snapshot of MTS machine acquisition during fatigue test, showing opening of the notch (COD) due to the application of cyclic loading between P_{\max} and P_{\min} .

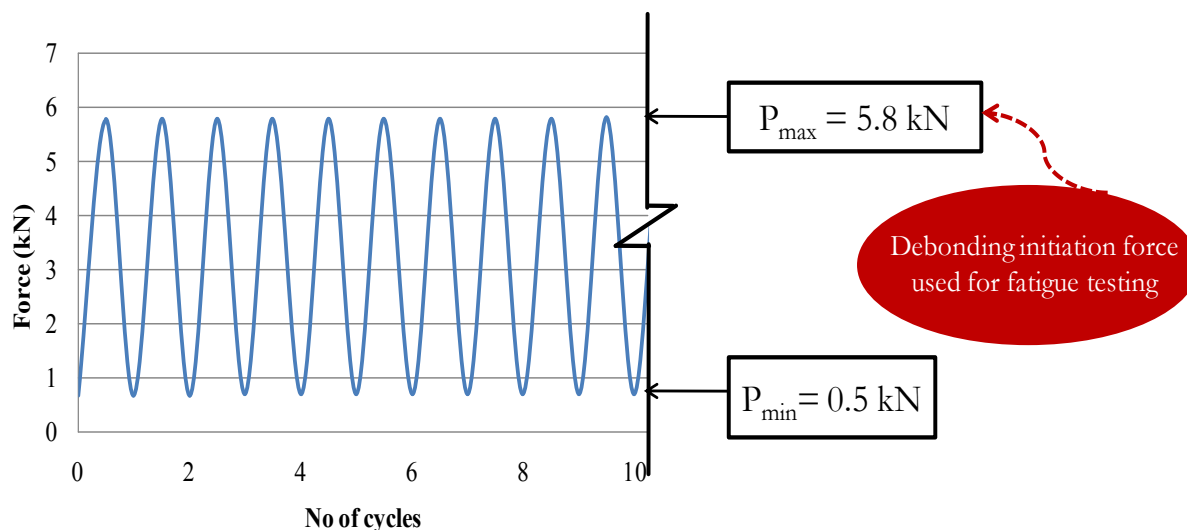


Figure V-26: Experimental protocol of cyclic loading for 30R0F repair

The primary objective of conducting these fatigue tests is to monitor the following two parameters as a function of the number of cycles

- ✚ Evolution of the notch opening at P_{\max}
- ✚ Interface debonding propagation

Figure V-27 shows the strain field color contrast indicating the crack propagation from the notch to interface location under monotonic loading before the application of cyclic loading. Similarly, Figure V-28 shows the strain field color contrast indicating the interface debonding location at 100000 cycles. And the length of debonding is measured by using artificial extensometer as shown in this figure. Figure V-29 show seven strain fields indicating interface debonding propagation with the number of cycles for 30R0F repaired specimen.

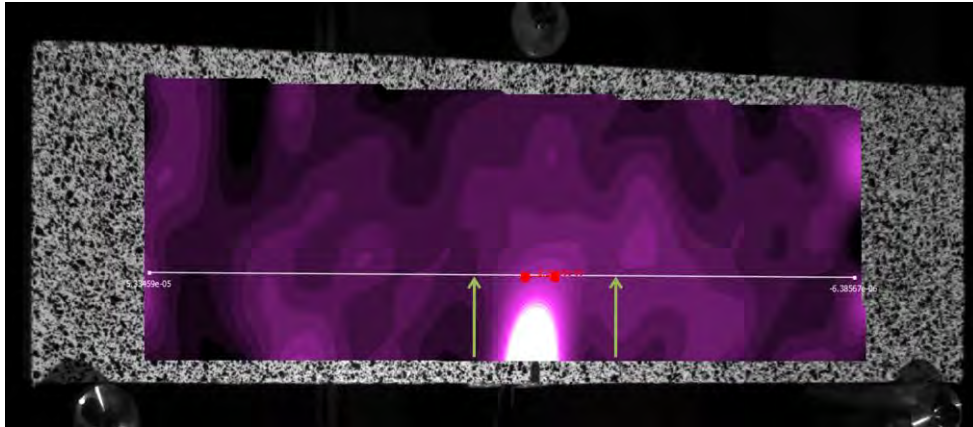


Figure V-27: Strain field color contrast showing propagation of crack from notch tip to interface location under monotonic loading for 30R0F repair

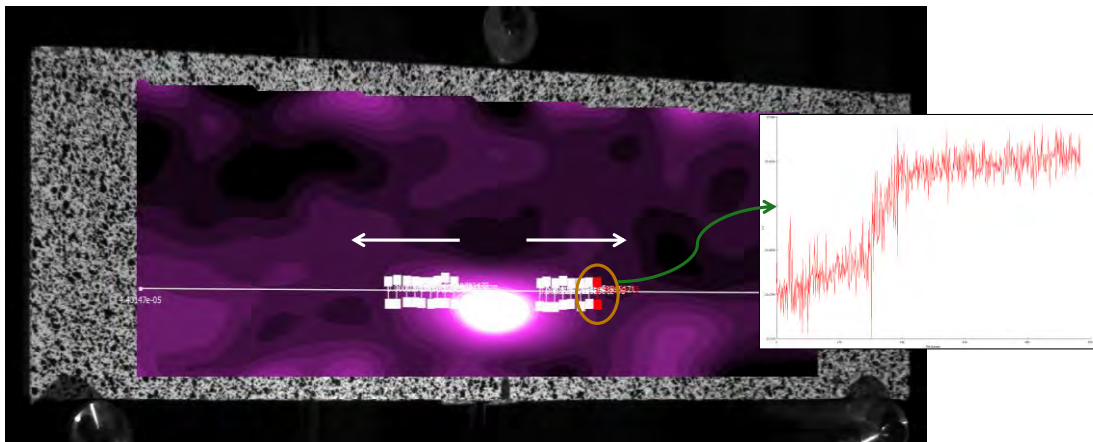


Figure V-28: Strain field color contrast showing interface debonding location and using artificial extensometer to determine the debonding length for 30R0F repair (100000 cycles)

Image No: 398
No of Cycles : 1000

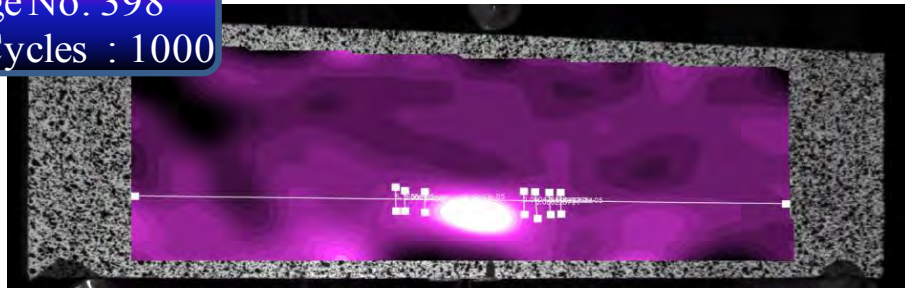


Image No: 456
No. of Cycles : 10000

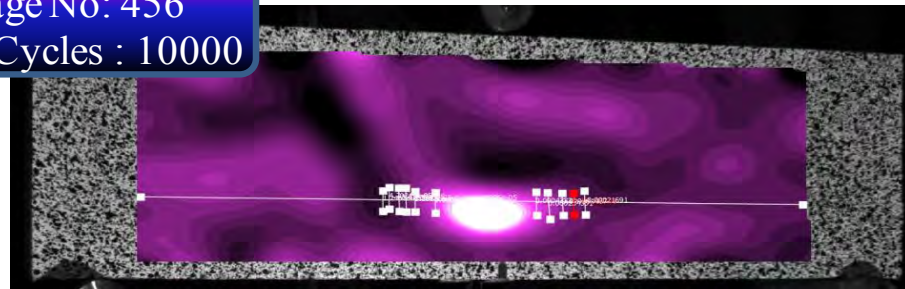


Image No: 498
No. of Cycles : 20000

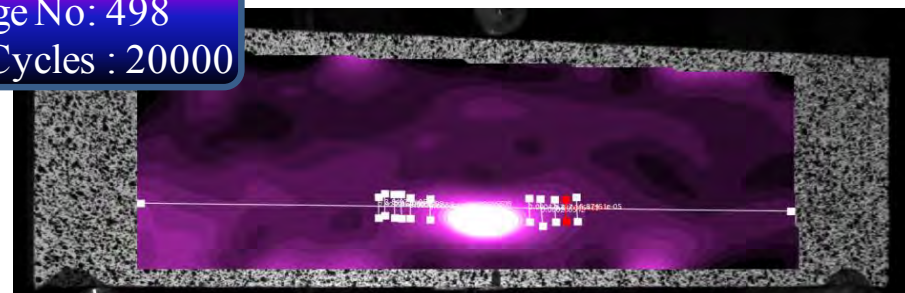


Image No: 574
No of Cycles : 40000

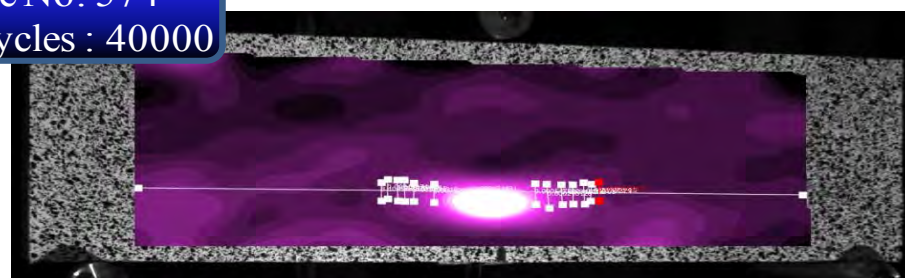
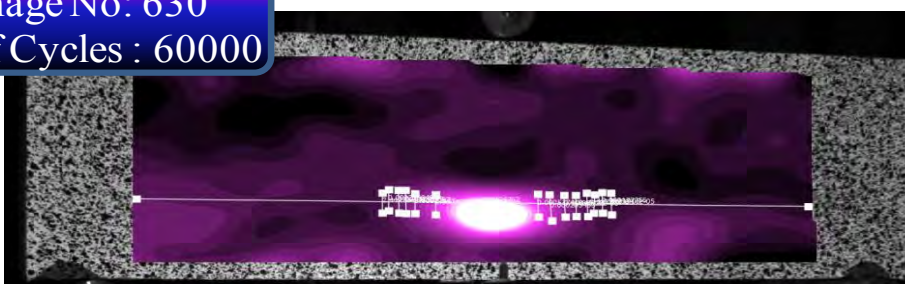


Image No: 630
No of Cycles : 60000



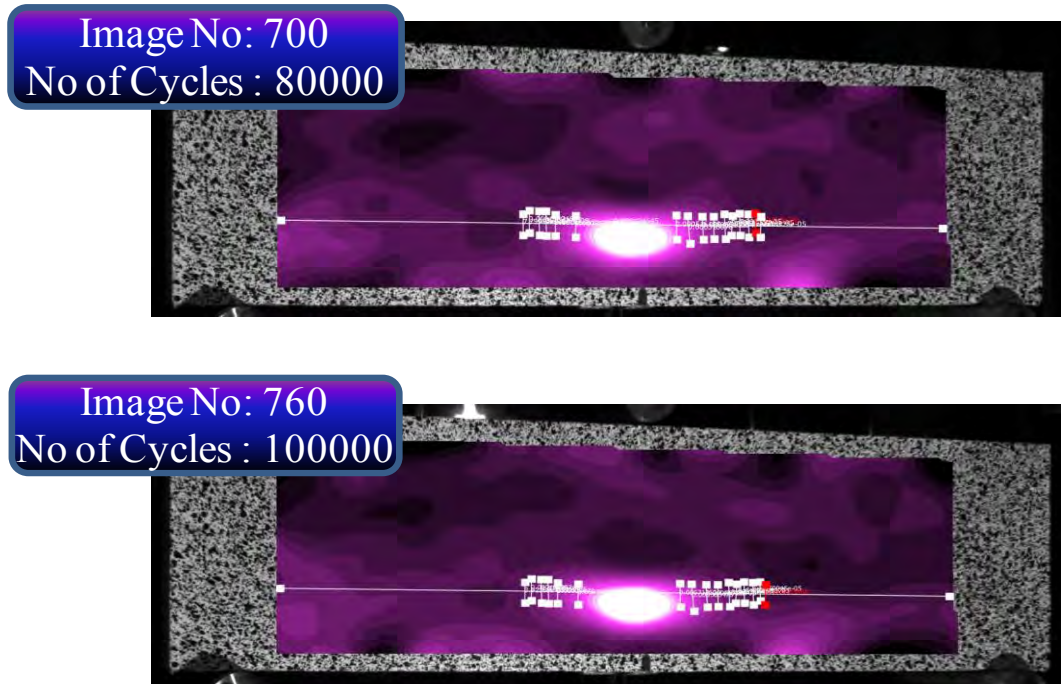


Figure V-29: Seven Strain fields showing interface debonding propagation with number of cycles and using artificial extensometer to determine the debonding length for 30R0F repair

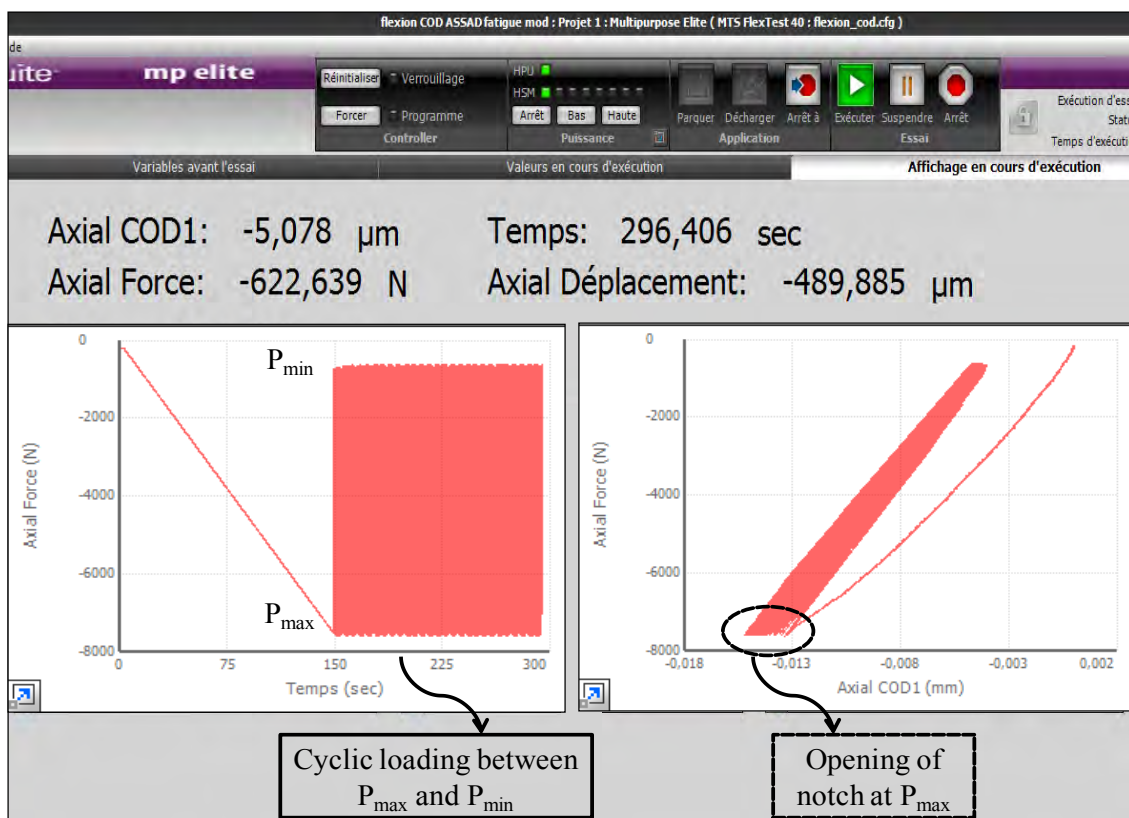


Figure V-30: Snapshot of MTS acquisition during fatigue test, showing opening of notch (COD) due to the application of cyclic loading between P_{max} and P_{min}

V.5.2 Results and discussions

V.5.2.1 Evolution of notch opening with the number of cycles

Curves presented from Figure V-31 to Figure V-34 show the evolution of the notch opening with respect to the number of loading cycles, measured at maximum load (P_{\max}) for composite beams with four different repair materials. In order to make a comparison among different repair mix compositions at a given number of cycles, an average COD is presented in Figure V-35.

Results show that in case of beams repaired with control mortar (CC), the opening of notch develops very quickly from the first cycle. And in case of beams repaired with 30R0F mortar the opening of the notch is limited upto certain extent as compared to control mortar repair.

The opening of the notch is very well limited in beams repaired with fiber reinforced material (with or without rubber aggregates). This is the consequence of the ability of fibers to transfer stresses through the cracks, that results in the control of notch opening not only in monotonic loading but also under fatigue loading.

It is also observed that addition of rubber aggregates along with the fibers in the repair material didn't change the role of fibers. However, once again, the combine use of rubber aggregates and fibers in the repair material produces a positive synergetic effect by further controlling the evolution of the notch opening (comparing results of composition 0R30F, 30R0F and 30R30F). Curve presented in Figure V-36 shows the evolution of notch opening (COD) with the number of cycles.

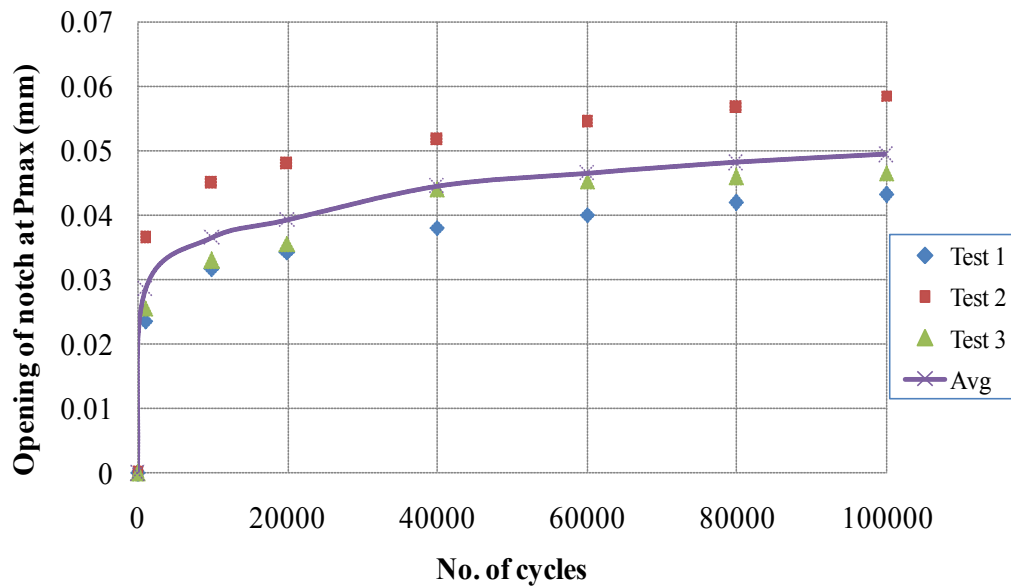


Figure V-31: Opening of notch at P_{max} with number of cycles for 0R0F (CC) repair.

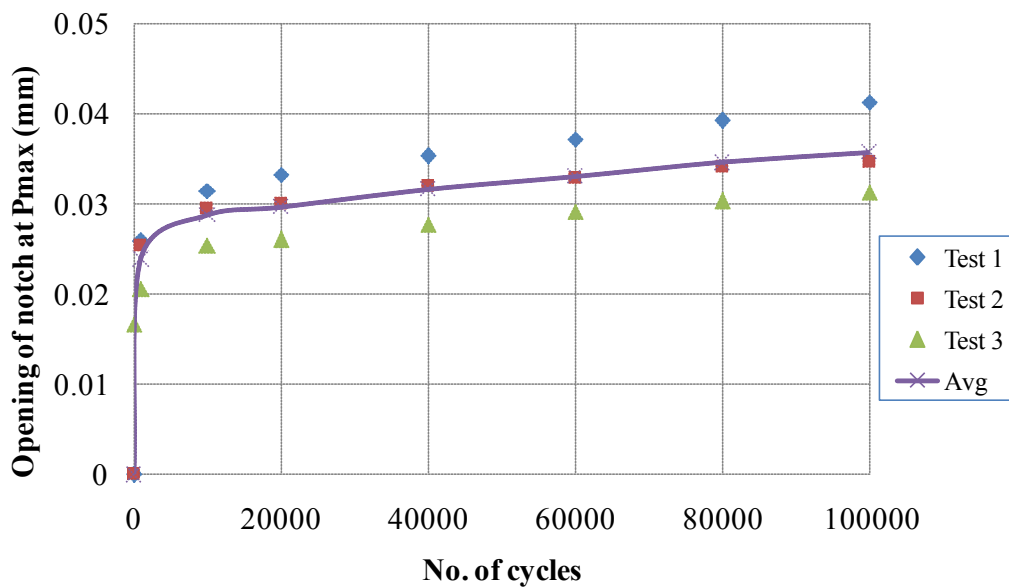


Figure V-32: Opening of notch at P_{max} with number of cycles for 0R30F repair

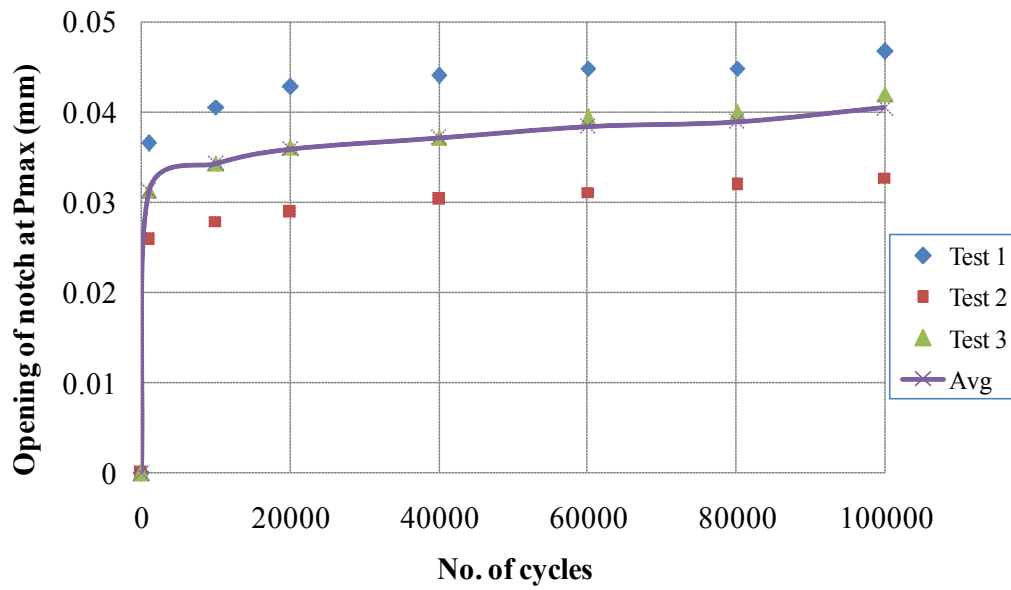


Figure V-33: Opening of notch at P_{\max} with number of cycles for 30R0F repair

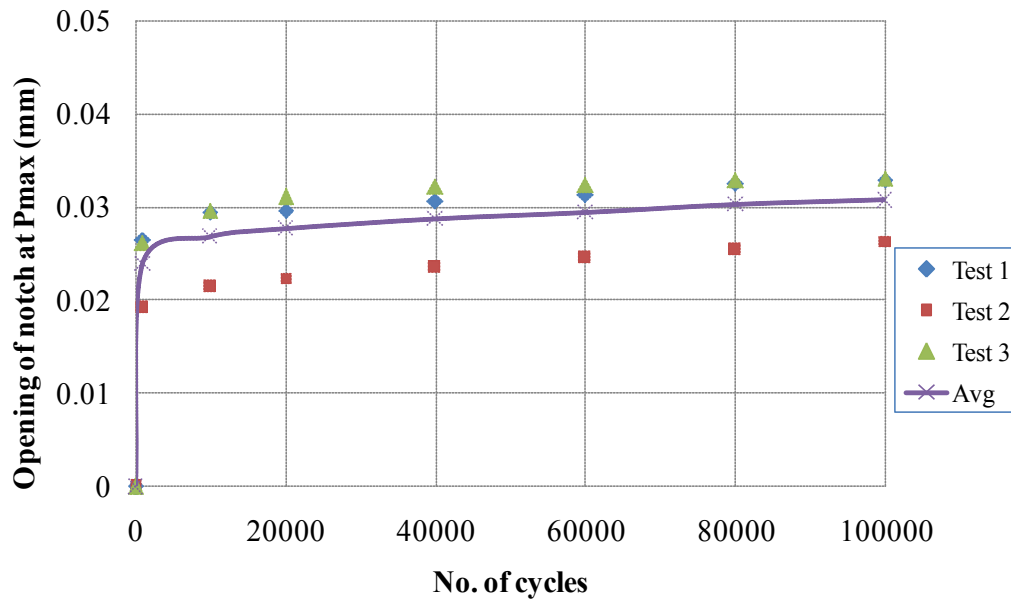


Figure V-34: Opening of notch at P_{\max} with number of cycles for 30R30F repair

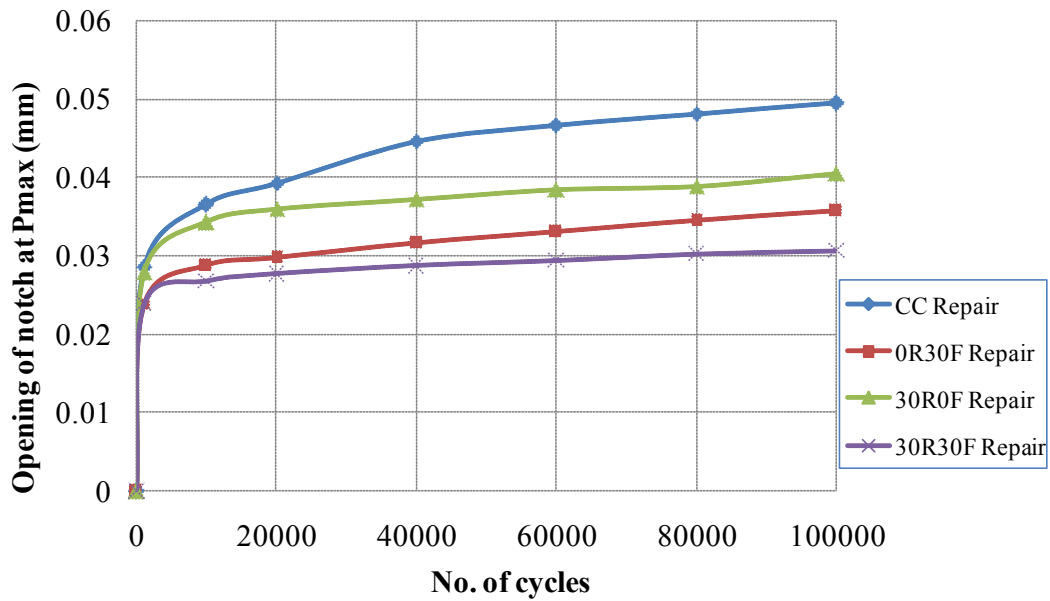


Figure V-35: Opening of notch at P_{max} with number of cycles for different repair mortar mixes

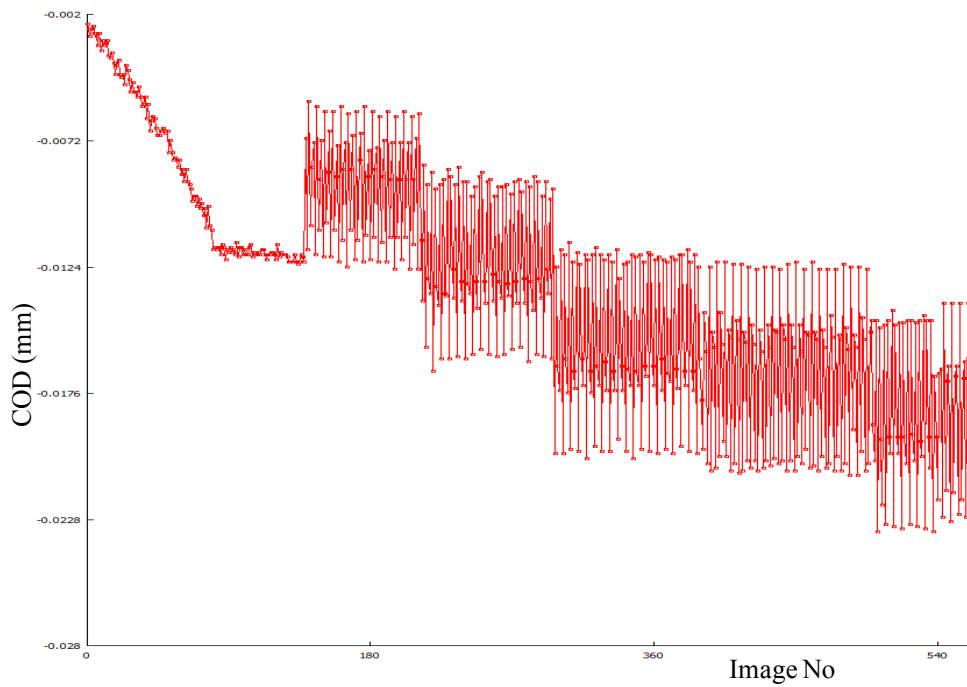


Figure V-36: Curve between COD and image number (recorded at every 20000 cycles), showing evolution of notch opening with number of cycles

V.5.2.2 Interface debonding propagation with number of cycles

The interface debonding propagation with the number of loading cycles for four different repair mix compositions is presented in curves shown from Figure V-37 to Figure V-40. For the comparison, the average interface debonding lengths with the number of cycles is presented in Figure V-41.

Under fatigue tests, the trends are quite similar to the one observed under monotonic loading. The interface debonding propagation is rapid in the repairs without fibers and this is very limited in the case of the fiber-reinforced overlays (with or without rubber aggregates). The efficacy of fiber-reinforced repair material can be explained by this simple example. In case of composite beams repaired with 0R0F or 3R0F mortar, the debonding length reaches to 70 mm from the very first cycles, whereas 20000 cycles are required for 0R30F mortar and more than 100000 cycles are necessary for 3R30F mortar to cause an equivalent damage.

The use of rubberized mortar as a repair material also limits the propagation of debonding, especially for some initial number of cycles. Since, the role of rubber aggregates vanishes very quickly once the crack opening becomes large with number of loading cycles.

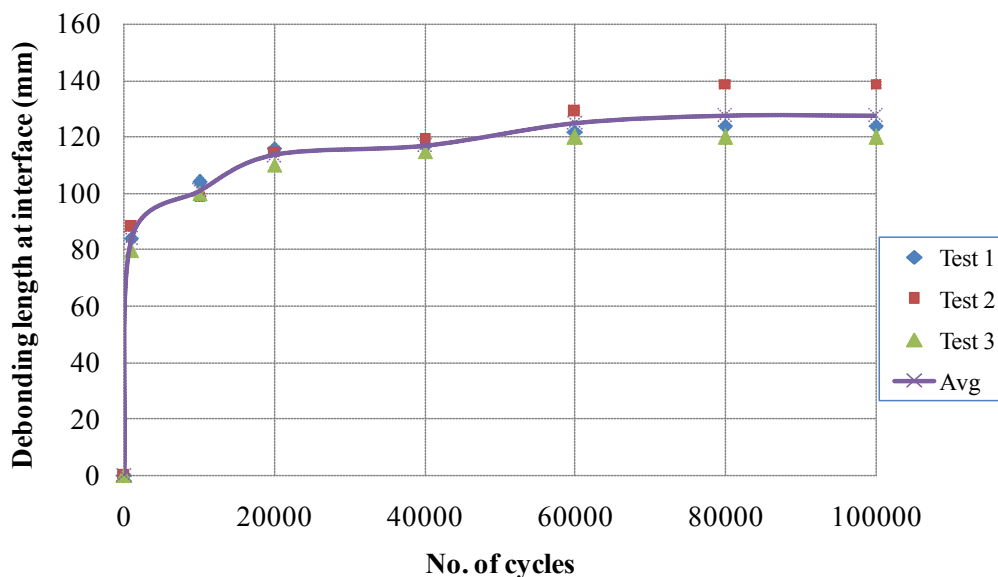


Figure V-37: Propagation of debonding length at interface with number of cycles for 0R0F (CC) repair

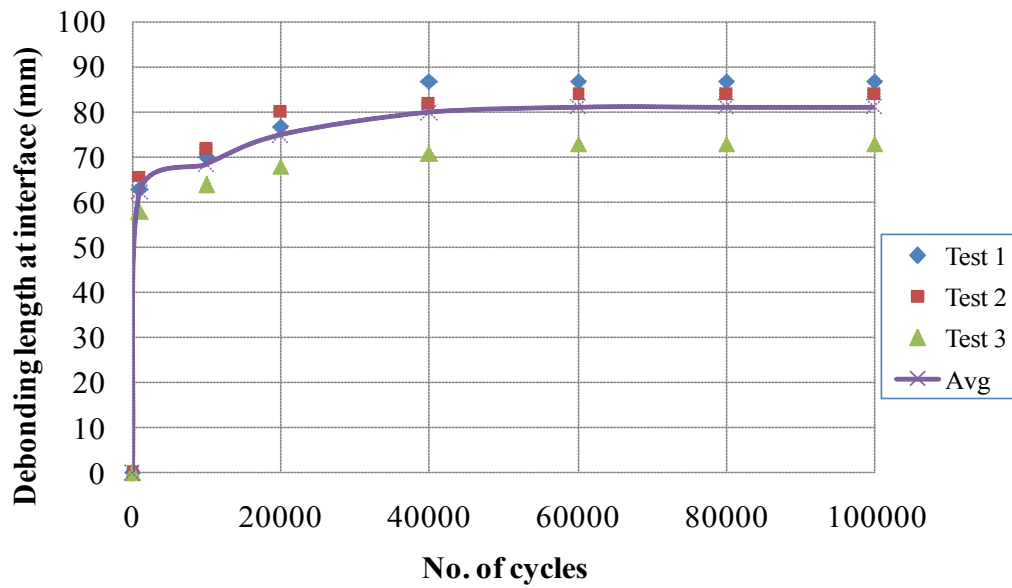


Figure V-38: Propagation of debonding length at interface with number of cycles for 0R30F repair

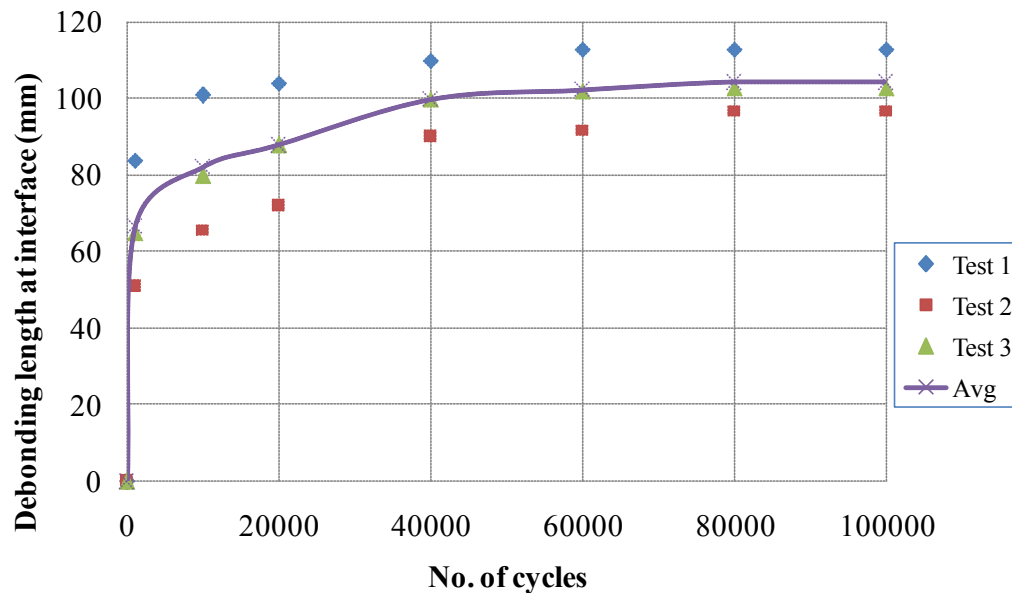


Figure V-39: Propagation of debonding length at interface with number of cycles for 30R0F repair

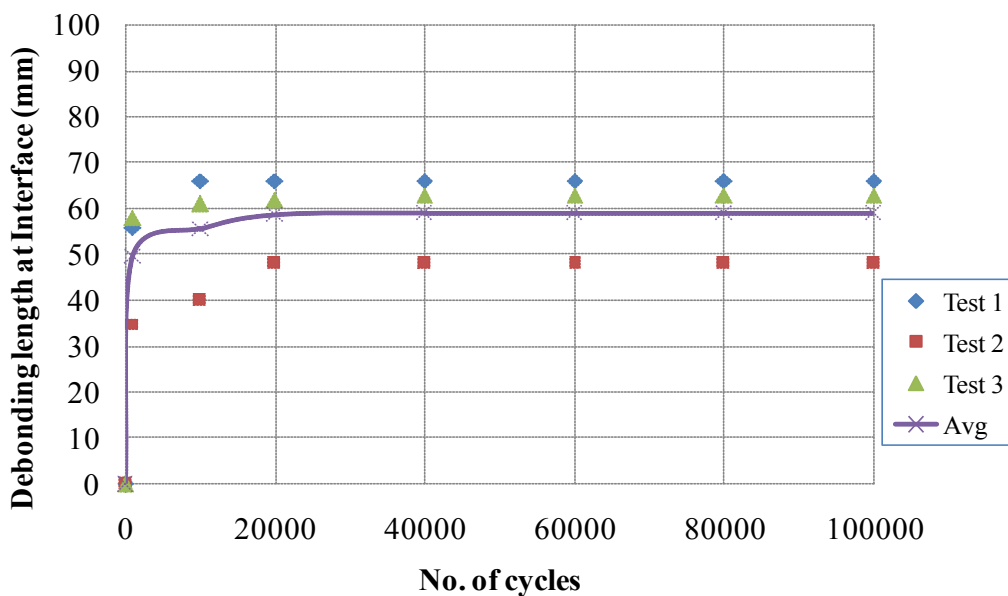


Figure V-40: Propagation of debonding length at interface with number of cycles for 30R30F repair

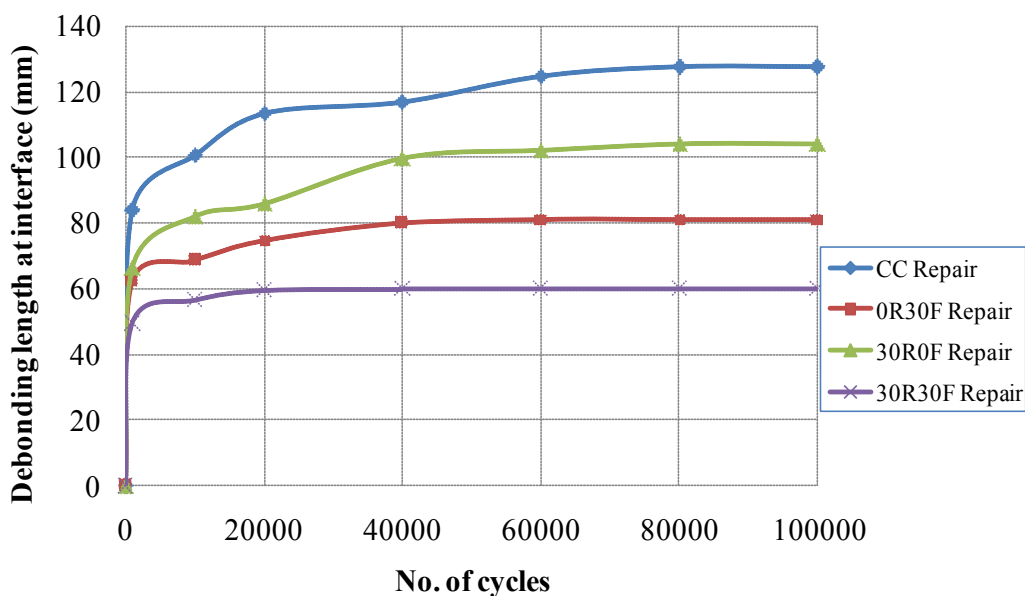


Figure V-41: Propagation of debonding length at interface with number of cycles for different repair mortar mixes

For better understanding the contribution of rubber aggregates, the fiber-reinforcement and combine use of rubber aggregates and fiber-reinforcement under fatigue loading, a curve is presented in Figure V-42 showing the relationship between interface debonding propagation and evolution of notch opening for our studied repair mix compositions. One can notice that for same notch opening, the debonding length is always less in specimens repaired with rubberized mortar (30R0F) as compared to the one repaired with control mortar (CC). Although, the difference in debonding length with the above mentioned repair mixes is not so significant. In the case of specimens repaired with fiber reinforced material (0R30F), the debonding length along with the opening of notch is very well limited as compared to control mortar repair. The mix containing both rubber aggregates and fibers (30R30F) behaves best among all of the studied repair mix compositions. Under fatigue loading, the debonding length along with the opening of notch is significantly reduced in specimens repaired with 30R30F mortar. This shows that positive synergetic effect provided by the combine use of rubber aggregates and fibers remains valid even under fatigue loading. The effectiveness of fibers to transmit stress through crack opening does not change even in the presence of rubber aggregates. Finally, it can be concluded that the incorporation of rubber aggregates and fibers in the repair material of thin bonded cement-based overlays is helpful to delay the debonding initiation and also to limit the interface debonding propagation.

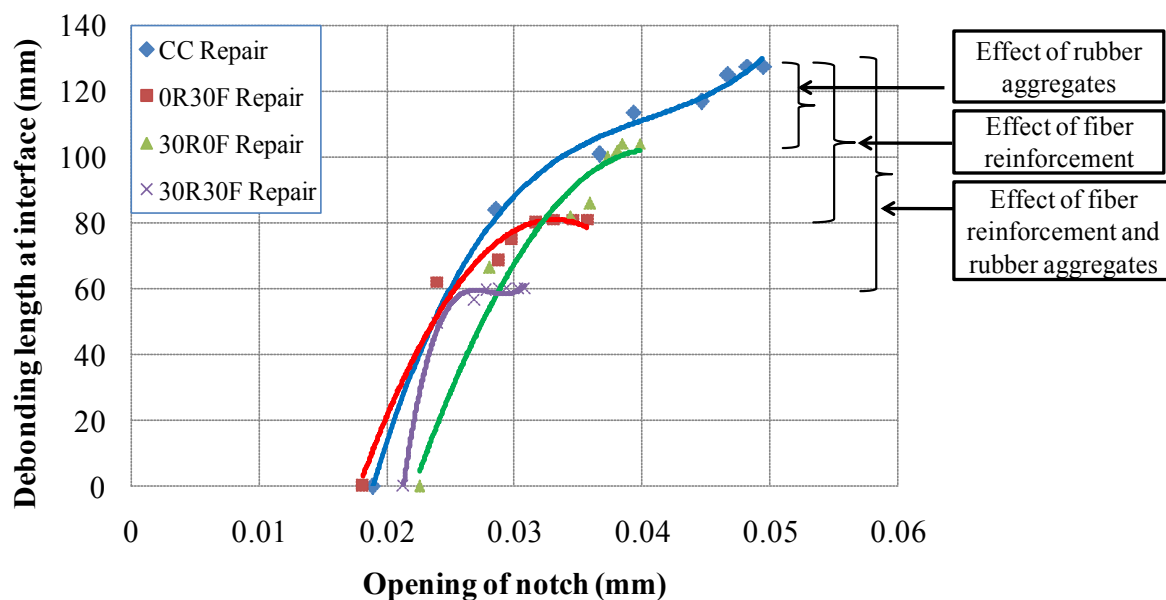


Figure V-42: Debonding length at interface vs. opening of notch for different repair mortar mixes

V.6 CONCLUDING REMARKS

This chapter reports the structural behaviour of repaired beams under flexural loading (monotonic and fatigue). Four mix compositions, i.e. 0R0F (CC), 0R30F, 30R0F and 30R30F were selected as a repair material. The reason for selecting these four repair mix compositions is to better understand the contribution of rubber aggregates, fibers and particularly the combine use of rubber aggregates and fibers towards the durability of the repair system. The main focus of this work is to determine the load at which debonding initiates and propagates along the interface between repair and substrate under monotonic and fatigue loading.

Under monotonic loading, the load required to initiate the interface debonding is the lowest for specimens repaired with control mortar (CC). In case of specimens repaired with rubberized mortar (30R0F), the interface debonding initiation is delayed as compared to reference control mortar. Since, rubber aggregates in mortar control the micro-cracking, which as a result increase the debonding initiation force. Along with the debonding initiation force, the notch opening at which debonding initiates is also increased due to the enhanced strain capacity of rubberized mortar. For fiber reinforced repairs (with or without rubber aggregates), the debonding initiation force is always higher as compared to control mortar repair. The maximum debonding initiation force is observed in specimens repaired with 30R30F. As far as interface debonding length is concerned, it is significantly limited in fiber reinforced repair materials. And the minimum debonding length is observed in specimens with 30R30F repair material.

Under fatigue loading, the efficiency of fibers in the repair material (with or without rubber aggregates) remains unaltered. Results present the same trend as the one obtained under monotonic loading. The efficiency of the composite specimens repaired with four different materials can be explained by this simple example. In order to attain the 100 mm interface debonding length, almost 10000 cycles are required for specimens repaired with 0R0F (CC) mortar. For acquiring the same debonding length, 40000 cycles are required in specimens with 30R0F repair. And in case of specimens repaired with 0R30F mortar, the debonding length is limited to 80 mm even after 100000 cycles. Similarly, the debonding length is also limited to 60 mm even after 100000 cycles for specimens repaired with 30R30F mortar. These results show that the synergetic effect provided by the combine use of rubber aggregates and fibers remains valid under fatigue loading also. These results prove that the

contribution of fibers towards the durability of thin bonded cement-based repairs does not change in the presence of rubber aggregates also.

All composite repaired beams used in this study were cast on sandblasted substrates. If one makes a comparison among debonding lengths obtained in this study with one of the previous study conducted in LMDC by using untreated substrates (T-H. Nguyen et al., 2010), then the debonding lengths are well limited with the sandblasted substrates. This shows that the substrate surface preparation also restricts the interface debonding propagation. It is also important to recall that most of these results are obtained through DIC technique. This technique seems relevant and exciting in order to detect cracks, the load at which debonding initiates and to follow interface debonding propagation.

Finally, it can be concluded that in thin bonded cement-based overlays, the debonding between repair and substrate is mainly caused by cracking of repair layer and differential shrinkage phenomena between freshly cast repair material and relatively stabilized substrate. Under these conditions, the best possible solution to control debonding is to use a repair material having an improved strain capacity and that can also provide post cracking residual strength. In this regard, the use of rubber aggregates in repair material is helpful to control micro-cracking, which as a result delay the debonding initiation. And after cracking of repair layer anything which can transfer the stress through these cracks can contribute towards the sustainability of this repair system. So, the fiber-reinforcement of repair material can be a suitable solution to improve the post cracking strength of repair material. This fiber-reinforcement of repair material is also helpful to limit the interface debonding propagation. So, the combine use of rubber aggregates and fibers in the repair material of thin bonded cement-based overlays can be a suitable solution to delay the debonding initiation and also to limit the interface debonding propagation.



CONCLUSIONS AND PROSPECTS

CONCLUSIONS AND PROSPECTS

Given the aging of civil engineering structures, there is general agreement that repairs are gaining importance in the rehabilitation of concrete structures. In this regard, the main objective of this research is to investigate the application of innovative cement-based materials in order to enhance the durability of thin bonded cement-based overlays. For this purpose, mortar incorporating rubber aggregates and fiber-reinforced was used. In this respect, special attention was paid on the fatigue performance of repair system.

Under cyclic loading, the bridging strength degradation of fiber reinforced and/or rubberized mortar was analyzed. Moreover, the impact of substrate surface preparation on the bond behaviour of repair system was also explored. In this regard, a comprehensive experimental program was conducted. Results obtained from all these experimental investigations are concluded in four different steps.

In the first step, different tests were conducted in order to determine the basic mechanical properties of fiber-reinforced and/or rubberized mortar. The results obtained from these mechanical tests can be summarized as follows:

- ✚ By the incorporation of rubber aggregates in mortar, a significant reduction in 28 days compressive strength is observed as compared to control mortar.
- ✚ Addition of rubber aggregates in mortar significantly reduces the compression modulus of elasticity. This reduction of modulus of elasticity as a result improves the strain capacity of mortar.
- ✚ The tensile strength is significantly reduced by the incorporation of rubber aggregates in mortar as compared to control mortar, but along with that an improvement in strain capacity of mortar is also observed.

Conclusions and prospects

- ✚ The tensile strength of mortar incorporated with metallic fibers is almost identical to the reference control mortar. On the contrary, the post peak residual strength is significantly enhanced by the incorporation of metallic fibers.
- ✚ The combine use of rubber aggregates and fibers in mortar not only improves the strain capacity, but also improves the residual post peak strength which is a solution to control crack opening and debonding in overlays. Also, it can be said that the presence of rubber aggregates didn't change the role of fiber-reinforcement. Therefore, the combination of both rubber aggregates and fibers in mortar produces a positive synergetic effect.
- ✚ Significant increase in total shrinkage is observed in a mortar mix incorporating rubber aggregates (30R0F). This increase in shrinkage is not only because of mass loss, but the low stiffness of rubber aggregates also plays a vital role in order to enhance shrinkage length change. In this regard, the combine use of rubber aggregates and fibers (30R30F) in mortar appeared to be a suitable solution to limit the shrinkage additionally induced due to the low stiffness of rubber aggregates.

In the second step, the importance of substrate surface preparation on bond behaviour of repair system was acknowledged. Different surface preparation techniques were evaluated by conducting bond tensile tests and the obtained results are concluded below:

- ✚ Bond tensile strength perpendicular to the interface is significantly improved by preparing the substrate surface and removing the top weak laitance or dirt deposit.
- ✚ Two different surface preparation techniques were evaluated by conducting the bond tensile tests. Among them, more bond strength improvement is observed with sawed substrate surface as compared to sandblasted one.
- ✚ Although, more bond strength is obtained with sawn substrate surface, but it was decided to use sandblasted one in this research work. Since, sand blasting surface preparation technique is easy to implement in actual conditions instead of cutting the whole surface.

In the third step, uniaxial tensile fatigue tests were conducted in order to establish the cyclic bridging law, which is capable to predict the cyclic bridging degradation behaviour of fiber

Conclusions and prospects

reinforced and/or rubberized mortar. Moreover, the impact of using the above mentioned composites as a repair material on interfacial bond strength degradation is also evaluated under tensile fatigue loading. The major outcomes of all these tests are presented below:

- ✚ The cyclic bridging degradation behaviour of fiber reinforced and/or rubberized mortar is a quite complicated phenomena and can be influenced by many parameters like material composition, maximum pre-cracked width value, loading conditions, etc.
- ✚ The bridging strength decreases with the number of fatigue cycles for the same maximum crack width, whatever the nature of the composite.
- ✚ The maximum cyclic bridging strength degradation occurs in plain mortar. For fiber reinforced mortar, cyclic bridging strength degradation is limited at large pre-cracked width values. In case of rubberized mortar, cyclic bridging strength degradation is limited at less pre-cracked width values.
- ✚ A combine use of rubber aggregates and fibers in mortars appeared to be a suitable solution to limit the cyclic bridging strength degradation. It confers to the composite an interest for durable application such as cement-based thin bonded overlays.
- ✚ The cyclic interfacial bond degradation behaviour can be influenced upto certain extent by repair material composition, especially with rubberized repairs. But the behaviour remains same by varying maximum pre-cracked width values.
- ✚ Interfacial bond strength decreases with the number of fatigue cycles for same maximum pre-cracked width value irrespective of the nature of the composite used as a repair material.
- ✚ Maximum cyclic bond strength degradation occurs in composite specimens repaired with control mortar and seems to be limited in composite specimens repaired with rubberized mortar.

Finally, the structural performance of thin bonded composite beams (repair on top of sandblasted substrates) is evaluated under monotonic and fatigue loading. Three point bending tests were conducted along with Digital 3D Image Correlation (DIC) technique. This DIC technique was used to detect the crack initiation and propagation and also to measure the

debonding along the interface. In the light of obtained results, one can draw the following conclusions:

- ✚ Under monotonic loading, the debonding initiation force is always higher for fiber reinforced repairs (with or without rubber aggregates) as compared to composite beams repaired with reference control mortar. The maximum debonding initiation force is observed in composite beams with fiber-rubberized repair material (30R30F).
- ✚ Under fatigue loading, the debonding propagation along the interface is more pronounced in the repairs without fibers and it is very much limited in the case of the fiber-rubberized overlays (30R30F). This shows that the synergetic effect provided by the combine use of rubber aggregates and fibers remains valid under fatigue loading also.
- ✚ Above all, DIC technique seems relevant and exciting tool in order to detect cracks, the load at which debonding initiates and to follow interface debonding propagation. This technique provides the flexibility to do back analysis of resulting strains obtained by post processing of images. So, this allows us to trace the crack path and one can place the artificial extensometer at an exact crack or debonding location in order to precisely identify the moment at which crack or debonding crosses this location.
- ✚ Finally, the use of rubber aggregates obtained by grinding end-of-life tyres in cement-based materials can be considered as a contribution to maintain a clean environment by limiting the landfill for residual waste.

Main Perspectives:

From the last two decades, several researches have been conducted in LMDC on this topic of thin bonded cement-based repairs. This present research responded some important questions related to cyclic crack bridging degradation of fiber reinforced and/or rubberized mortar and sustainability of using studied composites as overlay material. Similarly, the impact of substrate surface preparation towards the durability of thin bonded cement-based overlays is also highlighted here. In response to these questions, this research also proposed some other research directions in the field of thin bonded cement-based overlays which are listed below:

Conclusions and prospects

- ✚ To further explore the possibility of using studied composites as a repair material in real application, cyclic bridging strength degradation of studied composites could be analyzed for some more pre-cracked width values.
- ✚ The cyclic bridging degradation behaviour of cement-based mortar with the different nature of fibers or combination of different fibers could be evaluated and their structural performance could also be analyzed in monotonic and fatigue loading.
- ✚ A finite element modelling of test simulating thin bonded cement-based overlays could be conducted. This model should rely on the cyclic bridging degradation laws already developed under the scope of this study.
- ✚ The durability of such kind of application, especially when rubberized cement-based composite is used in severe environment deserves consideration. This question is more pertinent by keeping in view the known fact that the vulcanized rubber does not develop adhesion with the cement matrix. So, the degradation mechanism of such composite may be accelerated under severe environmental conditions.



REFERENCES

REFERENCES

A

ACI 546R-04., 2013. Concrete Repair Manual. American Concrete Institute(ACI) ICRI Fourth Edition.

A. Bascoul and A. Turatsinze., 1994. Microscopical characterisation of mode I crack opening in mortar. *Materials and Structures*, 27: 71-78.

A. Fiore, G-C. Marano, C. Marti, and M. Molfetta., 2014. On the Fresh/Hardened Properties of Cement Composites Incorporating Rubber Particles from Recycled Tires. *Advances in Civil Engineering*, vol. 2014, Article ID 876158, 12 pages. doi:10.1155/2014/876158.

A. Garbacz , L. Courard and K. Kostana., 2006. Characterization of concrete surface roughness and its relation to adhesion in repair systems. *Materials Characterization*, 56: 281-289.

A. Toumi, T-H. Nguyen and A. Turatsinze., 2015. Modelling of the debonding of steel fibre reinforced and rubberised cement-based overlays under fatigue loading. *European Journal of Environmental and Civil Engineering*, 19: 672-686.

A. Toumi, T-H. Nguyen and A. Turatsinze., 2013. Debonding of a thin rubberized and fibre reinforced cement-based repairs: analytical and experimental study. *Materials and Design*, 49: 90-95.

A. Toumi, T-H. Nguyen and A. Turatsinze., 2013. Benefits of low modulus of elasticity and of fibre reinforcement of cement based mortars as thin bonded overlay materials. *Experimental Mechanics*, 53: 1791-1797.

A. Turatsinze, J.-L. Granju and S. Bonnet., 2006. Positive synergy between steel-fibres and rubber aggregates: Effect on the resistance of cement-based mortars to shrinkage cracking. *Cement and Concrete Research*, 36: 1692–1697.

A. Turatsinze, S. Bonnet and J.-L. Granju., 2005. Mechanical characterisation of cement-based mortar incorporating rubber aggregates from recycled worn tyres. *Building and Environment*, 40: 221-226.

A. Turatsinze, H. Farhat and J-L. Granju., 2003. Influence of autogenous cracking on the durability of repairs by cement- based overlays reinforced with metal fibres. *Materials and Structures*, 36: 673-677.

A. Turatsinze, M. Measson and J-P Faure., 2016. Rubberised concrete: from laboratory findings to field experiment validation. *International Journal of Pavement Engineering*. doi:10.1080/10298436.2016.1215688.

A. Fernández-Canteli, L. Castañón, B. Nieto, M. Lozano, T. Holušová and S. Seidl., 2014. Determining fracture energy parameters of concrete from the modified compact tension test in proceedings of *Frattura ed Integrità Strutturale Conference (30)*: Catania (Italy) September 15-17, 2014, pages 383-393, doi: 10.3221/IGF-ESIS.30.46

A.G. Evans, F.W. Zok and R.M. Mcmeeking., 1995. Fatigue of ceramic matrix composites. *Acta Metallurgica et Materialia*, 43: 859-875.

AM. Hartman and MD. Gilchrist., 2004. Evaluating four-point bend fatigue of asphalt mix using image analysis. *Journal of Materials in Civil Engineering* 16: 60-68.

AS3600.,2009. *Concrete Structures*. vol. 2009, Standards Sydney, Australia.

B

Bassam A. Tayeh, B.H. Abu Bakar and M.A. Megat Johari., 2013. Characterization of the interfacial bond between old concrete substrate and ultra high performance fiber concrete repair composite. *Materials and Structures*, 46: 743-753

B. Bissonnette, L. Courard, AM. Vaysburd and N. Belair., 2006. Concrete removal techniques: influence on residual cracking and bond strength. *Concrete International*, 28: 49-55.

B. Bissonnette, L. Courard, DW. Fowler and J-L Granju., 2011. Bonded cement-based material overlays for the Repair, the Lining or the strengthening of slabs pavements, Springer, volume 3 of Rilem state-of-the-art reports. doi: 10.1007/978-94-007-1239-3

B. Gencturk, K. Hossain, A. Kapadia, E. LABib and Y-L Mo., 2014. Use of digital image correlation technique in full-scale testing of prestressed concrete structures. *Measurement*, 47: 505-515.

B.N. Cox and L.R.F. Rose., 1994. Time-or cycle-dependent crack bridging. *Mechanics of Materials*, 19: 39-57.

C

Concrete Repair Manual, ACI International, Farmington Hills, MI, USA, 1999.

C. Ciobanu, I. Lazău and C. Păcurariu., 2013. Investigation regarding the effect of viscosity modifying admixtures upon the Portland cement hydration using thermal analysis. *Journal of Thermal Analysis and Calorimetry*, 112: 331-338

C. Redon and J-L Chermant., 1999. “Damage mechanics applied to concrete reinforced with amorphous cast iron fibers, concrete subjected to compression”, *Cement and Concrete Research*, 21: 197-204

CD. Johnston and RW. Zemp., 1991. Flexural performance of steel fiber reinforced concrete-influence of fibre content, aspect ratio and type. *ACI Materials Journal*, 88: 374-83.

D

D.A. Hordijk., 1991. Local approach to fatigue of concrete. PhD thesis, Delft, Hollande.

D.E. Otter and A.E. Naaman., 1988. Properties of steel fibre reinforced concrete under cyclic loading. *ACI Materials Journal*, 85:254-261.

D.H. Dauskardt, B.J. Dalgleish, D. Yao, R.O. Ritchie and P.E. Becher., 1993. Cyclic fatigue crack propagation in a silicon carbide whisker-reinforced alumina composite: role of load ratio. *Journal of Materials Science*, 28: 3258-3266.

D.W. Hobbs., 1971. The dependance of the bulk modulus, Young's modulus, creep, shrinkage and the thermal expansion of concrete upon aggregate volume concentration. *Matériaux et Constructions*, 4: 107-114.

E

E. Bonaldo, JAO. Barros and PB. Lourenço., 2005. Bond characterization between concrete substrate and repairing SFRC using pull-off testing. *International Journal of Adhesion and Adhesives*, 25: 463-474.

E. Brühwiler and E. Denarié., 2008. Rehabilitation of concrete structures using ultra high performance fibre reinforced concrete in proceedings of second international symposium on ultra high performance concrete, Kassel, Germany, 05-07 March 2008, pages 895-902.

E. Romeo., 2013. Two-dimensional digital image correlation for asphalt mixture characterisation. interest and limitations. *Road Materials and Pavement Design*, 14: 747-763.

EN 1504 (2003) Products and systems for the protection and repair of concrete structures Definitions – Requirements – Quality control and evaluation of conformity, CEN (Brussels).

EN 1542., 1999. Products and systems for the protection and repair of concrete structures - Test methods – Measurement of bond strength by pull-off, CEN (Brussels).

EN1992-1-1.,2004. Design of concrete structures. Part 1: General Rules and Rules for Buildings. vol.1.

F

F. Grandhaie., 1993. Le béton de fibres métalliques amorphes comme nouveau matériau de réparation. PhD thesis, Université de Paul Sabatier de Toulouse.

Fibraex a new generation of metallic fibers., 2016. <http://www.oilandgas.saint-gobain.com/uploadedFiles/SGoilandgas/Documents/SEVA/SEVA-FIBRAFLEX-GB1.pdf>.

G

G. Bao and R.M. McMeeking., 1991. Fatigue crack growth in fiber-reinforced metal-matrix composites. Technical report, Materials Department and Mechanical Engineering Department, University of California.

G. Chanvillard, P-C. Aitcin and C. Lupien., 1989. Field evaluation of steel fibre reinforced concrete overlay with various bonding mechanisms. *Transportation Research Record*, 1226: 48-56.

H

H. Chausson and J-L Granju., 1996. Rechargements minces adherents en béton renforcé de fibres métalliques: jeu des fibres dans l'amélioration de leur adhérence au support. In 2ème Colloque Francophone sur les bétons renforcés de fibres métalliques, Toulouse.

H. Farhat., 1999. Durabilité des rechargements en béton de fibres : Effets du retrait et de la fatigue. PhD thesis, Université de Paul Sabatier de Toulouse.

H. Stang and J. Zhang., 1994. Experimental determination of fatigue crack growth in fibre reinforced concrete in the proceeding of 10th International Conference on Experimental Mechanics, Lisbon, Portugal, pages 1347-1352.

H.C. Wu, T. Matsumoto and V.C. Li., 1994. Buckling of bridging fibres in composites. *Journal of Materials Science Letters*, 13: 1800-1803.

J

J. Kim and Y. Kim., 1996. Experimental study of the fatigue behaviour of high strength concrete. *Cement and Concrete Research* 26:1513-1523.

- J. Silfwerbrand., 1990. Improving concrete bond in repair bridge decks. *ACI Concrete International*, 12: 61-66.
- J. Silfwerbrand and J. Paulsson.,1998. Better bonding of bridge deck overlays. *Concrete International*, 20: 56-61.
- J. Silfwerbrand and H. Beushausen., 2006. Bonded concrete overlays - bond strength issues, in proceedings of International Conference on Concrete Repair, Rehabilitation and Retrofitting, Cape Town, South Africa, published by Taylor & Francis Group, London, pages 19-21, edited by M. Alexander et al. 2006.
- J. Silfwerbrand, H. Beushausen and L. Courard., 2011. Bond [chapter 4] in *Bonded cement-based material overlays for the repair, the lining or the strengthening of slabs and pavements*, RILEM State-of-the-Art Report of RILEM TC 193-RLS published by Springer, pages 51-79, edited by B. Bissonette et al., 2011.
- J. Zhang and H. Stang., 1997. Interfacial degradation in cement based fibre reinforced composites. *Journal of Materials Science Letters*, 16: 886-888.
- J. Zhang and H. Stang., 1998. Fatigue performance in flexure of fibre reinforced concrete. *ACI Materials Journal*, 95: 58-67.
- J. Zhang, H. Stang and V.C. Li., 1999. Fatigue life prediction of fiber reinforced concrete under flexural load. *International Journal of Fatigue*, 21: 1033-1049.
- J. Zhang, H. Stang and V.C. Li., 2000. Experimental study on crack bridging in FRC under uniaxial fatigue tension. *ASCE Journal of Materials in Civil Engineering*, 12: 66-73.
- J. Zhang, H. Stang and V.C. Li., 2001. Crack bridging model for fibre reinforced concrete under fatigue tension. *International Journal of Fatigue*, 23: 655-670.
- J-L. Granju., 1994. Rechargement mince adhérentes de dalles, dallages ou chaussées en béton : fibrage et limitation du décollement de la couche de rechargemen. In 1er Colloque francophone sur les bétons renforcés de fibres métalliques, Béthune, France. pages 105-113.
- J-L. Granju., 1996. Thin bonded overlays: about the role of fibre reinforcement on the limitation of their debonding. *Advanced Cement Based Materials*, 4: 7-21.

J-L. Granju., 2001. Debonding of thin cement-based overlays. *ASCE Journal of Materials in Civil engineering*, 13: 114-120.

JO. Holmen., 1979. Fatigue of concrete by constant and variable amplitude loading. Doctoral Thesis, NTH Trondheim.

L

L. Courard, T. Piotrowski and A. Garbacz., 2014. Near-to-surface properties affecting bond strength in concrete repair. *Cement & Concrete Composites*, 46: 73-80

L. Courard, A. Garbacz and L. Wolff., 2006. Evaluation and quality assessment in RILEM TC 184 – IFE Industrial floors, RILEM Report 33, published by RILEM Publications S.A.R.L., Pages 59-89, [chapter 4] edited by P. Seidler, 2006.

L. Courard and M. Nélis., 2003. Surface analysis of mineral substrates for repair works: roughness evaluation by profilometry and surfometry analysis. *Magazine of Concrete Research*, 55: 355-366.

L. Courard, D. Schwall, A. Garbacz and T. Piotrowski., 2006. Effect of concrete substrate texture on the adhesion properties of PCC repair mortar in the proceedings of International Symposium Polymers in concrete (ISPIC), Guimarães, Oficinas Gráficas de Barbosa & Xavier, Lda, Braga, Portugal, pages 99-110 edited by J.B. Aguiar et al., 2006.

L. Courard., 2005. Adhesion of repair systems to concrete: influence of interfacial topography and transport phenomena. *Magazine of Concrete Research*, 57: 273-282.

L. Courard., 2005. Adhesion of repair systems to concrete: Influence of interfacial topography and transport phenomena. *Magazine of Concrete*, 57: 273-282.

L. Czarnecki and B. Chmielewska., 2005. Factors affecting adhesion in building joints. *Cement lime Concrete*, 2: 74-85.

L. Czarnecki, A. Garbacz and K. Kostana., 2003. The effect of concrete surface roughness on adhesion in industrial floor systems in 5th Int Colloq—industrial floors, Esslingen, Germany, 168-174.

M

M. Grzybowski and C. Meyer., 1993. Damage accumulation in concrete with and without fibre reinforcement. *ACI Materials Journal*, 90: 594-604.

M. Mahal, T. Blanksvård, B. Täljsten and G. Sas., 2015. Using digital image correlation to evaluate fatigue behavior of strengthened reinforced concrete beams. *Engineering Structures* 105: 277-288

M. Skazlic, D. Bjegovic' and M. Serdar., 2008. Utilization of high performance fiber-reinforced micro-concrete as a repair material in the proceedings of 2nd International Conference on Concrete Repair, Rehabilitation and Retrofitting (ICCRRR), cape town, South Africa, printed by Taylor & Francis Group, London, ISBN 978-0-415-46850-3, pages 317-318.

M-D-S. Pedro and N-B-S. Eduardo., 2013. A state-of-the-art review on roughness quantification methods for concrete surfaces. *Construction and Building Materials*, 38: 912-923.

M.T. Do., 1989. Développement d'un essai de délamination par fatigue. Mémoire de maîtrise des sciences appliquées. Université de Sherbooke.

N

NF EN 12390-3., 2003. Essais pour béton durci. Partie 3 : Résistance à la compression des éprouvettes. AFNOR

P

P. Paris and F. Erdogan., 1963. A critical analysis of crack propagation laws. *Journal of Basic Engineering*, 85: 528-534.

PMD. Santos, ENBS. Julio and VD. Silva., 2007. Correlation between concrete-to-concrete bond strength and the roughness of the substrate surface. *Construction and Building Materials*, 21: 1688-1695.

Q

Q-T. Tran., 2006. Interface ancien-nouveau béton : Caractérisation du comportement adoucissant de l'interface en cours de décollement et son évolution dans le cas de sollicitation de fatigue. PhD thesis, Université de Paul Sabatier de Toulouse.

Q-T. Tran, A. Toumi and J-L. Granju., 2006. Experimental and numerical investigation of the debonding interface between an old concrete and an overlay. *Materials and Structures*, 39: 379-389.

Q-T. Tran, A. Toumi and A. Turatsinze., 2007. Modelling of debonding between old concrete and overlay: fatigue loading and delayed effects. *Materials and Structures*, 40: 1045-1059

Q-T. Tran, A. Toumi and A. Turatsinze., 2008. Thin bonded cement-based overlays: numerical analysis of factors influencing their debonding under fatigue loading. *Materials and Structures*, 41: 951-967.

Q-T. Tran, A. Toumi and A. Turatsinze., 2008. Thin bonded cement-based overlays: numerical analysis of factors influencing their debonding under monotonic loading. *Materials and Structures*, 41: 863-877

R

RILEM TC CPC 8., 1972. Modulus of elasticity of concrete in compression. *Materials and Structures*, 6: 507-512.

RILEM TC 162-TDF., 2001. Test and design methods for steel fibre reinforced concrete. *Materials and Structures*, 34: 3-6

RILEM TC 162-TDF., 2002. Test and design methods for steel fibre reinforced concrete, design of steel fibre reinforced concrete using the sigma-epsilon method: principles and applications. *Materials and Structures*, 35: 262-278.

RILEM. CPC7., 1994. Direct tension of concrete specimens 1975 TC14-CPC. Rilem technical Recommendations for the testing and use of construction materials, E & FN Spon, London, pages 23-24, doi: 10.1617/2351580117.011.

Rossi P., 1998 “Les bétons de fibres métalliques”, Presses de l’Ecole Nationale des ponts et chaussées, Paris, (in French)

S

S-U. Balouch and J-L. Granju., 1999. Corrosion of different types of steel fibres in SFRC and testing of corrosion inhibitors in proceedings of an international conference Infrastructure regeneration and rehabilitation-improving the quality of life through better construction. A vision for the next millennium, Sheffield: 735-747.

S. Asad Ali Gillani, A. Toumi, A. Turatsinze. Effect of incorporating rubber aggregates and fiber reinforcement on the durability of thin bonded cement-based overlays. 8th RILEM International Conference on Mechanisms of Cracking and Debonding in Pavements, Volume 13 of the series RILEM Book series pages 619-625, doi: 10.1007/978-94-024-0867-6_87. edited by A. Chabot et al., 2016.

S. Bonnet., 2004. Matériaux cimentaires à haute déformabilité par incorporation de granulats issus du broyage de pneus usages. PhD thesis, Université de Paul Sabatier de Toulouse.

S-S. Dinis, M-D-S. Pedro, and D-D-C. Daniel., 2012. Effect of surface preparation and bonding agent on the concrete-to-concrete interface strength. *Construction and Building Materials*, 37: 102-110.

S. Li, J. Wang and M.D. Thouless., 2004. The effects of shear on delamination in layered materials. *Journal of the Mechanics and Physics of Solids*, 52: 193-214.

T

T. Matsumoto and V.C. Li., 1996. Uniaxial cyclic behavior of discontinuous fiber reinforced composites. Proceedings of the 4th Materials Engineering Conference, Washington, D.C, pages 426-435. edited by P. Ken and F. Chong.

T-H. Nguyen, A. Toumi, and A. Turatsinze., 2010. Mechanical properties of steel fibre reinforced and rubberised cement-based mortars. *Materials and Design*, 31: 641-647.

T-H. Nguyen, A. Toumi, A. Turatsinze and F. Tazi., 2012. Restrained shrinkage cracking in steel fibre reinforced and rubberised cement-based mortars. *Materials and Structures*, 45: 899-904.

T-H. Nguyen., 2010. Durabilité des réparations à base cimentaire : Analyse comparée de l'influence des propriétés mécaniques du matériau de réparation. PhD thesis, Université de Paul Sabatier de Toulouse.

V

V. Pickerd., 2013. Optimisation and validation of the ARAMIS digital image correlation system for use in large-scale high-strain-rate events. Published by Maritime Division DSTO Defence Science and Technology Organisation Australia.

V. Ramakrishan, G. Oberling and P. Tatnall., 1987. Flexural fatigue strength of steel fibre reinforced concrete. *America Concrete Institute*, 105: 225-245.

V. Ramakrishan and G. Oberling., 1987. Performance characteristics and fatigue strength of polypropylene fibre reinforced concrete. *America Concrete Institute*, 105: 159-178.

V. Sabathier., 2004. Rechargements minces adhérentes à base cimentaire renforcés de fibres métalliques : Condition de leur durabilité, modélisation et calcul. PhD thesis, Université de Paul Sabatier de Toulouse.

VC. Li and T. Matsumoto., 1998. Fatigue crack growth analysis of fibre reinforced concrete with effect of interfacial bond degradation. *Cement and Concrete Composites*, 20: 353-63.

W

W. Zhong and Wu. Yao., 2008. Influence of damage degree on self-healing of concrete. *Construction and Building Materials*, 22: 1137-1142.

W.G. Buttlar, B.C. Hill, Y.R. Kim, M.E. Kutay, A. Millien, A. Montepara, G.H. Paulino, C. Petit, I.O. Pop, E. Romeo, R. Roncella, S.A. Safavizadeh, G. Tebaldi, A. Wargo., 2014. Digital image correlation techniques to investigate strain fields and cracking phenomena in asphalt materials. *Materials and Structures*, 47: 1373-1390

Z

Zena R. Aljazaeri, John J. Myers., 2016. Fatigue and Flexural Behavior of Reinforced-Concrete Beams Strengthened with Fiber-Reinforced Cementitious Matrix. *Journal of Composites for Construction* : doi/10.1061/%28ASCE%29CC.1943-5614.0000726.

Z. Suo and JW. Hutchinson., 1990. Interface crack between two elastic layers. *International Journal of Fracture*, 43: 1-18.



ANNEXES

Annexe A

Methods to plot stress-crack width curves from stress-strain relationship obtained by direct tension test

From direct tension tests conducted on notched specimen, the stress-crack width curve (σ - w) cannot be obtained directly. These curves are derived from stress vs. displacement relationship (σ - δ) obtained during the test. Two methods are commonly used for obtaining (σ - w) relationship from the (σ - δ) relationship. According to first method (D.A. Hordijk., 1991), the crack opening width (w) is the displacement that occurs in the post peak region and can be obtained by subtracting the elastic displacement δ_{el} and irreversible displacement δ_{irr} from total displacement as shown in Figure A-1.

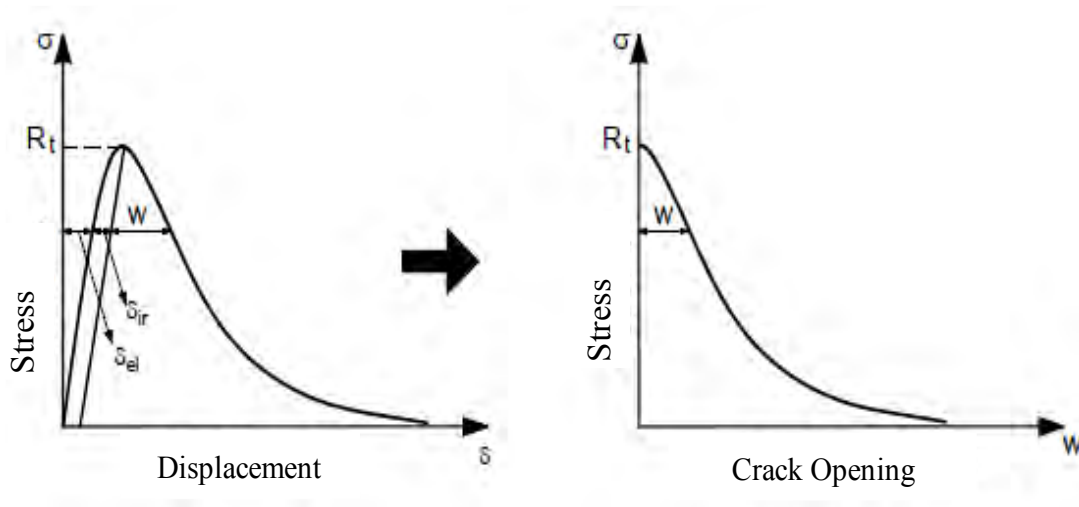


Figure A-1: Curve σ - w produced from σ - δ curve obtained by direct tensile test (D.A. Hordijk.,1991)

Second way to plot the (σ - w) curves is proposed by RILEM (RILEM TC 162-TDF., 2002). According to RILEM recommendation, the crack opening width (w) can be computed by subtracting the average value of the peak displacement δ_{pk} from total displacement δ for any given value of stress i.e. $w \geq 0$ as shown in Figure A-2.

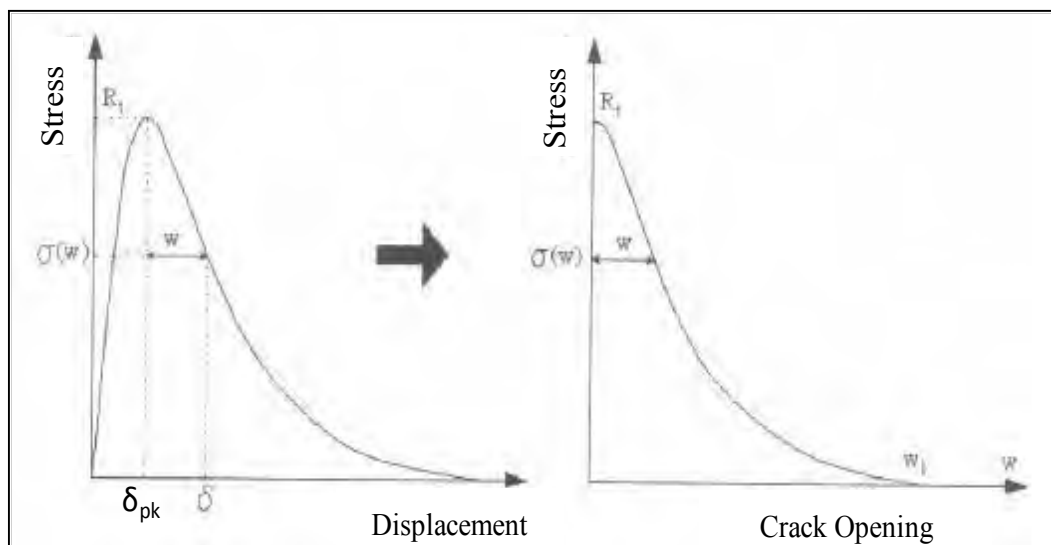


Figure A-2: Curve σ - w produced from the σ - δ curve obtained by direct tensile test according to RILEM recommendations TC 162-TDF (2002)

Annexe B

Effect of incorporating metallic fibers and rubber aggregates on fracture energy of mortars (G_f)

The fracture energy (G_f) can be obtained from area under load-displacement or load-COD (crack open displacement) curve as shown in Figure B-1. Simple, direct tension tests were conducted on the notched specimens for all of our studied mortar mixes. The area under the curve represents the work of fracture (W_f), from which the fracture energy (G_f) is defined as:

$$G_f = W_f / A_{lig}$$

where:

A_{lig} is a ligament cross-sectional area.

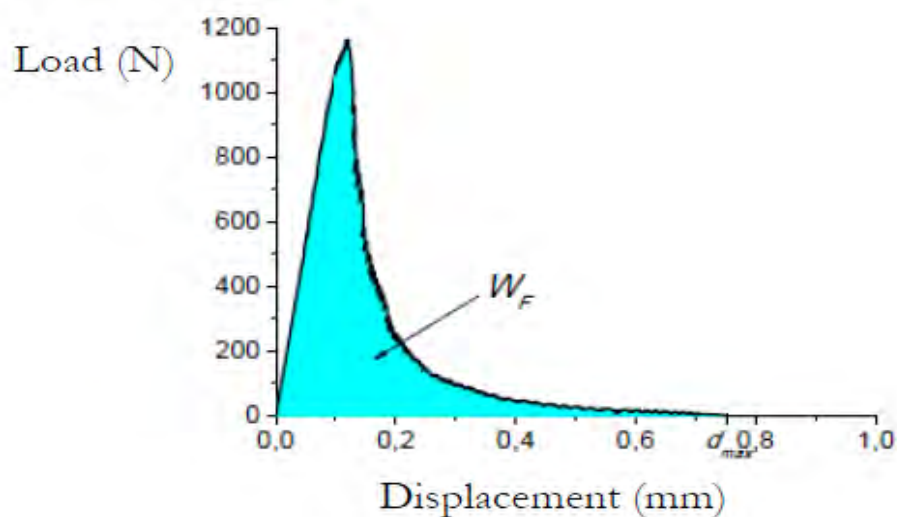


Figure B-1: Load-displacement curve of concrete specimens (A. Fernández-Canteli et al., 2014)

Fracture energy for all of our studied mortar mix compositions are presented in Figure B-2. For each mix composition, the fracture energy is calculated from the average of three curves and following conclusions can be made on the basis of energy analysis:

- ✚ Significant increase in fracture energy is observed for fiber-reinforced mortar as compared to reference control mortar.
- ✚ Incorporation of rubber aggregates along with metallic fibers (30R30F) produce a positive synergetic effect and further enhances the energy dissipation capacity of mortar.

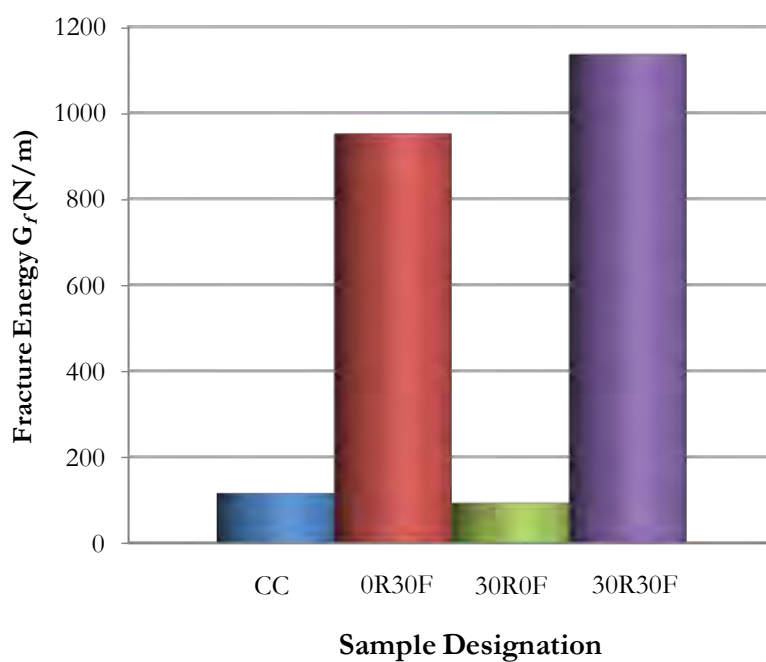


Figure B-2: Influence of fiber reinforcement and rubber aggregates incorporation on fracture energy

Annexe C

Bond tensile test along with DIC technique for monitoring debonding along interface

The purpose of conducting bond tensile test along with this DIC technique is to evaluate the delamination of repair from the base (opening at interface) measured by this technique and to compare it with the values of opening measured by COD. The accuracy of this technique is evaluated in a direct tension test before practically using this digital 3D image correlation technique for tracing the cracking pattern and to determine the interface debonding of repaired beams under simple flexure and flexural fatigue loading. In order to carry out 3D image correlation, sample preparation is necessary like painting it white and then black spot on this white painted surface as shown in Figure C-1. Figure C-2 shows the full testing arrangements (lights, cameras, etc.) necessary to use this digital image correlation technique.

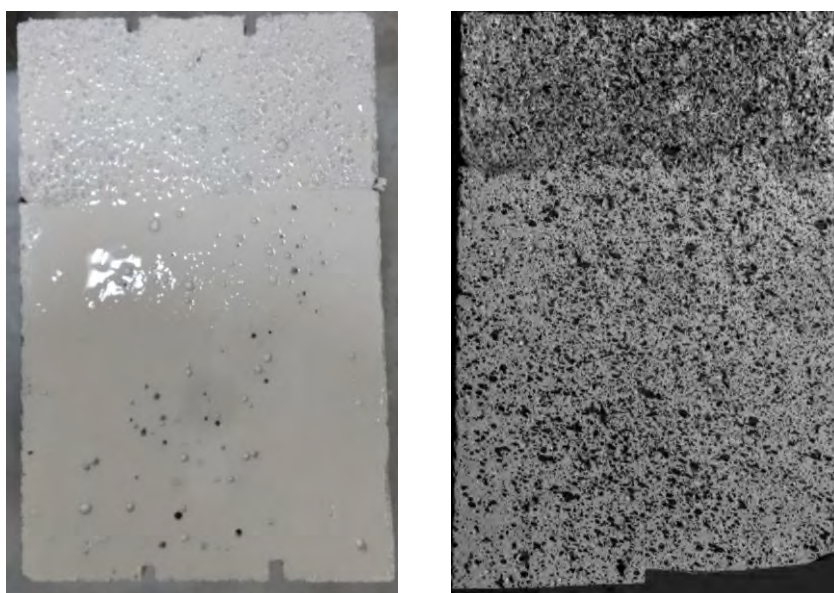


Figure C-1: Painting of sample before testing through DIC Technique

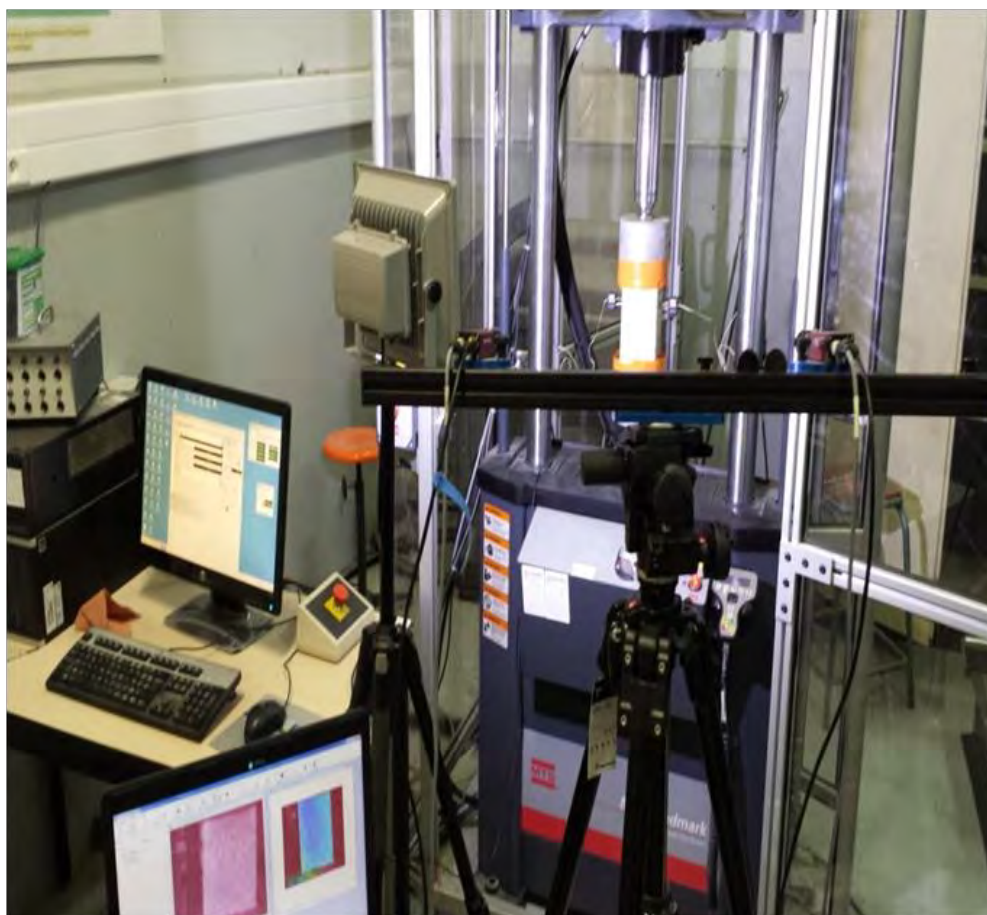


Figure C-2: Testing arrangements for using Digital 3D Image Correlation Technique

Comparison of crack opening values obtained from digital 3D image correlation and COD

Results of crack opening displacement at interface measured from digital 3D image correlation technique (D1) and from COD are shown in Figure C-3. Since D1 (crack opening at interface) is obtained by placing artificial extensometer at interface location in post treatment. This artificial extensometer determines opening at the interface by measuring the elongation occurs in it from the first image (reference image) to the last image. This artificial extensometer has a capability which allows us to compute the point at which debonding initiated and how it is propagating. Figure C-3 shows that crack opening at interface obtained from this digital 3D image correlation technique is in agreement with the value obtained from COD. Figure C-5 shows four displacement maps indicating how debonding propagates at the interface with the increase of notch opening.

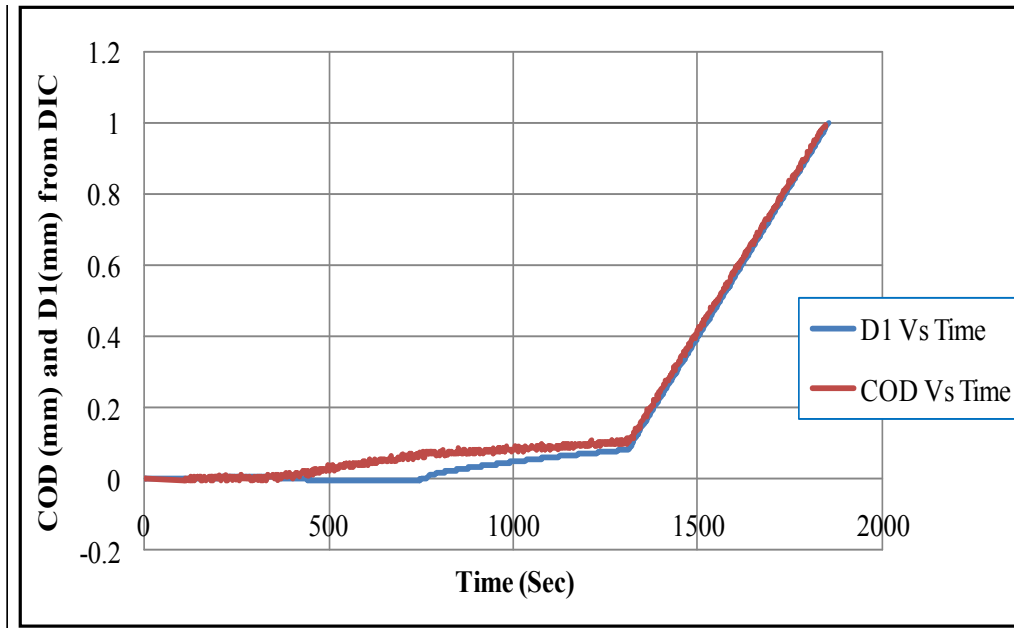


Figure C-3: Crack opening at interface under direct tension measured by COD and by using extensometer D1 in post treatment through DIC Technique

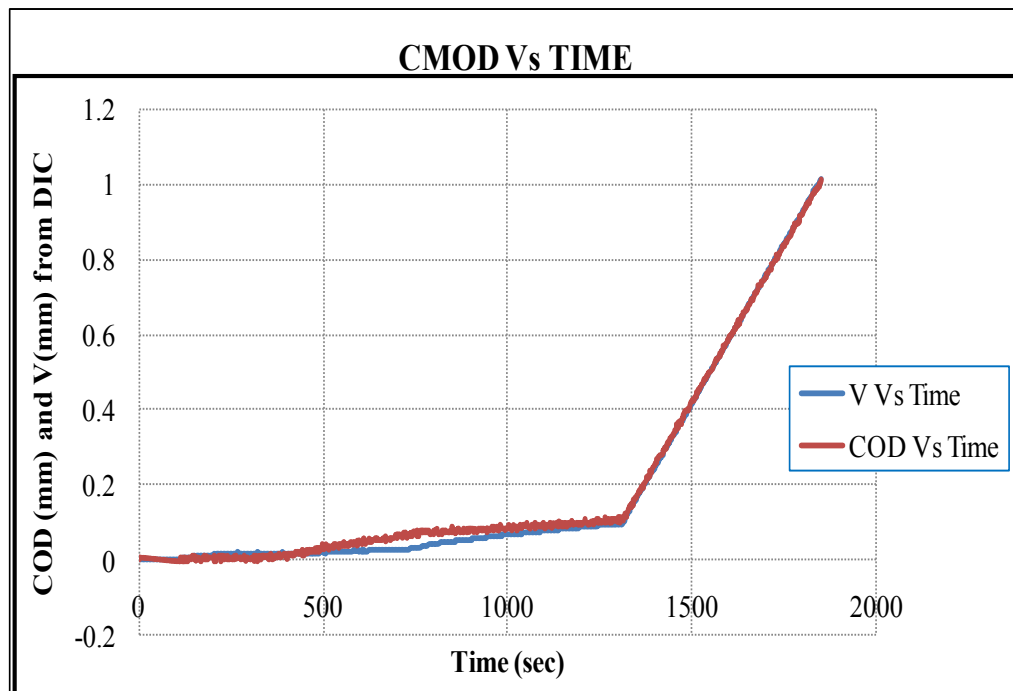


Figure C-4: Crack opening at interface under direct tension measured by COD and vertical displacement V from DIC Technique

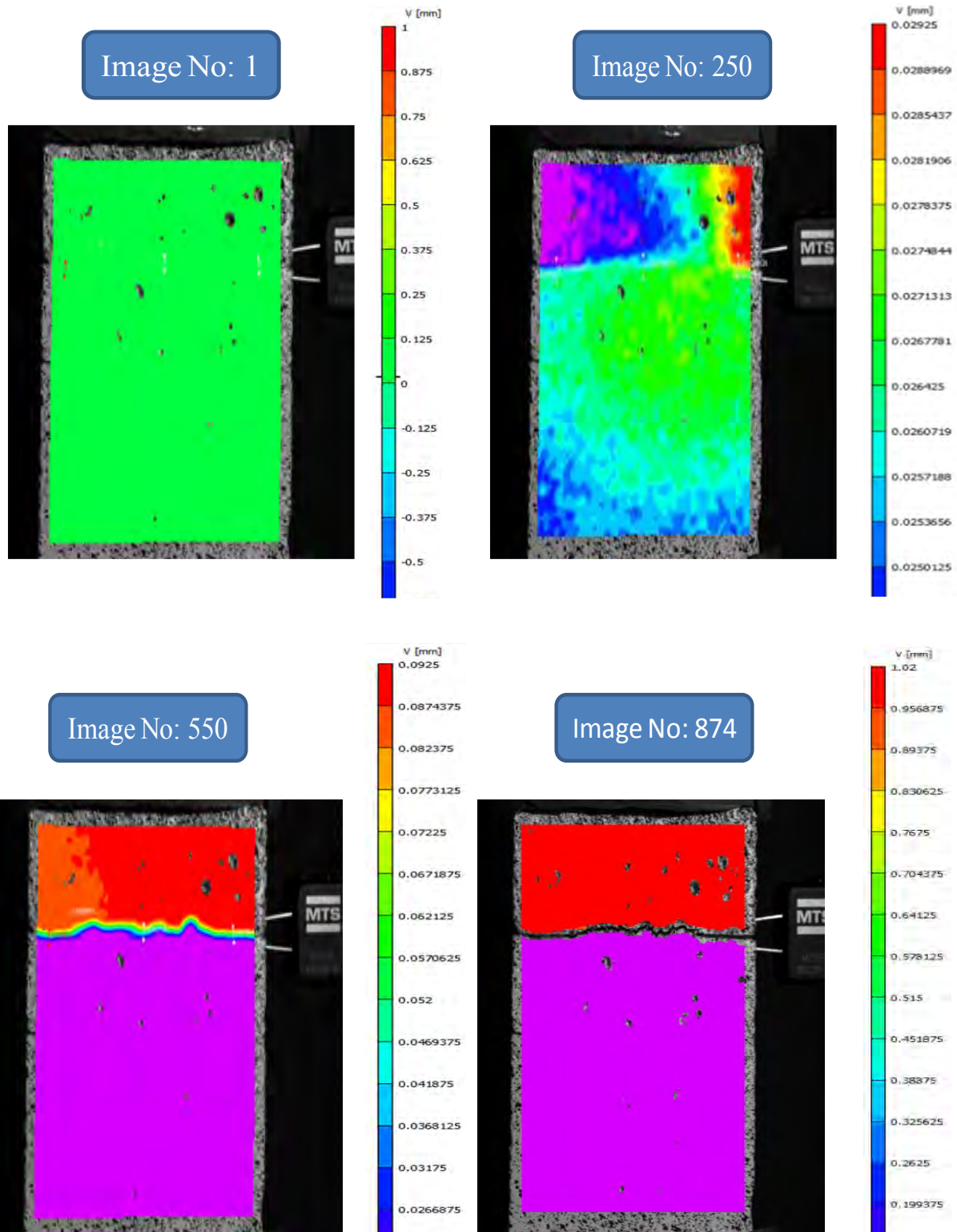


Figure C-5: Four vertical displacement maps showing debonding propagation

Manta G-504B/C

Feature	Specification
Resolution	2452 x 2056
Sensor	Sony ICX655AL/AQ with Super HAD CCD™ technology
Type	Progressive Scan CCD
Sensor size	Type 2/3
Cell size	3.45 μm
Lens mount	C / CS-Mount
Housing variants ¹	Standard (straight view), Angled head, Board level
Maximum frame rate at full resolution	9 fps
Maximum image bit depth	12-bit
On-board FIFO image buffer	32 MB, up to 6 frames at full resolution
Mono formats	Mono8, Mono12Packed, Mono12
Color formats	BayerGB8, BayerGB12Packed, BayerGB12, Mono8, RGB8Packed, YUV411Packed, YUV422Packed, YUV444Packed, BGR8Packed, RGBA8Packed, BGRA8Packed
Exposure control	38 μs to 60 s; 1 μs increments
Gain control	0 – 32 dB
Binning	Horizontal: 1 to 8 columns; Vertical: 1 to 14 rows
Decimation	Horizontal and Vertical: 1, 2, 4, 8 factor
Opto-isolated I/Os	2 inputs, 2 outputs
RS-232	1 TxD, 1 Rx D
Voltage requirements	8 – 30 VDC, or PoE
Power consumption	3.9 W @ 12 VDC; 4.6 W PoE
Trigger latency ²	Idle state: 12.8 μs; Frame valid state: 34.0 μs
Trigger jitter ²	Idle state: 9.1 μs; Frame valid state: 30.3 μs
Operating temperature	+5°C to +45°C ambient temperature without condensation
Storage temperature	-10°C to +70°C ambient temperature without condensation
Body dimensions (L x W x H)	86.4 x 44 x 29 mm
Mass	PoE model: 210 g; Non-PoE model: 200 g
Hardware interface standard	PoE, IEEE 802.3af 1000BASE-T, 100BASE-TX
Interface standard	GigE Vision Standard V1.2
Camera control interface	GenICam SFNC V1.2.1 compliant
Regulatory	CE, FCC Class B, RoHS (2011/65/EU)

¹ For more information on housing variants, see the [Modular concept](#).







² It is possible to start the exposure of the next frame while the previous frame is read out:

- Idle state: sensor is ready and camera is idle, waiting for the next trigger
- Frame valid state: sensor is reading out and camera is busy. If the next frame is requested by an external trigger in this state, higher latency may occur as compared to the idle state.

Annexe D

Technical data about materials

- ✚ Cement CEM I 52.5 R
- ✚ Sand 0/4 mm
- ✚ Super-plasticizer (BASF Glenium 27)
- ✚ Viscosity agent (BASF Rheomac 890F)
- ✚ FibraFlex fibers provided by SEVA (Saint Gobin)
- ✚ Sand used for Sandblasting (0.3/1.2 mm)

FICHE TECHNIQUE PRODUIT			CIMENTS						
									
			USINE DU TEIL CEM I 52,5 R CE CP2 NF						
SERVICES EXCLUSIFS 			Déclaration de Performance n° 0333-CPR-1201						
Centre de Relation Clientèle 0825 888 007* Numéro indigo : 0.196 TTCimr									
NF EN 197-1 NF P 15-318									
CARACTERISTIQUES PHYSIQUES ET MECANIQUES									
	DP (min)	Stabilité (mm)	Résistances mécaniques (MPa)		MV (g/cm ³)	SSB (cm ³ /g)	Demande en eau (%)	Q41 (J/g)	L*
			2 jours	28 jours					
Val. moyenne	126	1,0	40,6	71,8	3,15	4150	28,7	363	64
Val. garantie	> 60	< 10	> 28	> 50					
CARACTERISTIQUES CHIMIQUES									
	Valeur moyenne	Valeur garantie							Valeur moyenne
SO ₃ (%)	3,50	< 4,5	Alcalins équivalents [Na ₂ O + 0,658 K ₂ O] (%)						0,2
Chlorures Cl ⁻ (%)	0,04	< 0,1	Alcalins actifs [suivant la norme NF P 18-454] (%)						0,2
Perte au feu 950°C (%)	2,00	< 5	Vc coefficient de variation des alcalins actifs						0,13
Insolubles (%)	0,40	< 5							
S ⁻ (%)	0,01	< 0,2							
CONSTITUANTS PRINCIPAUX ET SECONDAIRES :									
Clinker Portland Le Teil	95,0%							Constituant secondaire	5,0%
C ₃ S + C ₂ S (%)	78							Calcaire	
CaO/SiO ₂	3,1								
MgO (%)	0,8								
C ₃ S (%)	67								
C ₂ S (%)	10								
C ₃ A (%)	9								
C ₄ AF (%)	8								
								Total des constituants	100%
AUTRES CONSTITUANTS									
Gypse (%)									4,7
Agent de mouture AMA14E - Teneur sous forme d'extrait sec (%)									0,07
ou Agent de mouture AMA32E - Teneur sous forme d'extrait sec (%)									0,07
LIVRAISON EN SAC									
				Date de révision : 01/04/2015					
Les données figurant sur la présente fiche technique sont la propriété de Lafarge Ciments et ne peuvent être reproduites partiellement ou totalement sans notre autorisation préalable. Les résultats indiqués ne sont mentionnés qu'à titre purement indicatif, ils sont susceptibles de variation dans les limites des normes applicables et ne sauraient en conséquence engager la responsabilité de Lafarge Ciments. Les résultats de nos autocontrôles périodiques sont disponibles sur demande auprès de votre interlocuteur commercial habituel.									





SABLIERES MALET - Site de PORTET

27 avenue de Palarin
31120 Portet sur Garonne
Tel:0561728080

Fiche Technique
- NOV 2015 / 01

Engagement du 26/11/2015 au 25/05/2016

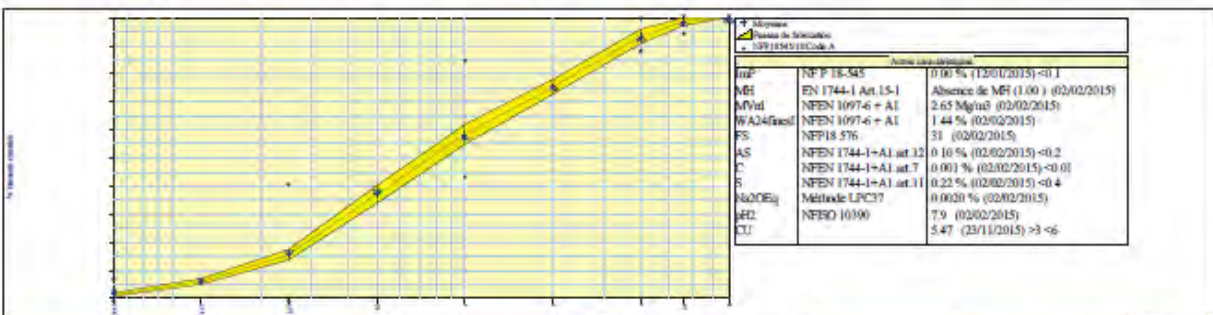
Page 1/1

Sable 0/4RL code 02108 SMP

Pétrographie : Alluvionnaire Siliceux de Garonne
Elaboration : Roulé Lavé
Site de production : PORTET SUR GARONNE
MARQUAGE CE : CE2+ - N°Certification: 0333-CPR-041006

Partie normative											
Valeurs spécifiées sur lesquelles le producteur s'engage											
Classe granulaire		Norme								Spécification	
0	4	NFP15-545 Art 10 - EN12620/EN13130 - Granulats pour bétons hydrauliques,mortiers								Code A	
		0.063	0.125	0.25	0.5	1	2	D	1.4D	2D	
								4	5.6	8	FM MB
Etendue e		6		40		40		10			0.6
Incertitude U		1		2		4		2	1		0.15 0.5
V.S.S.+U		7.0		42		88		100	100		3.52 2.00
V.S.S.		8.0		40		84		99	100	100	3.37 1.50
V.S.I.		0.0		0		44		89	95	100	2.77
V.S.I.-U		0.0		0		40		87	94		2.62
Ecart-type max.				12.12		12.12					0.18

Partie informative											
Résultats de production											
du 28/05/15 au 23/11/15											
	0.063	0.125	0.25	0.5	1	2	4	5.6	8	FM	MB
Maximum	2.3	8	19	43	64	79	97	100	100	3.28	0.49
Xf+1.25xEcart-types	2.0	7	17	40	62	78	96	100	100	3.26	0.48
Moyenne Xf	1.4	6	15	37	58	75	93	99	100	3.14	0.33
Xf-1.25xEcart-types	0.8	5	14	34	55	73	91	97	100	3.03	0.18
Minimum	0.4	5	13	33	53	72	89	96	100	2.95	0.22
Ecart-type	0.47	0.9	1.5	2.5	2.7	2.1	2.1	1.1	0.0	0.090	0.120
Nombre de résultats	29	29	29	29	29	29	29	29	29	29	29
Norme											
Demier	23/11/2015	23/11/2015	23/11/2015	23/11/2015	23/11/2015	23/11/2015	23/11/2015	23/11/2015	23/11/2015	23/11/2015	23/11/2015



Norme	Caractéristique	Valeur
NFP 15-545	0.10 % (12/01/2015) < 0.1	
MF	EN 1744-1 Art. 15-1	Absence de MF (1.00) (02/02/2015)
MVid	NFEN 1097-6 + A1	2.63 Mg/m³ (02/02/2015)
WA24finel	NFEN 1097-6 + A1	1.44 % (02/02/2015)
FS	NFP18-576	31 (02/02/2015)
AS	NFEN 1744-1+A1 art.12	0.10 % (02/02/2015) < 0.2
C	NFEN 1744-1+A1 art.7	0.001 % (02/02/2015) < 0.01
S	NFEN 1744-1+A1 art.11	0.22 % (02/02/2015) < 0.4
Méthode LFC37		0.0030 % (02/02/2015)
FDL	NFEN 10390	7.9 (02/02/2015)
CU		5.47 (23/11/2015) > 3 < 6

Le producteur :

Document remis à :



The Chemical Company

GLENIUM® 27



Superplastifiant haut réducteur d'eau pour béton à faible E/C, hautes performances et long maintien d'ouvrabilité

Description

Le GLENIUM® 27 est un adjuvant non chloré d'une nouvelle génération chimique à base d'éther polycarboxylique modifié. Cet adjuvant a été développé pour l'utilisation dans l'industrie du béton où haute qualité, durabilité, performance et ouvrabilité sont requises.

La nouvelle chimie du GLENIUM®

Le GLENIUM® se différencie des superplastifiants traditionnels par son action nouvelle et originale qui améliore de façon très significative le pouvoir dispersant sur le ciment.

Cette nouvelle structure chimique agit sur le grain de ciment par répulsion électrostatique et effet stérique, c'est à dire en créant un obstacle physique au rapprochement des particules de ciment. L'état dispersé est ainsi amélioré.

De plus, cette réaction est la combinaison de deux actions successives. Dès l'incorporation du GLENIUM® dans le mélange cimentaire, une première partie active agit immédiatement et la seconde est présente mais inactive. L'hydratation du ciment, qui se déroule normalement, fait évoluer le pH du mélange vers la basicité, ce qui provoque la libération progressive des molécules complémentaires.

Celles-ci travaillent de la même manière que les premières et prolongent donc l'état de dispersion évitant ainsi la floculation et donc le raidissement précoce du mélange.

Domaines d'application

Le GLENIUM® 27 est particulièrement recommandé pour l'élaboration de béton nécessitant un long maintien d'ouvrabilité et des performances mécaniques initiales élevées.

Le GLENIUM® 27 est donc adapté à l'industrie du béton prêt-à-l'emploi et aux chantiers de Génie Civil.

Propriétés

L'excellent effet de dispersion du GLENIUM® 27 permet de conserver une maniabilité très plastique ou fluide pendant plus de 1 heure 30 avec un faible rapport eau/ciment et sans effet de retard de prise.

Le GLENIUM® 27 apporte les avantages suivants au niveau de la mise en place, des performances et de la qualité intrinsèque du béton :

augmente

- la résistance à la compression à jeune âge et à long terme,
- la résistance à la flexion à jeune âge et à long terme,
- le module d'élasticité,
- l'adhérence sur les aciers,
- la résistance à la carbonatation,
- l'imperméabilité,
- la résistance aux agressions atmosphériques,
- la qualité des parements et de la texture du béton.

diminue

- la vibration,
- le retrait,
- le risque de fissuration,
- le fluage.

Caractéristiques

• Aspect	liquide
• Couleur	brun
• Masse volumique (MA 002)	1,05 ± 0,02 g/cm ³
• pH (MA003)	7,0 ± 1
• Teneur en chlorures (MA 004)	< 0,1 %
• Extrait sec	20 ± 2%
• Na ₂ O eq	< 2 %
• Transport	non classé
• Etiquetage	pas de symbole exigé



The Chemical Company

GLENIUM® 27

Mode d'emploi

Le GLENIUM® 27 est un adjuvant pour béton qui doit être incorporé isolément. L'effet optimal est obtenu par incorporation du GLENIUM® 27 dans le béton en différé, c'est-à-dire après l'addition de 70 % de l'eau de gâchage dans le malaxeur. Toutefois, il est possible d'incorporer le GLENIUM® 27 dans l'eau de gâchage.

Eviter d'ajouter le GLENIUM® 27 sur les granulats.

Recommandations

En cas de gel, réchauffer le produit jusqu'à une température proche de + 30°C et agiter mécaniquement.

Compatibilité

Le GLENIUM® 27 est compatible avec la majorité des ciments.

Le GLENIUM® 27 n'est pas compatible avec certains plastifiants et superplastifiants. Consultez votre représentant local BASF CC France pour toute synergie.

Dosage

Plage normale d'utilisation :

0,3 à 3,0 % du poids du ciment, soit 0,28 à 2,86 L pour 100 kg de ciment.

Pour d'autres utilisations, consultez votre représentant local BASF CC France.

Conditionnement

Container de 1000 L, fût de 210 L, bidon de 10 L ou vrac.

Stockage

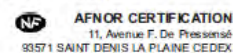
Stocker le GLENIUM® 27 dans des conditions de températures supérieures à + 5°C.

BASF Construction Chemicals France SAS a couvert sa responsabilité civile tant en exploitation qu'après livraison de ses produits par une police d'assurance souscrite auprès de la Compagnie HDI Gerling France. Les garanties de cette police sont complétées par la police "parapluie" responsabilité civile du Groupe souscrite auprès de la société d'assurances HDI Gerling Allemagne.

Nos fiches techniques ont pour objectif de vous conseiller d'après nos connaissances les plus récentes, nous nous réservons donc le droit de modifier à tout moment le contenu de celles-ci.

L'emploi des produits doit être adapté aux conditions spécifiques à chaque situation. Pour toute précision complémentaire, nous vous conseillons de prendre contact avec l'une de nos agences BASF Construction Chemicals France.

Nos fiches de données de sécurité sont disponibles sur simple demande par Internet (www.basf-cc.fr) ou par téléphone (au 01.69.47.50.00).



11, Avenue F. De Pressensé
93571 SAINT DENIS LA PLAINE CEDEX

BASF Construction Chemicals France SAS

Z.I. Petite Montagne Sud - 10, rue des Cévennes - Lisses - 91017 Evry Cedex
Tél. : 01 69 47 50 00 Fax : 01 60 86 06 32 <http://www.basf-cc.fr>



The Chemical Company

RHEOMAC® 890 F

Agent de viscosité pour bétons, mortiers et coulis de ciment.

Description

Le RHEOMAC® 890 F est un ajout liquide prêt à l'emploi à base de polymères synthétiques à haut poids moléculaire.

Cet ajout agit dès son incorporation, sur la texture de la pâte cimentaire.

L'action du RHEOMAC® 890 F sur cette texture permet une meilleure cohésion du mélange en garantissant un équilibre idéal entre fluidité et résistance à la ségrégation (propriétés normalement opposées).

Domaines d'application

Le RHEOMAC® 890 F peut être utilisé en béton prêt à l'emploi et dans les préfabriquations dans de nombreux domaines :

- Bétons Autoplaçants/Autonivellants (BAP/BAN).
- Bétons coulés sous l'eau.
- Coulis de ciment.
- Bétons légers.
- Bétons hautes performances (BHP).
- Bétons projetés.
- Bétons pompés.
- Mortiers de remplissage.
- etc...

Propriétés

Les biopolymères en solution dans la pâte cimentaire s'adsorbent sur la surface des grains de ciment, ayant ainsi une action sur la viscosité et sur les propriétés rhéologiques du mélange.

Les longues chaînes moléculaires du RHEOMAC® 890 F agissent par formation de "ponts" entre particules ultrafines de la pâte cimentaire. De plus, ces molécules s'orientent naturellement dans le sens d'écoulement du mélange.

En conséquence, le RHEOMAC® 890 F présente des avantages en phase statique et en phase dynamique sur le mélange cimentaire.

Phase statique

Le réseau tridimensionnel créé par les longues chaînes moléculaires dans la pâte cimentaire, assure la stabilité du mélange et améliore ainsi la résistance au ressuage et à la ségrégation.

Phase dynamique

L'orientation naturelle des molécules, dans le sens de l'écoulement, garantit une meilleure cohésion interne et améliore la déformabilité du mélange.

Cette chimie particulière apporte donc de nombreux avantages :

- Capacité à retenir l'eau.
- Amélioration de la stabilité.
- Diminution du ressuage et de la ségrégation.
- Diminution de la sensibilité des bétons aux variations de quantités d'éléments fins.
- Diminution de la sensibilité des bétons aux variations d'humidité des matériaux.
- Facilite le cheminement autonome du béton :
 - remplissage de formes complexes ou avec des réservations,
 - enrobage des armatures,
 - longues distances avec un seul point de coulage,
 - répartition le long du coffrage.
- Optimisation de la quantité de fines.

Ces caractéristiques sont particulièrement intéressantes pour le BAP et le BAN.



The Chemical Company

RHEOMAC 890 F

Caractéristiques

• Aspect	liquide
• Couleur	transparent
• pH (MA003)	7,5 +/-1,5
• Masse volumique (MA002)	1,01 - 1,02 g/cm ³
• Extrait sec	3 ± 1%
• Na ₂ O eq	< 1,5 %

Mode d'emploi

Le RHEOMAC® 890 F est particulièrement recommandé en synergie avec les superplastifiants de la gamme GLENIUM®.

La réactivité du RHEOMAC® 890 F est optimale si le produit est ajouté séparément sur un béton mouillé à environ 70 % (dosage différé). Toutefois, il est possible de le doser dans l'eau de gâchage.

Dosage

De 0,1 à 1,0 % du poids de ciment. Le dosage varie en fonction de la qualité et de la quantité d'éléments fins présents dans la formule utilisée. Il est recommandé d'effectuer des essais préalables.

Conditionnement

Container de 1.000 l, fût de 210 l, bidon de 10 l ou vrac.

Stockage

Conserver le RHEOMAC® 890 F dans des conditions de températures comprises entre + 5° C et + 40° C.

BASF Construction Chemicals France SAS a couvert sa responsabilité civile tant en exploitation qu'après livraison de ses produits par une police d'assurance souscrite auprès de la Compagnie GERLING FRANCE. Les garanties de cette police sont complétées par la police "parapluie" responsabilité civile du Groupe souscrite auprès de la société suisse d'assurances GERLING KONZERN de Zürich.

Nos fiches techniques ont pour objectif de vous conseiller d'après nos connaissances les plus récentes, nous nous réservons donc le droit de modifier à tout moment le contenu de celles-ci.

L'emploi des produits doit être adapté aux conditions spécifiques à chaque situation. Pour toute précision complémentaire, nous vous conseillons de prendre contact avec l'une de nos agences BASF Construction Chemicals France.

Nos fiches de données de sécurité sont disponibles sur internet : www.basf-cc.fr et sur simple demande au 01.69.47.50.00.



BASF Construction Chemicals France SAS

Z.I. Petite Montagne Sud - 10, rue des Cévennes - Lisses - 91017 Evry Cedex
Tél. : 01 69 47 50 00 Fax : 01 60 86 06 32 <http://www.basf-cc.fr>



Caractéristiques

Dimensions

Références disponibles sur stock	Longueur en mm	Largueur en mm	Epaisseur en µm	Nombre de fibres/kg	Surface spécifique en m ² /kg
FF5E0	5	1	24	1 100 000	11,6
FF10E0	10	1	24	580 000	11,6
FF15E0	15	1	24	385 000	11,6
FF20E0	20	1	24	275 000	11,6
FF20L6	20	1,6	29	150 000	9,6
FF30L6	30	1,6	29	100 000	9,6

SAINT-GOBAIN SEVA a le droit permanent d'améliorer la qualité de ses produits et services. Les caractéristiques de FIBRAFLEX® font l'objet de spécifications détaillées qui peuvent être consultées à la demande. Les renseignements indiqués dans cette fiche sont donc donnés à titre indicatif et ne sont pas contractuels.



Photographie de FIBRAFLEX® au microscope

Densité

• 7,2

Résistance à la traction

• ≥ 1400 MPa.

Composition

• Métal amorphe (Fe,Cr)₈₀ (P,C,Si)₂₀.

Résistance à la corrosion

• Excellente résistance dans les milieux salins (chlorures, sulfates) et acides.
 • Essais de corrosion dans HCl (0,1 N) et FeCl₃ (0,4 N) : pas de réaction après 24 heures.

Conditionnement

• Sacs de 10 kg.
 • Palettes de 500 kg.
 • Big-bags de 250 kg.



Contact

SAINT-GOBAIN SEVA
 Département **FIBRAFLEX**
 43 Rue du Port de Fer
 B.P. 176
 71105 Chalon-sur-Saône cedex
 FRANCE
 Tél. : +33 (0)3 85 47 25 88
 Fax : +33 (0)3 85 47 25 99
 www.fibraflex.com


SAINT-GOBAIN
 SEVA

DU 0,3/1,2H

Composition chimique type

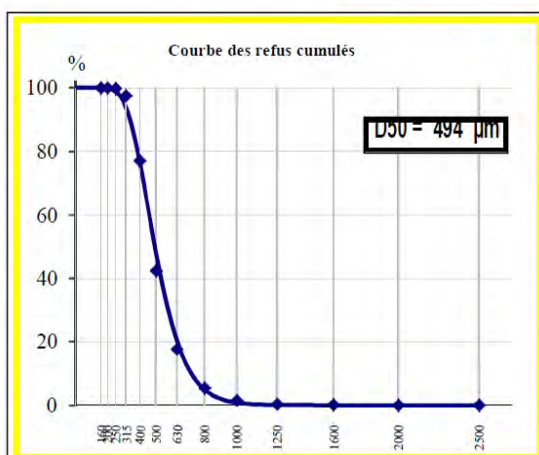
SiO ₂	99,30 %
Fe ₂ O ₃	0,022 %
Al ₂ O ₃	0,300 %
TiO ₂	0,013 %
CaO	0,008 %
K ₂ O	0,100 %

Caractéristiques physiques types

densité réelle (Pycnomètre)	2,65
dureté (Mohs)	7
pH	#7
densité apparente sable sec ("Prolabo")	1,5 à 1,6
perte au feu (à 1000°C)	moy 0,2%
résistance pyroscopique (SFC ISO R528) ..	1750 °C

GRANULOMETRIE MOYENNE STATISTIQUE

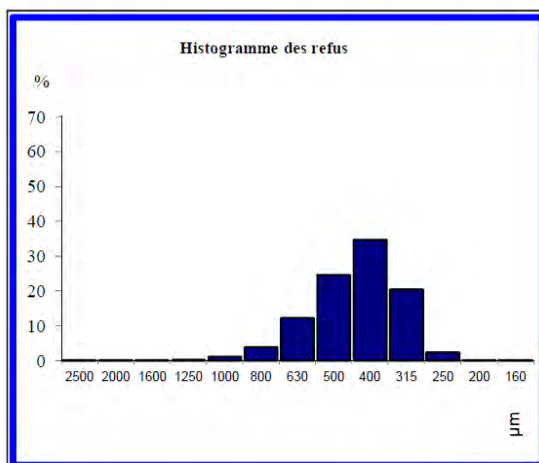
(% en masse - Valeurs indicatives)

TAMISAGE
AFNOR X.11-507

ouverture des mailles µm	refus cumulés %
> 2500 µm	0,0
> 2000 µm	0,1
> 1600 µm	0,2
> 1250 µm	0,4
> 1000 µm	1,5
> 800 µm	5,4
> 630 µm	17,7
> 500 µm	42,4
> 400 µm	77,1
> 315 µm	97,5
> 250 µm	99,8
> 200 µm	100,0
> 160 µm	100,0

TAMISAGE
AFNOR X.11-507

Classe µm	refus par tamis %
> 2500 µm	0,0
2500-2000 µm	0,1
2000-1600 µm	0,1
1600-1250 µm	0,2
1250-1000 µm	1,1
1000-800 µm	3,9
800-630 µm	12,3
630-500 µm	24,6
500-400 µm	34,7
400-315 µm	20,4
315-250 µm	2,4
250-200 µm	0,1
200-160 µm	0,0



CENTRE DE PRODUCTION DE DURANCE
Lieu-dit Landes de Gueyze Route du Brocq
47 420 DURANCE
Tel : +33 (0)5 53 65 53 77 Fax : +33 (0)5 53 65 85 18

SIEGE: Immeuble le Colisée - Bâtiment C
8 avenue de l'Arche - ZAC DANTON
92419 COURBEVOIE
Tel : +33 (0)1 53 76 82 00 Fax : +33 (0)1 42 25 32 23
site web : www.Sibelco.fr

TITRE: Dégradation de la résistance résiduelle en traction d'un béton : Effet d'un renfort par des fibres et des granulats en caoutchouc - Application aux rechargements minces adhérents à base cimentaire.

RESUME

Ce travail est centré sur l'étude du décollement de couches minces adhérentes à base cimentaire sur un substrat en béton sous chargement mécanique. Comme matériaux de réparation, des mortiers renforcés par des fibres et/ou incorporant des granulats en caoutchouc sont utilisés. Dans ces conditions, l'étude de la durabilité des réparations implique nécessairement celle de la dégradation de la résistance sous chargement de fatigue. Dans ce contexte, des essais de fatigue par traction, contrôlés par l'ouverture de la fissure (CMOD) sont effectués sur des échantillons composites afin d'établir la loi de dégradation de la résistance du mortier renforcé par des fibres et / incorporant des granulats en caoutchouc.

Les résultats montrent que, pour une ouverture de fissure maximale donnée, la résistance résiduelle diminue avec le nombre de cycles et ce quelle que soit la nature du composite. La dégradation maximale de la résistance résiduelle se produit dans le cas du mortier non fibré. Pour des grandes ouvertures de fissure, un renfort par des fibres permet de limiter cette dégradation sous un chargement de fatigue. Dans le cas du mortier incorporant des granulats en caoutchouc, la dégradation de la résistance résiduelle est limitée pour les petites ouvertures de fissure. Une association granulats caoutchouc-renforcement par des fibres permet de limiter les dégâts sur une large étendue d'ouvertures de fissure. Cette solution confère au composite un intérêt pour une application durable dans le cas des réparations minces adhérents à base cimentaire.

En tenant compte des principales pathologies rencontrées dans cette application tels que la fissuration de la couche de réparation suivie par le décollement de l'interface, différentes techniques de préparation de la surface du support ont été évaluées. Parmi celles-ci, un traitement de la surface par sablage, facile à mettre en œuvre dans les conditions réelles, a été utilisé.

Pour évaluer la performance structurale, des poutres composites constituées d'un rechargement mince sur des substrats dont la surface a été préalablement traitée par sablage ont été soumises à des essais de flexion trois points (monotone et fatigue). Pour le suivi de l'évolution de la fissuration dans le rechargement et du décollement à l'interface, la technique de corrélation d'image 3D est employée. Il en résulte que l'incorporation des granulats caoutchouc dans le matériau de réparation est efficace pour contrôler la fissuration, et par conséquent pour retarder l'initiation du décollement. De plus, le renforcement du matériau de réparation par des fibres est également efficace pour limiter la propagation du décollement en contrôlant l'ouverture de la fissure. Ainsi, l'utilisation simultanée des granulats caoutchouc et des fibres dans le matériau de réparation par couches minces à base cimentaire peut être une solution appropriée pour retarder l'initiation du décollement et également pour limiter sa propagation, autrement dit pour la durabilité de l'application. Les granulats en caoutchouc utilisés étant obtenus par broyage de pneus usagés non réutilisables, cette approche apporte une valeur ajoutée en valorisant un sous produit industriel et en contribuant à la sauvegarde d'un environnement sain.

Mots clés: Réparation, renforcement de fibres, granulats de caoutchouc, préparation des surfaces du substrat, durabilité, fatigue, décollement, technique de corrélation d'images.

TITLE: Degradation of the residual strength of concrete: Effect of fiber-reinforcement and of rubber aggregates - Application to thin bonded cement-based overlays

ABSTRACT

This work is devoted to the study of the debonding of thin bonded cement-based overlays from the concrete substrate under mechanical loading. As repair materials, fiber-reinforced and rubberized cement-based mortars are used. Under these conditions, assessment of durability of the repairs necessarily involves the study of the degradation of the bridging strength under fatigue loading. In this context, tensile fatigue tests controlled by crack mouth opening displacement (CMOD) are conducted on composite specimens in order to establish the degradation law of fiber-reinforced and/or rubberized mortar.

The bridging strength decreases with the number of fatigue cycles for the same maximum crack width, whatever the nature of the composite. The maximum cyclic bridging strength degradation occurs in plain mortar. The cyclic bridging strength degradation for large pre-cracked widths is limited for mortar reinforced with metallic fibers. In case of rubberized mortar, cyclic bridging strength degradation is limited at less pre-cracked width values. A combine use of rubber aggregates and fibers in mortar appeared to be a suitable solution to limit the cyclic bridging strength degradation for a wide range of pre-cracked widths. It confers to the composite an interest for durable application such as cement-based thin bonded overlays.

Taking into account the main cause of distress in thin bonded cement-based applications i.e. cracking and interface debonding, different surface preparation techniques were evaluated in this research. Among them, the sandblasting one is usually implemented in actual conditions.

In order to investigate the structural performance, composite beams consisting of a thin repair layer on top of sandblasted substrates are subjected to three point bending tests (monotonic and fatigue). For monitoring the evolution of cracking in the repair layer and of debonding at interface, digital 3D image correlation technique is used. It emerges as a conclusion that the rubber aggregates incorporation in repair material is helpful to control micro-cracking, which results in the delay of the debonding initiation. Moreover, a fiber-reinforcement of repair material is also helpful to limit the interface debonding propagation by restraining opening of the crack. So, the dual-use of rubber aggregates and fibers in the repair material of thin bonded cement-based overlays can be a suitable solution to delay the debonding initiation and also to limit the interface debonding propagation. This shows that the synergetic effect provided by the combine use of rubber aggregates and fibers remains valid under fatigue loading also.

The used rubber aggregates are obtained by grinding end-of-life tyres. In such conditions, the approach brings an added value, the recycling of this industrial by-product being also a contribution to the maintenance of a clean environment. Incidentally, this approach also helps towards the development of a circular economy.

Key words: Repair, fiber-reinforcement, rubber aggregates, substrate surface preparation, durability, fatigue, interface debonding, digital image correlation.